Annual Report on Nuclear Physics Activities

July 1, 1980 - June 30, 1981

Editors:
R. Beck, G. Büche, G. Flügge, N. Kernert
Institut für Kernphysik
Institut für Angewandte Kernphysik

Kernforschungszentrum Karlsruhe

KERNFORSCHUNGSZENTRUM KARLSRUHE

Institut für Kernphysik
Institut für Angewandte Kernphysik

KfK 3280

ANNUAL REPORT

on

NUCLEAR PHYSICS ACTIVITIES

July 1, 1980   -   June 30, 1981

Editors:

R. Beck, G. Büche, G. Flügge and N. Kernert

Kernforschungszentrum Karlsruhe GmbH, Karlsruhe

ABSTRACT

This report surveys the activities in fundamental research from
July 1, 1980 to June 30, 1981 at the three institutes of the KfK
which are concerned with nuclear physics. The research program
comprises laser spectroscopy, nuclear reactions with light ions
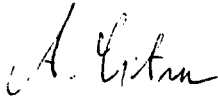and physics at medium and higher energies.

ZUSAMMENFASSUNG

Der vorliegende Bericht gibt einen Überblick über die Arbeiten
an den drei Kernphysikalischen Instituten des Kernforschungszentrums
Karlsruhe im Zeitraum vom 1. Juli 1980 bis zum 30.Juni 1981. Das
Forschungsprogramm umfaßt die Gebiete Laserspektroskopie, Kernreak-
tionen mit leichten Kernen, sowie Mittel- und Hochenergiephysik.

Die drei kernphysikalisch arbeitenden Teilinstitute des
Kernforschungszentrums Karlsruhe legen zum ersten Mal einen
gemeinsamen Bericht über die Arbeiten des vergangenen Jahres
vor. Dieser Bericht soll neben dem seit einiger Zeit durch-
geführten gemeinsamen Seminar die Zusammenarbeit der
Institute unterstreichen.

Ein Teil der Arbeiten macht Gebrauch von dem im Kernfor-
schungszentrum vorhandenen Zyklotron, andere sind auf Nutzung
auswärtiger Großforschungseinrichtungen orientiert, wobei
aber die technischen Möglichkeiten des Kernforschungszentrums,
insbesondere auch die leistungsfähige Grossrechenanlage,
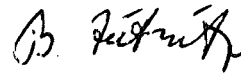eine wesentliche Voraussetzung darstellen.

Wir hoffen, daß durch diesen Bericht einem größeren Inter-
essentenkreis ein Einblick in die kernphysikalischen Arbeiten
im Kernforschungzentrum Karlsruhe ermöglicht wird.

(Prof.Dr.A.Citron)   (Prof.Dr.G.Schatz)   (Prof.Dr.B.Zeitnitz)

Am Institut für Kernphysik 1 wurden drei Arbeitsgruppen im Bereich der kernphysikalischen Grundlagenforschung eingerichtet:

1. Physik schneller Neutronen: Am polarisierten Neutronenstrahl des Karlsruher Zyklotrons werden Streuexperimente an sehr leichten Kernen durchgeführt. Ziele sind die präzise Bestimmung von Nukleon-Nukleon-Phasen aus n-p-Streuexperimenten mit polarisierten Teilchen sowie die Untersuchung der Struktur des ^{4}Helium-Kernes. Ähnlichen Zielen dienen hochauflösende Messungen von neutroneninduzierten Reaktionen am Flugzeitspektrometer des Zyklotrons.
Experimentierhalle und Kollimatoranlage sind fertiggestellt, erste Messungen wurden bereits erfolgreich ausgeführt.

2. Elementarteilchenphysik: Die Gruppe hat in einer deutsch-französischen Kollaboration mit Physikern aus sechs Laboratorien das Detektorsystem CELLO erstellt und Anfang 1980 am e^+e^- Speicherring PETRA in Betrieb genommen. Der Detektor dient Experimenten zur Untersuchung von e^+e^- Stößen bei den höchsten zur Zeit erreichbaren Energien. Mit seinem modernen Flüssig-Argon-Kalorimeter ist CELLO besonders geeignet, die elektromagnetische Komponente in diesen Reaktionen zu untersuchen. Damit werden z.B. genaue Studien der Quanten-Elektrodynamik, detaillierte Untersuchungen von Quark- und Gluon-Jets und die Suche nach neuen Quarks und ihren Eigenschaften möglich. Der Detektor arbeitet seit März 1980 in allen seinen Komponenten zufriedenstellend. Die 1980/81 genommenen Daten werden gegenwärtig analysiert.

3. Experimentelle Methoden: Eine kombinierte kryotechnische Anlage zur Erzeugung niedriger Temperaturen (<10 mK) und starker Magnetfelder (10 Tesla) befindet sich zur Zeit im Bau und wird Ende des Jahres 1981 in Betrieb gehen. Mit dieser Polarisationsanlage sollen große polarisierte Proben verschiedener Atomkerne für Streuexperimente mit schnellen polarisierten Neutronen erzeugt werden. Als Protonentarget wurde mit einer selbst entwickelten Hydrieranlage eine große Titan-Hydridprobe erfolg-

reich hergestellt.

Außer diesen Arbeiten wurden Voruntersuchungen für kernphysika-
lische Experimente an der geplanten deutschen Spallationsneutronen-
quelle, insbesondere auf dem Gebiet der Neutrinophysik, durchgeführt.

Im Institut für Kernphysik II wird Mittelenergiephysik bei CERN und am SIN betrieben.

Bei CERN hat sich unsere Gruppe in Fortsetzung einer langen Tradition auf dem Gebiet exotischer Atome auf das Projekt LEAR (Low Energy Antiproton Ring) konzentriert. Dieses Projekt, für dessen Zustandekommen sich Karlsruhe sehr stark eingesetzt hat, verspricht einmalige Arbeitsmöglichkeiten mit langsamen Antiprotonen. Schon für die erste Meßperiode sind zwei Experimentiervorschläge angenommen worden, von denen der eine ganz von Karlsruher Physikern getragen wird, während sie beim anderen in einer Kollaboration maßgeblich mitwirken. Der Karlsruher Vorschlag nutzt die von Herrn Simons vorgeschlagene Idee der Zyklotronfalle aus. Dieses Gerät soll am SIN erprobt und dann zum LEAR gebracht werden. Auch an den technischen Problemen der Erstellung von LEAR, insbesondere am Einsatz der Elektronenkühlung, ist Karlsruhe personell und finanziell beteiligt.

Die Experimente beim SIN befassen sich schwerpunktsmäßig mit Fragen der Pionwechselwirkung mit überschaubaren Systemen aus wenigen Nukleonen. Dies gilt für die komplementären Experimente mit Protonen bzw. Pionen im Eingangskanal. Durch Heranziehung der zusätzlichen Informationen, die man unter Ausnutzung von Polarisation erhalten kann, werden theoretische Annahmen, insbesondere über die Existenz von Dibaryonzuständen, überprüft.

Auch das von Karlsruhe entworfene Niederenergiespektrometer wird vorwiegend der Untersuchung sehr einfacher Systeme bei Energien nahe der Pionenschwelle dienen.

Die Arbeiten des Institutes für Angewandte Kernphysik II
auf dem Gebiete der kernphysikalischen Grundlagenforschung
betreffen im wesentlichen drei Arbeitsgebiete:

1. Am Karlsruher Isochronzyklotron werden Kernreaktionen
   untersucht, die durch α-Teilchen und ^{6}Li-Ionen von
   26 MeV/Nukleon induziert werden. Im Vordergrund stehen
   dabei die Bestimmung der Neutronendichte von Kernen aus der
   elastischen Streuung von α-Teilchen und die Untersuchung
   des Aufbruchs von ^{6}Li-Ionen im Kernfeld. In Zusammenarbeit
   mit einer Gruppe von der Universität Krakau wurde beim Be-
   schuß von ^{40}Ca mit ^{6}Li-Ionen ein spaltungsähnlicher Prozeß
   entdeckt. Für Experimente mit schweren Ionen, die in naher
   Zukunft am Zyklotron zur Verfügung stehen werden, wird z.Z.
   ein Magnetspektrometer aufgebaut.

2. Mit laserspektroskopischen Methoden werden an sehr geringen
   Mengen ($\lesssim$ ng) radioaktiver Atome Isotopieverschiebungen
   optischer Spektrallinien gemessen und daraus Kernradien be-
   stimmt. Derartige Messungen gestatten es, die Abhängigkeit
   der Ladungsradien der Kerne von der Neutronenzahl über einen
   größeren Bereich zu verfolgen und u.a. Aussagen über die Kom-
   pressibilität der Kernmaterie zu machen.

3. Am Van-de-Graaff-Beschleuniger des Institutes werden Neutronen-
   einfangquerschnitte gemessen, die für das Verständnis der
   Elementsynthese in Sternen von Bedeutung sind. Dabei liegt
   das Schwergewicht darauf, durch kernphysikalische Messungen
   Aussagen über die physikalischen Bedingungen zu gewinnen,
   unter denen der sogenannte s-Prozeß der Elementsynthese ab-
   gelaufen ist.

CONTENTS

1. LASER SPECTROSCOPY

1.1 Laser Spectroscopic Measurements of Isotope Shifts in Calcium Isotopes

A. Andl. K. Bekk, S. Göring, A. Hanser, G. Nowicki[+],

H. Rebel, G. Schatz, and R.C. Thompson

Kernforschungszentrum Karlsruhe, IAK II

[+]Present address: MBB, Schrobenhausen

There is considerable experimental and theoretical interest in charge and matter distributions in the chain of calcium isotopes between the doubly magic nuclei ^{40}Ca and ^{48}Ca. High resolution laser spectroscopy is one experimental technique particularly well suited to the study of charge distributions of the unstable as well as the stable isotopes of calcium. We report measurements of rms charge radii obtained by this technique for all the isotopes between ^{40}Ca and ^{48}Ca.
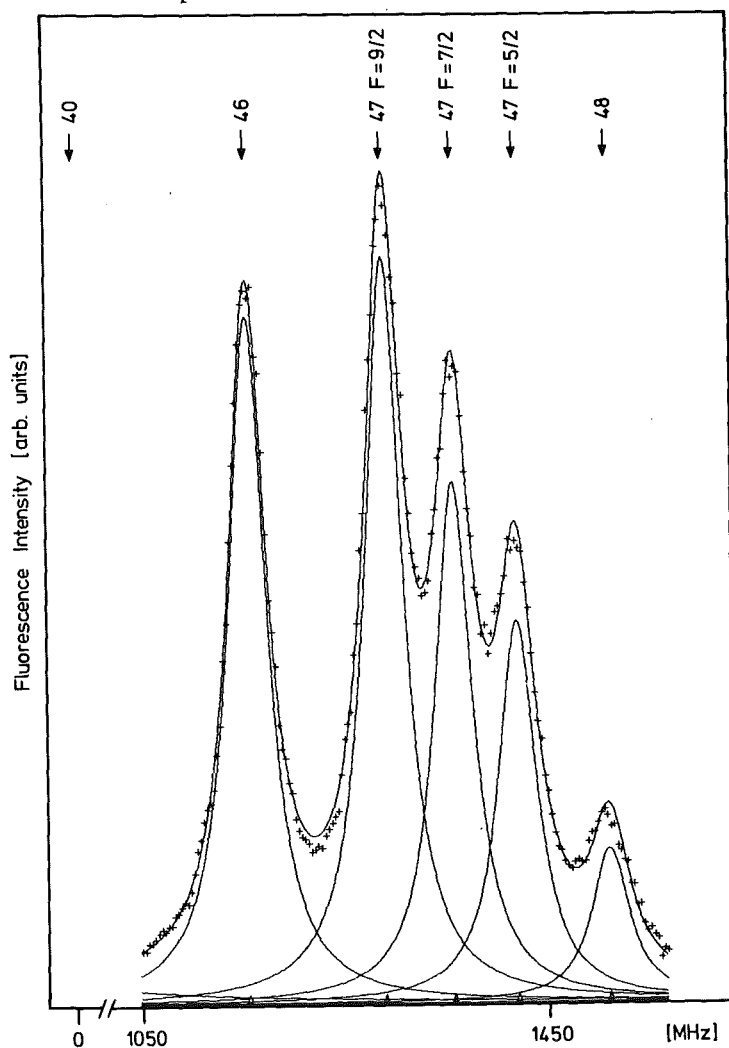
Fig. 1 Spectrum of ^{46,47,48}Ca. For the measurement of ^{47}Ca ($t_{1/2}$ = 4.54 d) the sample contained only ∿170 pg. In order to increase the observed signal without introducing optical pumping effects the polarization of the incoming laser beam was modulated at 5 MHz using a Pockels cell. This allowed for an increase in laser power (and hence signal) by a factor of at least 3, the only disadvantage being a small amount of broadening.

The measurements are based on the observation of the resonance fluorescence induced in a well-collimated atomic beam by the light of high resolution tunable cw dye lasers. Typical uncertainties in the measured isotope shifts were 1.5 MHz; the experimental line-width was about 42 MHz.
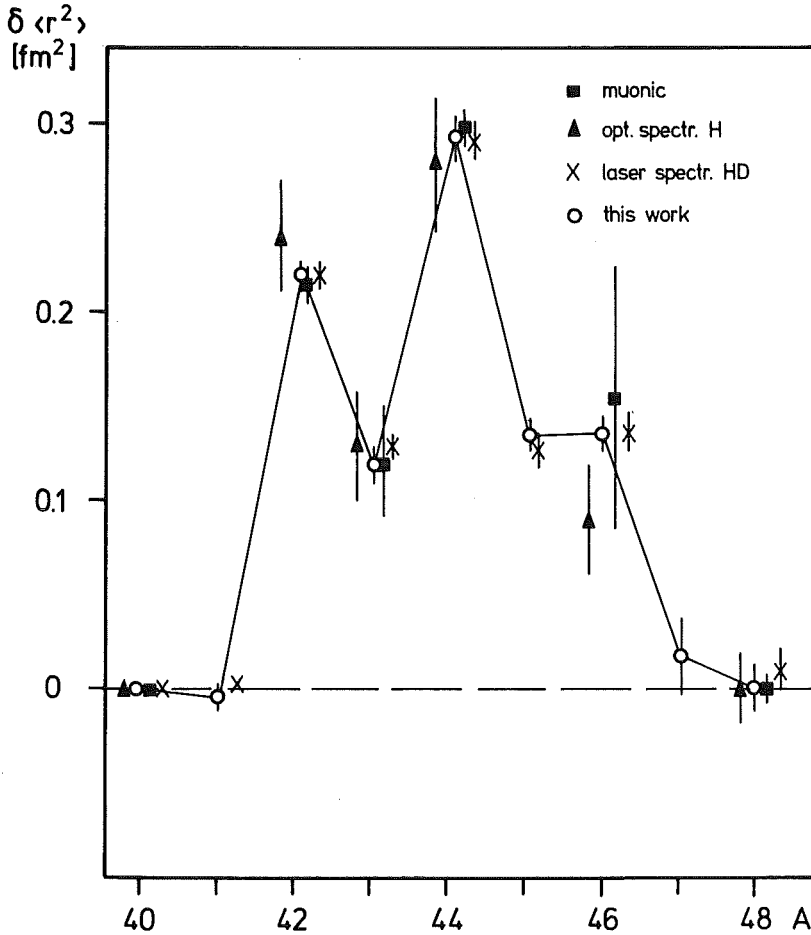

Fig. 2
Changes in rms charge radii for calcium isotopes, derived from the present work. Also shown for comparison are the muonic data, recent conventional optical spectroscopy results and the results of the Heidelberg laser spectroscopy group.
The present results confirm the existence of a considerable odd-even staggering in this region; the rms charge radii of ^{41}Ca and ^{40}Ca are equal whereas those of ^{47}Ca and ^{48}Ca differ slightly.

As an explanation of the peculiar behaviour of the nuclear charge radii in the ^{40}Ca – ^{48}Ca isotopic series – the parabolic dependence on the number n of neutrons in the $f_{7/2}$ shell and the odd-even staggering – an admixture of excited states $|J_c = 2\ f_{7/2}^n\ (J_1)\ J = J_o>$ to the shell model states $|J_c = 0\ f_{7/2}^n\ (J_o)\ J = J_o>$ is suggested (1). In fact with only one parameter (the mixing matrix element) the experimental data are fairly well described.

Reference

(1)   J. Talmi, Private communication.

1.2   Attempt to Measure the Isotope Shift and Hyperfine Structure of ^{49}Ca ($T_{1/2}$ = 8.7 min)

A. Andl, K. Bekk, A. Hanser, and R.C. Thompson

Kernforschungszentrum Karlsruhe, IAK II

An attempt was made to determine the isotope shift and hence the rms radius of the charge distribution of ^{49}Ca. This is an interesting quantity because ^{49}Ca, like ^{41}Ca, has one neutron outside a closed shell, in this case the $f_{7/2}$ shell. With a nuclear spin I = 3/2 there are three ^{49}Ca hyperfine components. The isotope shift in calcium consists mainly of the mass effect; the field effect is negative. This means that for ^{49}Ca the expected large increase of $\delta\langle r^2\rangle$ over the ^{48}Ca value will lead to significant overlap of the resonance lines from the two isotopes.

For the production of ^{49}Ca four samples (each containing 1.5 mg of calcium enriched to 95 % ^{48}Ca) were irradiated with neutrons in the Karlsruhe Research Reactor FR2. After the electromagnetic mass-separation each sample contained $\sim$80 fg ^{49}Ca, with a relative abundance ^{48}Ca:^{49}Ca of 800 : 1.

Because of the very small quantities involved, the closeness of the resonance lines of ^{48}Ca and ^{49}Ca and the short half life (8.7 m) a "photon burst" method (1) was used for detection of the fluorescence. This method takes advantage of the time-correlation of the fluorescence quanta when an atom is excited many times in an intense laser beam. A count is registered only when within a given time interval (in this case 3.5 μs, the approximate time-of-flight of an atom through the laser beam) a preset number of photons (in this case 4) are detected. As the lifetime of the excited $^{1}P_1$ level is $\sim$4.5 ns, many hundred excitations are possible in this time interval. Optical pumping effects were avoided by the use of a fast modulation of the laser beam polarization. With this technique the background (which consisted mainly of scattered laser light) could be nearly completely eliminated; also the Lorentzian wings of neighbouring lines could be strongly suppressed.

The spectra were stored in a multi-channel analyzer (operating in multiscaling mode) which was synchronized with the laser scan of 600 MHz. From each sample spectra were recorded for approximately 10 minutes.
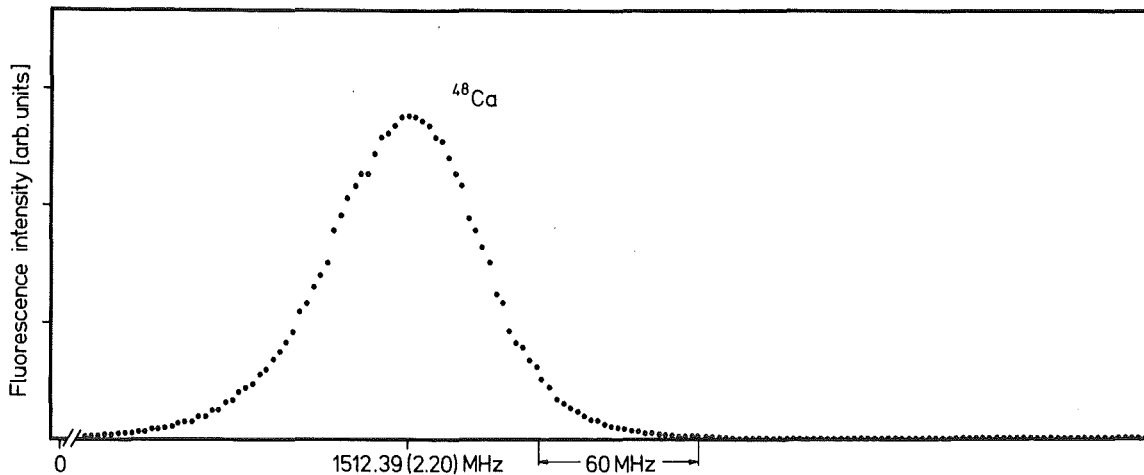
Fig. 1   Sample spectrum. The ^{49}Ca lines cannot be seen.

Fig. 1 shows one of the resulting spectra: only the ^{48}Ca line can be seen. As the ^{49}Ca components would almost certainly have been seen if they lay well away from the ^{48}Ca line, they probably lie under the ^{48}Ca profile. Symmetry tests of the ^{48}Ca profile were carried out but due to an inherent asymmetry (probably arising from laser scan nonlinearity) it was not possible to detect the presence of the ^{49}Ca lines. If it is taken that the lines lie under the ^{48}Ca line we obtain a field effect of -150 ± 100 MHz and hence a notable $\delta<r^2>_{48,49}$ of $.8 \pm .5$ fm^2. However, the possibility cannot be ruled out that the ^{49}Ca lines are hidden in the statistical noise in the wing of the ^{48}Ca peak.

Reference

(1)   G.W. Greenlees, D.L. Clark, S.L. Kaufman, D.A. Lewis, J.F. Tonn, nd J.H. Broadhurst, Optics Comm.,23 (1977) 236.

1.3   Spectroscopy of the 283.3 nm Resonance Line of Lead
           Using a Frequency Doubled Dye Laser

           R.C. Thompson, K. Bekk, S. Göring, A. Hanser,
           H. Rebel, and G. Schatz
           Kernforschungszentrum Karlsruhe, IAK II

Measurements of isotope shifts and hyperfine structure of the resonance line in lead are in progress. Lead is of special interest because it has a magic number of protons and ^{208}Pb is doubly magic. A large number
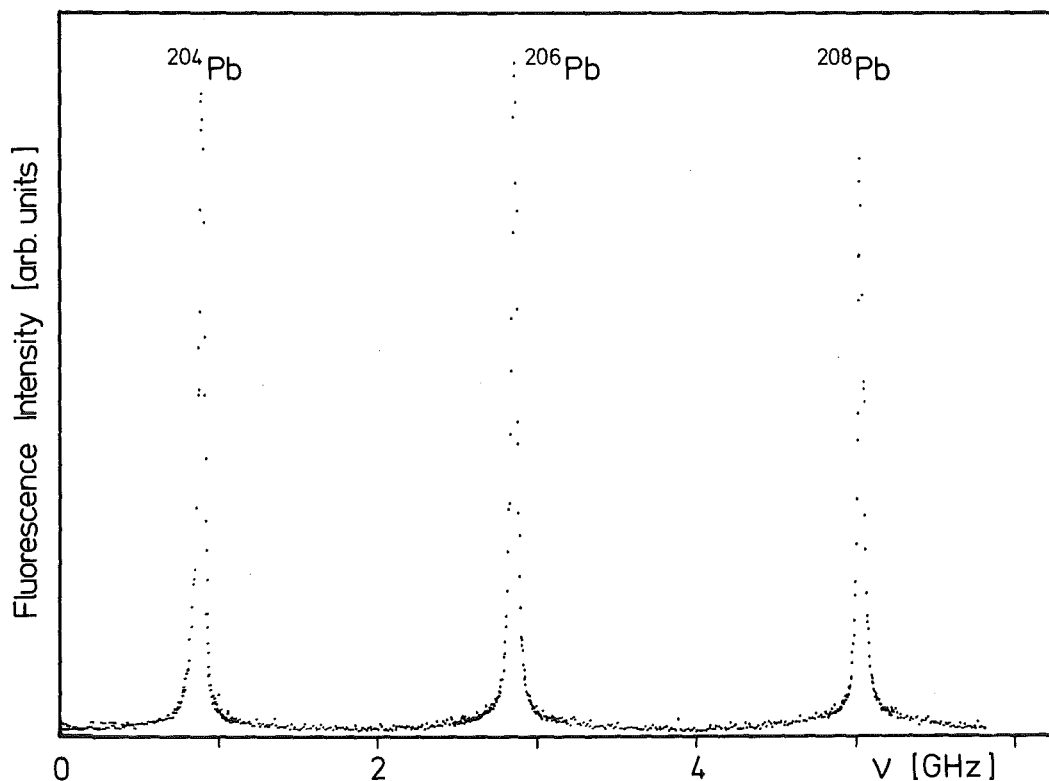
Fig. 1   Fluorescence spectrum after excitation of the Pb resonance
line ($6s^2\ 6p^2\ {}^3P_0 - 6s^2 6p7s\ {}^3P^o_1$) at $\lambda = 283.3$ nm with a
^{204,206,208}Pb sample.

of isotopes are accessible to study without needing to resort to on-line
techniques, and extraction of nuclear information (mean square charge radii
and nuclear moments) from the measurements is a relatively straight-forward
process, due to the large mass of lead.

The method used is similar to that used for studies in barium and
calcium. One important difference is that the resonance line (at 283.3 nm)
is not accessible to tunable cw dye lasers, so a frequency doubling
crystal is used to generate this wave-length from intense radiation
at 566.6 nm from a ring dye laser. Using this technique we have been able
to generate up to 0.3 mW of tunable single-mode radiation at the resonance
wavelength. This is perfectly adequate for the performance of the experiment.

A further difference in the experimental method is that as it is not convenient to frequency-double two dye lasers, the optical reference frequency is not provided by a second atomic beam of the element under study, but rather by a stable Fabry-Perot etalon. This is placed in a temperature-controlled mount and the spacing is electronically stabilized with use of a stable single-mode He-Ne laser. A second dye laser, running at 566.6 nm, is locked to a transmission mode of the etalon and this provides the necessary optical reference frequency.

Preliminary data have been obtained (without use of the reference laser) for the four stable isotopes. Fig. 1 shows a typical trace for the even isotopes $^{204-208}$Pb. As a result of these experiments further modifications to the apparatus are in progress. The observed experimental line-width of less than 50 MHz will enable us to reach a precision higher than that of current classical spectroscopy experiments in lead (1). Preliminary tests show that a string of at least ten stable and unstable isotopes can be produced in sufficient quantities for study.

References
(1) F. Moscatelli, O. Redi, R.L. Wiggins and H.H. Stroke,
    European Conference Abstracts, Vol. 5A, p. 225 and references therein.

2. LOW ENERGY PHYSICS

2.1 NEUTRON PHYSICS

2.1.1 High Resolution Neutron Spectroscopy at the 190 m Neutron Flight Path

H.O. Klages, G. Schmalz, M.S. Abdel-Wahab[+], D. Eversheim[++],
B. Haesner, F. Hinterberger[++], L. Husson, J. Kecskemeti,[+++]
P. Schwarz, and J. Wilczynski

Kernforschungszentrum Karlsruhe, IK1

[+] Now at University of Kairo
[++] University of Bonn
[+++] Acad. of Science, Budapest

The time-of-flight neutron facility at the Karlsruhe cyclotron (1) contains 3 experimental areas which are connected by evacuated beam lines. Fig. 1 shows a schematic view of the apparatus.
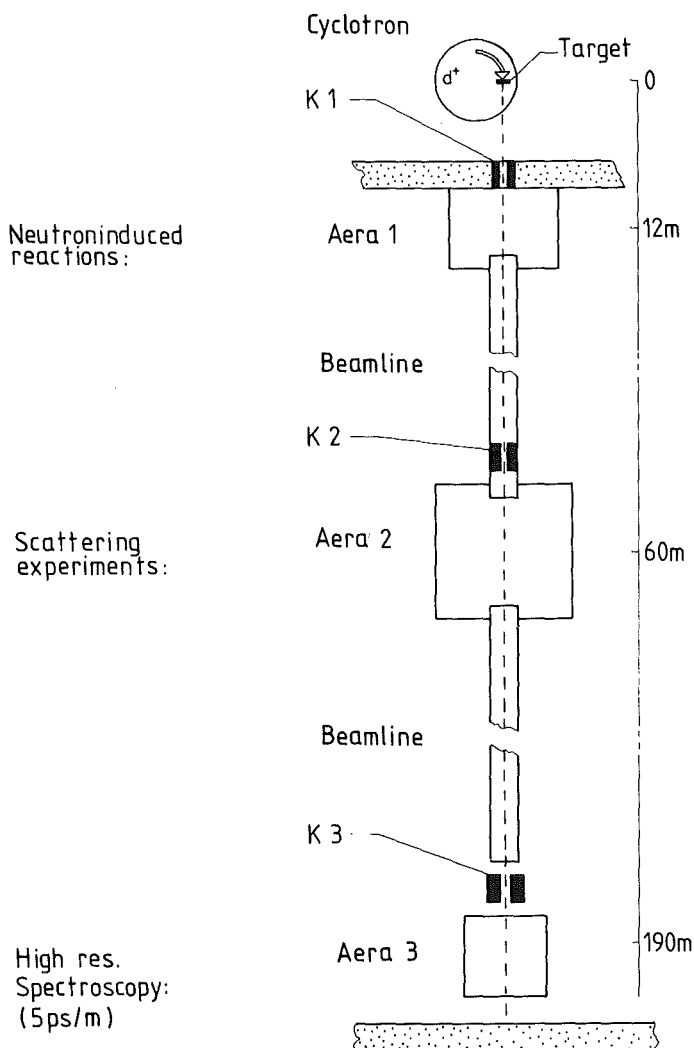
Fig. 1
Schematic set-up of the Karlsruhe neutron time-of-flight spectrometer. Neutron source and experimental areas are connected by evacuated beam tubes. Various collimators (K1 - K3) define the diameter of the neutron beam.
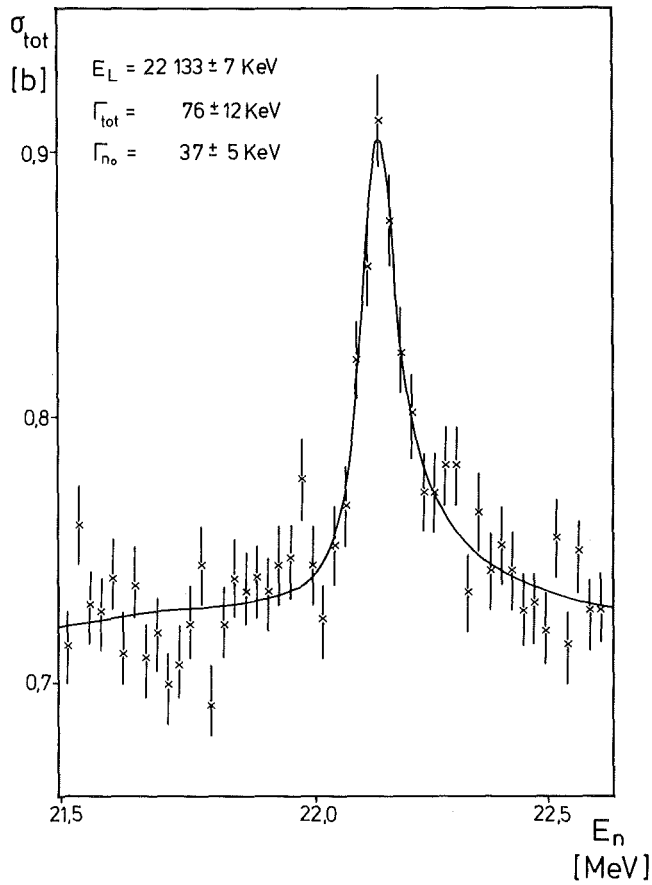
Fig. 2
The total cross section
of ^{4}He for neutrons near
the $3/2^+$ resonance in the
nucleus ^{5}He. The solid
line shows the result of
a one-level Breit-Wigner-
fit to the data.

$E_L = 22\,133 \pm 7\,KeV$

$\Gamma_{tot} = 76 \pm 12\,KeV$

$\Gamma_{n_o} = 37 \pm 5\,KeV$

$n + {}^{20}Ne$

Fig. 3   The total cross section of ^{20}Ne for fast neutrons in the energy
range from 1.5 to 40 MeV

Inside the accelerating chamber of the Isochronous Cyclotron bunches
of deuterons with energies around 50 MeV are deflected onto a thick uranium
target. The high repetition rate of the cyclotron pulses of 33 Mc is
reduced to 30 - 100 Kc by means of a special internal suppression system (2).
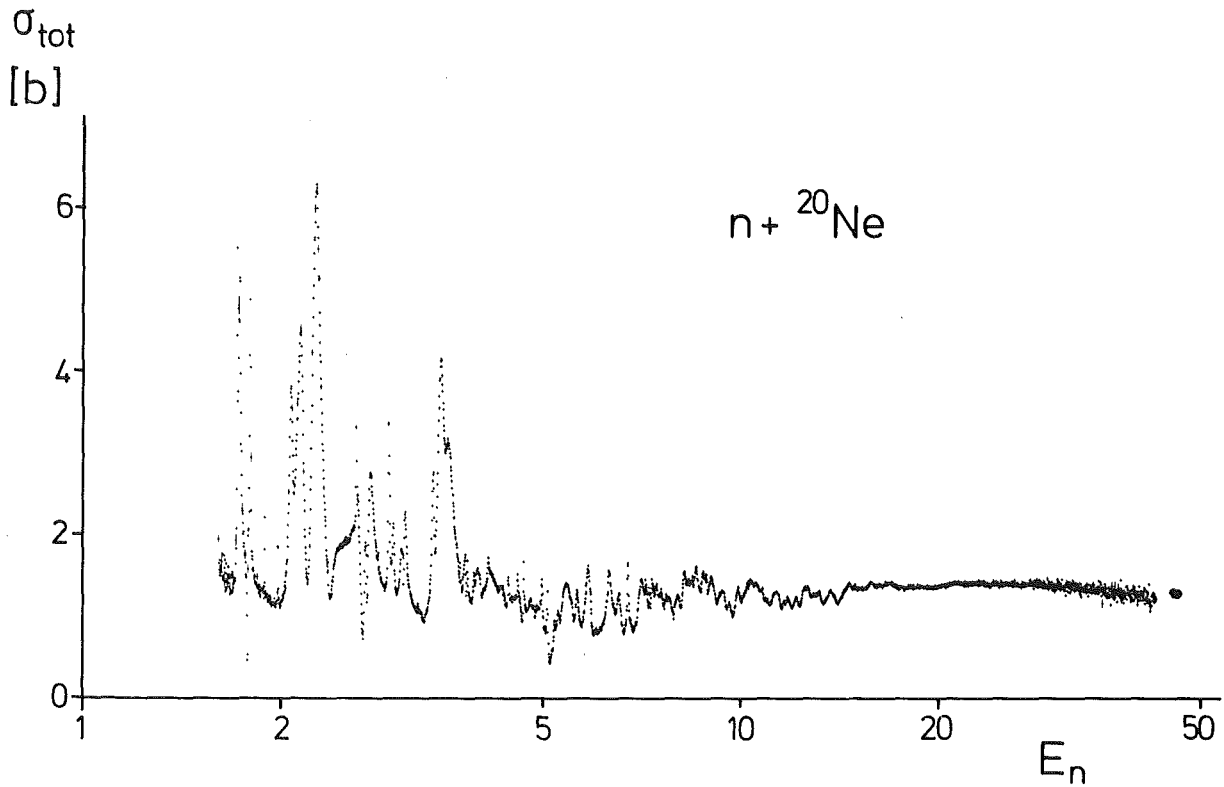
Up to 50 micropulses can be bunched to form a macropulse. These techniques
lead to an average beam of 10 μA on the target. For this value we obtain
more than 10^{12} neutrons$\cdot$ster$^{-1} \cdot$ sec^{-1} at zero degree. The single "neutron-
flash" has a pulse width of about 1 nsec. The energy spectrum of the
pulsed neutron source contains all energies up to 40 MeV.

The use of the collimated neutron beam for scattering experiments
and for the investigation of (n, charged particle)-reactions is described
in the contributions 2.1.4, 2.1.6 and 2.1.8 of this report.

For a high resolution measurement of total neutron cross sections
the detector is placed at a distance of 190 m from the uranium target.
The collimator K1 defines a neutron beam with a diameter of 20 mm at
the experimental area 1, where the material to be investigated is mounted
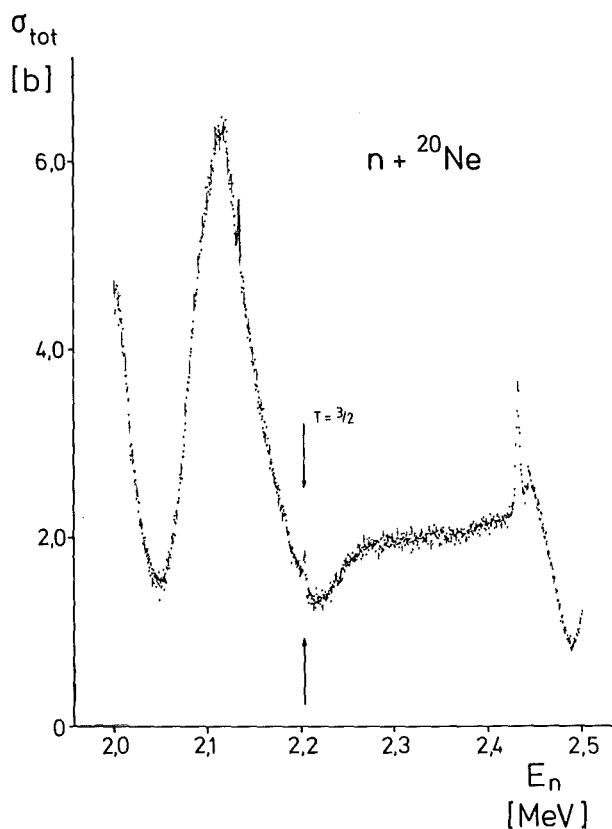into the neutron beam. A sample in-sample out measurement of the

Fig. 4
Enlarged part of the
n+^{20}Ne cross section;
the lowest T=3/2 reso-
nance in ^{21}Ne is indicated
by the arrows.

energy dependent transmission gives direct access to the total cross section.

Neutron time-of-flight spectra are taken using a TDC covering 65 536 channels, 250 psec width each. This is done by means of a specially designed TDC in connection to an on-line computer. A new development of an even faster TDC is described in contribution 2.1.5 in detail.

In the framework of the investigation of light nuclei we measured the total cross sections of the stable hydrogen and helium isotopes, respectively. The well-known resonance at 22.1 MeV in the ^{4}He+n-system was clearly resolved. Fig. 2 shows the cross section together with a single level fit to the data. The associated resonance parameters (3) have been improved by a factor of 4. No narrow structure has been found for the hydrogen isotopes and for ^{3}He.

In a collaboration with a group from the University of Bonn the neutron cross sections of ^{10}B, ^{11}B and ^{20}Ne were measured to investigate the systematic behaviour of isospin forbidden transitions with increasing mass number (4). Fig. 3 shows the total cross sections of ^{20}Ne for neutrons from 1.5 to 40 MeV using a logarithmic energy scale for better
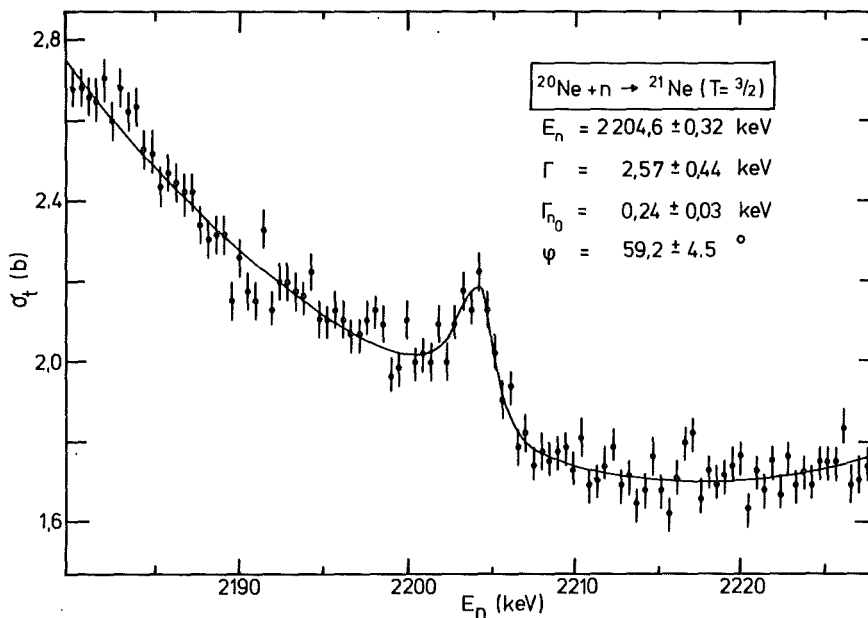

Fig. 5   One-level Breit-Wigner-fit to the lowest T=3/2 resonance in the n+^{20}Ne cross section

representation at low energies. In Fig. 4 a part of the spectrum is enlarged to show the region of interest, where the lowest T=3/2 resonance is located in the nucleus ^{21}Ne. Fig. 5 shows a single-level Breit-Wigner-fit to the data and the deduced parameters.

The full resolution of the Karlsruhe spectrometer, which is better than 5 psec/m is necessary for this type of investigations.

References

(1) S. Cierjacks et al., Rev. Sci. Instr. 39 (1968) 1249.

(2) S. Cierjacks in: Nuclear structure studies with neutrons,
     eds. J. Erö, J. Szücs (Plenum Press, London, 1974) p. 229.

(3) F. Aijzenberg-Selove, Nucl. Phys. A320 (1979), 1.

(4) F. Hinterberger et al., Nucl. Phys. A253 (1975) 125.

2.1.2   POLKA, a Polarized Fast Neutron Beam Facility at the
         Karlsruhe Cyclotron

H.O. Klages, P. Doll. H. Hucker, L. Husson,

P. Plischke, and G. Schmalz

Kernforschungszentrum Karlsruhe, IK1

In 1979 a new activity was started at the Karlsruhe Isochronous Cyclotron. Adjacent to the existing experimental area a new hall has been constructed for fast neutron scattering experiments.

Fig. 1 shows a schematic view of the central part of the experimental arrangement, which was planned and installed in the meantime.

The external beam line of the cyclotron was extended into the new experimental area. The deuteron beam from the cyclotron hits a neutron producing target at a fixed energy of 52 MeV. A bending magnet behind the target leads to a beam dump. The target is surrounded by concrete walls 1 m to 1.5 m thick. At forward angles a special shielding composed of iron, boron-loaded polyethylen and lead is part of this walls. At five angles collimator-tubes are embedded in the shielding. Any open tube allows the extraction of a well collimated beam of fast neutrons into the scattering area outside the walls.
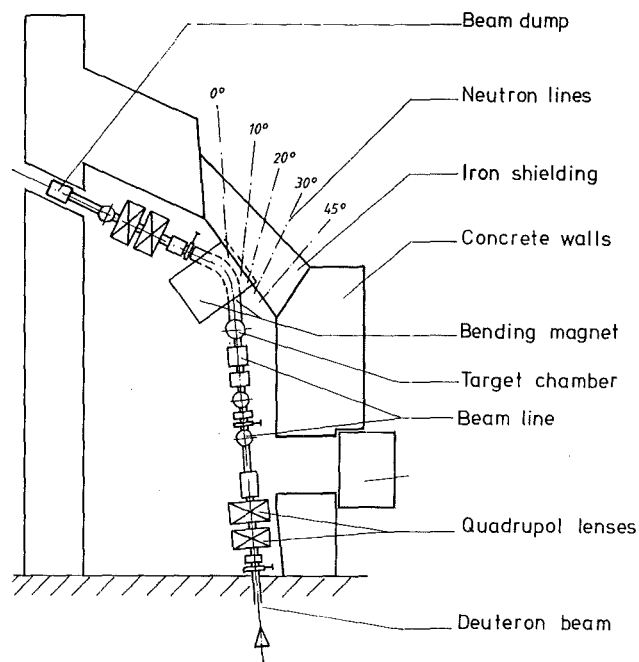
Fig. 1   Schematic view of the neutron collimator facility POLKA for
         the production of fast polarized neutron beams at the
         Karlsruhe cyclotron

The main interest of the neutron collimator facility lies in
experiments with polarized neutrons at energies up to 70 MeV.

By far the best method to produce polarized neutron beams at
the Karlsruhe Cyclotron is to use the polarization transfer in the
reactions $D(\vec{d},\vec{n})$ and $T(\vec{d},\vec{n})$, respectively. For the first time, the
polarized deuteron source (1) at the cyclotron will be used in connec-
tion with a liquid deuterium target. At 0° the emitted neutrons have
energies up to 50 MeV. The main advantage lies in the fact that the
polarization transfer coefficient $K_y^{y'}$ is nearly independent of energy
and has the same value for the high energy part of the breakup neutrons
at is has for the reaction peak (2).

In spite of the low intensity of the beam out of the polarized
source (max. 50 nA) using a thick target (10 MeV energy loss) one can
obtain about 10^6 neutrons/sec, collimated to a beam of 60 mm diameter
at a distance of 5 m from the target.

An experimental set-up including a scintillating scatterer detector as well as 16 detectors for the scattered neutrons is nearly completed. The arrangement for the on-line measurement of the deuteron beam polarization and the computer-based data acquisition system has been designed. The test runs for the shielding and the measurements of neutron beam profiles will be carried out in the near future. The first experiments planned are the measurements of the elastic $\vec{n}$-^{4}He-scattering and the $\vec{n}$-p scattering for the neutron energy range from 20 to 50 MeV.

References

(1)   H. Brückmann et al., Z. Physik 224 (1969) 468.

(2)   R.L. York et al., Proc. 5th Int. Symp. on Pol. Phen. in Nucl. Phys., Santa Fé, (1980) 528.

2.1.3   Calibration of Neutron-Detectors Using Standard Neutron Beams

B. Haesner, H.O. Klages, P. Schwarz, H. Klein[+], and H. Schölermann[+]

Kernforschungszentrum Karlsruhe, IK1

[+]Physikalisch-Technische Bundesanstalt, Braunschweig

In the scattering experiments at the Karlsruhe cyclotron (2.1.4 and 2.1.8) we used two special neutron detectors, a liquid ^{3}He-scintillation-detector (2.1.4) and a large volume (130 ltr) NE 213-detector (2.1.9). To get absolute cross sections it is necessary to know the efficiencies of these detectors. To measure absolute efficiencies one must have a well known neutron source. At the PTB in Braunschweig exists a neutron dosimetry facility where detectors can be calibrated with monoenergetic neutron beams. There the absolute neutron flux is known to better than 3 %. At this facility neutron energies from 2 to 20 MeV are available.

The two neutron detectors were calibrated at the facility of the PTB for neutron energies of 2.5 MeV and 20 MeV for the liquid ^{3}He-scintillation detector and for 6 MeV, 9 MeV, 12 MeV and 20 MeV for the large detector.

The detectors were mounted behind each other at a distance of 11.6 m for the ^{3}He-detector and 12.3 m for the large detector from the neutron target. The neutron beam was collimated down (1) to 60 mm diameter.
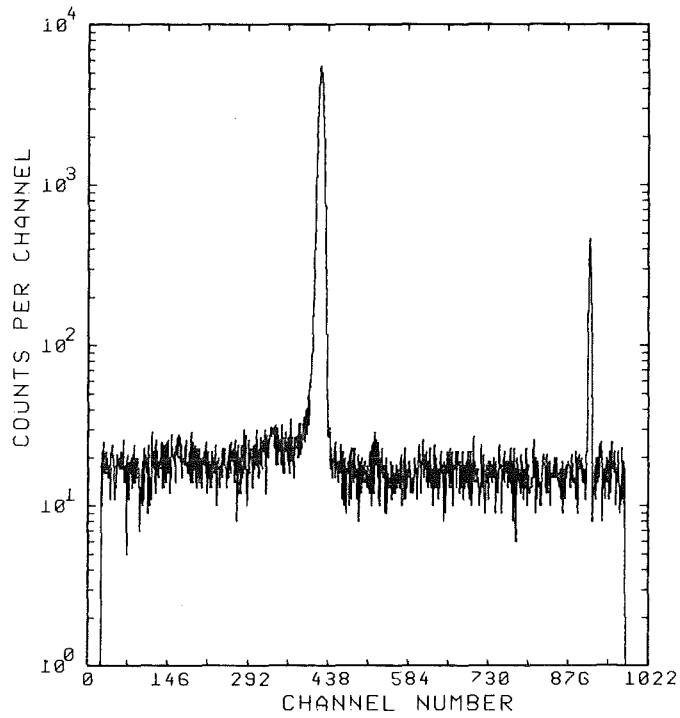
Fig. 1   Time-of-flight spectrum for neutrons of 2.45 MeV (^{3}He-detector)-
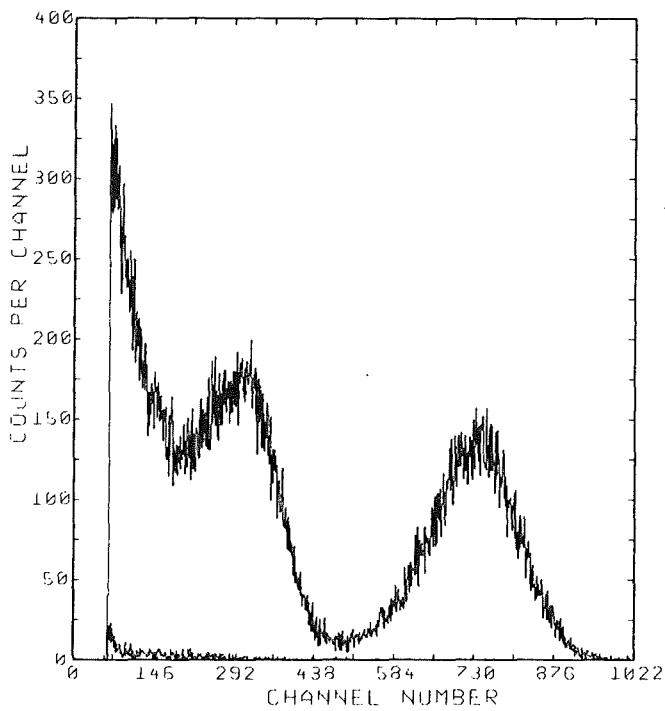
Fig. 2   Pulse-height-spectrum of the ^{3}He-detector bombarded with neutrons of

2.45 MeV. The small curve in this spectrum results from the background.

The ^{3}He detector could be moved out of the beam when the measurement
was done with the NE 213 detector.

For every neutron energy three individual runs have been taken,
one to determine the absolute neutron flux, another one to determine the
background and finally a run with the neutron detector which had to be
calibrated.

A small shielded scintillation detector was used to monitore all
individual measurements. This detector was set up all the time at an
angle of 145° and a distance of 6.45 m from the neutron target.

The neutron flux was measured with a proton telescope. The energy of
the neutrons was determined by time-of-flight techniques. Fig. 1 shows
a TOF-spectrum for the ^{3}He-detector. The strong peak in this spectrum results
from neutrons of the T(p,n)^{3}He reaction, and the smaller peak from prompt
gamma-quanta. This picture shows also that the peak to background ratio is
nearly 10^3. For the determination of the efficiency ε of the neutron detec-
tor the pulse-height spectrum of this detector was measured in coincidence
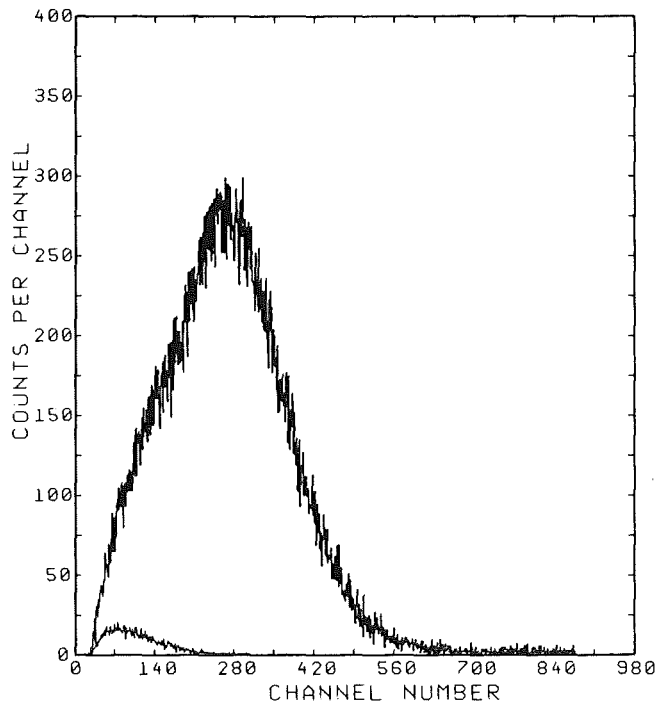
Fig. 3   Pulse-height-spectrum of the NE 213-detector bombarded with
         neutrons of 12 MeV.

with events of the neutron peak. Fig. 2 and 3 show the pulse-height spectra of the two detectors. The neutron energy for the liquid ^{3}He detector was 2.45 MeV (Fig. 2) and for the NE 213-detector 12 MeV (Fig. 3). In both spectra the random background is very small due to the good shielding. For the liquid ^{3}He-detector the calibration ought to be done with the reaction $n+^3He \rightarrow p+t$. The reaction peak can be easily identified in the pulse-height-spectrum.

The results of a first evaluation are:

1. Liquid ^{3}He

ε = 0.042, E_n = 2.45 MeV

ε = 0.002, E_n = 20   MeV

2. NE 213-detector (2.1.9)

ε = 0.29, E_n = 6 MeV

ε = 0.42, E_n = 9 MeV

ε = 0.58, E_n = 12 MeV

ε = 0.55, E_n = 20 MeV.

Reference

(1) D. Schlegel-Bickmann et al., NIM 169 (1980) 517-526.

2.1.4   Differential Cross Sections for the Elastic Scattering
          of Neutrons from ^{3}He

B. Haesner, P. Doll, L. Husson, J. Kecskemeti, H.O. Klages,

G. Schmalz, P. Schwarz, and J. Wilczynski

Kernforschungszentrum Karlsruhe, IK1

In connection with the investigation of the A=4-system with neutron and ^{3}He in the entrance channel differential cross sections for the elastic n-^{3}He-scattering were measured. The experiment was carried out at the experimental area 2 of the Karlsruhe neutron time-of-flight spectrometer. The experimental set-up and the detectors for the scattered neutrons are described in chapter 2.1.8.
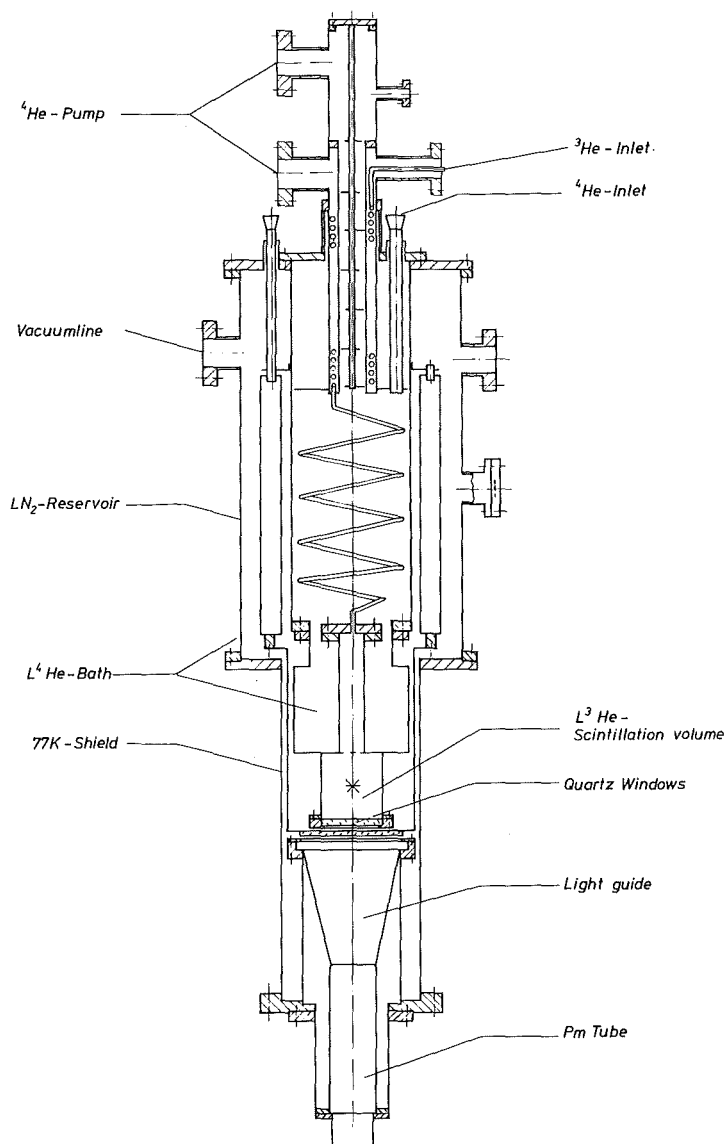
Fig. 1   Liquid ^{3}He-scintillation-detector

A liquid ^{3}Helium-scintillation detector (Fig. 1) served as a
scatterer. Its active volume (70 mm $\emptyset$ x 75 mm high) was chosen to
match the collimated "white" neutron beam of the Karlsruhe cyclotron.
The data acquisition was performed measuring 5 parameters, see chapter
2.1.8. Angular distributions for 13 different scattering angles from 25°
to nearly 180° in the lab. system are evaluated for 20 energy bins from
2 to 30 MeV. Fig. 2 shows an isometric representation of the elastic scattering
of neutrons from ^{3}He for a neutron energy of 10 MeV and a scattering angle
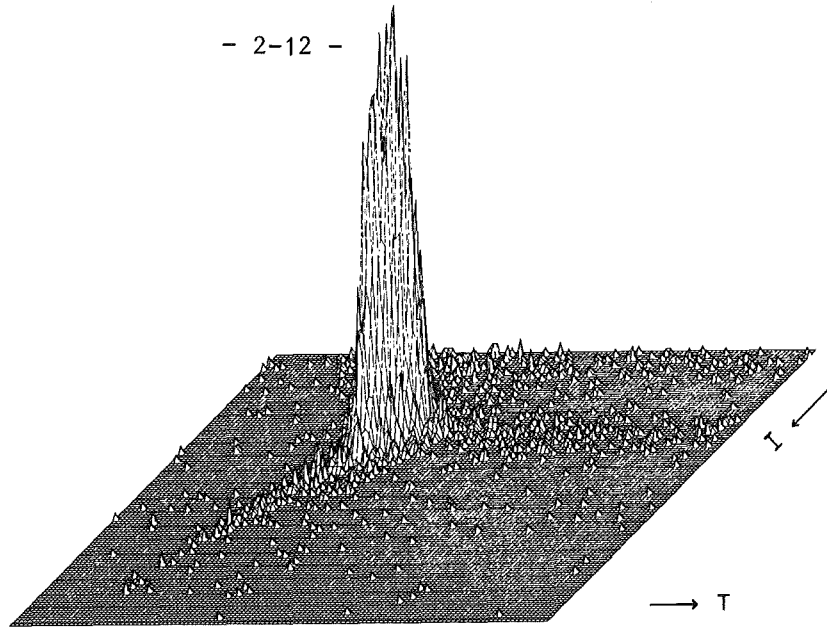
Fig. 2   Isometric representation of the scattering for neutrons with
          an energy of 10 MeV from ^{3}He at an angle of 160° (lab). T is
          the time-of-flight between scatterer and side detector and I
          represents the energy which is deposited in the scatterer. The
          events in the peak are due to neutrons elastically scattered
          from ^{3}He while the background in the matrix results from inelastic
          process or multiscattering events or random coincidences.

of 160° in the lab. system. It makes evident that the multiparameter
data analysis allows a clean separation of the true elastic events
from the background. The complete analysis of the measured data has
not been finished. Preliminary results are shown in Fig. 3.

    The liquid ^{3}He-detector was used simultaneously as a scatterer
and as a monitor. Using the reaction $n + {}^3He \rightarrow p + t$ one has a unique control
of the flux of the neutrons and of the density of the nuclei in the
scatterer. Another advantage of this detector for monitoring is its
unsensitivity to an electronical threshold because the peak of the reaction
$n + {}^3He \rightarrow p + t$ can be separated in the impulse height spectra for
all neutron energies due to the positive Q-value of 0.77 MeV.

    The knowledge of the reaction cross section allows an absolute
measurement of the neutron flux if the density of the liquid is known.
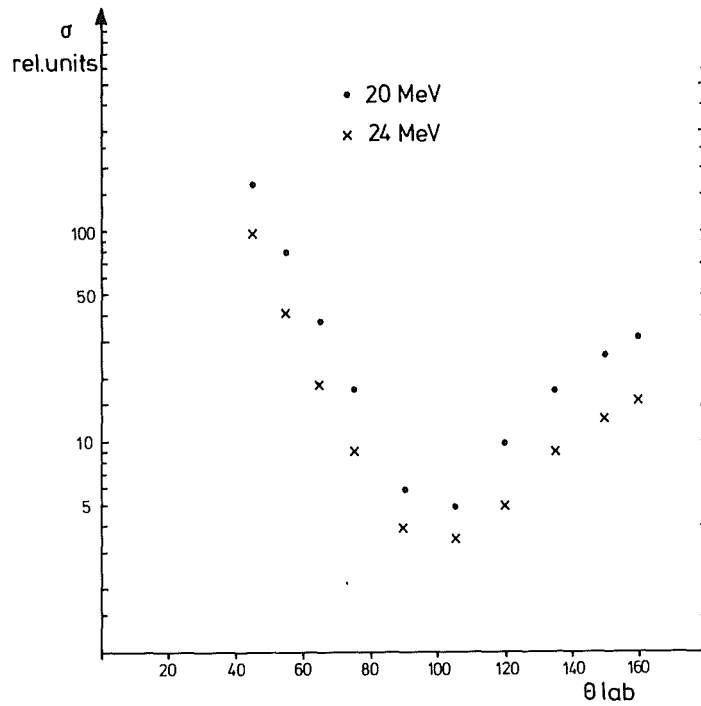
Fig. 3   Preliminary differential cross sections for the elastic
           n-^{3}He-scattering at 20 and 24 MeV.

2.1.5   **A Time-to-Digital-Converter (TDC) with Subnanosecond Resolution**
          at High Repetition Rates by Dual Digital Interpolation
          G. Schmalz and H.O. Klages
          Kernforschungszentrum Karlsruhe, IK1

The neutron-time-of-flight spectrometer at the Karlsruhe Isochronous
Cyclotron is a very efficient device. Its energy resolution for fast
neutrons is unexcelled. An essential part of this is the highly precise
measurement of the time-of-flight of gamma quanta and fast neutrons
over a flight-path length of about 190 m. Therefore, it is necessary to
measure time-intervals of some microseconds absolutely with a resolution
distinctively better than a nanosecond. Moreover, the system must not have
any nonlinearity. Commercial TDC's do not meet these specifications.

For this reason a TDC was developed which is directly connectable
to an on-line data acquisition system.
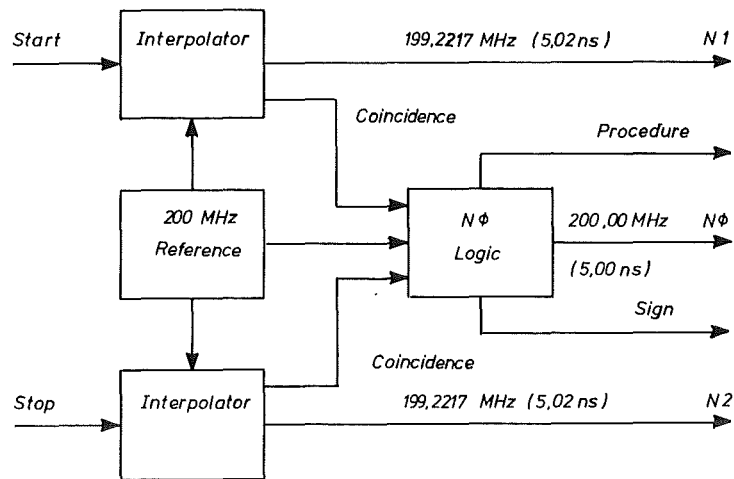
Fig. 1   Block diagram of the TDC, the interpolators, the 200 Mc
time base and the logic.
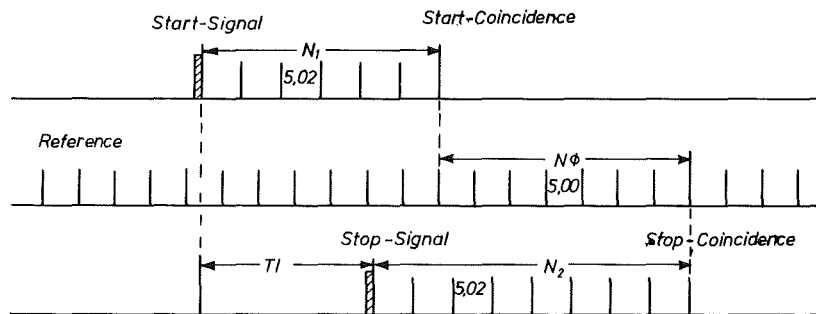
$$N_1 \times 5{,}02 + N_\phi \times 5 = TI + N_2 \times 5{,}02$$

$$TI = 5 \times N_\phi + 5{,}02 \ (N_1 - N_2) \ \cdot$$

$$TI = 5 \left[N_\phi + \tfrac{257}{256} \ (N_1 - N_2) \right] [ns]$$

$$TI = [\ 256 \ N_\phi + 257 \ (N_1 - N_2) \ ] [bit]$$

Fig. 2   Time diagram of a measurement and the equation to compute
the time-interval (TI) equivalent address.

Specifications of the TDC

Repetition rate	100 Kc max.
Resolution	20 ps
Measuring-time preset	99 μs max.
Output	24 bit TTL parallel

Principle of measurement

To measure the time-interval between a start-pulse and a stop-pulse the periods of an extremely stable clock are counted. The quantization error of $\pm$ 1 period is avoided by using a dual interpolation, i.e., an interpolation for the start-pulse and an interpolation for the stop-pulse. By this method the resolution is improved to a small fraction of the period length of the time base.

Fig. 1 shows the block diagram of the TDC, the interpolator, the 200 Mc time base and the necessary logic circuit.

The oscillators of the two separate interpolators are phase coherently triggered by the start- and the stop-pulses, respectively. Their oscillator-period is precisely $5 \times 2^{57}/256 = 5.02$ ns by locking the VCO's to the 200 Mc time base in a PLL circuit and are fed into a counting chain. The outputs of the oscillators are mixed with the 200 Mc clock and the phase-crossover points (coincidences) are detected and stop the counting. The number of counts between start-pulse and start-coincidence is N_1, that of the stop-interpolator N_2. The first coincidenc signal starts a counter for the periods of the time-base-clock, the second coincidence stops this counter. The result is $N_\emptyset$. These three values N_1, N_2, $N_\emptyset$ are fed into a parallel-working computer and have as a result a time equivalent address. So the time-interval-measurement is reduced to a digital counting and computing. The results of a first test-setup show that after some corrections of the printed boards (200 Mc multiplier and computing board) the TDC will fulfill the given specifications.

Fig. 2 shows the time-diagram of a measurement and the equation for the computing of the time interval between start- and stop-pulse.

2.1.6   A New Evaluation of n+^{3}He Reaction Cross Section Data

J. Kecskemeti[+] B. Haesner, and H.O. Klages

Kernforschungszentrum Karlsruhe, IK 1

[+]Acad. of Science, Budapest

The reaction n+^{3}He was investigated in the energy range E_n=1-30 MeV with the aim to determine the absolute cross sections for the reactions n+^{3}He→p+t and n+^{3}He→d+d, respectively. The experiments were carried out making use of the white neutron beam of the Karlsruhe time-of-flight facility.

The target, consisting of a large volume liquid ^{3}He cryostat, served simultaneously as a 4π scintillation detector with 100 % efficiency for the charged reaction products. Because of their total energy deposit the p+t and d+d channels give well defined peaks in the spectra, as shown in Fig. 1. The continuous distribution is due mainly to the recoiled ^{3}He nuclei from elastic scattering and partly to the break-up processes with much lower cross sections.
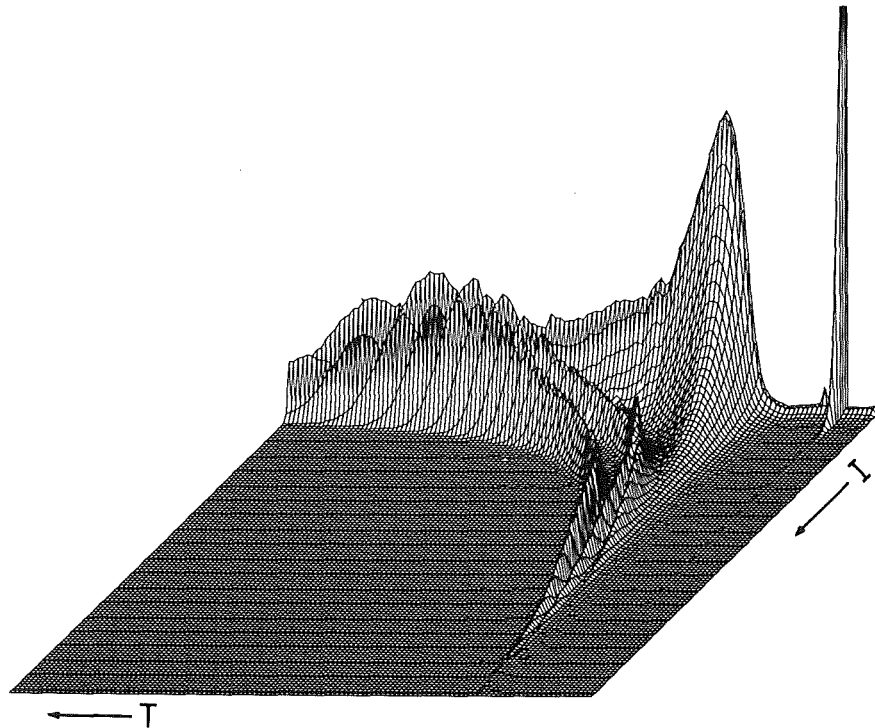
Fig. 1   Isometric display of the neutron-^{3}He-interaction using a pulsed white neutron beam. T is the time-of-flight for the incoming neutrons whereas I denotes the pulse height in the liquid scintillator. The outermost ridge is due to the p+t-channel, the second maximum shows the d+d-events. The continuum at low pulse heights stems from elastic scattering and break-up processes.

During the experiments the neutron flux was monitored with
a very large volume "black neutron detector". A first evaluation of
the data was done using the calculated efficiency of this detector.
Because of normalization problems only relative cross sections could
be obtained.

In order to overcome this shortage and also to avoid systematic
errors from possible uncertainties of the efficiency calculations a
new evaluation was made which is independent of the neutron flux and
of the target properties. The main idea was to use the fact that in
each possible final state of the $n+^3He$ reaction at least one charged
particle is contained so that the total detected event number is propor-
tional to the well known total $n+^3He$ cross section. Consequently, one
has to determine the relative contributions of the p+t and d+d peaks in
the measured spectra and then to multiply these ratios by the total
cross sections to get the absolute reaction cross sections.

The problem to be solved in this evaluation method was to determine
the continuation of the measured spectra below the detection threshold
to zero energy.
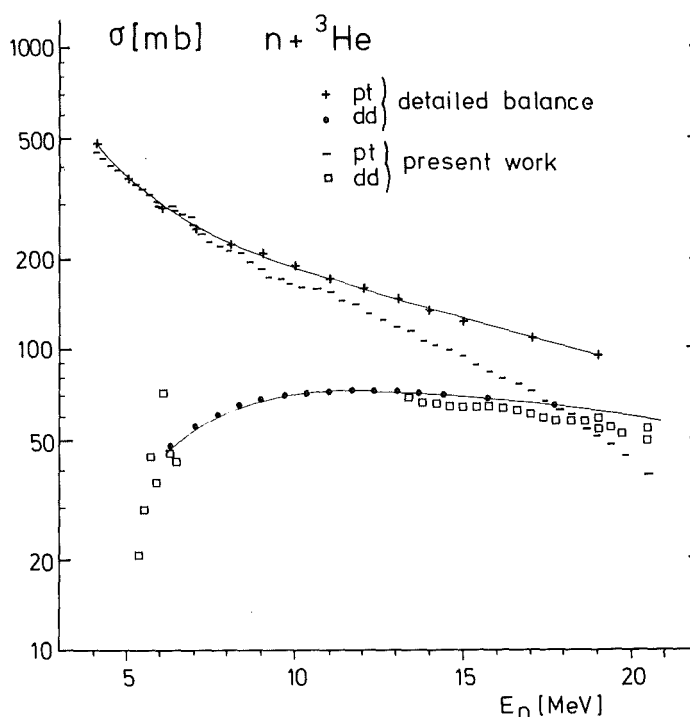
Fig. 2   The evaluated reaction cross section data compared to detailed
          balance calculations based on an inverse reaction cross section
          evaluation by Drosg (1).

As already mentioned the distribution in this region is determined by the elastic scattering and because of the good linearity of the ^{3}He light response it has the shape of the c.m. angular distribution. It seems, therefore, to be reliable to get the continuation from the extrapolation of a smooth fit to the continuous distribution above the threshold.

In the present preliminary evaluation fourth and sixth order polynomial χ^2 fits were performed. In order to avoid the effect of the finite amplitude resolution no fit was made in regions where the d+d or the backward elastic peak dominate. The total n+^{3}He cross sections were taken from a previous Karlsruhe measurement. The results for the reaction cross sections are shown in Fig. 2 together with those from a detailed balance calculation using the inverse cross section data of a compilation by Drosg (1). The statistical errors are generally less than 3 %, except for the low energy d+d data (= 10 %). The systematic error of the above procedure was estimated as follows:

We performed the calculations with continuing the measured spectra with a constant distribution. Since this corresponds to the physically true assumption that the elastic angular distribution does not drop at small angles, the results give an upper limit for the cross sections. At small energies (4 MeV) these were about 20 % higher than those from the polynomial fit. The deviation becomes smaller at higher energies, and is less than 10 % for E_n > 15 MeV.

A more complete analysis of the data, taking into account the finite amplitude resolution and the neutron energy resolution is in progress. It is hoped that this way we get decomposed the d+d and backward elastic peaks in the range E_n = 7-13 MeV with a simultaneous description of the angular distribution of the elastic scattering.

Reference
(1) M. Drosg, Nucl. Science and Engineering <u>67</u> (1978) 190.

2.1.7   Calibration of Neutron-Detectors by Means of a ^{252}Cf-Source

P. Doll, A. Chalupka[+] B. Haesner, J. Kecskemeti, H.O. Klages,

P. Schwarz, and J. Wilczynski

Kernforschungszentrum Karlsruhe, IK 1

[+]Universität Wien

     Due to the dependence of the efficiency of neutron-detectors on the geometry of the detector and the energy of the neutrons it is highly desirable to understand the response of a given neutron detector to a well-known neutron field. It is convenient to use a ^{252}Cf-fission source for the production of such a field with reasonable neutron intensities below 8 MeV. The ^{252}Cf-source was embedded in a low mass ionization chamber (1). This device gives a signal when spontaneous fission of ^{252}Cf occurs thus allowing a time-of-flight measurement for the neutrons emitted in the fission process. The energy spectrum of the fission neutrons is well represented by a Maxwell distribution (2,3). Our aim was to calibrate two detectors: a liquid ^{3}He-scintillation detector (2.1.4) and a liquid NE 213 scintillator (17.8 cm $\emptyset$, 6.4 cm long). The ^{3}He-detector had to be calibrated for the ^{3}He (n,p) T reaction channel only. Knowing
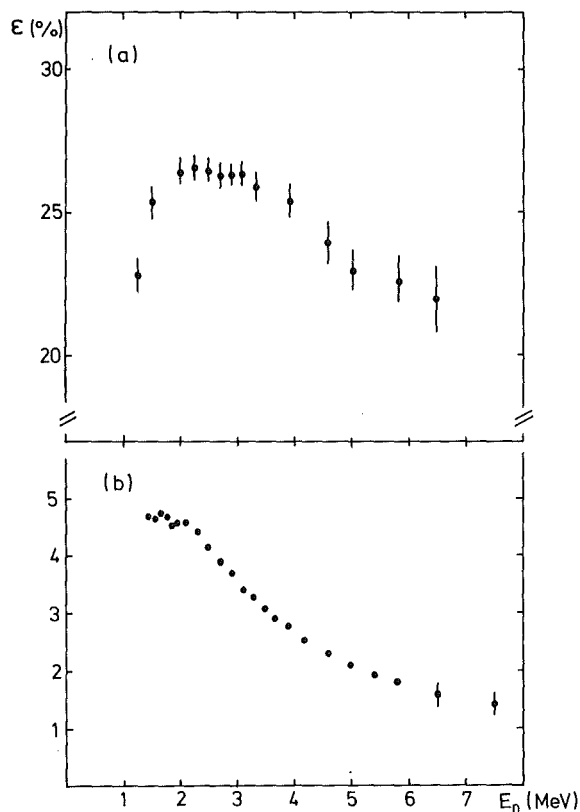
Fig. 1

Efficiency curve for the NE 213-detector (a) and the ^{3}He-detector (b).

the cross section for this reaction we obtain a monitor absolutely calibrated for neutron fluxes up to about 8 MeV.

We used an open geometry for the experimental set-up. A tungsten collimator of 44 cm thickness defined a neutron beam of 6 cm ∅ at 220 cm distance from the source. We were able to close the collimator while conserving his outer geometry, allowing a comparatively precise determination of background neutrons scattered from the environment. However, it turned out that this method is not adequate for the low-energy part of the neutron spectrum ($\leqq$ 1.5 MeV), due to contributions of neutrons having a long time-of-flight after scattering from the walls. With a fission rate of 71000 per second the source emits 3.7 times more neutrons into the full solid angle and about 12 neutrons per second into the detector. For both detectors time-of-flight and pulse-height spectra were measured. For the NE 213 scintillator neutron-gamma discrimination techniques were applied, in addition. The pulse-height spectra for individual neutron-energy intervals exhibited for the ^{3}He-scintillator a clear separation of elastic scattering events from p plus t events in the reaction channel. The stability of the NE 213 detector was checked by means of a ^{22}Na source in subsequent runs. By integrating the pulse-height spectra for subsequent neutron-energy intervals and dividing by the amount of neutrons emitted by the Cf-source in the corresponding energy interval, we obtained the absolute efficiency of the detector. In case of the ^{3}He-detector we only concentrate on the p plus t reaction peak in the pulse-height spectra.

Fig. 1b shows the efficiency for the ^{3}He (n,p)t reaction as a function of the neutron energy. Correspondingly, Fig. 1a shows the efficiency curve for the NE 213 detector.

However, there still exists a discrepancy between the cross sections determined in the present experiments and those evaluated by reciprocity considerations (4) from the inverse reaction. Once we have solved this problem we will be able to normalize other neutron scattering experiments, which overlap with the present experiment from 5-10 MeV of neutron energies, by using the ^{3}He-scintillator as monitor.

References

(1) A. Chalupka, Nucl. Instr. Meth. <u>164</u> (1979) 105.

(2) J.W. Boldeman, Proc. Int. Symp. Neutron Standards on
     Applications, Gaithersburg, MD, 1977, p. 181.

(3) J.W. Boldeman, D. Culley and R.J. Cawley, Proc. Int.
     Conf., Neutron Physics and Nucl. Data, Harwell, 1978,
     to be published.

(4) A. Paulsen and H. Liskien, IAEA-PL-246-2/21, p. 135.

2.1.8   Elastic Scattering of Neutrons From Deuterium in the
         Energy Range 2 MeV - 30 Mev

         P. Schwarz, P. Doll, B. Haesner, L. Husson, J. Kecskemeti,
         H.O. Klages, G. Schmalz, and J. Wilczynski
         Kernforschungszentrum Karlsruhe, IK1

In the framework of the investigation of light nuclear systems two
measurements of the elastic neutron-deuteron scattering were performed.
The collimated "white" neutron beam of the Karlsruhe cyclotron enabled
the measurement of differential cross sections in the energy range from
2 MeV to 30 MeV simultaneously.
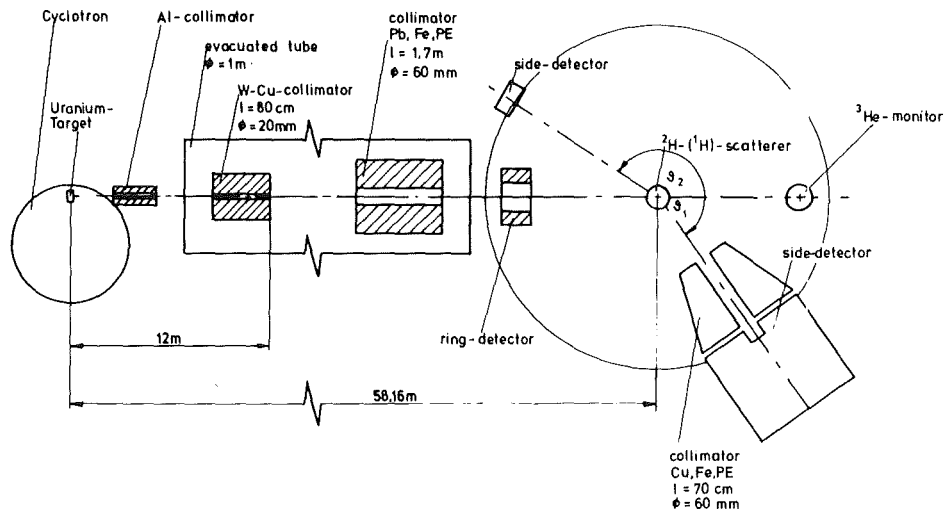
Fig. 1   Experimental set-up at the 60 m flight path of the
          Karlsruhe cyclotron.

Fig. 1 shows the experimental set-up. In the first measurement a partial deuterated NE 213 scintillating scatterer was used for normalizing the neutron-deuteron cross section to the neutron-proton cross section. Two side detectors, one commercial $\emptyset$ 7" x 3" NE 213 scintillator and one so called "black neutron detector" with a scintillation volume of 130 1 (see 2.1.9), were used to detect the scattered neutrons. In the second experiment a totally deuterated NE 213 scatterer was used with the same side detectors positioned at 14 different angles successively and an additional ring detector for the cross section near to 180°. The absolute calibration of the incident neutron flux was done by a ^{3}He-cryostat (see 2.1.4).

The measured data were sampled in a multiparameter-analyzer. The obtained coincident informations for each event were:
1.   Time-of-flight of the incident neutron
2.   recoil-energy in the scatterer detector
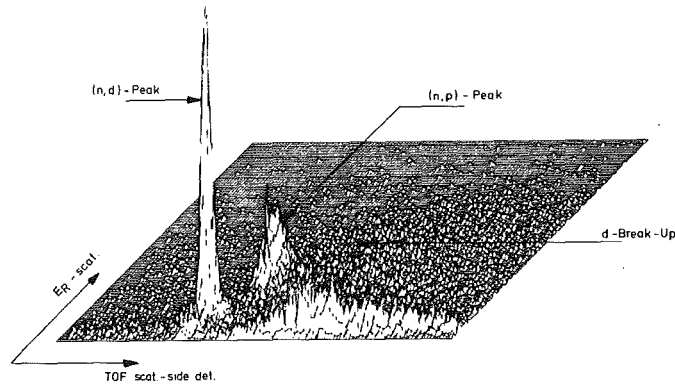
Fig. 2   Kinematical matrix for 14 MeV neutrons. The recoil energy in the scatterer is plotted against the TOF of the scattered neutrons for a scattering angle of 45°.

3.   pulse-shape-discrimination of the scatterer-detector

4.   time-of-flight between scatterer and side-detector

5.   recoil-energy in the side-detector

Data reduction was done in the following way: firstly 24 cuts were laid into the time-of-flight of the incident neutron to obtain 24 cross sections for well defined energy bins. In the second step the pulse-shape-discrimination was used to get rid of the gamma-background. Fig. 2 shows the third step of data reduction for the first measurement at the energy bin 13-15 MeV. The well defined kinematical situation delivered one peak for the n-d scattering and one peak for the n-p scattering in the matrix displayed. By applying narrow windows on both axes a separation of true events against random concidences, multiple scattering, and d-break-up was possible. In the last step one increment pulse height spectrum for each incident energy bin and each angle was built by gating the data lists with all informations and projecting the true events on the recoil axis of the side-detector. The integrals of these spectra are proportional to the differential cross section.

In the first measurement the absolute determination of the cross section depends on the normalization to the n-p scattering and the relative efficiency of the two side-detectors. In the second measurement the knowledge of the absolute detector-efficiencies, of the absolute neutron-flux, and of the target-thickness is necessary. The final results are expected to be accurate within 3 % and will be obtained still in 1981.

2.1.9   Features of Large Volume Neutron Detectors

P. Schwarz, B. Haesner, and H.O. Klages

Kernforschungszentrum Karlsruhe, IK1

For the absolute calibration of fast neutron fluxes two so-called "black neutron detectors" (1,2) were built. Fig. 1 shows a side view of these two neutron-calorimeters. The first one (Fig. 1a) is 600 mm long and has a diameter of 500 mm. At its front it has an entrance channel of 100 mm length and 80 mm diameter. Five Valvo XP 2041 photomultiplier tubes are collecting the light output of the NE 213 scintillator. The second detector (Fig. 1b) has the following dimensions: length 900 mm, diameter 700 mm, entrance-channel length 200 mm, and channel diameter 80 mm.
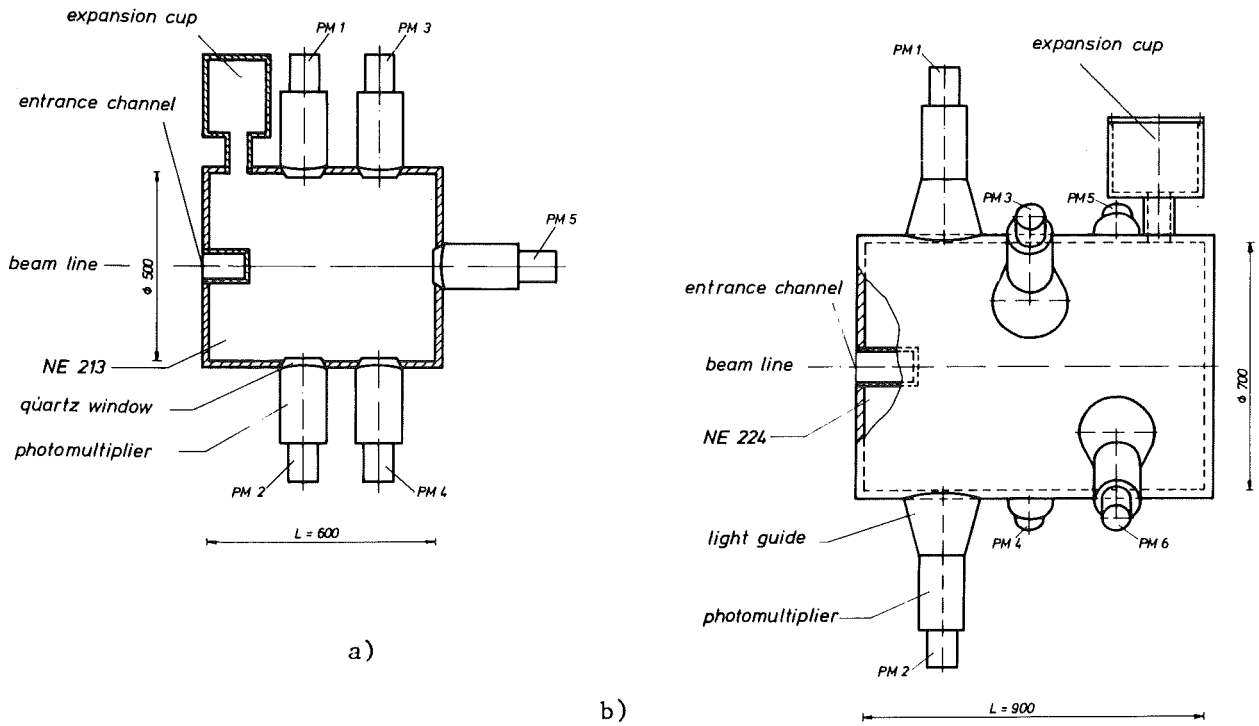
Fig. 1 Schematical set-up of (a) the first black detector type and (b) the second design
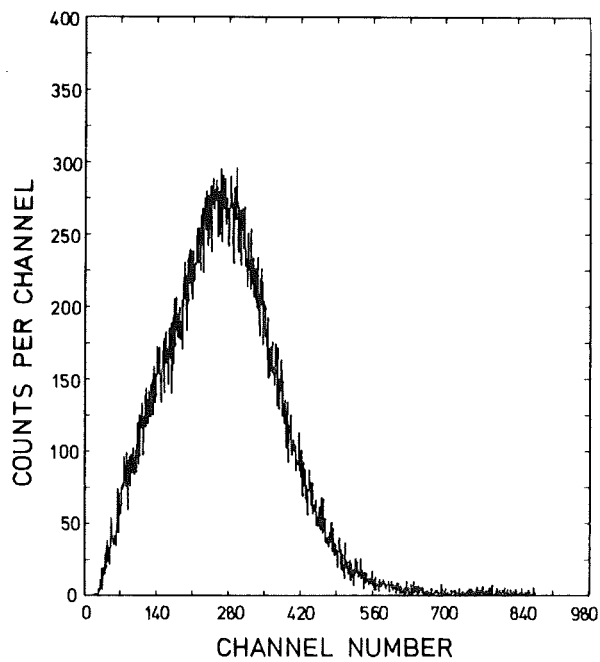
Fig. 2
Light output spectrum for 12 MeV neutrons measured with a fourfold coincidence condition

Six Valvo XP 2041 tubes are sampling the light out of the NE 224 scintillator.

The size and shape of the first black detector was fitted to the energy range (E_n < 30 MeV) of the white neutron beam of the Karlsruhe cyclotron by a Monte-Carlo-simulation, in which seven reaction-channels of neutrons with the scintillation material are included. Multiple scattering, light-attenuation in the scintillator and electronical processing of the scintillation-signals are included, too.

Several electronical set-ups were tested with calibrated monoenergetic neutron beams at the PTB in Braunschweig (see 2.1.3). For an energy equivalent signal the dynode outputs of all five multipliers were added during 400 ns. To get a timing signal for time-of-flight measurements two different set-ups were used. At first the anode-signals of the tubes 1,2,3 and 4 (Fig. 1a) were time-averaged in coincidence.

The obtained pulse height spectrum for 12 MeV neutrons is displayed
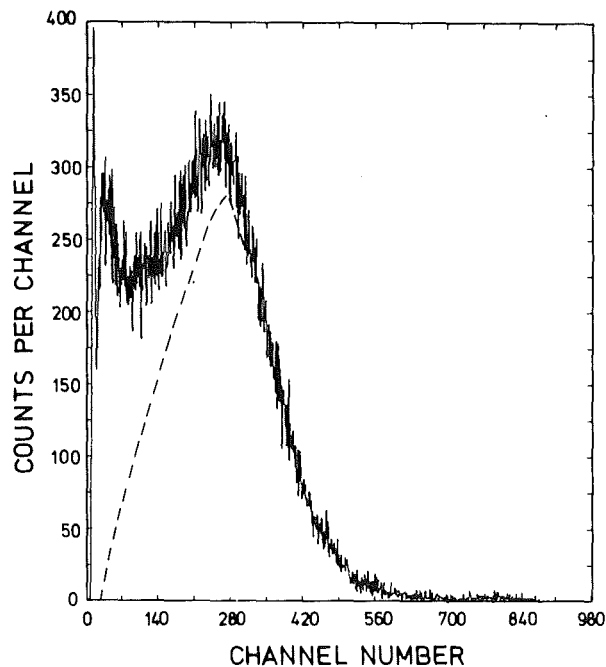
Fig. 3   Light output spectrum for 12 MeV neutrons, measured with a twofold coincidence. The dashed line indicates the normalized spectrum measured with the fourfold coincidence condition.

in Fig. 2. The good calorimetric property of this detector is indicated
by the deep valley at small amplitudes. The efficiency of the detector
in the described set-up is 58%. A second timing method with the multipliers
1 and 2 in coincidence delivered the energy-spectrum shown in Fig. 3.
The efficiency for this method is 78 %. The dashed line in Fig. 3 indicates
the normalized spectrum shape of the four fold coincidence timing shown
in Fig. 2. The above mentioned Monte-Carlo-Simulation identified the region
left of the dashed line as multiple scattered neutrons from the carbon
nuclei in the scintillator. Since carbon has a largely smaller light
output than hydrogen, those neutrons do not fulfill the sharper four fold
coincidence condition. In all further measurements the decrease in effi-
ciency was permitted in order to get the good calorimetrical property
of the detector for neutron flux calibration. The time resolution obtained
by this method was 2.5 ns.

For the measurement of neutrons with higher energies up to 50 MeV
the second detector type (Fig. 1b) was built. To reach the same or even
higher efficiency the scintillation volume was increased from 130 l
(first detector) to 350 l. Caused by the larger volume, the light paths
to the multiplier tubes were increased. Therefore, the scintillator NE
224 was chosen, which has a light attenuation length of 2.5 m, whereas
NE 213 has a light attenuation length of 1.5 m only. A comparison of
both detectors at the white neutron beam revealed an efficiency increase
of about 15 % over the energy range 5 MeV to 30 MeV.

Tests of the new detector at monoenergetic neutron beams will
be performed.

References

(1)   W.P. Poenitz, NIM 109 (1973)

(2)   F. Gabbard, Symposium on Neutron Standards and Applications,
      March 28-31, 1977, National Bureau of Standards, Gaithersburg,Maryland

2.1.10   Neutron-Neutron Scattering using the Neutron-
         Spallation Source (SNQ)

         R. Maschuw
         Kernforschungszentrum Karlsruhe, IK1

In connection with the discussion about nuclear physics experiments
at the SNQ the possibility of a free neutron-neutron scattering experiment
has been investigated. The high flux of thermal neutrons in the pulse peak
supplies very high neutron density inside the moderator. This allows to
observe free neutron-neutron scattering from an evacuated scattering volume
in the moderator outside the biological shield through collimating neutron
pipes. With the proposed features of the SNQ (1) providing a mean flux
of 10^{14} neutrons/sec cm^2 in a scattering volume of 7000 cm^3 a counting
rate of about 5 scattered neutrons per second outside the biological shield
may be expected. The peak flux should be as high as possible as it enters
directly into the counting rate.

The quadratically flux dependent nn scattering effect will be separable
from the linearly dependent background by flux variation.

For absolute calibration of the nn-cross section flux measurements
inside the scattering volume and np reference measurements have to be
performed.

Reference
(1) KfK-Report 3175

2.1.11   The Isomeric Ratio in Thermal and Fast Neutron
         Capture of ^{241}Am*

         K. Wisshak, J. Wickenhauser, F. Käppeler, G. Reffo[+],
         and F. Fabbri[+]
         Kernforschungszentrum Karlsruhe, IAK II
         [+]Centro Nazionale Energia Nucleare, Bologna, Italy
         *submitted for publication to Nucl. Sci.Eng.

A new experimental method has been used to determine the isomeric
ratio IR in neutron capture of ^{241}Am in a differential experiment.
Thin ^{241}Am samples have been activated with monoenergetic neutrons of

14.75 meV and quasi monoenergetic neutrons of ∿30 keV. The decay of the ^{242g}Am nuclei produced has been determined by observing the emitted beta spectrum in a mini orange-spectrometer. The measurements have been performed relative to gold. The ratio $R_1 = \sigma_\gamma \, (^{241}\text{Am} \to \, ^{242g}\text{Am})/\sigma_\gamma(\text{Au})$ was found to be $R_1 = 5.79 \pm 0.33$ at 14.75 meV and $R_1 = 2.73 \pm 0.16$ at ∿ 30 keV. The corresponding isomeric ratios $IR = \sigma_\gamma(^{241}\text{Am} \to \, ^{242g}\text{Am})/\sigma_\gamma \, (^{241}\text{Am})$ are $IR = 0.92 \pm 0.06$ at 14.75 meV and $IR = 0.65 \pm 0.05$ at ∿ 30 keV.

Detailed theoretical calculations of the total capture cross section, the isomeric ratio and the capture gamma-ray spectra were performed in the energy range from 1 to 1000 keV taking advantage of recently available information on the discrete level scheme of ^{242}Am. With the present knowledge on the level scheme of ^{242}Am it seems to be difficult to reproduce the strong energy dependence of IR as indicated by the experimental results.

2.1.12   Fast Neutron Capture Cross Sections and Related
           Gamma-Ray Spectra of ^{93}Nb, ^{103}Rh, and ^{181}Ta*

G. Reffo[+], F. Fabbri[+], K. Wisshak, and F. Käppeler

Kernforschungszentrum Karlsruhe, IAK II

[+]Comitato Nazionale Energia Nucleare, Bologna, Italy

*submitted for publication to Nucl. Sci. Eng.

The capture cross sections of ^{93}Nb, ^{103}Rh and ^{181}Ta were measured in the neutron energy range between 10 and 70 keV, using ^{197}Au as a standard. Most of the data points were obtained with a total uncertainty of ∿4 %. This was possible because of a detailed discussion of the systematic uncertainties involved. Extensive Hauser-Feshbach calculations were performed which yielded not only the neutron cross sections of the isotopes considered up to 4 MeV neutron energy but also partial capture cross sections and capture gamma-ray spectra. For these calculations a consistent set of input parameters was determined from available experimental information or from empirical systematics. The effect of these parameters on the results is discussed.

2.1.13   Determination of the Capture Widths of Neutron Resonances
          in ^{56,58}Fe in the Energy Range from 10 to 100 keV

          F. Käppeler, L.D. Hong, and K. Wisshak
          Kernforschungszentrum Karlsruhe, IAK II

        The capture widths of resonances in ^{56}Fe and ^{58}Fe have been
determined using a pulsed 3 MV Van de Graaff-accelerator and the ^{7}Li(p,n)
reaction. The samples were positioned at a flight path of 60 cm,
capture events were detected by two C_6D_6 detectors and gold was used as
a standard cross section. In spite of the short flight path an energy
resolution of 1.7 ns/m was obtained which was sufficient to perform a
detailed resonance analysis. The distance from sample to detector was
large enough compared to the primary flight path to discriminate background
due to capture of resonance scattered neutrons by time of flight. In this way,
e.g., the capture width of the broad s-wave resonances in ^{58}Fe (43.4 keV
and 66.7 keV) could be determined with improved accuracy. In Fig. 1 the experi-
mental capture yield of ^{58}Fe is shown in the energy range from 36 to 70 keV.
The solid line is the result of a shape analysis using the FANAC code
of F. Fröhner.

        During the experiments data were recorded from the two detectors
in coincidence and anticoincidence mode. This allowed to deduce information
on the relative gamma-ray multiplicity for individual resonances,
which possibly may be related to the respective resonance spins.

        As data analysis is not yet finished completely, final resonance
parameters and uncertainties cannot be given. However, the statistical
accuracy of the strong resonances is certainly better than 5 %.
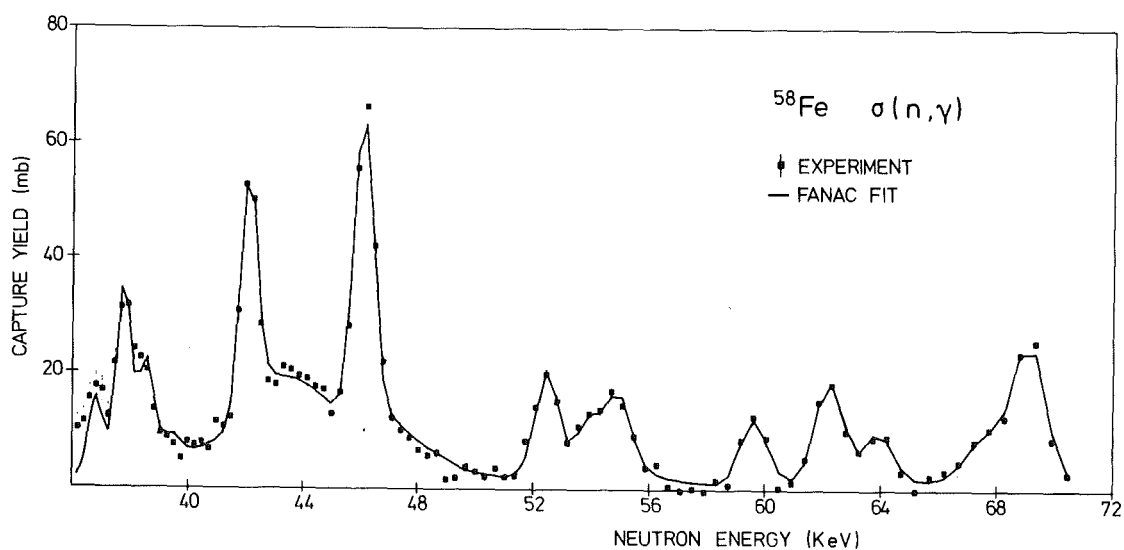
Fig. 1   Neutron capture cross section of ^{58}Fe

2.1.14   <u>Determination of the Capture Width of s-Wave</u>
         <u>Resonances in ^{56}Fe, ^{58,60}Ni and ^{27}Al</u>

K. Wisshak, F. Käppeler, G. Reffo[+],and F. Fabbri[+]

Kernforschungszentrum Karlsruhe, IAK II

[+]Comitato Nazionale Energia Nucleare, Bologna, Italy

The capture widths of s-wave resonances in ^{56}Fe (27.7 keV), ^{58}Ni (15.5 keV), ^{60}Ni (12.5 keV) and ^{27}Al (34.7 keV) have been determined using a setup completely different from previous experiments. A pulsed 3 MV Van de Graaff-accelerator and the ^{7}Li(p,n) reaction served as a neutron source. Capture gamma rays were observed by three Moxon-Rae detectors with different converter materials and gold was used as a standard. The samples were positioned at a flight path of 8.0 cm only. This allowed the use of very thin samples avoiding large multiple scattering corrections. Events due to capture of resonance scattered neutrons in the detector or surrounding materials were completely eliminated by time-of-flight. To demonstrate the experimental signal-to-background ratio Fig. 1 shows a time-of-flight spectrum taken with a ^{60}Ni sample. The corresponding background was measured with an empty position in the sample changer frame. The s-wave resonance at 12.5 keV is clearly isolated from the neighbouring p-wave resonances. The sample thickness used is 0.45 mm. In addition, data were taken with 0.3 and 0.15 mm thick samples.
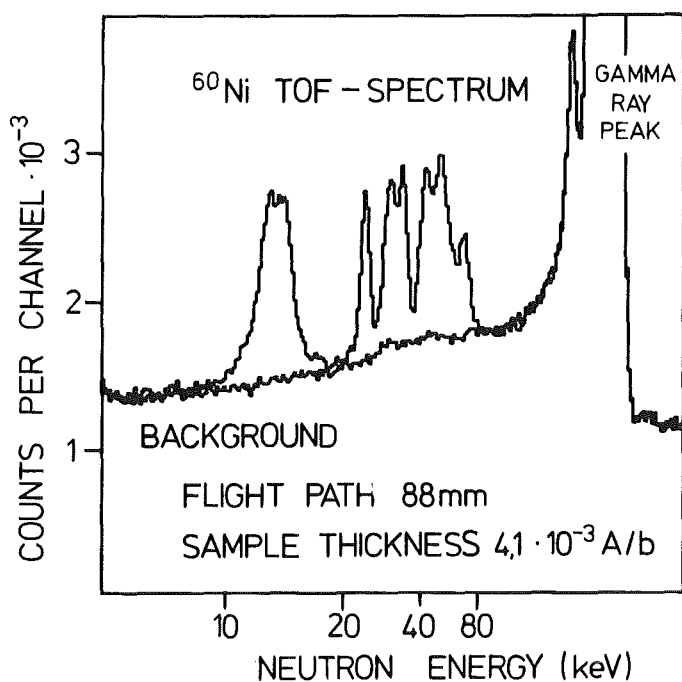
Fig. 1 :Experimental TOF spectrum of the ^{60}Ni sample and the corresponding background.

The main systematic uncertainty in a relative measurement using Moxon-Rae-detectors is caused by deviations of the detector efficiency from the ideal linear increase with gamma-ray energy. This holds especially in the present case as the capture gamma-ray spectra of the samples and the reference sample are quite different. To reduce this uncertainty, data were taken simultaneously from three detectors with different converter materials (graphite, mixed bismuth-graphite and pure bismuth). In addition detailed calculations of the capture gamma-ray spectra have been performed in the framework of the statistical model taking advantage of all available experimental information (e.g. on level schemes, gamma-decay branchings, level densities,cross sections etc.). These spectra together with the relative shape of the detector efficiency taken from literature allow to correct the data of each detector separately.

At present data evaluation is in progress.

2.1.15   The Neutron Capture Cross Sections of the Neon Isotopes
          in the Energy Range 5-400 keV
          J. Almeida and F. Käppeler
          Kernforschungszentrum Karlsruhe, IAK II

The ^{22}Ne(α,n)^{25}Mg reaction taking place in the He-burning shell of red giant stars is believed to be the major neutron source for the s-process. The study of the observed abundances of the heavy elements indicates (1) that 8.2 ± 0.5 neutrons per Fe-seed should be captured by these heavy elements, while the stellar models show that up to 39 neutrons per Fe-seed may be produced by the ^{22}Ne(α,n) reaction; the excess neutrons should be captured by isotopes lighter than ^{56}Fe. Due to their large abundances, ^{20,22}Ne are among the most important neutron absorbers. For this reason, we measured at the 3 MV pulsed Van de Graaff the capture cross sections of the three stable neon isotopes, using the time-of-flight method and a gold sample as a cross section standard. The flight path was 60 cm and the resolution achieved 1.2 ns; at 30 keV neutron energy this leads to an energy resolution of 0.22 keV.

The experimental set-up was essentially the same as that used by B. Leugers (2) with some modifications (3) leading to a larger efficiency and a better signal-to-background ratio. The sensitivity was thus improved
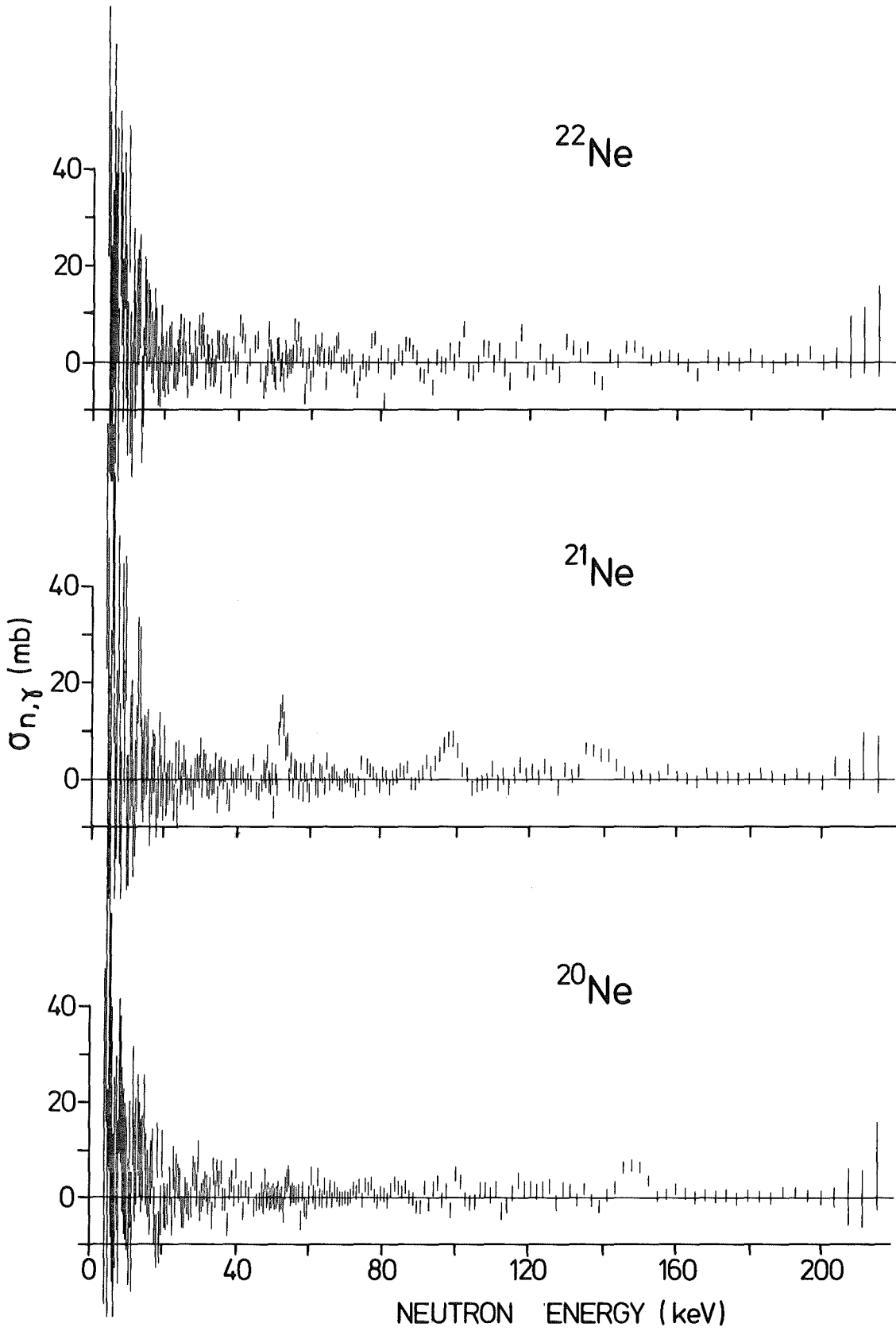
Fig. 1   Measured neutron capture cross sections of the neon

isotopes in the energy range 5-200 keV

by about 50 %, and 8 weeks of measuring time were needed to obtain the results shown in Fig. 1. The resonances at 138 keV and 147 keV in ^{21}Ne and ^{20}Ne, respectively, were known from a previous transmission measurement (4). The 52 keV and 98 keV capture resonances in ^{21}Ne have not been seen in the total cross section. In ^{22}Ne, two wide resonances were observed in the total cross section at 260 and 305 keV; they were not found in this capture measurement, although the energy range from 200 to 400 keV was covered with an energy resolution of ∿1 keV and a sensitivity of 3 mb.

The quantity of interest for the astrophysical problem mentioned above is the Maxwellian averaged capture cross section at kT ∿ 30 keV, corresponding to a temperature T ∿ 3.5 x 10^8 K. From our measured cross sections we obtain the following averages at kT = 30 keV: 1.5 ± 0.6, 1.6 ± 0.8, 0.9 ± 0.6 mb for ^{20,21,22}Ne, respectively. The implications of these results for the neutron balance in the s-process are being investigated.

References

(1) F. Käppeler, H. Beer, K. Wisshak, D.D. Clayton, R.L. Macklin, and R.A. Ward, to be published in Ap.J.Suppl.Series

(2) B. Leugers et al., KfK-Report 2686 (1978)

(3) J. Almeida et al., KfK-Report 3068 (1980)

(4) J. Almeida et al., KfK-Report 3068 (1980)

2.1.16   s-Process Studies in the Light of New Experimental
          Cross Sections: Distribution of Neutron Fluences and
          r-Process Residuals[*]

F. Käppeler, H. Beer, K. Wisshak, D.D. Clayton[+],
R.L. Macklin[++], and Richard A. Ward[+++]

Kernforschungszentrum Karlsruhe, IAK II

[+]Max-Planck-Institut f. Kernphysik, Heidelberg and Rice University, Houston, Texas

[++]Oak Ridge National Laboratory, Oak Ridge, Tenn., USA

[+++]Max-Planck-Institut für Physik und Astrophysik, München

[*]submitted to The Astrophysical Journal, Part 1

A best set of neutron-capture cross sections has been evaluated for the most important s-process isotopes. With this data base,

s-process studies have been carried out using the traditional model which assumes a steady neutron flux and an exponential distribution of neutron irradiations. The calculated σN-curve is in excellent agreement with the empirical σN-values of pure s-process nuclei. Simultaneously, good agreement is found between the difference of solar and s-process abundances and the abundances of pure r-process nuclei. We also discuss the abundance pattern of the iron group elements where our s-process results complement the abundances obtained from explosive nuclear burning. The results obtained from the traditional s-process model such as seed abundances, mean neutron irradiations, or neutron densities are compared to recent stellar model calculations which assume the He-burning shells of red giant stars as the site for the s-process.

2.1.17 A Double Energy – Double Velocity Measurement for Fragments from Fast Neutron Induced Fission of ^{235}U*

R. Müller[+], A.A. Naqvi[++], F. Käppeler, and F. Dickmann

Kernforschungszentrum Karlsruhe, IAK II

[+]Universität Tübingen, Physikalisches Institut
present address: Siemens AG, D-8000 München

[++]Present address: Dept. of Physics, University of Petroleum and Minerals, Dhahran, Saudi-Arabia

*submitted to Phys. Rev. C.

We report on a complete (2E, 2v)-experiment for fast neutron induced fission on ^{235}U. The energy dependence of fragment properties so far known only for thermal neutron induced fission is studied. Experimental problems as well as difficulties in data analysis are considered in detail in order to obtain clean and unbiased results. In particular, a self consistent determination of the fragment kinetic energies TKE was achieved by comparing the results obtained via the respective velocities and pulse heights. We find systematic discrepancies of 2 MeV if TKE is determined from the observed pulse heights using the calibration scheme of Schmitt et al. Therefore, refined calibration constants were deduced using accurate radiochemical mass yields.

Measurements were performed at neutron energies of 0.50 and 5.55 MeV. Our results include mean values of fragment properties before and after neutron evaporation e.g. of fragment velocities and masses, total kinetic

energies, and the respective variances. We also show the distributions of fragment mass, of TKE and of the variance of TKE. In addition, the number of prompt fission neutrons ν is given as a function of fragment mass. Our mass resolution of 2.1 amu reveals fine structure not only in the fragment mass distribution but also in TKE (A*) and ν(A*).

For the lower neutron energy of 0.50 MeV the present results compare reasonably well with similar measurements performed with thermal neutrons. Apparently the 0.5 MeV increase in saddle point excitation does not alter the results significantly. The improved accuracy of this measurement is demonstrated by comparison of our neutron emission data with direct measurements of fission neutrons. At the higher neutron energy of 5.55 MeV we observe the expected decrease of shell and pairing effects which indicate an increase in nuclear temperature. These results are in qualitative agreement with the model of Wilkins, Chasman and Steinberg. However, a striking discrepancy exists for the number of fission neutrons where we find that the increase in the total number of fission neutrons is totally accounted for by heavy fragments alone.

2.1.18   Neutron Capture Cross Section of ^{80}Kr in the Energy Range from 4 to 290 keV

G. Walter, F. Käppeler, D. Erbe, and Z.Y. Bao

Kernforschungszentrum Karlsruhe, IAK II

We have measured the ^{80}Kr(n,γ)^{81}Kr cross section in an energy range from 4 to 290 keV relative to ^{197}Au. As a low lying isomeric state is known to exist in ^{81}Kr our data, by the method of measurement, represent the sum of the capture cross sections to the ground state and the isomer.

The experiment was performed by the time-of-flight (TOF) technique using a pulsed proton beam from the Karlsruhe 3.75 MV van de Graaff-accelerator with a repetition rate of 1 MHz. Neutrons were produced by the ^{7}Li(p,n)^{7}Be reaction and collimated by a ^{6}Li/^{10}B-arrangement. The four samples (Au, empty, ^{80}Kr, C) were mounted on a sample changer and are sequentially brought into the measuring position. The deexcitation gamma rays of the ^{81}Kr nucleus were detected by two Maier-Leibnitz-detectors. Coincident events were rejected from the main spectra and separately recorded for later correction of multiple weighting.
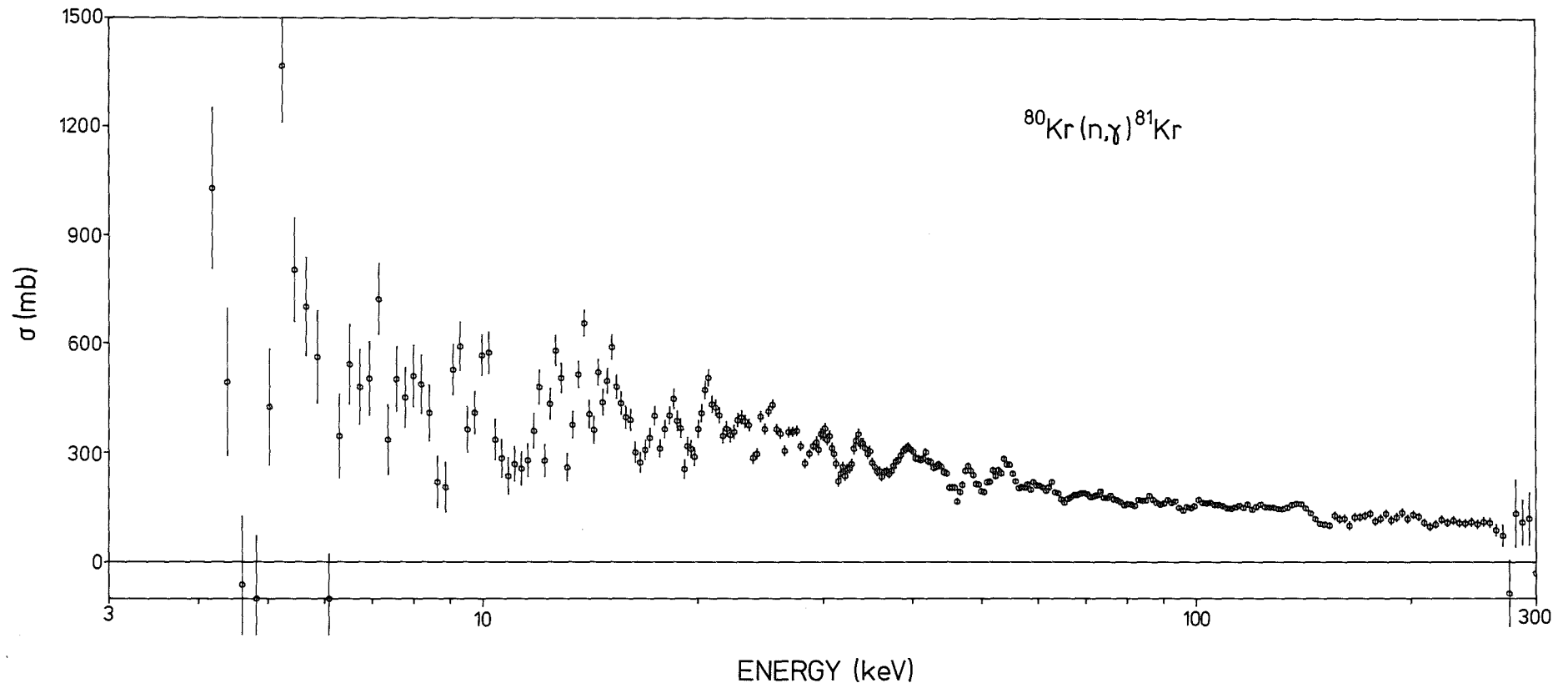
Fig. 1   Neutron capture cross section of ^{80}Kr. The errors given are due only to statistics.

We achieved an overall time resolution of 1.2 ns corresponding to an energy resolution of 200 eV at 30 keV. Monitoring of the neutron flux was performed by a ^{6}Li-glass detector at 90° to the beam axis. Fig. 1 shows the result of this measurement. From the data we calculated the Maxwell-averaged cross section to (282+13) mb. The quoted uncertainty arises mainly from systematic errors.

2.1.19 ^{176}Lu:Cosmic Clock or Stellar Thermometer?*

H. Beer, F. Käppeler, K. Wisshak, and Richard A. Ward[+]

Kernforschungszentrum Karlsruhe, IAK II

[+]Max-Planck-Institut für Physik und Astrophysik, Garching

*Astrophysical Journal Supplement Series (in press)

We quantitatively examine the various experimental and theoretical aspects of the stellar synthesis of the long-lived ground state of ^{176}Lu (3.6×10^{10} y). We discuss the various regimes of stellar temperature and free-neutron density in which either: (i) the internal electromagnetic couplings between ^{176}Lu^o and ^{176}Lu^m (3.68 hours) are sufficiently slow that they may be treated as separate nuclei, or (ii) the internal couplings are able to establish rapidly thermal equilibrium between ^{176}Lu^o and ^{176}Lu^m. Case (i) above allows ^{176}Lu^o to be used as a cosmic clock of galactic s-process nucleosynthesis. As experimental input to the cosmic clock, we have measured the 30-keV neutron capture cross sections: $\sigma(^{170}$Yb$)$ = 766 $\pm$ 30 mb and $\sigma(^{175}$Lu$)$ = 1266 $\pm$ 43 mb. This latter value also yields the branching ratio, B, to ^{176}Lu^o from neutron capture on ^{175}Lu as: B(24 keV) = 0.362 $\pm$ 0.038. Using abundance and cross-section systematics, we derive an upper limit on the mean s-process age of solar material of 11 x 10^9 y before the solidification of the meteorites. By requiring the solar abundance of ^{170}Yb to be consistent with the same σN systematics, we can also bracket the allowable range for the average s-process neutron density as: 10^7 cm^{-3} $\lesssim$ <n> $\lesssim$ 4 x 10^7 cm^{-3}. However, for sufficiently high stellar temperatures, case (ii) above implies that the total effective half-life of ^{176}Lu against beta decay becomes a very strong function of the stellar temperature: $t_{1/2}(^{176}$Lu$)$ = 18.5 exp(14.7/T$_8$) hours for T$_8$ > 1, and thus the ^{176}Lu $\rightarrow$ ^{176}Hf decay would constitute a sensitive stellar s-process thermometer. We show that the fact that ^{176}Lu does

exist in the solar system can place firm constraints on the temperature and neutron density of current models for the site of the s-process. Our preliminary studies indicate that the decay of $^{176}Lu^o$ can be unambiguously used as a cosmic clock of nucleosynthesis only if the s-process occurs in nature at temperatures $T_8 < 1.9$.

2.1.20   Neutron Capture Nucleosynthesis of Nature's Rarest Stable Isotope*

H. Beer and R.A. Ward[+]

Kernforschungszentrum Karlsruhe, IAK II

[+]Max-Planck-Institut für Physik und Astrophysik, Garching

*Nature 291, 308 (1981)

^{180}Ta with a solar abundance of 2.46×10^{-6} ($Si \equiv 10^6$) is nature's rarest stable isotope. Until now it was not possible to explain its origin satisfactorily by spallation which is the commonly assumed source of ^{180}Ta. This is due to insufficient knowledge of the ^{180}Ta level scheme. In the present investigation an alternative production mechanism is proposed. The ^{180}Ta abundance is explained by a small branching in the s- or post r-process neutron capture nucleosynthesis. In this picture the population of an isomeric state in $^{180}Hf^m$ is of crucial importance. The population of this isomer by 30 keV neutron capture on ^{179}Hf has been determined to 0.9 ± 0.1 %.

2.1.21   On the Origin of the Solar System Abundances of ^{113}In, ^{114}Sn, and ^{115}Sn*

R.A. Ward[+] and H. Beer

Kernforschungszentrum Karlsruhe, IAK II

[+]Max-Planck-Institut für Physik und Astrophysik, Garching

*Astron. & Astrophys. (in press)

The neutron-capture cross section of ^{114}Cd to the 53.38 h ground state in ^{115}Cd has been measured via neutron activation. Using this result in conjunction with the total neutron-capture rate of ^{114}Cd, the relative

population of ^{115}Cd^o (53.38 h) was found to be 0.78 $\pm$ 0.13 at an energy appropriate to 30 keV stellar neutrons. In addition, we have quantitatively examined the isomeric structure of the key nuclei: ^{113}Cd, ^{114}In, ^{115}Cd, and ^{115}In which all crucially influence the neutron-capture flows of the s-process as well as the final beta-decays of the r-process in the Cd-In-Sn region. Using temperature and free-neutron histories of various stellar s-process environments, we find that a simple combination of separate s- and r-process components can generally reproduce most of the solar abundances of ^{113}In and ^{115}Sn under typical stellar conditions. Resulting implications for various models of the p-process are also discussed.

2.1.22   Fast Neutron Capture on ^{180}Hf and ^{184}W and the

Solar Hafnium and Tungsten Abundances*

H. Beer, F. Käppeler, and K. Wisshak

Kernforschungszentrum Karlsruhe, IAK II

*Submitted to Astron. and Astrophys.

The capture cross sections of ^{180}Hf and ^{184}W were measured by the activation method and via direct detection of prompt gamma rays, respectively. The Maxwellian averaged cross sections for kT = 30 keV were used to decompose the solar isotopic Hf- and W-abundances into s- and r-process contributions. Examination of the r-process contributions yielded evidence that the abundances of Hf and W might be smaller than quoted in recent abundance compilations. Therefore it is proposed to reconsider the information from meteorite analyses and to perform new measurements, if necessary.

2.1.23   Measurement of the Neutron Capture Cross Sections

^{152}Sm (n,γ) ^{153}Sm, ^{151}Eu (n,γ) ^{152}Eu^m, ^{152,158,160}Gd(n,γ)

and the Study of the s-Process Branching at ^{151}Sm-^{152}Eu

H. Beer, R.A. Ward$^+$, and F. Käppeler

Kernforschungszentrum Karlsruhe, IAK II

$^+$Max-Planck-Institut für Physik und Astrophysik, Garching

The ^{151}Sm-^{152}Eu decay has already been used by Burbidge et al. (1) to estimate the time scale of s-process neutron capture. At ^{151}Sm the s-process path is branched due to the competition of

neutron capture and β^--decay. A second branching occurs at ^{152}Eu. This is the result of β-decay and electron capture both from the 9.3 h isomeric state and the 12.4 yr ground state. The s-process flow through these various branching points leads to the production of the rare nucleus ^{152}Gd. The solar abundance of this isotope is not explained quantitatively by p-process nucleosynthesis. The p-process calculations of Audouze and Truran (2) and Woosley and Howard (3) account only for a small fraction (4-6 %) of the ^{152}Gd abundance. Therefore the s-process must act as the main source of the solar ^{152}Gd. As the ^{151}Sm and ^{152}Eu branching points depend on temperature and neutron density, the s-process yield of ^{152}Gd provides constraints for these important parameters.

For a quantitative study of the ^{151}Sm-^{152}Eu branching neutron capture cross section measurements on ^{152}Sm(n,γ), ^{151}Eu(n,γ)^{152}Eu^m ^{152,158,160}Gd(n,γ) were carried out using the activation technique as described elsewhere (4). In Table 1 the results are summarized. The quoted capture cross sections already constitute the Maxwellian averages for kT = 25 keV.

Table 1: Capture cross sections measured by the activation technique

Target nucleus	$\dfrac{\langle\sigma v\rangle}{v_T}$ (mb) at kT = 25 keV
^{151}Eu	2051 $\pm$ 148*
^{152}Sm	440 $\pm$ 27
^{152}Gd	1144 $\pm$ 71
^{158}Gd	242 $\mp$ 21
^{160}Gd	159 $\pm$ 15

*Cross section to the 9.3 h isomer in ^{152}Eu

The temperature dependence of the ^{152}Eu and the ^{151}Sm decay has been calculated by Cosner and Truran (5) between T = 10^8 K and 10^9 K. Using their results together with the present capture cross sections and supplementary
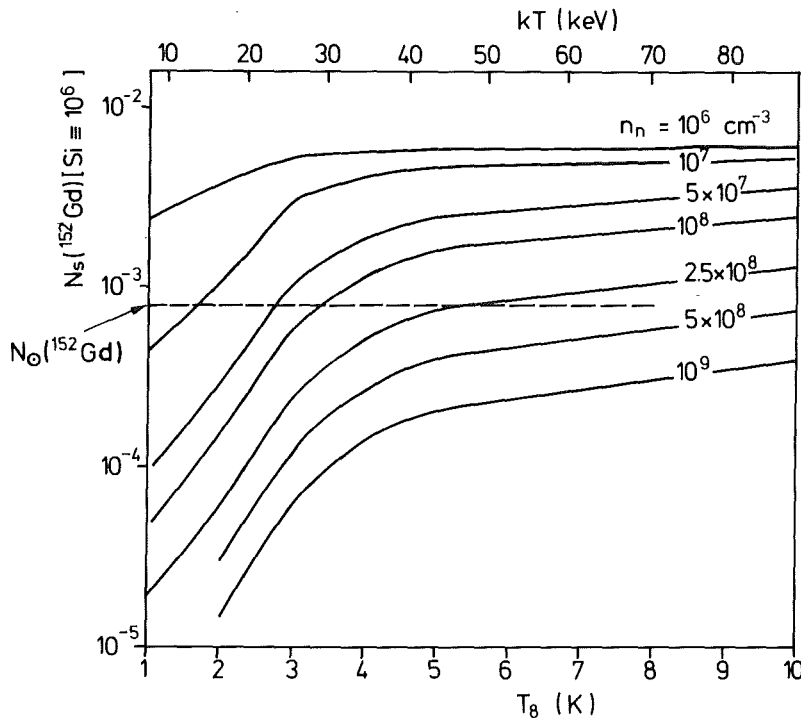
Fig. 1   The abundance of ^{152}Gd that can be made in s-process

nucleosynthesis under various stellar temperatures (T_8)

and neutron densities (n_n). The solar abundance of

^{152}Gd is indicated by the dashed line.

data from literature, the s-process production of ^{152}Gd can be calculated

as a function of temperature and neutron density. This is shown in

Fig. 1. The solar ^{152}Gd abundance is indicated by a dashed line.

The assumption of a typical s-process temperature of 3.5 x 10^8 K

(kT = 30 keV) would imply a mean neutron density of n_n = 10^8 Neutrons/cm^3

($\phi \cong$ 2.4 x 10^{16} Neutrons/cm^2 s) in order to reproduce the solar ^{152}Gd

abundance.

References

(1) E.M. Burbidge, G.R. Burbidge, W.A. Fowler, F. Hoyle,
     Rev. Mod. Phys. 29 (1957) 547.

(2) J. Audouze and J.W. Truran, Ap. J. 202 (1975) 204.

(3) S.E. Woosley and W.M. Howard, Ap. J. Suppl. 36 (1978) 285.

(4) H. Beer and F. Käppeler, Phys. Rev. C21 (1980) 534.

(5) K. Cosner and J.W. Truran, private communication.

2.1.24   Activation Measurements of Relevance to the
          ^{85}Kr Branching: ^{84}Kr(n,γ)^{85}Kr and ^{86}Kr(n,γ)^{87}Kr

H. Beer, R.-D. Penzhorn[+], and F. Käppeler

Kernforschungszentrum Karlsruhe, IAK II

[+]Kernforschungszentrum Karlsruhe, IRCh

An accurate quantitative analysis of the ^{85}Kr branching is of
great importance for the pulsed s-process model of Cosner, Iben,
and Truran (1). Calculations carried out by these authors with
estimated neutron capture cross sections yielded strong overproduction
of ^{86}Kr and ^{87}Rb as well as corresponding underproduction of ^{86,87}Sr
relative to solar abundances.
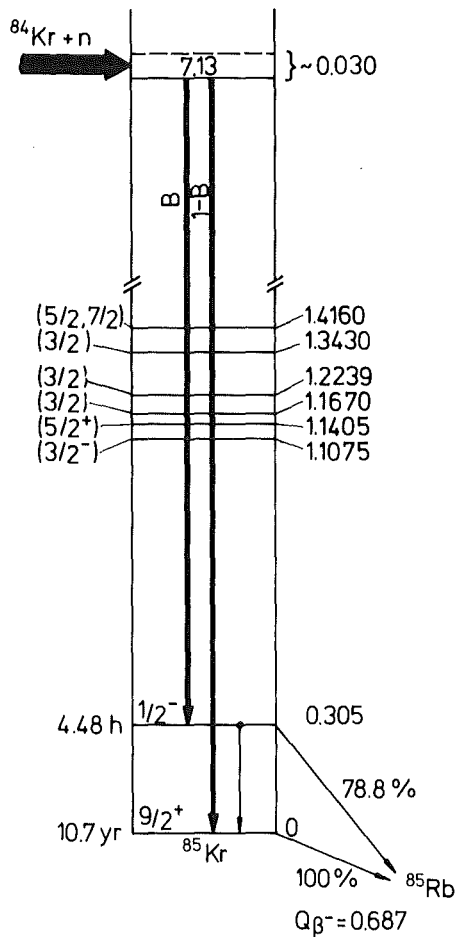
Fig. 1
Details of the neutron
capture and isomeric branching
of ^{85}Kr (all indicated energies are
in MeV).

In order to decide whether this discrepancy is model-dependent
or simply the result of wrong capture cross sections, the present
activation measurements were performed. A recent analysis of
Käppeler et al. (2) showed that besides the capture cross section

of ^{86}Kr the most important quantity needed is the population of

the 4.5 h isomeric state of ^{85}Kr by 30 keV neutron capture. Fig. 1 demon-

strates that a quick thermal equilibration of this isomer with the

ground state via other excited levels is very unlikely because the next state

is situated at 1.1075 MeV. Therefore the ground and the isomeric state must

be treated as two different species that contribute to the s-process capture

flow depending upon their respective initial populations.
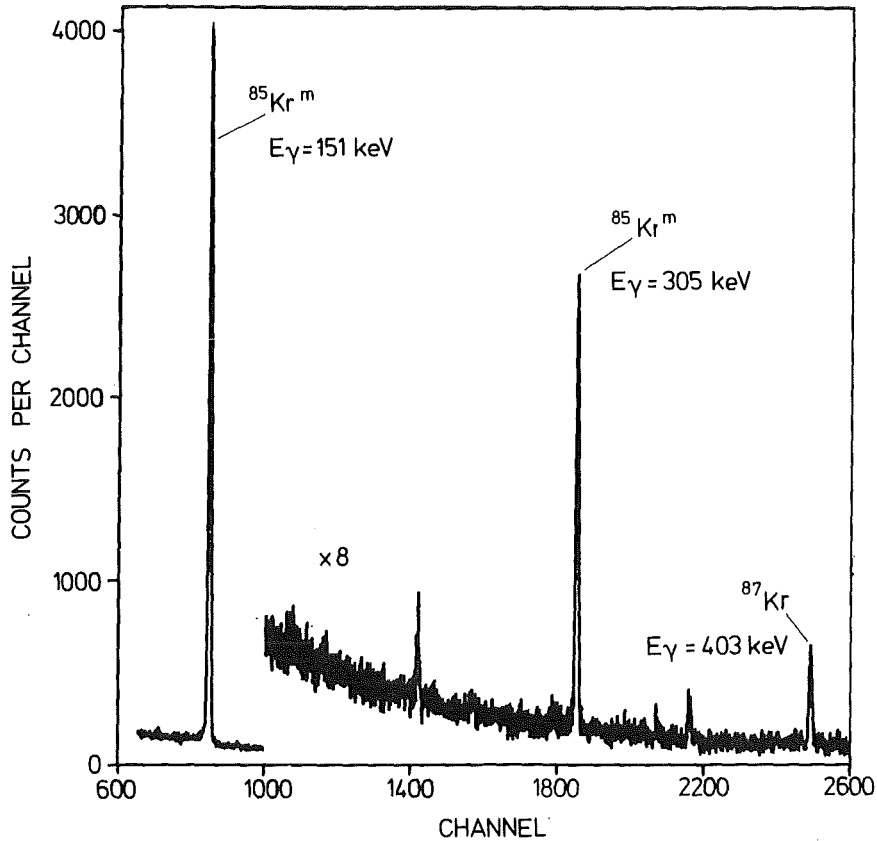
Fig. 2   The gamma-ray spectrum from the activation of natural Kr
measured with a Ge(Li) detector. The gamma-ray lines are related
to the activated radionuclei ^{85}Kr^{m} and ^{87}Kr via the characteristic
gamma energy E_γ and the half life of the decay.

In view of the fact that no stable compounds of krypton are
known, it was not possible to prepare a conventional Kr-sample
suited for the activation method of Beer and Käppeler (3).
However, this problem could be circumvented by the incorporation
of Kr into the crystal lattice of zeolite 5A (4). This matrix has
been shown to withstand high temperatures and intense neutron irradia-
tion (5). The employed zeolite 5A pellets had a loading of 66.3± 1.4 cm^3

(STP) Kr/g zeolite (referred to unloaded matrix). From this material an activation sample was prepared by pressing 50 mg into a self-supporting tablet of 6 mm diameter. Fig. 2 shows the gamma-ray spectrum of this sample together with the characteristic decay lines of $^{85}Kr^m$ and ^{87}Kr. The spectrum was obtained in a 1 h counting period. While this first activation, which demonstrates the feasibility of the technique, was carried out with natural krypton, mainly with the aim of determining the capture cross section to the 4.5 h $^{85}Kr^m$ isomeric state, future experiments are in preparation with enriched ^{86}Kr. These ^{86}Kr-zeolite samples will permit an even more accurate measurement of the ^{86}Kr capture cross section.

References

(1) K. Cosner, I. Iben, jr., J.W. Truran, Ap. J. 238, (1980) L91.

(2) F. Käppeler, H. Beer, K. Wisshak, D.D. Clayton, R.L. Macklin, and R.A. Ward, submitted to The Astrophysical Journal and KfK 3210, August 1981

(3) H. Beer and F. Käppeler, Phys. Rev. C21 (1980) 534.

(4) R.-D. Penzhorn, P. Schuster, H.E. Noppel, and L.M. Hellwig, IAEA-SM-245/10, (1980) 291.

(5) D.W. Breck, Zeolite-Molecular Sieves, John Wiley and Sons (1974).

2.1.25   A Determination of the Xenon Isotopic Neutron Cross Sections for the Evaluation of the Solar Xenon Abundance and for the Analysis of Isotopic Anomalies

H. Beer, G. Reffo[+], F. Fabbri[+], and F. Käppeler

Kernforschungszentrum Karlsruhe, IAK II

[+]Comitato Nazionale Energia Nucleare, Bologna, Italy

The element xenon with 9 stable isotopes exhibits a unique pattern for the study of isotopic anomalies: two isotopes, respectively, are exclusively synthesized in the s-, r- and p-process whereas the abundances of the remaining three isotopes are a mixture of s- and r-process contributions. Among the various anomalies of xenon pure s-process xenon was found by Srinivasan and Anders (1) and the complementary pattern characterized by a simultaneous enrichment of the light and heavy isotopes was reported by Lewis et al. (2). This latter pattern has been interpreted by Clayton and Ward (3) as a deficiency in normal solar s-process xenon. The analysis of the above anomalies requires accurate neutron capture cross sections of $^{128,129,130,131,132}Xe$.

In addition, the capture cross sections of s-only ^{128,130}Xe are
important to estimate the solar xenon abundance through s-process
systematics. In the case of xenon, the common abundance determinations
from meteorite analyses or from the emission spectrum of the sun fail
for physical reasons. The capture cross section of ^{134}Xe
might be of importance in connection with a possible partial s-process
synthesis of this isotope according to the pulsed s-process model
of Cosner, Iben and Truran (4).

As highly enriched isotopes are not easily available for the
measurement of the isotopic xenon capture cross sections, activation
measurements on ^{124,132,134}Xe were supplemented by Hauser-Feshbach
calculations for the other isotopes. In these calculations the measured
cross sections are important because they allow the determination
of an improved set of average model parameters for the individual
nuclei in the isotopic chain. The measurements were performed using
the activation technique of Beer and Käppeler (5). The natural Xe-sample
consisted of a compound of sodiumperxenat (Na_4XeO_6) pressed to a self-
supporting tablet. This sample was sandwiched between two gold foils
which served as a neutron capture standard.

In Table 1 the results of the measurements and of the calcula-
tions are summarized. The activation measurements yielded also the Maxwellian
averaged capture cross section of ^{23}Na, $\frac{<\sigma v>}{v_T} = 2.78 \pm 0.15$ mb. This value
is in excellent agreement with existing differential cross section data
and therefore ensures the correct stoichiometry of the compound.

Table 1   Maxwellian averaged capture cross sections

Target nucleus	$\frac{<\sigma v>}{v_T}$ (mb) at kT = 25 keV	
	experimental	theoretical
^{124}Xe	1134 $\pm$ 114	-
^{128}Xe		298
^{129}Xe		622
^{130}Xe		220
^{131}Xe		464
^{132}Xe	69 $\pm$ 4	77
^{134}Xe	34 $\pm$ 2	38
^{136}Xe		2.5
^{23}Na	2.78 $\pm$ 0.15	

References

(1) B. Srinivasan and E. Anders, Science <u>201</u> (1978) 51.

(2) R.S. Lewis, B. Srinivasan, E. Anders, Science <u>190</u>, (1975) 1251.

(3) D.D. Clayton and R.A. Ward, Ap. J. <u>224</u> (1978) 1000.

(4) K. Cosner, I. Iben, jr., J.W. Truran, Ap. J. <u>238</u> (1980) L91.

(5) H. Beer and F. Käppeler, Phys. Rev. <u>C21</u> (1980) 534.

2.2   NEUTRINO PHYSICS

2.2.1   Calculation of the Neutrino Flux and Background Contributions from a Spallation Neutron Source

J. Wilczynski

Kernforschungszentrum Karlsruhe, IK1

By using a Monte Carlo Code (2) the neutrino flux produced by a proton beam incident on a heavy target was calculated. The neutrinos are produced in the decay of the stopped charged pions and muons. Because of the capture of the negative charged pions and muons by the nuclei of the target material the neutrino flux is dominated by the ν_μ from π^+ decay and the ν_e, $\bar\nu_\mu$ from μ^+ decay.

In Fig. 1 the total number of ν_μ from π^+ decay is presented as a function of proton energy and target material. The ν_μ yield is a linear function of the proton energy and decreases with increasing mass number of the target material. The energy dependent ν_μ and $\bar\nu_\mu$, ν_e flux at a distance of 6 m from the spallation source is shown in Fig. 2 for 1.1 GeV protons incident on a Pb target. The ν_μ spectrum is dominated by the neutrinos from μ^+ decay at rest (E = 29.8 MeV), while the small continuous background of the spectrum originates from π^+ decay in flight. The energy spectrum of the $\bar\nu_\mu$ and ν_e is continuous because of the three-body-decay of the muon and shows a cutoff energy of $E = \frac{1}{2} m_\mu \cdot C_2$.

The time dependence of the neutrinos from π^+ and μ^+ decay is shown in Fig. 3 assuming a 200 ns proton pulse width, a frequency of 100 Hz, and an average proton current of 1 mA. The energy of the pulsed proton beam incident on a Pb target was assumed to be 1.1 GeV. Due to the difference in the lifetimes of the pion and the muon the ν_μ contribution dominates during the 200 ns proton pulse, while the $\bar\nu_\mu$, ν_e contribution increases much slower.
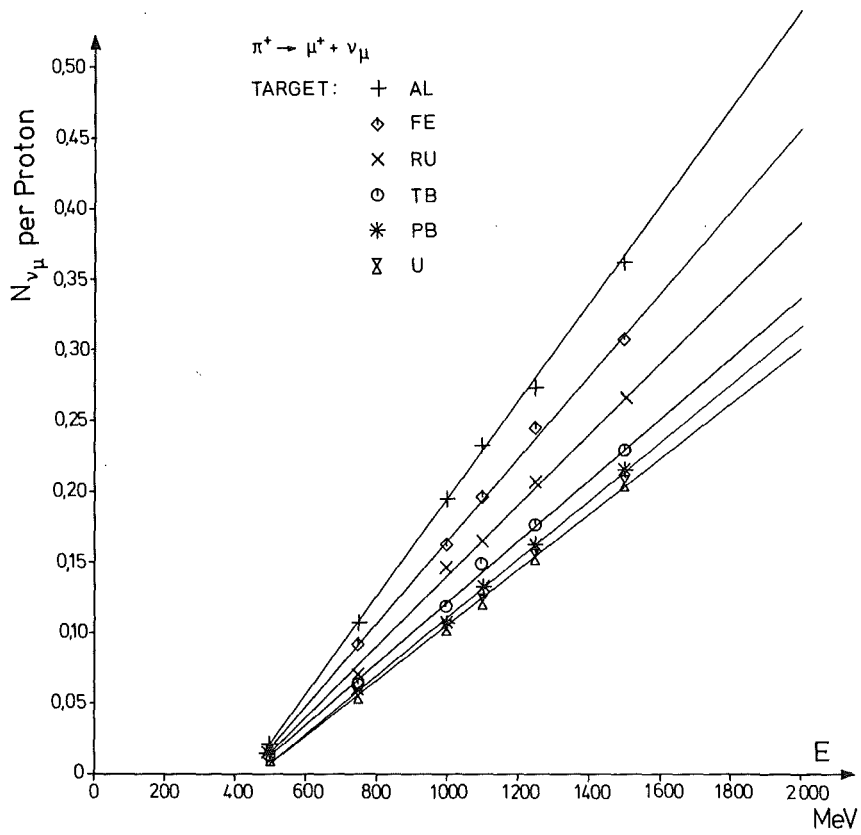
Fig. 1   The number of ν_μ produced per proton as a function of proton energy and target material
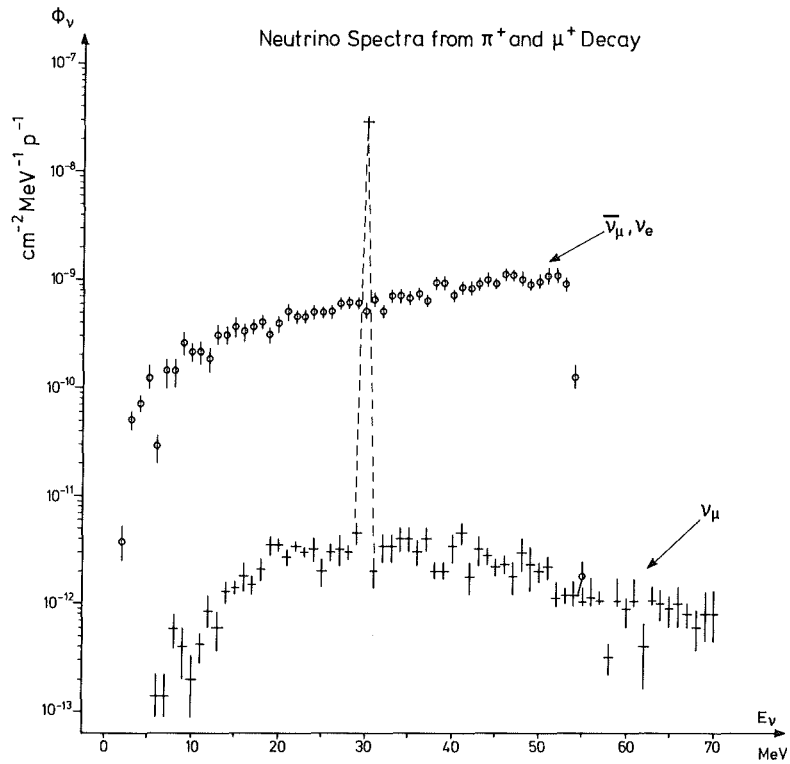
Fig. 2   Energy dependent neutrino flux at 6 m for 1.1 GeV protons incident on a Pb target
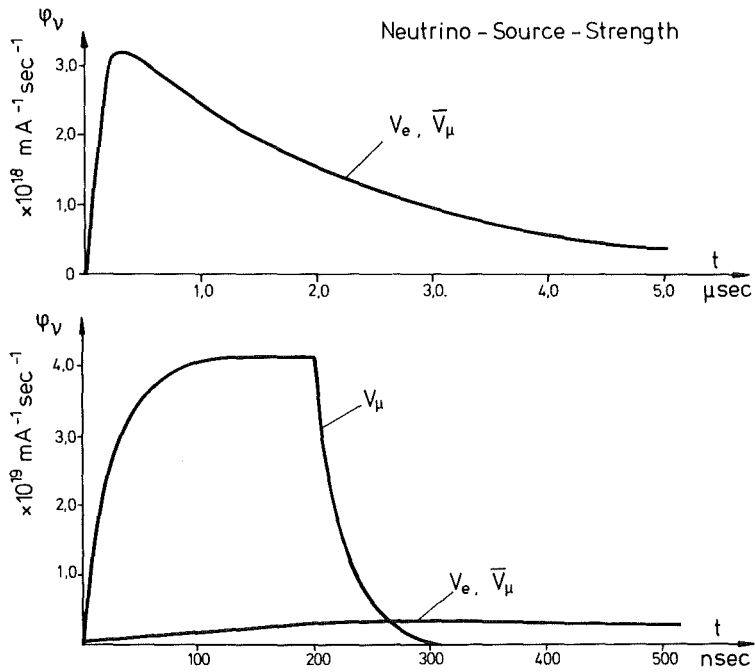
Fig. 3   Time dependence of the neutrino source strength at the
spallation neutron source (t_p = 200 ns, $\bar{I}_p$ = 1 mA, f = 100 Hz)
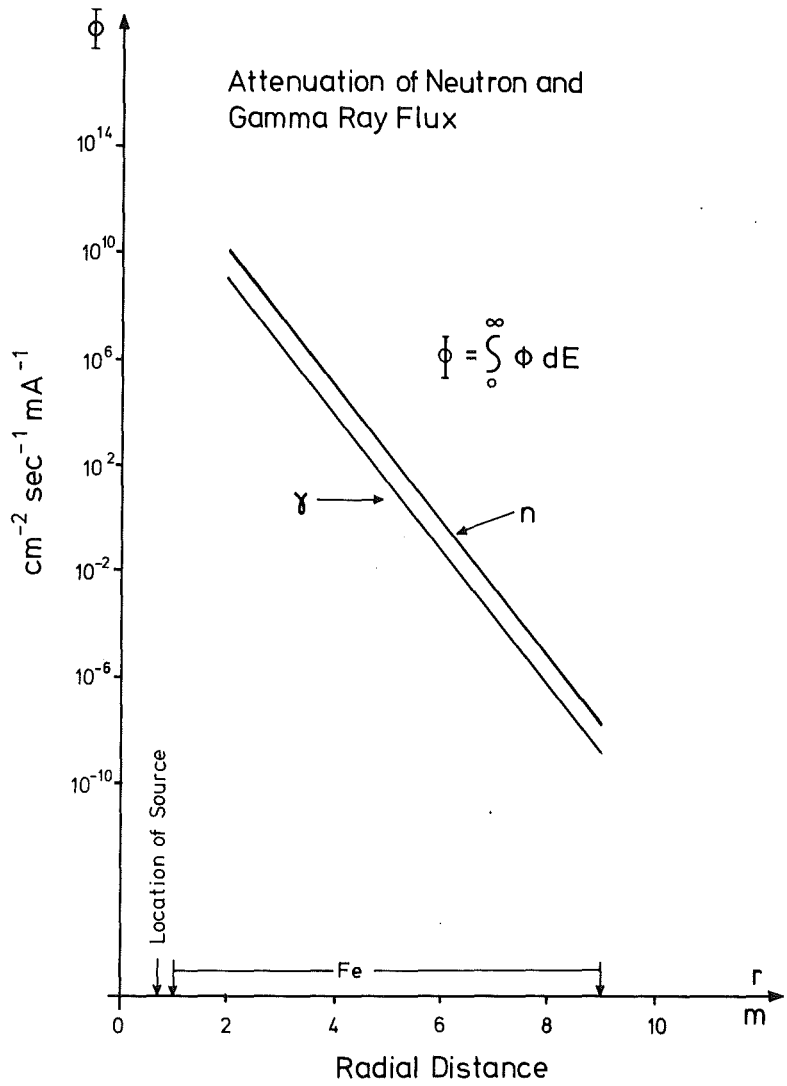
Fig. 4   Attenuation of the neutron and gamma-ray flux as a function
of the iron shield thickness
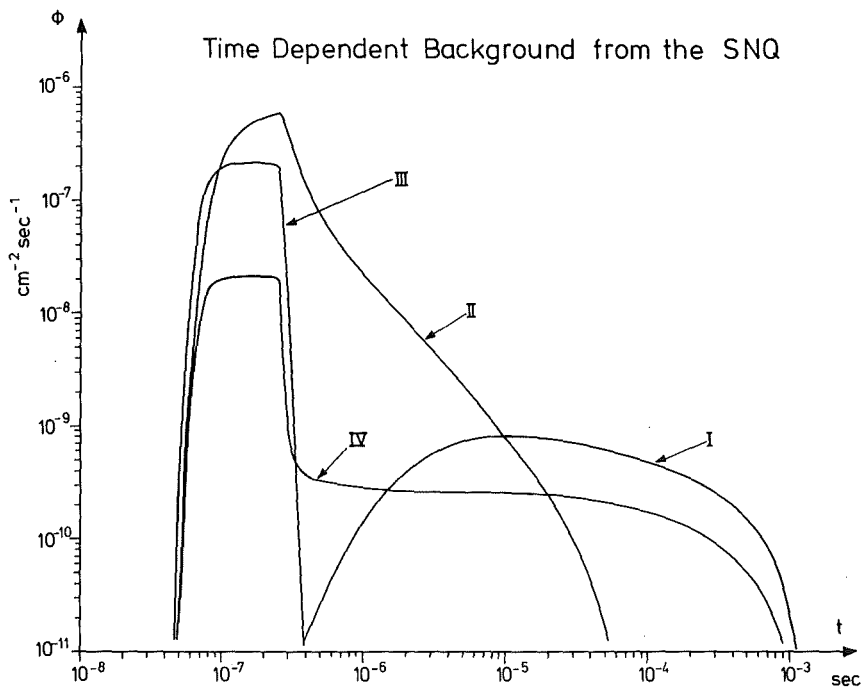
Fig. 5   Time dependence of the neutron and gamma-ray flux at a distance
          of 12 m from the spallation source
          I: thermal neutrons
          II: low energy neutrons; 0.4 eV $< E_n < 1$ MeV
          III: fast neutrons, $E_n > 1$ MeV
          IV: gamma rays

The neutron and gamma-ray background from the spallation source was calculated by radiation transport codes, which use the method of discrete ordinates (3). The attenuation of the energy integrated neutron and gamma ray flux is presented in Fig. 4 as a function of the thickness of the source shielding. The curves show the expected exponential behaviour. In the case of a shield thickness of 8 m of iron the neutron and gamma ray flux will be suppressed by about 18 orders of magnitude. This will be sufficient to reduce the background event rate in a neutrino detector to a negligible level. Fig. 5 shows the time dependence of this background from the spallation source assuming the same parameters as in Fig. 3 for a shielding of 8 m of iron. Details of the calculations of the neutrino fluxes and background contributions are described in Ref. 1.

References

(1)   Neutrino-Physics at the Spallation Source II Neutrino Fluxes, Shielding Considerations and Detector Analysis, KfK-Report 3174, June 1981, T.A. Gabriel, R.A. Lillie, B.L. Bishop, J. Wilczynski, and B. Zeitnitz.

(2)   CALOR: A Monte Carlo Program Package for the Design and Analysis of Calorimeter Systems , ORNL-TM-5619 (April, 1977), T.A. Gabriel et al.

(3)   A Users Manual for ANSIN, A One Dimensional Discrete Ordinates Transport Code with Anisotropic Scattering, K-1693, W.W. Engle. Time Dependent Neutron and Photon Transport Calculations Using the Method of Discrete Ordinates, ORNL-4662, S.A. Dupree et al.
The DOT III Two-Dimensional Discrete Ordinates Transport-Codes ORNL-TM-4280 (September 1973), W.A. Rhoades and F.R. Mynatt.

2.2.2   Neutrino Physics at the Spallation Neutron Source
         B. Zeitnitz
         Kernforschungszentrum Karlsruhe, IK1

As part of the feasibility study for a high intense spallation neutron source SNQ ref. (1) the advantages of the intense proton beam for parallel use in neutrino physics were discussed. The computations required in this context were carried out as a collaboration of the KfK
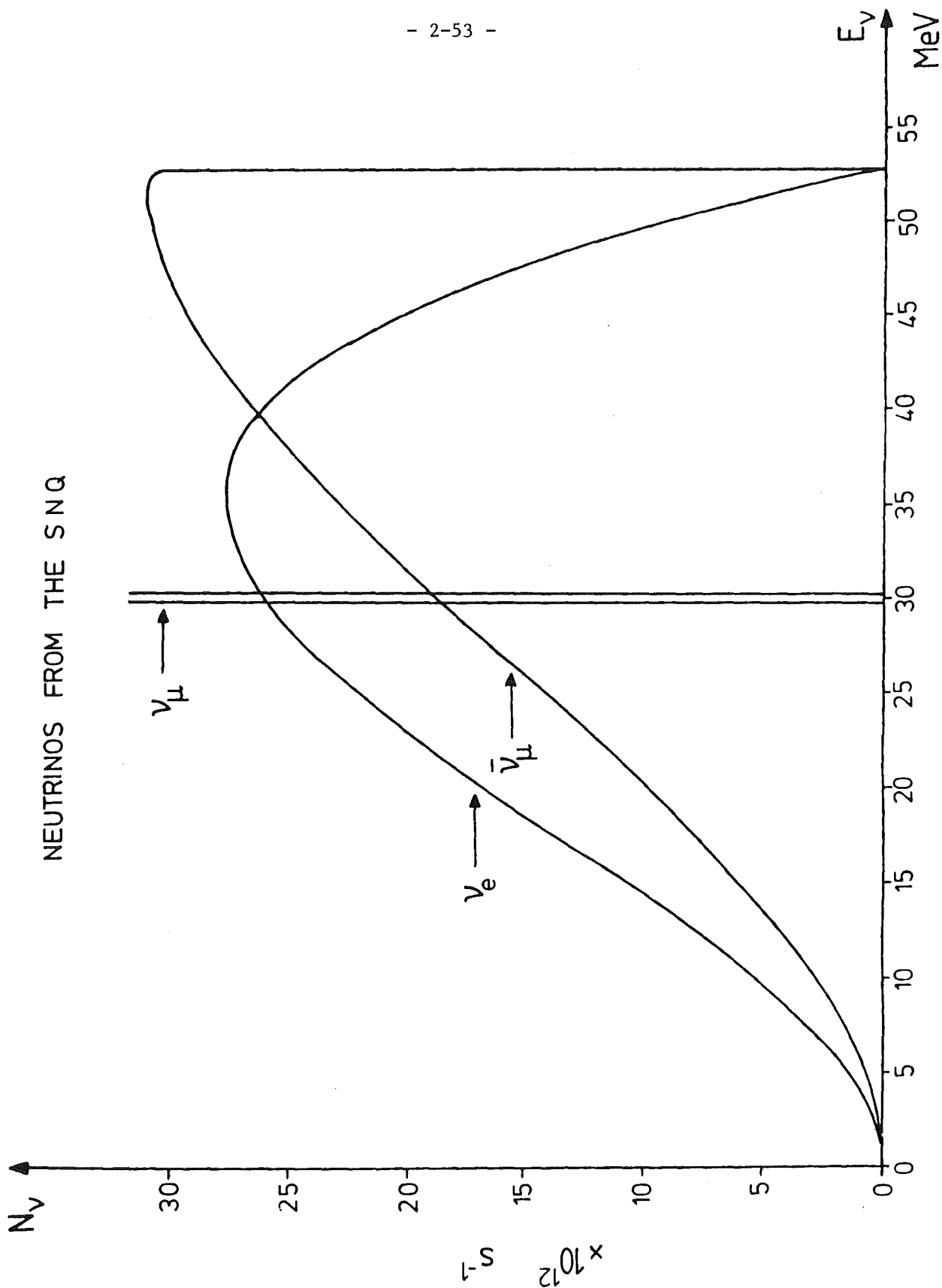
Fig. 1: Energy distributions of the neutrinos generated at the SNQ spallation neutron source (beamstop). The total numbers of all three kinds of neutrino are equal. The indicated source strengths apply to 1 mA averaged proton current for E_p = 1100 MeV

and the Oak Ridge National Laboratory by T.A. Gabriel (ORNL) and J. Wilczynski (KfK). The results were published in detail in ref. (2) and (3).

The protons do not only give rise to the production of neutrons in the spallation target. At the same time a considerable number of pions π^+ is produced which emit neutrinos while decaying. At the proton energy proposed for the SNQ ($E_{p_+} = 1100$ MeV) and lead as the target material the number of π^+ per proton is $N_{\pi^+}/N_{p} = 0.133$.

The pions are stopped within 10^{-10} s still in the target zone so that only a small fraction of about 5×10^{-3} decay while on flight. Whilst the negative pions, when at rest, are captured by nuclei and finally absorbed, the positive pions, with a lifetime $\tau_\pi = 26$ ns, decay into a positive muon and a muon neutrino. This means that practically only the positive pions and the positive muons play a role at the SNQ spallation neutron source. The muon with a lifetime $\tau = 2.2$ μs subsequently decays into a positron and (because of conservation of the lepton and muon numbers) into an electron neutrino and a muon antineutrino. Thus we have

$$\pi^+ \rightarrow \mu^+ + \nu_\mu \qquad\qquad \tau = 26.03 \times 10^{-9} \text{ s} \qquad (1)$$
$$\mu^+ \rightarrow e^+ + \nu_e + \bar{\nu}_\mu \qquad\qquad \tau = 2.197 \times 10^{-6} \text{ s} \qquad (2)$$

Since the pion at rest decays into two particles, the muon neutrinos from (1) have a constant energy of $E_\nu = 29.79$ MeV. By contrast, continuous distributions with an end μ energy of 52.83 MeV are obtained for the neutrinos produced by the three-particle decay (2). Fig. 1 shows the respective energy distributions.

Since the decays take place with the particles at rest, the intensities of all three kinds of neutrino are equal and isotropic in space. The source strengths given in Fig. 1 were calculated for an averaged proton current $\bar{I}_p = 1$ mA. For each kind of neutrino and the desired parameters of the spallation neutron source $E_p = 1100$ MeV and $\bar{I}_p = 5$ mA an averaged source strength is obtained of

$$\bar{Q}_\nu = 3 \times 4.1 \times 10^{15} \text{ /s}.$$

This means that the facility would be the most powerful source for the

three kinds of neutrino, ν_μ, ν_e, $\bar{\nu}_\mu$. However, in future experiments involving neutrinos not only the average flux but likewise a suitable time structure and the highest possible peak flux will play a role. With typical values of a proton-pulse-length of t_p = 200 nsec and frequency of f = 100 Hz one would obtain a peak source strength of μ-neutrinos of the order of $Q_\nu \sim 10^{20}$ s^{-1}. This would allow a new quality of low energy neutrino physics.

Typical counting rates, discrimination against cosmic and source background etc. is discussed in ref. (2) and (3), see also page 2-46. A list of interesting types of experiments which could be performed at this type of intense source is given in the following:

Experiments with Beam Stop Neutrinos

1. Test of conservation laws
   a) Lepton number, Myon number, e.g., additive or multiplicative?
   b) Neutrino oscillations
2. Neutrino-Electron Interactions
   Elastic scattering: ν_μ + e, ν_e + e, $\bar{\nu}_e$ + e
3. Neutrino-Hadron Interactions,
   inelastic scattering from nucleons,
   deuterons and light nuclei
4. Detection of exotic particles like axions.)

References
(1) Realisierungsstudie zur Spallations-Neutronenquelle, KfK-Report 3175.
(2) Neutrino-Physics at the Spallation Neutron Source I, KfK-Report 3155, March 1981, B. Zeitnitz.
(3) Neutrino-Physics at the Spallation Neutron Source II Neutrino Fluxes, Shielding Considerations and Detector Analysis, KfK-Report 3174, June 1981, T.A. Gabriel, R.A. Lillie, B.L. Bishop, J. Wilczynski, and B. Zeitnitz.

2.3   NUCLEAR REACTIONS AND NUCLEAR SPECTROSCOPY

2.3.1   The Dependence on Energy and Mass Number of the Alpha-Particle
        Optical Potential: A Support for the Folding Model Approach*
        E. Friedman[+], H.J. Gils, H. Rebel, and R. Pesl
        Kernforschungszentrum Karlsruhe, IAK II
        [+]The Racah Institute of Physics, The Hebrew University
        of Jerusalem, Israel
        *Nucl Phys. A363 (1981) 137.

    Data for elastic scattering of alpha particles by ^{40,42,44,48}Ca, ^{50}Ti, ^{52}Cr and ^{90}Zr at 104 MeV, by ^{40}Ca, ^{46,48,50}Ti, ^{58}Ni, ^{90}Zr and ^{208}Pb at 140 MeV and by ^{58,60,62,64}Ni at 173 MeV were analyzed using a Fourier-Bessel description of the optical potential. All data extend to large angles thus allowing unique determination of volume integrals and rms radii of the potentials. The variations with mass number and energy of these quantities are investigated and conclusions are drawn about studies of nuclear radii with the help of optical potentials.

2.3.2   104 MeV Alpha-Particle Scattering from ^{90,92}Zr
        V. Corcalciuc[+], H.J. Gils, H. Rebel, J. Buschmann,
        R. Pesl, R. Dumitrescu[+], S. Zagromski, and K. Feißt
        Kernforschungszentrum Karlsruhe, IAK II
        [+]Institute of Physics and Nuclear Engineering, Bucharest, Romania

    Recent investigations of the elastic alpha-particle scattering optical potential have shown that the overall radial shape of the real part is significantly better represented by a squared Saxon-Woods form rather than by the standard Saxon-Woods parametrization. Is this result also valid for the extended optical potential which provides the coupling to excited states? What are the implications when extracting isoscalar transition rates from alpha-particle scattering? In addressing these questions differential cross sections for the elastic and inelastic scattering of 104 MeV alpha particles from ^{90,92}Zr have been measured.
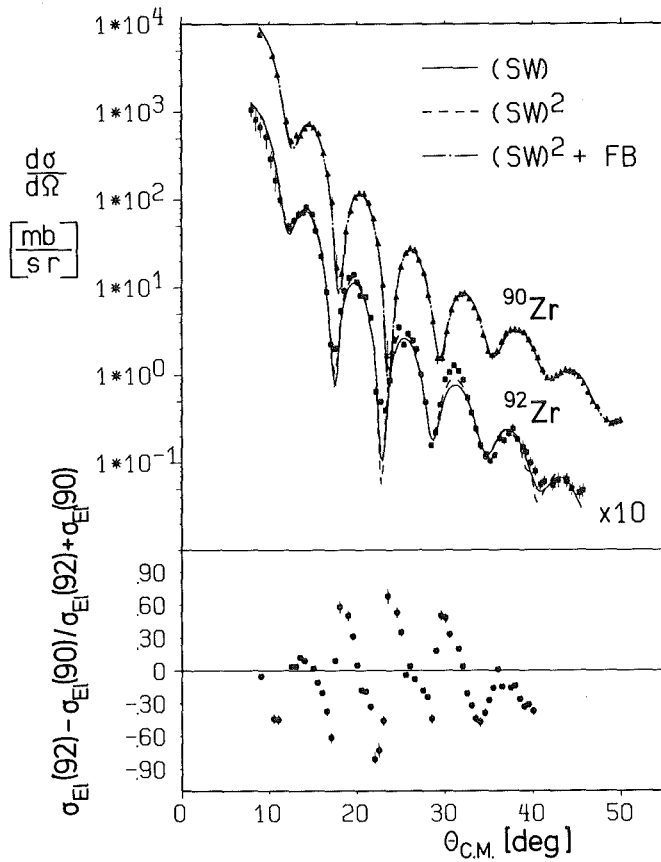
Fig. 1   Elastic scattering of 104 MeV Alpha Particles from ^{90,92}Zr :
          Optical model analysis with different radial shapes of
          the real potential (large angle data for ^{90}Zr$(\alpha,\alpha)^{90}$Zr indicating
          nuclear rainbow scattering are not shown).

First, the elastic scattering has been considered with the aspect of
small isotopic differences (see Fig. 1). For the case of ^{90}Zr where the
experimental cross sections extend beyond the nuclear rainbow angle
a "model-independent" procedure (Fourier-Bessel method) could be applied in
the optical model analysis. The resulting real potential (and its error

band representing realistic uncertainties) is displayed in Fig. 2 and
compared with the best-fit Saxon-Woods square form. With inclusion of the
inelastic scattering cross sections the experimental data are analyzed
in terms of coupled channels on the basis of a flexible anharmonic vi-
brator model and using different parametrizations of the radial shape
of the deformed optical potentials. The results favour the squared Saxon-
Woods type for the real part. Additionally a semi-microscopic folding model
has been invoked for extracting isoscalar quadrupole and hexadecapole
transition rates.
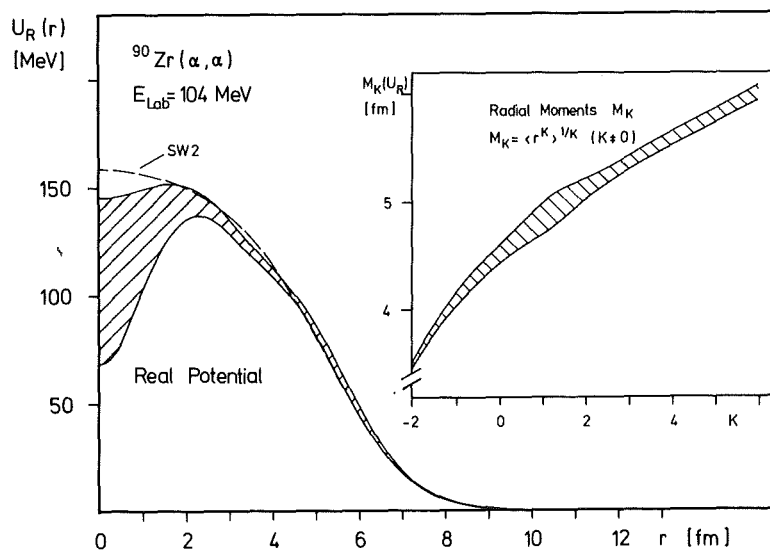
Fig. 2   Real part of the optical potential and its radial moments
for $^{90}Zr(\alpha,\alpha)^{90}Zr$ at E_{α} = 104 MeV.

2.3.3   Improved Phenomenological Effective Interactions for Folding
Model Analyses of Alpha-Particle Scattering

E. Friedman[+] and H.J. Gils

Kernforschungszentrum Karlsruhe, IAK II

[+]The Racah Institute of Physics, The Hebrew University of
Jerusalem, Israel

Density dependent folding model analyses of elastic alpha-particle

scattering at $E_\alpha \sim 100$ MeV provide interesting informations on the shape and size of neutron or total nuclear matter density distributions (1). However, with the widely used Gaussian effective interaction the representation of the experimental cross sections is still not of the same quality as obtained by a pure potential analysis using refined parametrizations of the potential like the squared Saxon-Woods form (SW^2). Moreover, the integral quantities of the folded potentials like the specific volume integral $J_v/4A$ and the root mean square (rms) radii considerably deviate from the phenomenological results (1,2). Also the errors of the extracted nucleon densities suffer from this insufficient simple two-parameter interaction. Therefore, it seems reasonable to search for improved parametrizations of the effective nucleon-alpha particle interaction.

We investigated different interaction forms like a Yukawa shape, sum of two Gaussians or Yukawas with different range, respectively. The sum of a Gaussian (which is very similar to the one previously used (1)) and a Yukawa shape (G+Y) with a long tail was found to describe best the elastic alpha-particle scattering from ^{40}Ca at two different
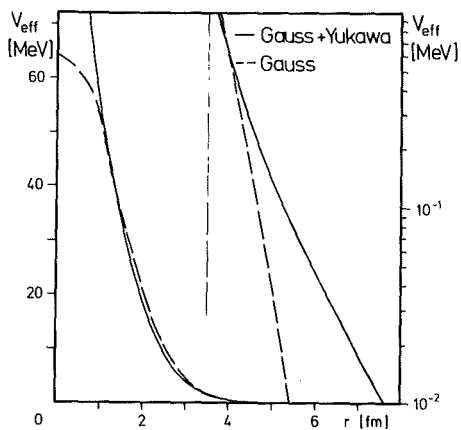
Fig. 1
Effective nucleon-alpha particle interaction with Gaussian plus Yukawa shape (solid line) in comparison to the previously used Gaussian interaction (dashed line).

E	SW^2 $-J_v/4A$	$\langle r_v^2\rangle^{1/2}$	χ^2/F	Potential $-J_v/4A$	FB $\langle r_v^2\rangle^{1/2}$	χ^2/F
(MeV)	(MeV fm^3)	(fm)		(MeV fm^3)	(fm)	
104	317.9	4.315	3.7	327 ± 2	4.37±0.06	2.0
140	313.3	4.365	1.8	322 ± 3	4.41±0.06	0.8

	Gauss			Folding	Gauss and Yukawa	
104	305.8	4.245	4.9	317.9	4.397	3.6
140	303.0	4.323	2.1	310.0	4.407	1.0

Table 1 Comparison of potential analyses and density dependent folding model analyses of elastic alpha particle scattering from ^{40}Ca at E_α = 104 and E_α = 141 MeV

energies E_α = 104 MeV and 141 MeV. Table 1 demonstrates that the density dependent folding model using this interaction yields even slightly better results than a potential analysis with SW^2 potentials. The integral quantities of the folding potentials closely approach the corresponding values of the "model independent" potential analysis by use of the Fourier-Bessel method (2,3). The shape of the interaction is compared to the previous Gaussian shape in Fig. 1. The considerably larger strength at small radii is of little influence on the folded potential for all radial regions (4) whereas the longer tail mainly yields also a longer tail in the potential.

References
(1) H.J. Gils, E. Friedman, H. Rebel, and Z. Majka, Phys. Rev. C21 (1980) 1245.
(2) H.J. Gils, E. Friedman, H. Rebel, J. Buschmann, S. Zagromski, H. Klewe-Nebenius, B. Neumann, R. Pesl, and G. Bechtold, Phys. Rev. C21 (1980) 1239.
(3) E. Friedman, H.J. Gils, H. Rebel, and R. Pesl, Nucl. Phys. A 363 (1981) 137; KfK-Report 3038 (1980).
(4) H.J. Gils, unpublished results.

2.3.4 Radial Sensitivity of Hadronic Probes and How Accurately are Nuclear Radii Determined

H.J. Gils, E. Friedman[+], and H. Rebel
Kernforschungszentrum Karlsruhe, IAK II
[+]The Racah Institute of Physics, The Hebrew University of Jerusalem, Israel

The radial distribution of nucleons in nuclei is a topic of

current interest as it provides a sensitive test of theories of nuclear structure. Hadronic probes have been shown to be quite useful in providing at least partial answers to the question of *neutron* densities, in particular by comparative studies when the "apparatus function" (effective probe-nucleus interaction) could be "calibrated" on a nucleus with a presumably known neutron distribution. The results of various types of experiments such as elastic scattering of alpha particles, of protons or pions etc. (1), although showing internal consistency, sometimes seem to be in conflict with each other. Apart from model assumptions and residual uncertainties such discrepancies could originate from differences in the radial sensitivity of different types of experiments. It is, therefore, interesting to investigate which parts of the nucleus are well probed, and how uncertainties of the radial moments are affected by the radial sensitivity. A critical comparison of the methods of evaluating the uncertainties in the different analysis is also important.

In order to study the radial sensitivity of different types of experiments on equal footing we applied the notch test method by introducing a local perturbation ("notch") into the neutron distribution of the ^{48}Ca nucleus. We considered four different experiments: the elastic scattering of alpha particles at 104 MeV, the elastic scattering of protons in the GeV region (3), the elastic scattering of 130 MeV pions (4), and strong interaction level shifts and widths in pionic atoms (5).

In the analyses the "notch" was set at different radial positions of the neutron distribution. The reproduction of the experimental data characterized by the χ^2-value per degree of freedom depending on the radial position of the notch is then the quantity measuring the radial sensitivity. Further details of the procedures may be found in Ref. (6). Examples of the resulting notch test curves are given in Fig. 1.

Although the notch test method is rather crude compared to "model independent" analyses (2) (which cannot directly be applied to all these experiments as discussed in Ref. (6)) the final results reveal some interesting details of the radial sensitivity of the different hadronic probes:

(i) All investigated probes are mainly sensitive to the slope of the
     densities between r=2 fm and 6 fm.

(ii) None of the probes is sensitive to the innermost part (r < 1 fm)
     of the nucleus.

(iii) Different radial sensitivity can only play a minor role for the discrepancies between densities resulting from different experiments. Underestimations of errors and model deficiencies seem to be more likely the reasons for that.
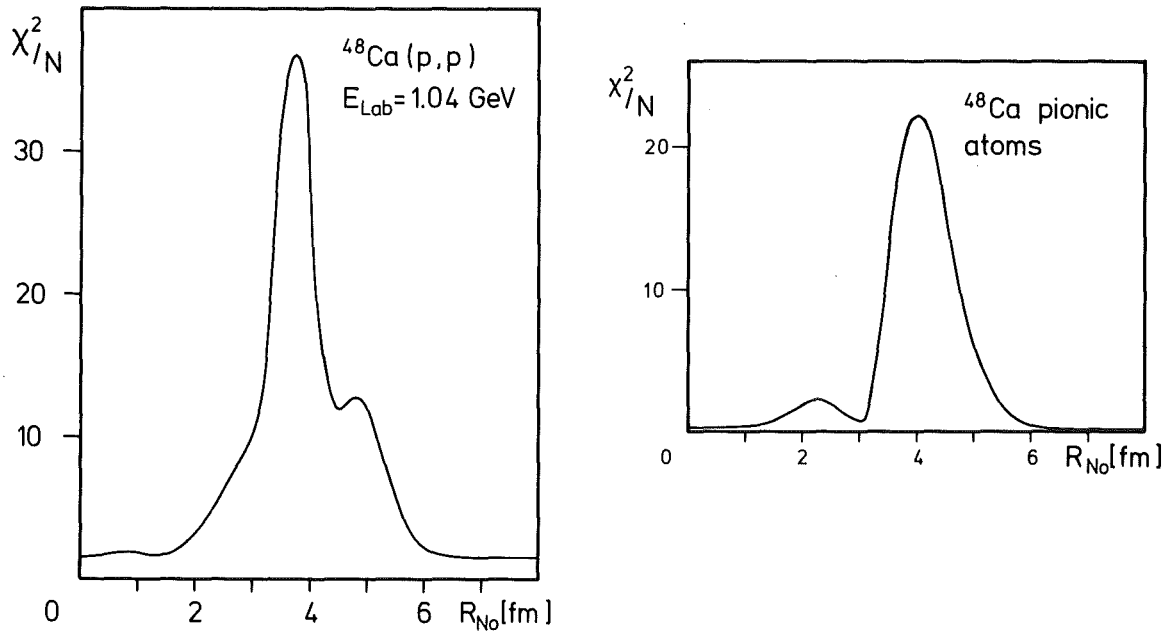
Fig. 1 χ^2 per point (a) for the elastic scattering of 1 GeV protons by ^{48}Ca, (b) for the shifts and width of the 2p level in pionic atoms of ^{48}Ca calculated as a function of the position of a 30 % notch in the neutron density.

References

(1)   H. Rebel, H.J. Gils, and G. Schatz (eds.),KfK-Report 2830 (1979).

(2)   H.J. Gils, E. Friedman, H. Rebel, J. Buschmann, S. Zagromski, H. Klewe-Nebenius, B. Neumann, R. Pesl, and G. Bechtold, Phys. Rev. C21 (1980) 1239.

(3)   G. Bruge, ed., unpublished report (Saclay 1978).

(4) J.P. Egger, R. Corfu, P. Gretillat, C. Lunke, J. Piffaretti,
     E. Schwarz, C. Perrin, J. Jansen, and B.M. Preedom, Phys. Rev.
     Lett. 39(1977) 1608.

(5) R.J. Powers, K.-C. Wang, M.V. Hoehn, E.B. Shera, H.D. Wohlfahrt,
     and A.R. Kunselman, Nucl. Phys. A336 (1980) 375.

(6) H.J. Gils, E. Friedman, and H. Rebel, KfK-Report 3039 (1980).

2.3.5   Combined Analysis of Pionic Atoms and Elastic Alpha-Particle Scattering

H.J. Gils and E. Friedman[+]

Kernforschungszentrum Karlsruhe, IAK II

[+]The Racah Institute of Physics, The Hebrew University of Jerusalem, Israel

Different types of experiments involving strongly interacting
particles have been used to gain information on nucleon density
distributions in nuclei (1). In most cases the experimental data
are analyzed with an effective ("optical") probe-nucleus potential,
which is related to the nucleon densities either phenomenologically
or in a more fundamental way. The results of such analyses may depend
on the models used. It is also possible that in different experiments
different parts of the nuclear density distributions are probed.
Therefore, it is interesting to perform simultaneous or combined
analyses of different experiments. Some of the model dependence
could be expected to be removed thereby and a combined analysis
could also reveal information which is inaccessible otherwise.

Experiments on elastic scattering of protons and alpha particles
are currently being analyzed (2,3) with "model independent" methods
where the traditional functions used for the nuclear densities
or the potentials are replaced by more bias free forms like Fourier-
Bessel series (FB) or sums of Gaussian functions (SOG). However,
this is not always possible. Measurements of strong interaction
level shifts and widths in pionic atoms provide only two experimental
numbers for each nucleus. Hence it is impossible to fit
parameters of a FB series. This limitation can be overcome by performing
a combined analysis of two different experiments. This was done
for elastic scattering of 100 - 140 MeV alpha particles and pionic
atoms in the calcium region.

Table 1   rms radii of neutron distributions of Ca nuclei from different procedures.

Procedure	^{42}Ca	^{44}Ca	^{48}Ca
Pionic atoms only	3.49 $\pm$ 0.03	3.50 $\pm$ 0.03	3.56 $\pm$ 0.03
Alpha scattering only	3.42 $\pm$ 0.17	3.54 $\pm$ 0.15	3.71 $\pm$ 0.20
Combined	3.44 $\pm$ 0.10	3.50 $\pm$ 0.08	3.69 $\pm$ 0.10

The strong interaction level shifts and width for the 2p level in pionic atoms of $^{40,42,44,48}Ca$ (4,5) and also the elastic alpha particle scattering cross sections (6,7) were taken from different groups for consistency checks. The procedure is essentially based on χ^2 fits used in the analysis of elastic alpha-particle scattering where the contribution due to the two experimental results from the pionic atoms is simply added to the χ^2 of the alpha particles to form the total χ^2. This total χ^2 is then minimized by varying the parameters of the neutron density ρ_n which was described by a FB series (8). Further details of the specific analyses of each experiment is described elsewhere (8,9).

In Table 1 the resulting rms radii of the neutron densities from pionic atoms only, alpha-particle scattering only and from the combined analyses are compared. The coupling of two problems is clearly demonstrated but what is more interesting is the reduction of the uncertainties compared to those from alpha-particle scattering only. Moreover, some unphysical structure occuring sometimes in analyses of alpha particles only - particularly in the nuclear interior - are strongly suppressed.

In conclusion, it is demonstrated that it is possible to combine in χ^2 fits different experimental methods and thereby gaining the informations extracted from separate analyses.

References

(1)   H. Rebel, H.J. Gils, and G. Schatz (eds.),   KfK-Report 2830 (1979).

(2)   L. Ray, Nucl. Phys. A335 (1980) 443.

(3)   E. Friedman and C.J. Batty, Phys. Rev. C17 (1978) 34.

(4) C.J. Batty, S.F. Biagi, E. Friedman, S.D. Hoath, J.D. Davies,
G.J. Pyle, G.T.A. Squier, D.M. Asbury, and A. Guberman,
Nucl. Phys. A322 (1979) 445.

(5) R.J. Powers, K.-C. Wang, M.V. Hoehn, E.B. Shera, H.D. Wohlfahrt,
and A.R. Kunselman, Nucl. Phys. A336 (1980) 475.

(6) H.J. Gils, E. Friedman, H. Rebel, J. Buschmann, S. Zagromski,
H. Klewe-Nebenius, B. Neumann, R. Pesl, and G. Bechtold,
Phys. Rev. C21 (1980) 1239.

(7) D.A. Goldberg, S.M. Smith, and G.F. Burdzik, Phys. Rev. C10
(1974) 1362.

(8) H.J. Gils, E. Friedman, Z. Majka, and H. Rebel, Phys. Rev. C21
(1980) 1245.

(9) E. Friedman and A. Gal, Nucl. Phys. A345 (1980) 457.

2.3.6 Method for Analysis of Inelastic Alpha-Particle Scattering*

H. Rebel, R. Pesl, H.J. Gils, and E. Friedman[+]

Kernforschungszentrum Karlsruhe, IAK II

[+]The Racah Institute of Physics, The Hebrew University of Jerusalem, Israel

*KfK -Report 3104 and Nucl. Phys. A 368 (1981) 61

The analysis of inelastic scattering of strongly interacting
particles from nuclei suffers from the model dependence introduced when
specifying the form factors (coupling potentials) e.g. in the frame work
of a vibrational model. Moreover, the relation between strength and
shape of the coupling potentials and corresponding quantities of the
transition densities is not well established, and the interpretation in
terms of transition rates and nuclear moments introduces additional
uncertainties. In the present studies of inelastic scattering of
104 MeV alpha particles from ^{50}Ti and ^{52}Cr we remove the constraints
due to pre-chosen forms of the coupling potentials by applying the
Fourier-Bessel method which is more flexible. It allows quite general
shapes and provides realistic estimates of the uncertainties of the
potentials and derived quantities (moments). Using the identities
between the integral moments of a folded potential distribution and of the
underlying nuclear matter distribution isoscalar transition rates have been
derived.

2.3.7   <u>Elastic Scattering of 156 MeV ^{6}Li Ions and the Optical Model</u>

J. Cook[+], H.J. Gils, H. Rebel, J. Buschmann, B. Neumann[++],

H. Klewe-Nebenius[++], and S. Zagromski

Kernforschungszentrum Karlsruhe, IAK II

[+] Wheatstone Laboratory, King's College, London, England

[++]Kernforschungszentrum Karlsruhe, IRCh

The differential cross sections for elastic scattering of 156 MeV ^{6}Li ions from ^{12}C, ^{90}Zr, ^{40}Ca and ^{208}Pb have been measured with good angular resolution. 156 MeV is the highest energy at which ^{6}Li data are currently available, and it has been observed that for light targets (^{12}C) rainbow scattering exists. This feature which is rather well understood in alpha particle scattering, suggests that there might be an increased sensitivity of elastic ^{6}Li scattering to the optical potential. This led us to investigate how sensitive the scattering is to different (phenomenological and semi-microscopic) potential forms and how well these potentials are determined. In addition to Saxon-Woods and Saxon-Woods squared forms, the more flexible Fourier-Bessel potential has been considered in the case of ^{12}C(^{6}Li,^{6}Li)^{12}C. Furthermore, we studied a double folding model (1) in which an effective nucleon-nucleon interaction is folded over the densities of both the projectile and target nuclei. For the nucleon-nucleon interaction the Bertsch M3Y interaction (2) has been chosen which has been widely applied for both light and heavy ions.
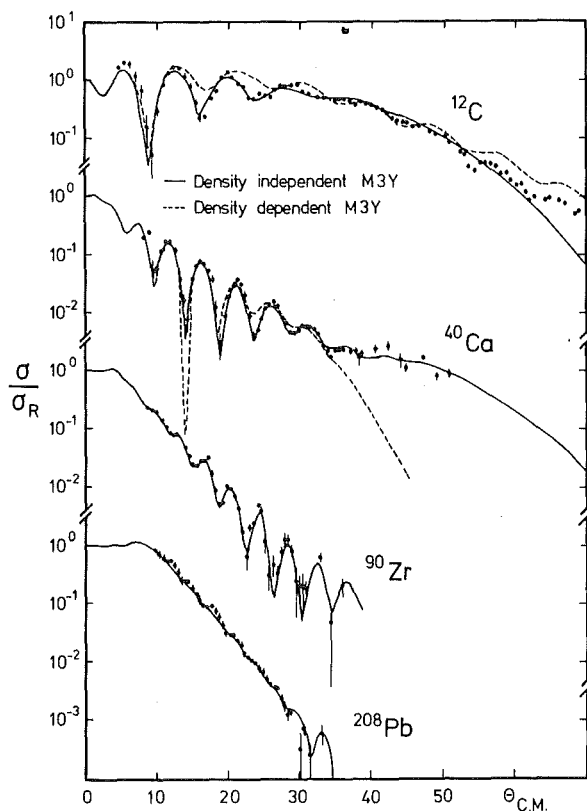
Fig. 1
Optical model description of 156 MeV ^{6}Li elastic scattering using folded real potentials and Saxon-Woods imaginary potentials. The full and dashed lines (for ^{12}C and ^{40}Ca only) compare results of calculations using density independent and density dependent versions of the M3Y interaction.

It turns out that the folded potentials must be multiplied by a normalization factor $N \cong 0.6$-0.7: a confirmation of a previously found (1) "anomaly" in scattering of loosely bound particles. The density dependent version of the M3Y interaction (2) seems to be not adequate and describes the data less satisfactorily.

References

(1) G.R. Satchler and W.G. Love, Phys. Rep. 55 (1979) 183.
(2) G. Bertsch, J. Borysowicz, H. McManus, and W.G. Love,
     Nucl. Phys. A 284 (1977) 399.

2.3.8   Description of Continuous Particle Spectra from
         ^{6}Li-Induced Nuclear Reactions by a DWBA Break-Up Model

B. Neumann[+], H. Rebel, H.J. Gils, R. Shyam[++],
R. Planeta, and H. Machner[+++]

Kernforschungszentrum Karlsruhe, IAK II

[+]Kernforschungszentrum Karlsruhe, IRCh

[++]Daresbury Laboratory, Warrington, United Kingdom

[+++]Institut für Kernphysik, Kernforschungsanlage Jülich

The measured energy spectra of light ejectiles after bombarding various targets with 156 MeV ^{6}Li ions are dominated by very broad bumps in forward direction, with maxima at energies roughly corresponding to the beam velocity. These bumps have been shown to originate from the projectile break-up. For a first survey the Serber model has been proven very useful for understanding the basic mechanism of the break-up phenomena. Within this model based on a quasi-free reaction mechanism the differential cross sections for the observed break-up fragments are mainly determined by the Fourier-transform of the wave function of relative cluster motion. Using a plane-wave approximation (PWA) this model describes fairly well the shapes of the break-up component of the spectra and the extracted widths of the intrinsic momentum distributions are in good agreement with results from quasi elastic knock-out reactions. PWA, however, fails in describing the angular distributions and absolute values of the cross sections. In addition to very simplified assumptions on the basic mechanism both the distortion of the incoming and outgoing waves by nuclear and Coulomb field and the absorption are neglected.

Baur et al. (1) have developed a break-up theory in the framework of the DWBA taking elastic and inelastic reactions into account. Using this theory we have calculated double differential cross sections of the break-up particles (in particular for alpha particles) from bombardment of ^{40}Ca by 156 MeV ^{6}Li ions. In order to separate the preequilibrium background from the measured results the coalescence model is invoked where complex particles are assumed to condensate from the excited nucleons during the preequilibrium cascade if they are within a momentum sphere of a certain coalescence radius. The value of this coalescence radius has been determined (r_o = 285 MeV/c) by matching the high energy tail of the experimental spectra measured at large emission angles (where the break-up component appears to be negligible). The coalescence model results are combined with the break-up model results in order to fit the measured spectra (see Fig. 1). The required normalization for the DWBA break-up cross
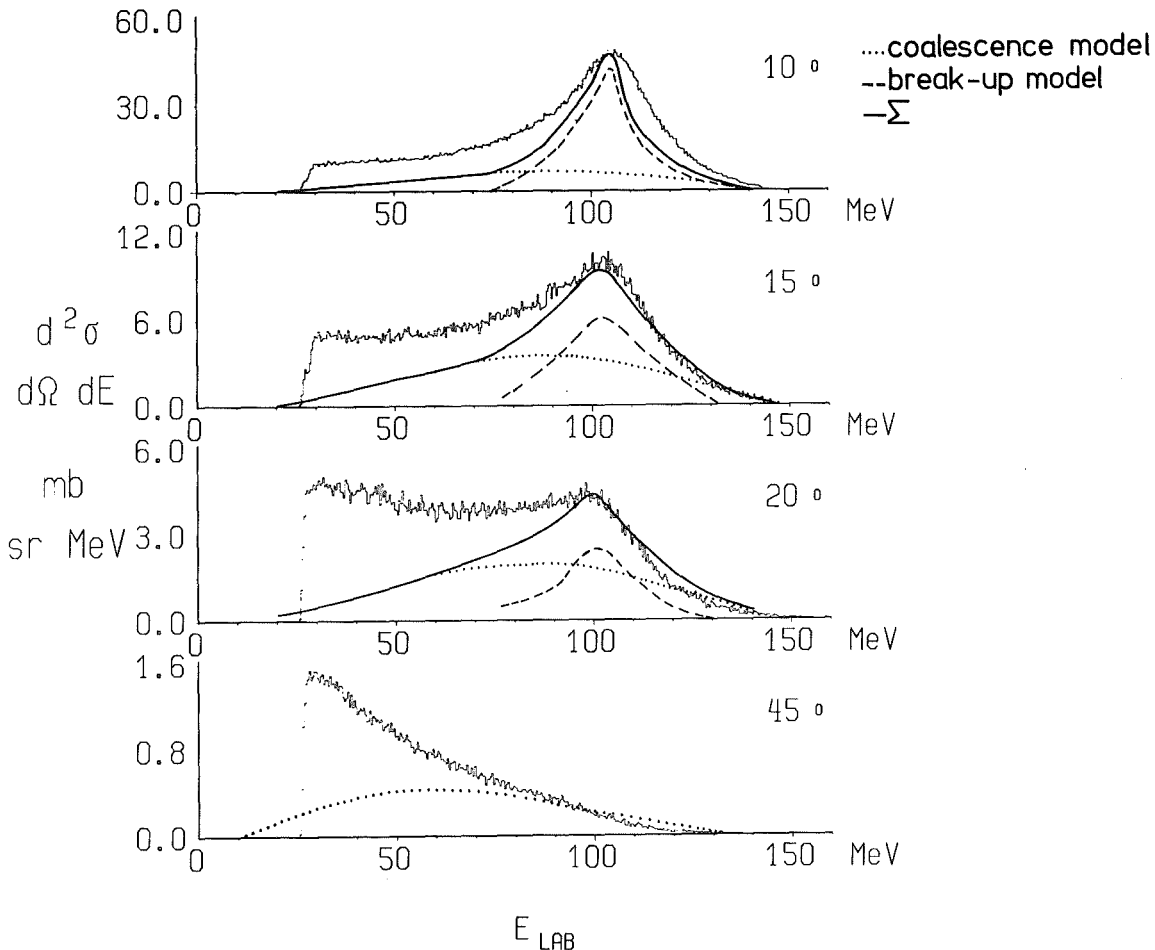
Fig. 1   Break-up model and coalescence model results compared with the measured alpha-particle spectra from bombarding ^{40}Ca by 156 MeV ^{6}Li ions.

sections agrees within 10 % with the value (of the zero-range normalization constant) derived by an independent calculation.

Reference

(1) G. Baur, F. Rösel, D. Trautman, and R. Shyam,
    Proceed. Symp. "Deep-Inelastic and Fusion Reactions with
    Heavy Ions", Berlin, Oct. 23-25, 1973, Lecture Notes
    in Physics, Springer-Verlag 1980, p. 268.

2.3.9   Mass Distribution of Residual Nuclei in the Reaction ^{6}Li+^{40}Ca at E_{Li} = 156 MeV

L. Freindl[+], K. Grotowski[+], Z. Majka[+], S. Micek[+],

R. Planeta , J. Buschmann, H. Klewe-Nebenius[++], H.J. Gils,

B. Neumann[++], and H. Rebel

Kernforschungszentrum Karlsruhe, IAK II

[+] Institute of Physics, Jagellonian University and
    Institute of Nuclear Physics, Cracow, Poland

[++]Kernforschungszentrum Karlsruhe, IRCh

Inclusive gamma-ray spectra have been measured for the reaction ^{6}Li+^{40}Ca at E_{Li} = 156 MeV. From these data the distribution of residual nuclei was deduced in order to obtain information on reaction mechanisms where relatively high angular momenta are involved. 260 gamma lines have been identified in the spectra. About 80 % of these lines have been assigned to the residual nuclei by at least one unique and one additional gamma transition. By this procedure a total of 36 residual nuclei were found. Details of the identification procedure can be found elsewhere (1). The deduced mass spectrum presented in Fig. 1 exhibits two distinct maxima. The maximum at higher values of A contains evaporation residues from the complete or incomplete fusion and products of the few nucleon transfer reactions. Concerning the second maximum in the mass region $18 \lesssim A \lesssim 22$ we suggest that it could be attributed to a symmetric fission-like mechanism. To support this hypothesis a charged particle coincidence measurement is desirable.
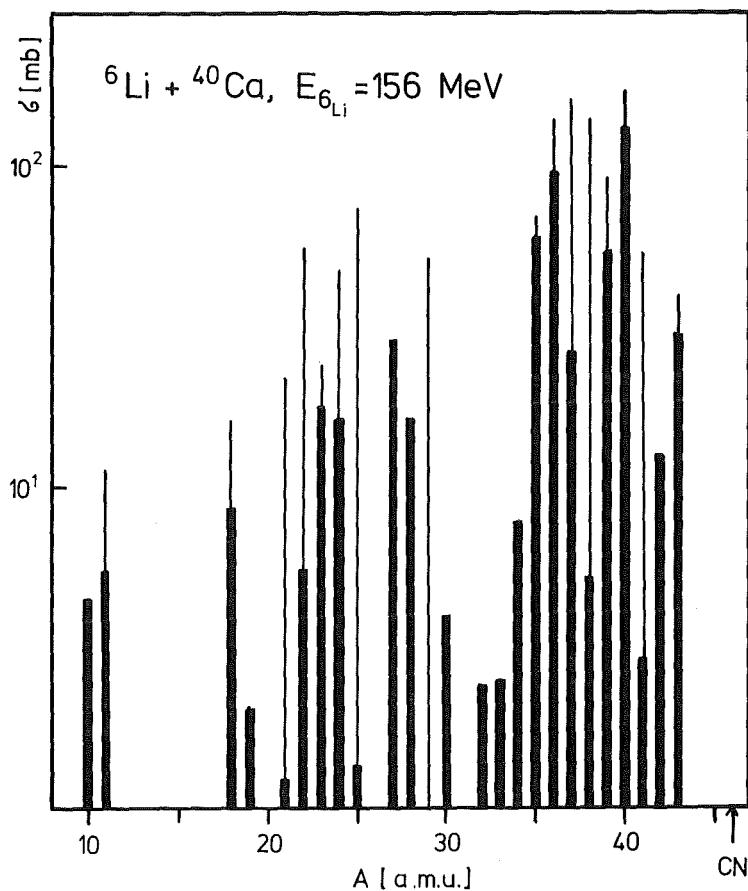
Fig. 1   Total mass spectrum of residual nuclei for the
          reaction ^{6}Li + ^{40}Ca at E_{Li} = 156 MeV.

Reference

(1) K. Grotowski et al., Phys. Rev. C23 (1981) 2513.

2.3.10   Investigation of Specific Reaction Paths in ^{6}Li-Induced Nuclear
          Reactions by Particle Gamma-Coincidence Measurements
          R. Planeta, B. Neumann[++], H. Klewe-Nebenius[++], J. Buschmann,
          H.J. Gils, H. Rebel, L. Freindl[+], K. Grotowski[+], and S. Micek[+]
          Kernforschungszentrum Karlsruhe, IAK II

          [+] Institute of Physics, Jagellonian University, Cracow, Poland

          [++]Kernforschungszentrum Karlsruhe, IRCh

          In order to obtain more detailed information on different reaction
paths in ^{6}Li induced nuclear reactions we have measured particle-gamma-
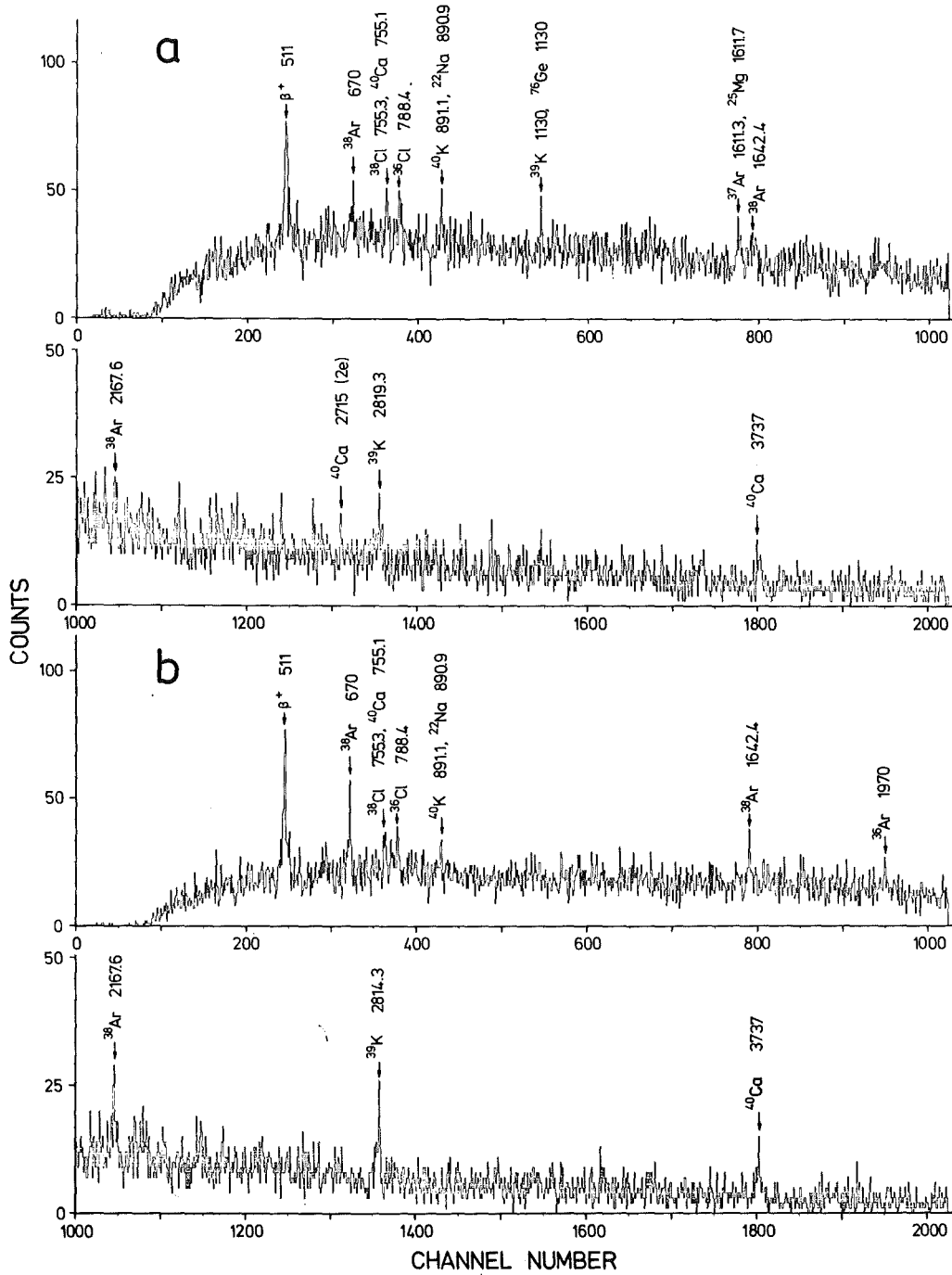
Fig. 1   Spectrum of gamma rays in prompt coincidence with (a) deuterons
and (b) alpha particles.

ray coincidences between the light charged ejectiles and gamma rays of the residual nuclei.

The charged particles were detected by means of a semiconductor telescope consisting of a silicon detector (ΔE) and a 15 mm thick high purity Ge detector (E). The telescope was placed at an angle of 12° with respect to the beam direction. The gamma rays were observed with a Ge(Li) detector placed at 135° to the beam direction. Particle-gamma-coincidences were stored event by event on magnetic tape.

The time resolution of the prompt peak in the TAC spectrum was typically about 10 ns. The data were analyzed off-line. As a first result of this analaysis the gamma-spectra in coincidence with alpha particles and deuterons for the reaction ^{6}Li + ^{40}Ca at E_{Li} = 156 MeV are presented in Fig. 1.

2.3.11 Is there a Giant Monopole Resonance in ^{12}C?

W. Eyrich[+], H. Hassold[+], A. Hofmann[+], B. Mühldorfer[+], H. Rebel, and U. Scheib[+]

Kernforschungszentrum Karlsruhe, IAK II

[+]Physikalisches Institut der Universität Erlangen-Nürnberg

The interest in the giant monopole resonance (GMR) lies mainly in the direct relation between the monopole frequency and the compression modulus of the nucleus. The existence of the GMR is now well established in heavy nuclei by scattering experiments at extreme forward angles (1). In light nuclei (A < 160) the information about the GMR is rather incomplete mainly due to the splitting of the giant resonances. There are
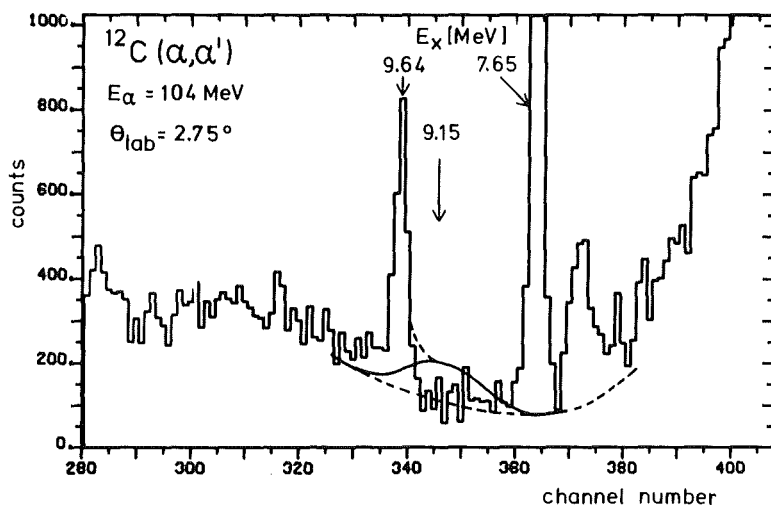
Fig. 1   Part of a ^{12}C (α,α') spectrum taken at Θ_{Lab} = 2.75°.

ambiguities and disagreements in the results of the different experiments concerning the spreading width, the strength and even the existence of the GMR (1-5).

Recently new evidence for monopole strength in ^{12}C from a ^{3}He scattering experiment at extreme forward angles has been reported (5). Besides the well-known E0-transition at E_x = 7.65 MeV, for which a strength of 8.6 % of the energy weighted sum rule (EWSR) was found, monopole strength of about 2.1 % of the EWSR was observed around E_x = 9.15 MeV (Γ = 1.8 MeV).

In the framework of our small angle scattering experiments on light nuclei using the 104 MeV alpha beam of the Karlsruhe Cyclotron we are able to check this result. Using three Si-telescopes for the particle detection at a distance of 115 cm from the target it was possible to measure at scattering angles as small as Θ_{Lab} = 2.5°. The energy resolution was about 150 keV. In Fig. 1 a part of a spectrum of alpha particles scattered from ^{12}C is shown taken at Θ_{Lab} = 2.75°. This part of the spectrum is dominated by the 0^+-state at E_x = 7.65 MeV as expected from the behaviour of the angular distribution of monopole strength at forward angles. We cannot find, however, evidence for remarkable monopole strength around E_x = 9.15 MeV. The smooth solid curve in Fig. 1 corresponds in form and strength to a 0^+-strength of 2.1 % of the EWSR as reported in ref. (5). We continue these measurements to confirm this preliminary result and to get more detailed informations about the strengths of the different multipolarities (especially monopole and isoscalar dipole modes) in the giant resonance region of ^{12}C.

References

(1) D.H. Youngblood, Proceedings of the Giant Multipole Resonance Topical Conference, Oak Ridge, TN, 1979.

(2) H. Rost, et al., Phys. Lett. 88B (1979) 51.

(3) A. Willis et al., Nucl. Phys. A344(1980) 137.

(4) F.E. Bertrand et al., Phys. Rev. C22 (1980) 1832.

(5) D. Lebrun et al., Phys. Lett. 97B (1980) 358.

2.3.12 Investigation of the Giant Resonance Region in Light Nuclei by Small Angle Scattering of 104 MeV Alpha Particles

W. Eyrich[+], H. Hassold[+], A. Hofmann[+], B. Mühldorfer[+],

H. Rebel, and U. Scheib[+]

Kernforschungszentrum Karlsruhe, IAK II

[+]Physikalisches Institut der Universität Erlangen-Nürnberg

The scattering of alpha particles at small angles is a very sensitive method for the investigation of strengths in nuclei at high excitation energies especially of giant multipole resonances (1,2). It turned out to be a powerful tool mainly for the identification of monopole and of isoscalar dipole strengths because at small angles the angular distributions of this multipolarities show significant differences compared to the angular distributions of higher multipolarities. In practice, however, the sensitivity of this method is limited by the experimental difficulties which arise in measurements at extreme forward angles. The main problem is the experimental background which is usually considerably larger than the physical strengths of interest. This background comes mainly from scattered projectiles where the scattering can take place at all beam defining elements, e.g., the slits of the analyzing magnet. A large number of these scattering events are registered in the detectors and generate a background especially in the region of higher excitation energies.

Using a magnetic spectrograph a large part of the experimental background is due to slit scattering from the aperture of the detecting system. It has been shown (3) that by defining the aperture by active collimators these events can be suppressed to a large extent. Using solid state detectors as it is done in our experiments this special problem does not occur, there is, however, another specific background which comes from elastic scattering events. At extreme forward angles the elastic peak dominates the spectrum so strongly that its tail leads to a background up to the giant resonance region which can predominate the strengths of interest in this energy region.

We have applied a method which permits to reduce the background from scattering from the beam defining elements as well as the events from the tail of the elastic peak. The idea is to get besides the energy information of the scattering event taken from the pulse height spectrum

of the solid state detector a second independent information about the
excitation energy. This information is obtained from the time-of-flight
of the alpha particles referred to the high frequency of the cyclotron.
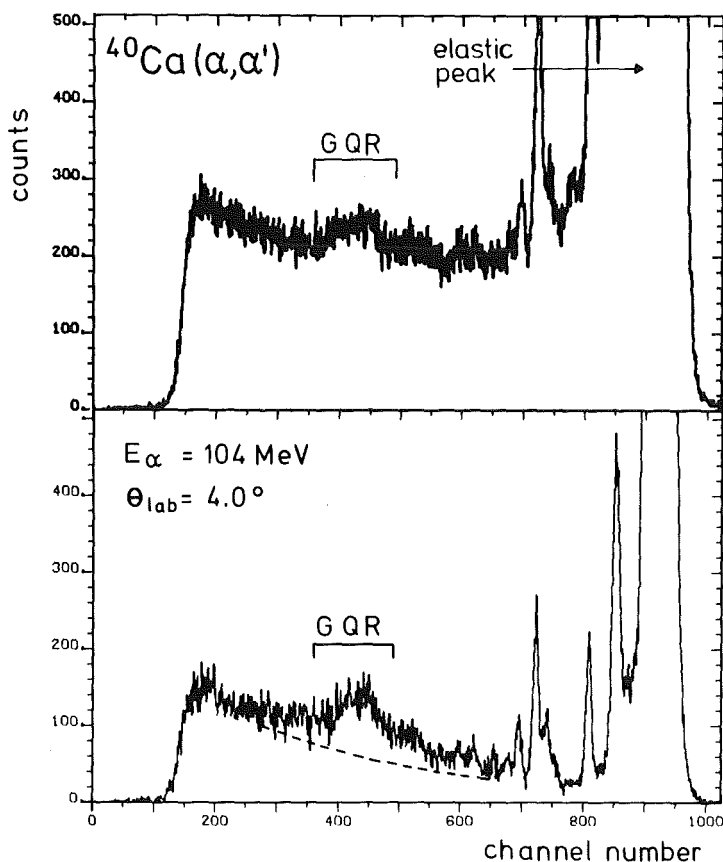
Fig. 1   Spectrum of inelastic alpha scattering on ^{40}Ca taken at 4° with-
out (upper part) and with additional time-of-flight information
(lower part).

Experimentally a time resolution of about 0.4 nsec was achieved. The distance
between the target and the detectors was about 1.10 m, the distance between the
target and the slits was larger than 4 m. Thus it was possible to get a second
energy information which made it possible to suppress the experimental background
for excitation energies higher than 5 MeV nearly quantitatively. This is demon-
strated in Fig.1 in the case of ^{40}Ca for a scattering angle of 4°. In the upper
part a spectrum is shown which was obtained without time-of-flight information,
in the lower part the corresponding spectrum with time-of-flight information is
displayed. To have a better control the elastic peak was not completely
cut off. One can see a drastic suppression of the background in the lower spectrum.
The remaining background at higher excitation energies belongs predominantly to
real physical events. In the region of the giant quadrupole resonance (GQR)
the ratio between the resonating strength

shape of the coupling potentials and corresponding quantities of the transition densities is not well established, and the interpretation in terms of transition rates and nuclear moments introduces additional uncertainties. In the present studies of inelastic scattering of 104 MeV alpha particles from ^{50}Ti and ^{52}Cr we remove the constraints due to pre-chosen forms of the coupling potentials by applying the Fourier-Bessel method which is more flexible. It allows quite general shapes and provides realistic estimates of the uncertainties of the potentials and derived quantities (moments). Using the identities between the integral moments of a folded potential distribution and of the underlying nuclear matter distribution isoscalar transition rates have been derived.

2.3.13   Neutron Decay of the Giant Quadrupole Resonance
         Region in ^{208}Pb

H. Steuer[+], W. Eyrich[+], A. Hofmann[+], H. Ortner[+], H. Rebel,
U. Scheib[+], R. Stamminger[+], and D. Steuer[+]
Kernforschungszentrum Karlsruhe, IAK II
[+]Physikalisches Institut der Universität Erlangen-Nürnberg

In the preceding annual report we showed first results of a direct measurement of the neutron decay of the giant resonance region in ^{208}Pb via an α-n coincidence experiment with 104 MeV alpha particles. In the meantime these measurements have been completed.

The aim of this experiment was to study the decay into the individual states of ^{207}Pb for small energy intervals corresponding to the fine structure observed in a previous α'-γ-experiment (1) where we measured the gamma quanta from the deexcitation of the residual nucleus ^{207}Pb in coincidence with the scattered alpha particles. Moreover it seemed to be most desirable to study the decay of the GR's and the underlying physical background separately. Therefore 4 Si(Li) alpha detectors arranged symmetrically with respect to the beam axis were placed at maxima ($\phi_{\alpha'lab} = 23.5°$) and minima ($\phi_{\alpha'lab} = 17°$) of the alpha-angular distribution of the GQR.

For the detection of the decay neutrons we applied time-of-flight technique. The achieved overall energy resolution of about 300 keV was sufficient to separate the decay into the individual states of ^{207}Pb. In order to obtain the spectra of the decay of the GR-region into the various states of ^{207}Pb kinematical plots were made event by event. The result is demonstrated in Fig. 1. In the upper part the neutron spectrum of the decay of the GQR-region of ^{208}Pb into ^{207}Pb summed over two positions of the n-detectors is shown for an alpha scattering angle of Θ_{lab} = 17°, in the lower part for an alpha scattering angle of Θ_{lab} = 23.5°. By folding the spectra with Gaussians of half widths known from the experimental energy resolution as shown by the dotted curves in Fig. 1, the population of the individual states in ^{207}Pb from the decay of the region of the GQR in ^{208}Pb can be gathered. The most surprising result which appears in all spectra is the fact that the isomeric $13/2^+$ state is populated so strongly by the decay of the GR-region.

The experimental results can be compared with the predictions of a statistical model calculation for the decay of different multipolarities
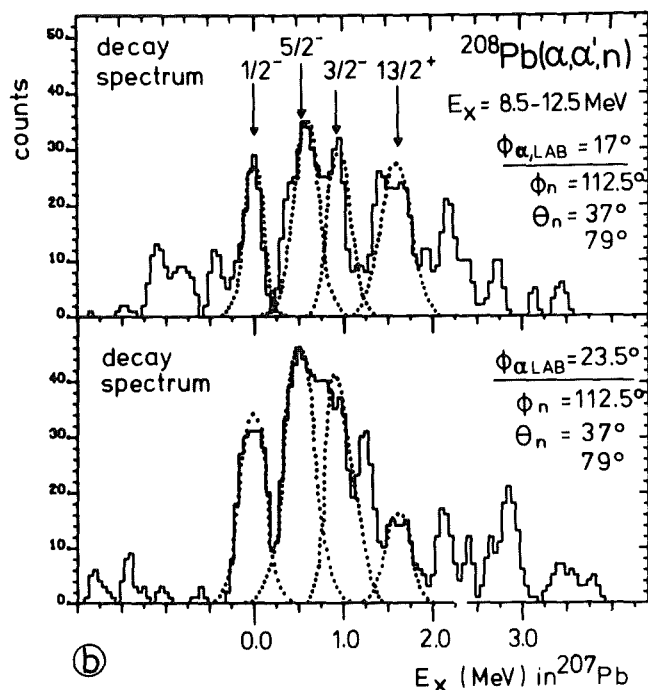
Fig. 1   n-spectra of the decay of the GQR-region in ^{208}Pb for the two alpha-scattering angles observed. The dotted curves represent Gaussians fitted to the experimental data.

assumed in the GR-region of ^{208}Pb. The relative intensities for the population of the three lowest states in ^{207}Pb obtained from this calculation assuming E2 strength agree roughly with the experimental data. This confirms the expectation that for heavy nuclei the statistical model provides at least a rough frame for the decay properties of the GR's. The 13/2$^+$ state, however, is practically not populated from the decay of E2 strength in the interesting energy region. The population from E4 strength is still relatively small whereas it is strong from E6 strength On the other hand the 1/2$^-$ groundstate is optimally matched to the quadrupole strength and is practically not populated from strengths with higher multipolarity. Therefore we claim that the states with the lower spins in ^{207}Pb are populated mainly from E2 strength, the 13/2$^+$ state, however, from higher multipolarities. Thus the decay of the quadrupole strength and the physical background can be roughly separated. From the strength of the 13/2$^+$ state in the experimental spectra one can estimate that up to half of the physical background in the region of the GQR has multipolarities equal or higher than four. Due to the fact that the minima are more pronounced in the alpha-angular distribution for E2-strength than for higher multipolarities one should expect that the 13/2$^+$ state is relatively stronger populated for the position of the alpha-detector in a minimum of the angular distribution of the GQR than in a maximum. This trend is confirmed by the experiment as can be seen by comparing the upper and lower part of Fig. 1.

In Fig. 2a-c the strength distributions in ^{208}Pb corresponding to the decay into the ground state (1/2$^-$), the first and second excited states (5/2, 3/2$^-$) and the third excited state (13/2$^+$) of ^{207}Pb are shown. The experimental thresholds of the α-n-experiment (indicated by solid arrows) lie about 1.3 MeV above the phyiscal thresholds (indicated by dashed arrows). All three spectra show significant fine structures. The patterns in the first and the second spectrum are roughly correlated, whereas there seems to be practically no correlation with the strength distribution corresponding to the 13/2$^+$ state.

In Fig. 2d an alpha-spectrum of those events is shown where the residual nucleus ^{207}Pb is populated in its states with lowest spin (ground state (1/2$^-$) and second excited state (3/2$^-$)). The alpha data for the decay into the 3/2$^-$ state were extracted from the α'-γ-experiment.
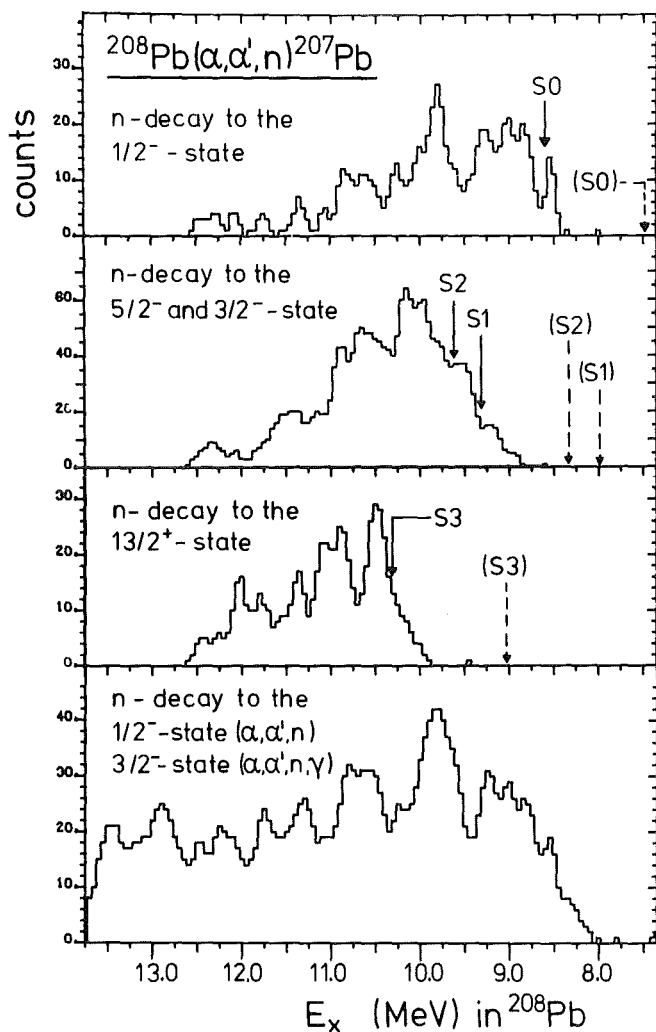
Fig. 2
Strength distributions in ^{208}Pb corresponding to the decay into the ground state (a), the first and second excited states (b) and the third excited state (c) in ^{207}Pb, extracted from the α'-n-coincidence experiment. The solid and dashed arrows indicate experimental and physical thresholds, respectively. In (d) the strength distributions of the decay into the ground state and into the second excited state, taken from the α'-γ-coincidence experiment are summed.

Thus no experimental threshold occur in the spectrum of Fig. 2d. Since the GQR decays mainly into the low-spin-states of ^{207}Pb this spectrum should describe especially the location of E2-strength. The fine structure observed in our experiment agrees relatively well with the distribution of the quadrupole strength found in (e,e')-experiment (2) and in a (γ,n)-experiment (3). This confirms that the fine structure components found in our coincidence spectra belonging to the decay into the low spin states of ^{207}Pb correspond mainly to quadrupole strength in the giant resonance region of ^{208}Pb.

References

(1) W. Eyrich, A. Hofmann, U. Scheib, S. Schneider, F. Vogler, and
    H. Rebel, Phys. Rev. Lett. 43, 1369 (1979).

(2) G. Kühner, D. Meuer, S. Müller, A. Richter, E. Spamer,and O. Titze,
    Proc. Int. Conf. on Nucl. Phys., Berkeley, California, August 1980,
    and submitted to Phys. Lett.

(3) N.K. Sherman, H.M. Ferdinande, K.H. Lokan, and C.K. Ross,
    Phys. Rev. Lett. 35, 1215 (1975).

2.4   NUCLEAR THEORY

2.4.1   The Three-Cluster Structures in ^{7}Li*

R. Beck, R. Krivec[+], and M.V. Mihailović[+]

Kernforschungszentrum Karlsruhe, IAK II

[+]permanent address: Institute J. Stefan, Ljubljana, Jugoslawien

The structure of light nuclei is described by a model which includes
the interplay of different two- and three-cluster structures as well as
the molecule-like vibrations of clusters. The model is applied to the
description of the low lying states of the nucleus ^{7}Li.

The space of the wave functions is spanned by antisymmetrized products
of two and three shell-model wave functions describing separated clusters.
In the case of two-cluster configurations the separation $\underset{\sim}{s}$ of the two shell
model potentials is used as the generator coordinate. In the case of three-cluster
configurations with fragments A,B and C the separation $\underset{\sim}{s}_1 = \underset{\sim}{s}_A - \underset{\sim}{s}_B$ between
the two shell model potentials for fragments A and B is taken as one of
the generator coordinates, the other one being the separation $\underset{\sim}{s}_2 = \underset{\sim}{s}_C - (A\underset{\sim}{s}_A + B\underset{\sim}{s}_B)/$
(A+B). The cluster configurations are characterized also by the spins of
fragments and their relative angular momenta (L_1 and L_2). The rotational
and the space inversion symmetry of the states is obtained by projecting
the basic states onto the eigenspace of the operators J,M and the parity
operator. An algebraic method based on an algorithm which expresses the
rotation of the coordinates in terms of rotation of the generator coordinates
is used.

The structure of the nucleus ^{7}Li is described by the two-cluster confi-
guration (^{4}He-^{3}H) and the three-cluster configurations (^{4}He-^{2}H(I_d)-n), with
I_d = 0,1, and the total spin I = 1/2, 3/2. In the wave function of three-
cluster structure the pair of values L_1 = 0, L_2 = 1 is included only.
The effective nuclear potential V2 of Volkov is used in the calculation.
The energy of the ground state described by a single configuration of
the two-cluster structure (^{4}He-^{3}H) is lowered by 0.66 MeV when this confi-
guration is coupled to two three-cluster configurations and the molecule-
like vibration is allowed through solving the Hill-Wheeler equation.
Both mechanisms have approximately equal effects. The ground state energy -
38.14 MeV is 0.3 MeV lower than in the model which describes the ^{7}Li
by a superposition of two-cluster structures (^{4}He-^{3}H) and (^{6}Li-n).

2.4.2   A Multi-Cluster Model for the Description of
          Low-Lying States in ^{6}Li

R. Beck, F. Dickmann, R. Krivec[+], and M.V. Mihailović[+]

Kernforschungszentrum Karlsruhe, IAK II

[+]permanent address: Institute J. Stefan, Ljubljana, Jugoslawien

The aim of the present investigation is to study the dependence of
effective nucleon-nucleon forces on the configuration space in few-nucleon
systems. The low-lying states in such nuclei exhibit cluster structures
which can be identified by the corresponding break-up channels. We
have chosen the nucleus ^{6}Li, because earlier calculations (1) with purely
central nucleon-nucleon interactions are unable to reproduce the experimental
energy levels. In the case of ^{6}Li, the lowest channels and their
energies (relative to the ground state) are ^{4}He-^{2}H (1.47 MeV), ^{5}He-^{1}H
(4.59 MeV) and ^{5}Li-n (5.66 MeV). Since these break-up energies are
close to each other, a realistic calculation should allow for mixtures
of all three clusterizations. In our model all clusterizations are repre-
sented by two-cluster wave functions where the nucleons in each cluster
occupy the lowest states in a harmonic oscillator potential. The wave
function $|\psi>$ is chosen as a weighted superposition of these three two-
cluster wave functions $|\phi_i(s_i)>$ where the separations s_i (i=1,2,3) between
different clusters are taken as generator coordinates,

$$|\psi\rangle = \sum_{i=1}^{3} \int d^3 s_i \, f_i(\underline{s}_i) |\phi_i(\underline{s}_i)\rangle. \tag{1}$$

The weight functions $f_i(\underline{s}_i)$ are determined variationally from the Hill-Wheeler equation

$$\sum_i \int d^3 s'_i \, f_i(\underline{s}'_i) \langle \phi_j(\underline{s}_j) | (H-E) P_M^{J\pi} | \phi_i(\underline{s}'_i) \rangle = 0. \tag{2}$$

The Hamiltonian H contains the kinetic energy of the nucleons and the two-body interactions including central, tensor and spin-orbit nuclear forces and Coulomb forces between protons. In order to calculate the matrix elements in eq. (2) analytically, we approximate the radial dependence of the forces by a sum of Gaussians. The operator $P_M^{J\pi}$ projects the wave functions δ onto the eigenspace of the angular momentum operators J^2 and J_z and of parity.

The status of our work is as follows: we have calculated matrix elements of the Hamiltonian between Slater determinant wave functions analytically as functions of the generator coordinates $\underline{s}_i$. Because of the complicated structure of these matrix elements, this was feasible only by using the symbolic algebra system REDUCE 2 on a computer. In order to obtain matrix elements between angular momentum eigenfunctions a FORTRAN program was written which uses the results of calculations with REDUCE 2.

Reference

(1) M.V. Mihailović and D. Mitić, to be published.

2.5   CRYSTAL AND SURFACE PHYSICS
2.5.1   Residence Sites for [111]In Implanted in Diamond*

H. Appel[+], J. Raudies[+], W.-G. Thies[+], A. Hanser,
and J.P.F. Sellschop[++]
Kernforschungszentrum Karlsruhe, IAK II
[+] Kernforschungszentrum Karlsruhe, IK 1, IGT and Univ. Karlsruhe, IEKP
[++]University of Witwatersrand, Nuclear Physics Research Unit,
   Johannesburg, Republic of South Africa

[111]In ions were implanted into diamond. After subsequent annealing

TDPAC techniques were applied for different crystal orientations with respect to the counter arrangement. A fraction of 5 % of the ions was determined that populated unique lattice sites with a well defined quadrupole interaction frequency $\nu_Q = (117.8 \pm 0.6) \cdot 10^6$ s^{-1} and preferred field gradient symmetry along <111> crystal directions.

2.5.2 Dynamic Nuclear Orientation of Surface Absorbed Radioactive Isotopes

D. Dubbers[+], B. Feurer, A. Hanser, T. Schneider[+], K. Wandelt[++], and W. Weibler[+]

Kernforschungszentrum Karlsruhe, IAK II

[+] Physikalisches Institut der Univ. Heidelberg

[++] Physikalisch-Chemisches Institut der Univ. München

A method for the study of local fields on surfaces and of the dynamics of surface adsorbed atoms and their valence electrons is being developed which uses the technique of dynamic nuclear orientation of radioactive nuclei. The nuclei of surface adsorbed paramagnetic atoms, as ^{84}Rb ($T_{1/2}$ = 34 d) on a LiF (1,0,0)-surface will be polarized by the induction of a forbidden electron-spin-resonance transition at low temperature. The nuclear polarization is monitored via the anisotropy in the decay of the nuclear gamma rays. In this way the frequencies of the ESR- or NMR-transitions can be determined from the changes they induce in the gamma-ray anisotropy. Classical ESR or NMR techniques, on the other hand, are not sensitive enough to be applied to sub-monolayer surface adsorbates. With the method proposed, coverage of less than 10^{-5} monolayers should be sufficient to yield a detectable signal.

Pure ^{84}Rb was produced in the following way for the investigations described above: a gas target containing ^{86}Kr enriched to 99 % was irradiated by the external 52 MeV deuteron beam of the Karlsruhe Isochronous Cyclotron. A beryllium absorber in front of the target degraded the energy of the beam particles to 39 MeV. This energy is most favourable for the ^{86}Kr (d,4n)-process as it resulted from irradiations at several energies. ^{84}Rb was separated from the mixture of Rb isotopes produced, using the Karlsruhe Electromagnetic Isotope Separator. The irradiation and mass separation techniques were the same as in the

production of pure [81]Rb for medical use which has been described else-
where (1). Several samples containing 200-300 µCi of the relatively long-
lived [84]Rb have been prepared.

Reference

(1) A. Hanser and B. Feurer, J. Appl. Rad. Isot., in press.

2.6 INSTRUMENTATION

2.6.1 A Brute Force Polarization Facility

R. Aures, R. Gumbsheimer, W. Heeringa, and R. Maschuw

Kernforschungszentrum Karlsruhe, IK 1

For investigations of spin dependent effects in the scattering
of polarized neutrons from polarized nuclei a brute force polarization
facility is under construction. It enables to polarize a large number
of different nuclei (see table 1) mainly restricted to metallic
elements due to their sufficient heat conductivity and nuclear spin
lattice relaxation even at very low temperatures.

The apparatus consists of a cryosystem containing a split
coil superconducting magnet and a ^{3}He/^{4}He-dilution refrigerator
(see Fig. 1). The magnet is designed to supply a field of 10 T with a
homogeneity of 1 % in a central volume of 6 cm diameter and 2.5 cm
height. This allows for an effective target size of 2 cm height
and 5 cm thickness. The attractive force between the two magnet
halves is taken up by six wedge shaped spacers which are arranged
in such a way that scattered neutrons can be observed at all angles.

The dilution refrigerator will be able to reach a temperature
below 10 mK. The cooling power at 10 mK is expected to amount 1-2 µW
at a circulation rate of 0.5 mmol ^{3}He/sec.

To minimize heat generation in the target by eddy currents the
cryostat will be mounted in a vibration free frame resting on airmont
shock absorbers.

„BRUTE FORCE" POLARISATION

Pumping line

Condensation line

N₂-Tank

Filter-

1K Pot

He-Tank

³He|⁴He-Refrigerator

10T Magnet

Probe
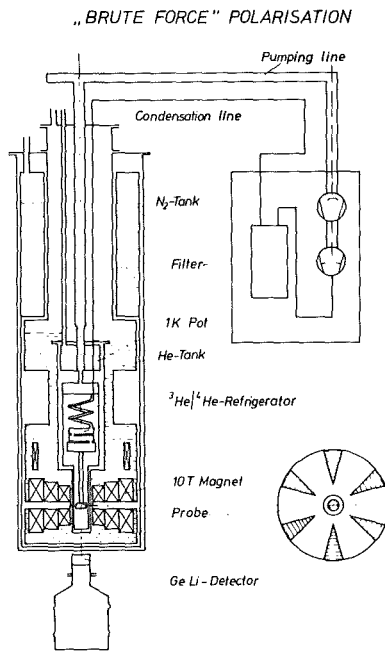
Ge Li - Detector

Fig. 1

Schematic view of the brute
force polarization facility

The temperature of the probe is determined by nuclear orientation
thermometry using radioactive gamma sources. The gammas will be detected
with a GeLi-detector, which is necessary because of the gamma
background expected in neutron scattering experiments. This detector
functions well even in a magnetic field of 1 T, so it can be put
close to the probe.

The cryostat with magnet and dilution refrigerator, under con-
struction at the Oxford Instruments Company, is nearly completed now.

In the meantime some experiments with another dilution refrigerator
have been performed. A minimum temperature of 7 mK was reached at the
mixing chamber which was measured by the anisotropy of an oriented
^{60}Co-single crystal (see Fig. 2). In addition a sample of TiH for
use as a polarized proton target (contribution 2.6.2) could already
be cooled to 17 mK.
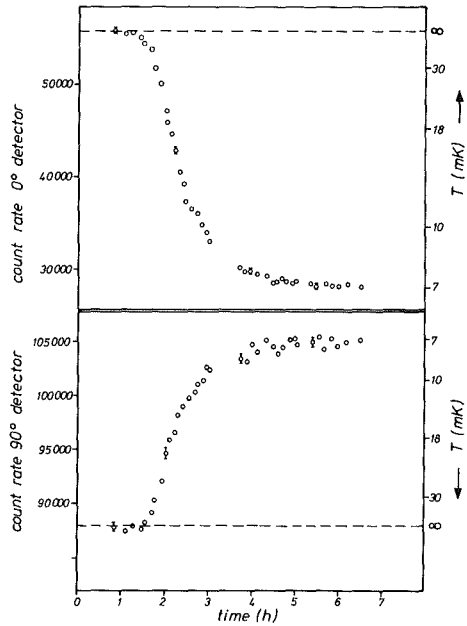
Fig. 2

Temperature at the mixing chamber of a ^{3}He/^{4}He-dilution refrigerator measured by the gamma anisotropy of a thermically coupled ^{60}Co-single crystal; detectors 3" x 3" NaJ.
coupled ^{60}Co single crystal; detectors 3" x 3" NaJ.

After delivery the polarization facility will be installed at the Van de Graaff accelerator for calibration measurements with fast polarized neutrons. The mechanics for the whole experimental arrangement consisting of beam line, neutron collimator, spin precessor, cryostat support, operating frame, neutron detector and neutron shielding is nearly completed.

Table 1

Isotope	Abundancy (%)	Polarization (%)	Isotope	Abundancy (%)	Polarization (%)
^{1}H	100.0	77.0	^{65}Cu	30.9	44.3
^{7}Li	92.6	56.6	^{93}Nb	100	67.4
^{11}B	80.3	48.9	^{115}In	95.7	63.4
^{27}Al	100	53.4	^{139}La	99.9	40.1
^{45}Sc	100	60.0	^{181}Ta	100.0	34.9
^{51}V	99.8	63.1	^{203}Tl	29.5	53.2
^{55}Mn	100	51.3	^{205}Tl	70.5	53.6
^{63}Cu	69.1	41.8	^{209}Bi	100	53.7

Nuclear polarizations achieved with the brute force method at B=10 T and T=10 mK of some (mostly mettalic) isotopes with high abundancies.

2.6.2 Metalhydrides for a Polarized Proton Target

W. Heeringa, R. Maschuw, and F.K. Schmidt

Kernforschungszentrum Karlsruhe, IK1

To investigate the spin-spin dependence of the neutron-proton interaction one needs a polarized proton target suitable for scattering experiments with polarized neutrons. It is planned to produce a brute force polarized proton target with density of about 10^{23} protons/cm² with the Karlsruhe polarization facility (see contribution 2.6.1). A magnetic field of 10 Tesla will polarize the protons at a temperature of 10 mK to a degree of 77 %.

To overcome the difficulties of poor heat conductivity and nuclear spin lattice relaxation at very low temperatures metalhydrides are chosen instead of pure hydrogen, water or hydrocarbons. Out of these titanium hydride (TiH_x) is favoured because of the high proton density achievable and the low average magnetic moment of the metal nuclei. Furthermore the diffusion properties of hydrogen in titanium enable easy production of TiH_x at pressures below 1 bar and temperatures below 1000 K.

Bulk material of Ti has been loaded with hydrogen homogeneously to concentrations up to $x = 1.1$ leaving the crystal lattice undestroyed. This is equivalent to a proton density of 5×10^{22} cm^{-3}. Freshly produced Ti turning could be hydrogenized up to the stoichiometric limit of $x = 2$. Pressing this material with several tons per cm² a proton density of about 8×10^{22} cm^{-3} could be achieved. The hydrogen content is well controlled during the hydrogenizing process and can be cross checked by gravimetic methods and degasing measurements. The accuracy in the determination of the hydrogen concentration is about 1 %.

2.6.3   High Pressure He Multiwire Proportional Chambers as Neutron Polarimeter

G. Giorginis, S. Kiontke, and R. Maschuw

Kernforschungszentrum Karlsruhe, IK1

A high pressure (<10 bar) He-polarimeter for polarized neutrons in the energy range from 20-70 MeV is being developed. The He-gas simultaneously serves as an analyzing target for a collimated polarized neutron beam as well as a detection medium for the recoil particles from the elastic n-^{4}He-scattering. Track identification of the recoil nuclei in the angular region of interest $\Theta_\alpha < 45°$ will be performed by use of multiwire proportional chambers.

Although the mass density of a gas target is low the detector has good efficiency as in a large solid angle ($\Omega_n = 2\pi$) every scattering process is observed by detection of the strongly ionizing He-recoil particle. Separation of the elastic n-^{4}He-scattering process from inelasticities such as n+^{4}He→2n+^{3}He, d+T, d+d+n etc. should be possible by combined measurement of range and energy loss of the charged particles. This simultaneously offers an energy resolution for the incoming neutrons which makes the polarimeter suitable for neutrons with a white energy spectrum.

For the final neutron polarimeter we think of a detector of 100 cm length and 60 cm diameter. 100 sense wire planes will be positioned cross wise perpendicular to the neutron beam direction. The spatial resolution in the wire plane will be tried to achieve by charge division on the meander-wound anode wire of each plane. Measuring the induced charge on the wire the energy loss of the charged particle is determined, too.

The feasibility of such a detector is investigated now with a smaller 10 b test chamber containing six sense wire planes of 32 anode wires with 5 mm spacing placed between cathode wire planes with 2 mm spacing using 20 μm WAu for all wires.
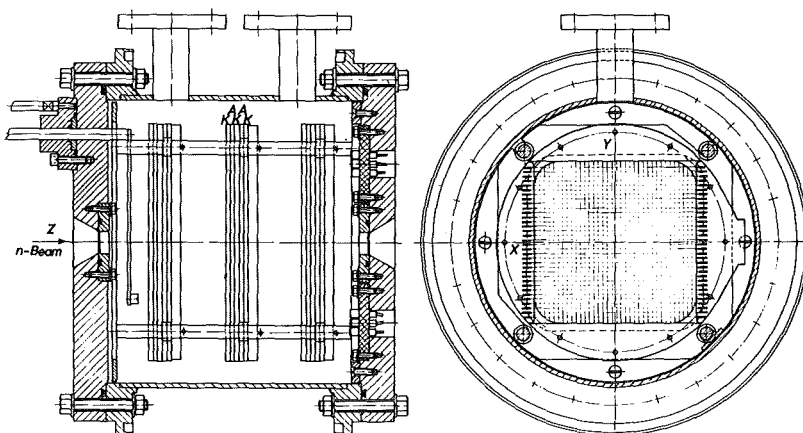
Fig. 1   High pressure (<10 b) He-MWPc. Test chamber
         for a neutron polarimeter.

Each sense wire is read out digitally via CAMAC into a LSI 11
micro-computer. Electronics and data handling are still under development.
First experiments with a 5.5 MeV alpha source showed good signal features
using 5 % CO_2 admixture to the He up to 6 bar pressure. With capacity
of $\cong 100$ pF terminated with 1 kΩ to ground the anode signals exceed 20 mV.
Although no gas-exchange is applied no change of the signal in shape
and size was observed over several days. With this test chamber optimum
gas composition, pressure dependence, wire geometry, signal handling,
spatial and angular resolution, track finding, energy resolution and
efficiency will be investigated.

2.6.4   Ion-Optical and Magnetic Properties of the Karlsruhe Magnetic
         Spectrograph "Little John"
         H.J. Gils
         Kernforschungszentrum Karlsruhe, IAK II

For nuclear reaction studies at the Karlsruhe Isochronous Cyclotron
a simple magnetic spectrograph called "Little John" will be built up (1).
The general ion optical design of the spectrograph consisting of two
quadrupoles, one 60° deflecting dipole and one sextupole magnet (QQDS con-
figuration) was previously described (2). The four magnets have been

developed according to this ion optical design. Some additional technical requirements caused small changes of the original ion optical design values. The final ion optical parameters for nine focal plane positions are compiled in Table 1. The different focal plane positions (which are determined by the measures of the vacuum system allow a variation of the dispersion and momentum acceptance by a factor of 2 in reasonable steps. The extreme focal plane positions are either determined by the ion optical limitations (FP1) or by the size of the experimental hall (FP9). Table 1 also demonstrates that both the horizontal and vertical magnifications remain rather constant when changing the dispersion. The variation of the total optical length improves the mass number resolution (due to the time-of-flight resolution) in parallel to the momentum resolution (2,3).
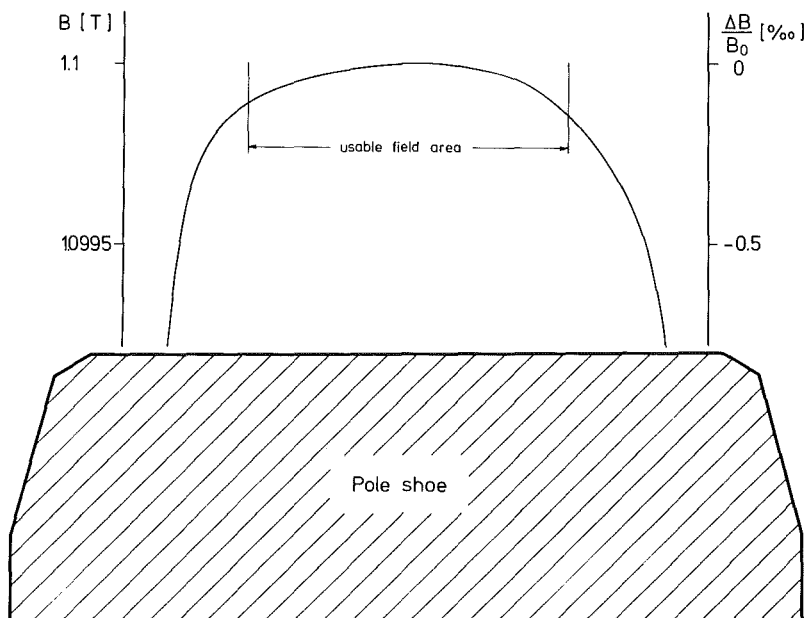
Fig. 1   Radial shape of the magnetic field of the 60° dipole magnet at B = 1.1 T

The 60° H-dipole magnet meanwhile has been constructed and the required field measurements have been performed (4). Since it has no correc-

tion coils or any other variable field adjustment elements the details of

Table 1   Ion optical properties of the magnetic spectrograph
         "Little John" at nine focal plane positions (FP1-FP9)

         *Option

FP	Optical length (m)	Magnification Horizontal	Vertical	Momentum Dispersion (cm/%)	Resolution (10^{-4})	Acceptance (%)
FP1	5.4	-.65	-5.8	1.9	3.4	$\pm$ 10.5
FP2	5.7	-.66	-6.0	2.2	3.0	$\pm$ 9.2
FP3	6.0	-.66	-6.2	2.5	2.7	$\pm$ 8.1
FP4	6.4	-.67	-6.3	2.7	2.5	$\pm$ 7.3
PF5	6.7	-.69	-6.4	3.0	2.3	$\pm$ 6.6
FP6	7.0	-.70	-6.4	3.3	2.1	$\pm$ 6.0
FP7	7.3	-.72	-6.4	3.6	2.0	$\pm$ 5.5
FP8	7.7	-.74	-6.3	3.9	1.9	$\pm$ 5.2
FP9*	8.0	-.76	-6.2	4.2	1.8	$\pm$ 4.8

the magnetic field (and the ion optical aberrations depending thereupon)
are mainly determined by the form and mechanical precision of the pole
pieces and yokes. The poles of the dipole magnet are parallel within
0.01 mm and the deviations from flatness are much less. Inside the used
area of the dipole field the homogeneity is better than 1.2×10^{-4} at
B = 1.1 T (field strength for primary beam particles B = 0.93 T).
An example of a radial cross section of the dipole field is given in
Fig. 1. The pole edges have an approximated Rogolski profile and are
clamped by field clamps. The fall-off of the field at B = 1.1 T
is shown in Fig. 2. The effective field boundary deviates from the
theoretical one by less than 0.5 mm for fields between 0.6 T and 1.5 T.

    The ion optical quality of the quadrupole magnets will be provided
by hyperbolic pole shapes and a required parallelity of the poles of
$\pm$ 0.01 mm. Mirror plates control the fall-off of the fields. For the
sextupole magnet which serves as correction magnet for the focal plane
tilt circular pole shapes with linear continuation are assumed to be
sufficient. The required parallelity of the poles is the same as for the quadrupoles.
The quadrupoles, the sextupole, and the power supplies are assumed to be
constructed and measured until August 1981.
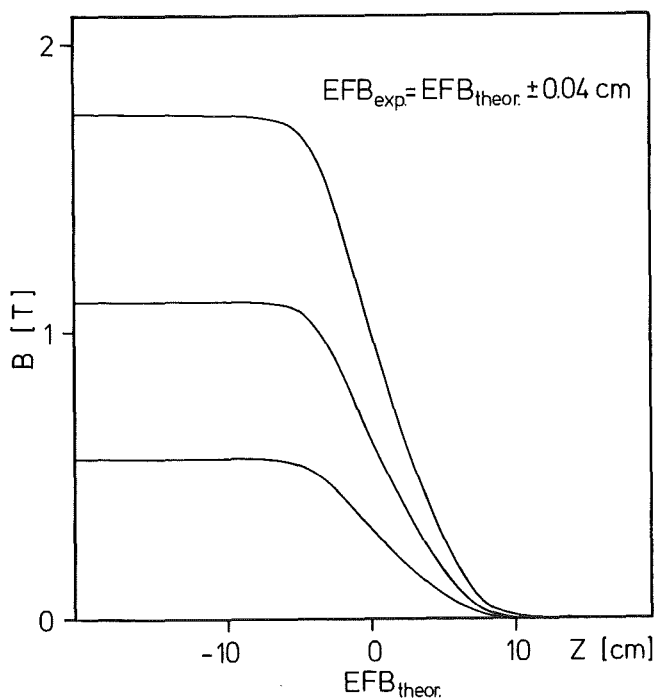
Fig. 2

Longitudinal fall-off of the
dipole field at the entrance
of the dipole magnet at B=1.78 T,
B = 1.1 T and B = 0.5 T.

$EFB_{exp.} = EFB_{theor.} \pm 0.04$ cm

B [T]

Z [cm]

$EFB_{theor.}$

References

(1) H.J. Gils, J. Buschmann, S. Zagromski, H. Rebel, Ch. Rämer,
     G. Bauer, K. Feißt, and J. Krisch, in KfK-Report 3068 (1980) p. 106.

(2) H.J. Gils; KfK-Report 2982 (1980).

(3) S. Zagromski; unpublished results (1980).

(4) Fa. Bruker, Analytische Meßtechnik GmbH, D-7512 Rheinstetten

2.6.5   Further Development of the Detection System
         for the Magnetic Spectrograph "Little John"

S. Zagromski
Kernforschungszentrum Karlsruhe, IAK II

The detection system for the magnetic spectrograph previously
described (1) has been constructed. Presently, the peripheral equipment
for the detector is being designed and collected.

The detector requires a gas supply. Depending on the experimental
details it will be filled with a suitable counter gas. This is

an argon(90 %)-methane(10%)-mixture(P-10 gas) or isobutane.

The pressure will be adjusted according to the requirements of energy loss in the ΔE-detector. Only parts of the inner space of the detector box comprise the active volume (first position sensitive detector, second position sensitive detector and energy loss (ΔE) detector). The spaces in between these are passive and should ideally be gasless. Because there are thin foils (2 microns hostaphan) between the detector elements, the passive volume has to be at the same pressure as the active volume. This is done by using counter gas or, to reduce multiple scattering in the gas, by using a lighter gas such as Helium.
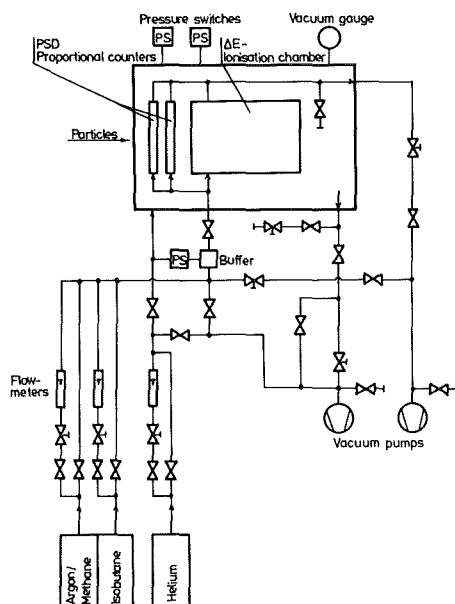
Fig. 1   Flow chart of the gas supply for the detector.

Both operation-modes (i) filling the passive volume with counter gas P-10 or isobutane and (ii) filling the passive volume with Helium are selectable on the board of the gas supply unit as required for the experiment. The later alternative is considered as the final operation mode, however, initially some experience is needed with the control of pressure

at the same level in the two circuits without deformation of the foils.
The pressures are controlled by using a gas flow system. The two outlets
of passive and active volume are connected to vacuum pumps through needle
valves. Pressure switches compare the inlet pressures relative to reference
pressures. When using the two different gases, the reference for the
active volume is the pressure in the passive volume and the reference
for the passive volume is a reference bottle. The switches open solenoid
valves whenever the pressures drop 0.1 mbar below that of the reference.
Fig. 1 shows a flow chart of the gas supply.

For coating the 2 micron hostaphan foils with gold strips which provide
the drift paths of the position sensitive detectors, the frame with the
foil (window of 56 x 6 cm²) is moved over an oven. A special
set up with a moving sled was constructed for this, driven by an electromotor.

Reference

(1)   S. Zagromski, unpublished results (1980).

2.6.6   A 4π-Spectrometer for Low Energy Beta Decays

G. Rupp, H. Beer, and F. Käppeler
Kernforschungszentrum Karlsruhe, IAK II

In activation measurements the induced activity of the irradiated
nuclei is normally counted via characteristic gamma-ray lines
with a high resolution Ge(Li) detector. This kind of data acquisition
has the advantage of an easy identification of the radionuclei through
the gamma-ray energy and guarantees a good signal-to-background-ratio.
For a variety of samples, however, neutron capture leads to a radio-
isotope with a decay scheme with only weak or uncertain gamma transitions. In these
cases one has to rely on counting the induced beta activity.

In order to meet the requirements of absolute activity counting,
a 4π Si(Li)- detector system was set up. Fig. 1 shows a cut through the
apparatus.

The activated sample is sandwiched between two movable Si(Li) detectors in an evacuated chamber. The use of Si(Li) detectors ensures a high efficiency and eliminates the effect of electron backscattering by summing the signals of both detectors. The good energy resolution of this system allows to separate the beta spectrum from accompanying conversion lines. The measurements will be carried out as a function of time to identify the radioisotope by means of its half-life.
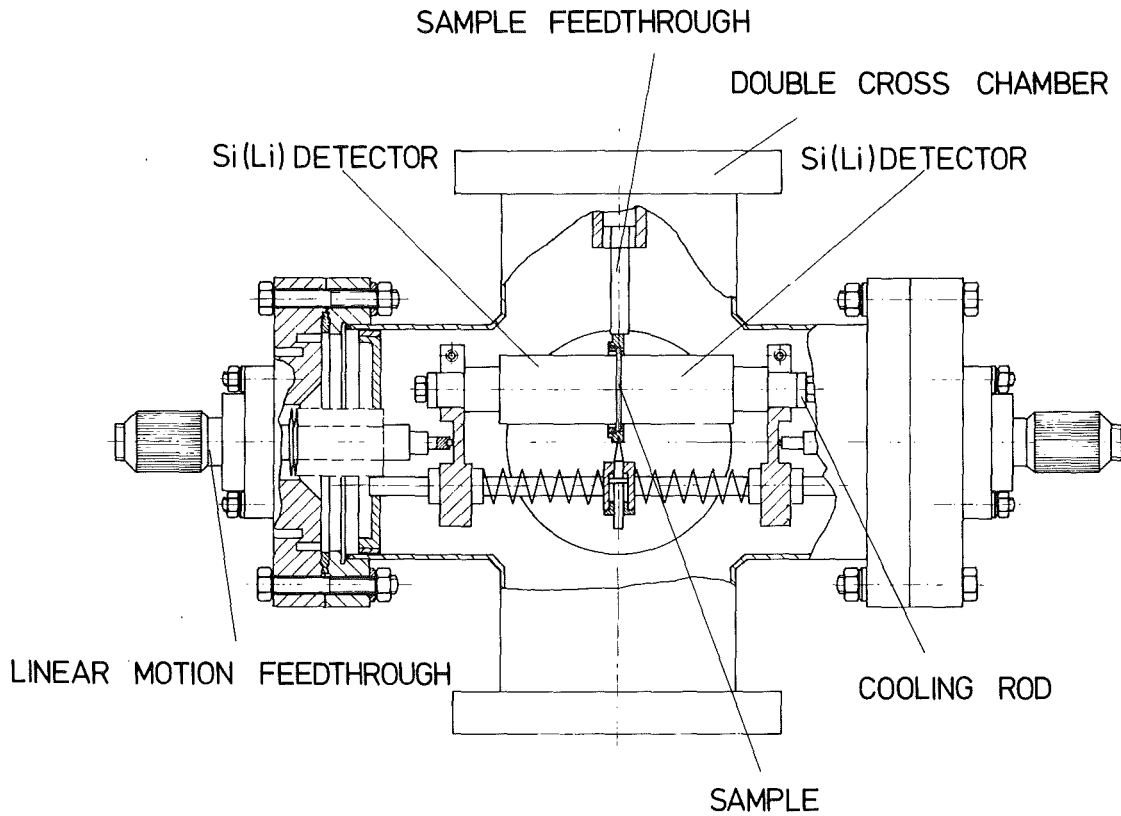
Fig. 1   A cut through the 4π Si(Li) beta-spectrometer
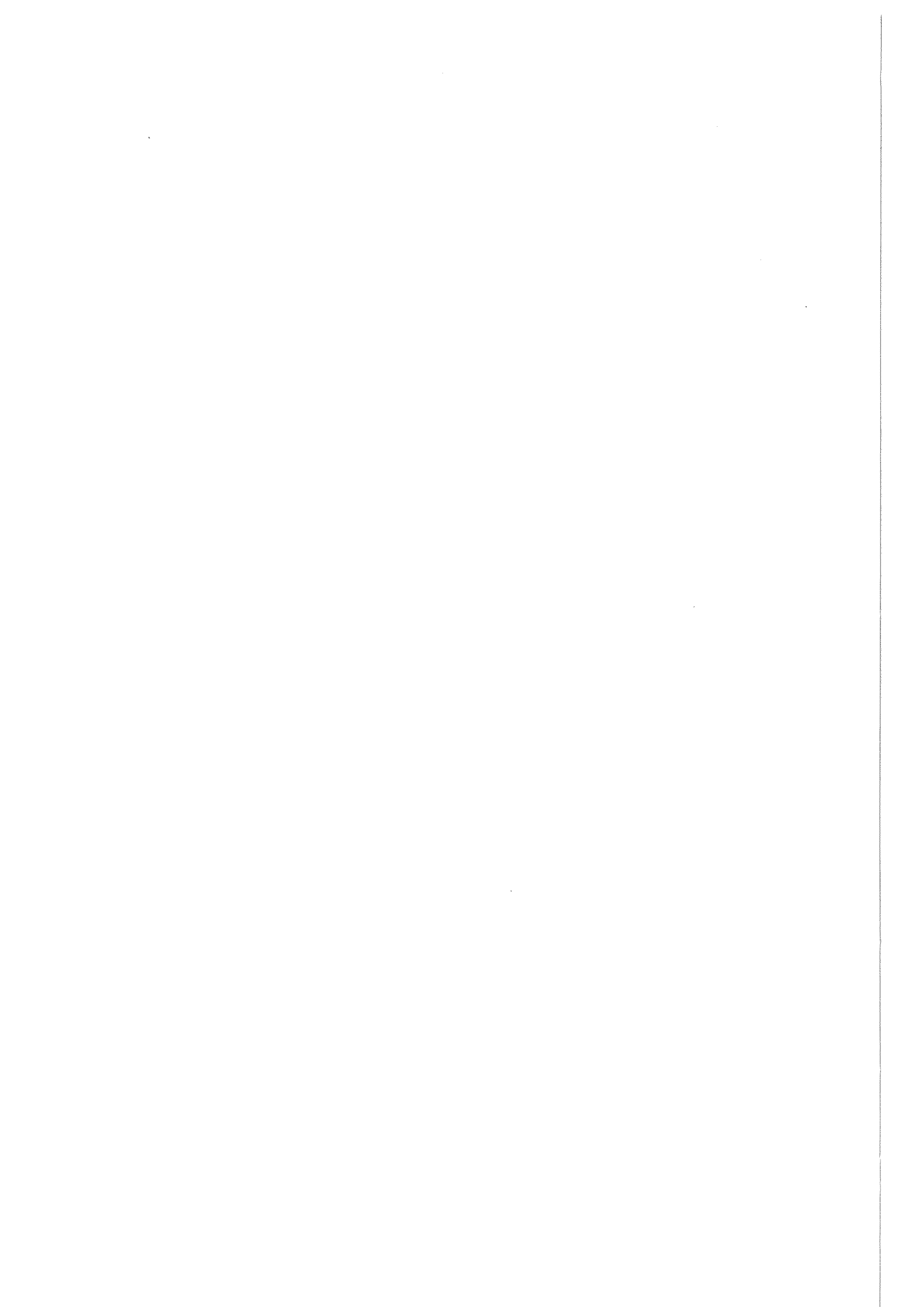
3. INTERMEDIATE ENERGY PHYSICS

3.1 MUONIC ATOMS AND QED

3.1.1 Measurements of Nuclear Quadrupole-Moments of Nuclei Around Z = 30

B. Effenberger, W. Kunold, W. Oesterle, M. Schneider, L.M. Simons
Kernforschungszentrum Karlsruhe, IK II und Universität Karlsruhe

R. Abela
Institut für Physik, Universität Basel, Switzerland

At the Swiss Institute for Nuclear Research (SIN at Villigen) the X-ray spectra of muonic arsenic ($^{75}_{33}$As) and copper ($^{63}_{29}$Cu) were measured. The experiment was performed at the μE1-channel in the momentum mode $150\pi-85\mu$.

The stopping of the muons was defined by a conventional scintillator telescope. The X-ray spectra were measured with an intrinsic Ge-diode. To detect the $2s \to 2p$ transition, which is weak in intensity, a coincidence measurement was performed using a CsF-detector, which identified the high-energetic $2p \to 1s$ transition, and the Ge-diode. The spectra for the $3d_{5/2} \to 2p_{3/2}$ transition of arsenic is shown in Fig. 1.

For the analysis muonic energies and relative intensities were computed by the programs 'RURP' and 'MUON'. The quadrupole-moments were determined by a χ^2-analysis.

Arsenic: Result of the $2s_{1/2} \to 2p_{3/2}$ transition:

$$Q = 0.3072 \pm 0.01346 \text{ b}$$

Result of the $3d_{5/2} \to 2p_{3/2}$ transition:

$$Q = 0.3154 \pm 0.0064 \text{ b}$$

weighted average: $Q = 0.3139 \pm 0.0058 \text{ b}$

Copper: Only the $3d \to 2p$ transition could be examined. Because copper has a smaller quadrupole moment than arsenic and has a lower Z-value,

too, its quadrupole splitting is smaller by about a factor of 2
compared to that of arsenic. Consequently, the relative error of
Q was larger in this case.

The result of the $3d_{5/2} \rightarrow 2p_{3/2}$ transition is:

$$Q = 0.22 \begin{array}{c} + \ 0.015 \\ - \ 0.0125 \end{array} b$$

Reference:

Y.M. Kim, Mesonic atoms and nuclear structure; North-Holland Publishing
Company, Amsterdam, 1971.
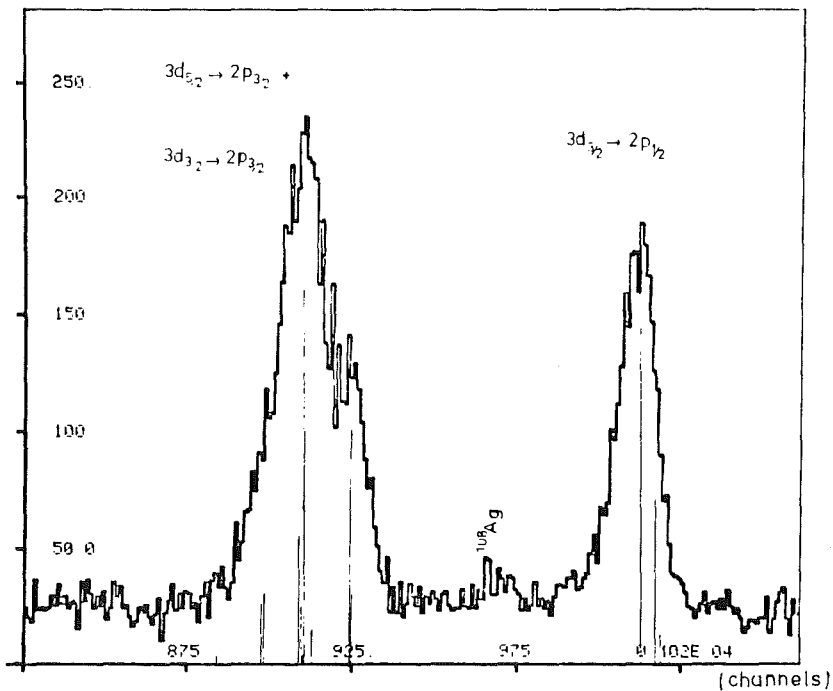
Fig. 1: The hyperfine structure splitting by quadrupole interaction
of the $3d_{5/2} \rightarrow 2p_{3/2}$ transition of arsenic is shown.
The $3d_{3/2} \rightarrow 2p_{3/2}$ transition, which is weak in intensity,
lies in the same energy region as the $3d_{5/2} \rightarrow 2p_{3/2}$ tran-
sition. The $3d_{3/2} \rightarrow 2p_{1/2}$ transition shows only a hyperfine
structure splitting by magnetic interaction.

3.1.2 Precision Determination of the Difference of the Charge Radii of ^{16}O and ^{18}O[*]

G. Backenstoss, W. Kowald, I. Schwanner, L. Tauscher, H. J. Weyer
Institut für Physik, Universität Basel, Basel, Switzerland

D. Gotta, R. Guigas
Kernforschungszentrum Karlsruhe, IK II und Universität Karlsruhe

The difference of the rms radii of the charge distribution of the oxygen isotopes was determined by a relative measurement of the muonic K-series X-rays. It is $r(^{18}O) - r(^{16}O) = (0.076 \pm 0.005)$ fm.

3.1.3 Search for a Dynamical E0 Excitation in the Muonic ^{68}Zn Atom[*]

R. Abela
Institut für Physik der Universität Basel, Switzerland

W. Kunold, L.M. Simons, M. Schneider
Kernforschungszentrum Karlsruhe, IK II und Universität Karlsruhe

Using a coincidence technique, the 2s-2p transition in muonic ^{68}Zn has been observed. The measured energies were compared with theory and no evidence for a dynamical E0 excitation was found indicating a value for the E0 matrix element much smaller than predicted.

3.1.4 Measurement of the g-Factor of the Bound Negative Muon

R. Abela[+], B. Effenberger[++], W. Kunold[++], M. Schneider[++],
L.M. Simons[++], W. Oesterle[++], J. Wuest[+].

[+] Institut für Physik der Universität Basel, Klingelberg-
    straße 82, CH-4056 Basel

[++] Kernforschungszentrum Karlsruhe, IK II und Universität Karlsruhe

For the first time the stroboscopic method was used for negative
muons. The g-factor of the negative muon, bound in the ground state
of muonic zinc, cadmium and lead was measured:

$$\text{Zinc:} \quad (g_{free} - g_{Zn})/g_{free} = (0.96 \pm 0.14) \cdot 10^{-2}$$

$$\text{Cadmium:} \quad (g_{free} - g_{Cd})/g_{free} = (2.67 \pm 0.26) \cdot 10^{-2}$$

$$\text{Lead:} \quad (g_{free} - g_{Pb})/g_{free} = (2.92 \pm 0.45) \cdot 10^{-2}$$

These results are about a factor of 5 more precise than previous ones
which were obtained from time differential measurements[1].
The quality can be increased by at least a factor of 10 in future
measurements. Fig. 1 shows a stroboscopic spectrum of carbon, which
was used as a reference spectrum.

Using the time differential μ^-SR method, the rest polarisation of the
muon in the atomic ground state of muonic sulfur and selenium (two modi-
fications: amorphous selenium, metallic selenium) in comparison to the
rest polarisation of the muon in the atomic ground state of muonic carbon
was measured:

$$P_S/P_C = 0.719 \pm 0.024, \quad P_{Se-metallic}/P_C = 0.75 \pm 0.09$$

$$P_{Se-amorphous}/P_C = 0.88 \pm 0.14$$

For the lifetimes of the muon in the atomic ground state
of sulfur and selenium the following results could be obtained[2]:

$$\tau_S = (561.1 \pm 1.9) \text{ nsec}, \qquad \tau_{Se} = (159.8 \pm 0.6) \text{ nsec}$$

Fig. 2 shows a time differential μ^-SR spectrum of carbon.

Using the muonic Hanle-effect with a carbon target, the direction
in polar coordinates of the polarisation vector of the μ^--beam in
the μE1-channel of SIN for the 150-85 MeV/c beam was determined:

$$\Phi = (191 \pm 3)^O, \qquad \theta = (9 \pm 1)^O.$$

The z-axis has the direction of the beam, the x-axis is vertical.
Fig. 3 shows the Hanle-spectrum of carbon.

References:

[1] T. Yamazaki et al., Physica Scripta 11(1975)133-139

[2] Eckhause et al., Nucl. Phys. 81(1966)575 - 584.
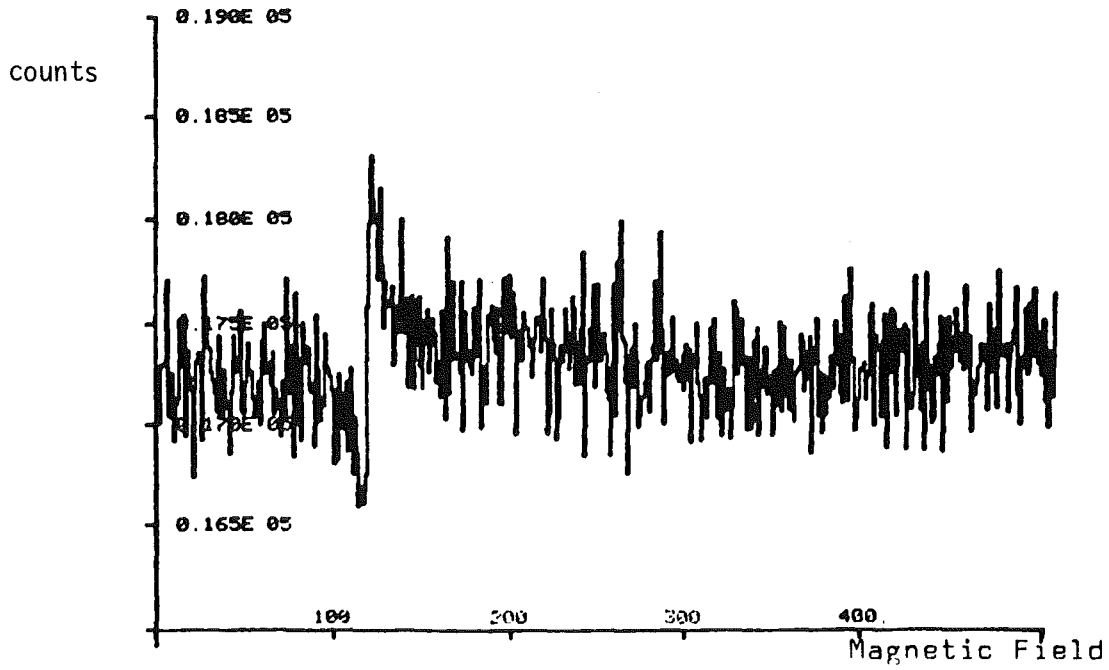
Fig. 1: Stroboscopic spectrum of muonic carbon
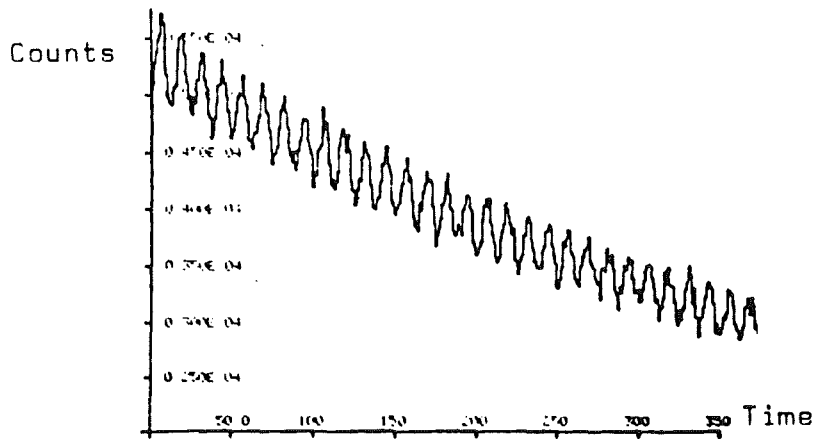
Fig. 2: Time differential μ^-SR spectrum of muonic carbon
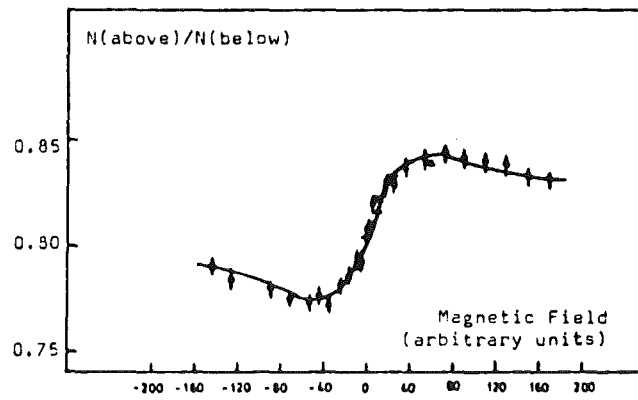
Fig. 3: Muonic Hanle-spectrum of carbon

3.1.5 Search for the $\mu^- e^+$ Conversion with a Low Level Counting Method*

L. M. Simons
Kernforschungszentrum Karlsruhe, IK II und Universität Karlsruhe

R. Abela, G. Backenstoss, W. Kowald, J. Wüest,
Institut für Physik, University of Basel, Switzerland

H. G. Seiler, M. Seiler,
Institut für Anorganische Chemie, University of Basel, Switzerland

The experimental facilities of the meson factories stimulated experiments aiming at lower upper limits for processes which are forbidden by separate lepton number conservation. Our experimental approach to measure a branching ratio of the process

$$\mu^- + A(Z,N) \rightarrow e^+ + A(Z-2,N+2)$$
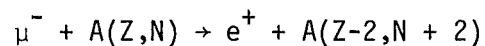
was not to detect the emitted positrons (as was done in a recent SIN experiment[1]), but was the detection of the recoil nucleus.

We looked for this nucleus by combining highly selective and sensitive radiochemical methods with low level counting techniques. This approach offers several advantages:

  a) no limitation of the useful μ^- beam intensity
  b) high detection efficiency
  c) high selectivity
  d) accumulation of produced nuclei in beam for several days, measurement off beam.

We have selected the process

$$\mu^- + {}^{127}_{53}I \rightarrow e^+ + {}^{127}_{51}Sb$$
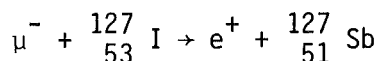
with the following sequence of decaying nuclei:

$${}^{127}_{57}Sb \xrightarrow[3.85\ d]{\beta^-} {}^{127}_{52}Te \xrightarrow[9.35\ h]{\beta^-} {}^{127}_{35}I$$
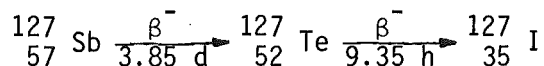
This particular choice involves a natural pure isotope and leads to a decay chain with two radioactive isotopes. It facilitates the task of chemical separation of ^{127}Te which is formed by this process and emits β^- with E_{max} = 690 keV. The chemical treatment aimed at the quantitative separation of ^{127}Te which was produced by the decay of ^{127}Sb.

The extracted amount of Te (together with inactive Te as a tracer) was then introduced into a dedicated low level counting detector and it was searched for a β^- activity showing a 9.35 h decay time. No indication of such an activity has been found. From this we obtain an upper limit for the branching ratio

$$R = \frac{(\mu^- + {}^{127}I \rightarrow e^+ + {}^{127}Sb^*)}{(\mu^- \rightarrow \nu_\mu)} < 3 \cdot 10^{-10}$$

with 90% confidence level.

Reference

[1] A. Badertscher et al., Phys. Lett. 79B(1978)371.

*Phys. Lett. 95B(1980)318-322

3.1.6 Nuclear Dynamic Resonance and Neutral Currents in Muonic $^{169}_{69}$Tm [*]

J. Missimer

Institut für Physik, Johannes Gutenberg-Universität, 6500 Mainz

L.M. Simons

Kernforschungszentrum Karlsruhe, IK II und Universität Karlsruhe

Dynamic resonance between the muon and nucleus induces an admixture
of even and odd parity states much larger than naive expectations
would suggest. The parity-violating admixture may induce a measu-
rable angular asymmetry between emitted X-rays and the spins of
the muon and nucleus. Such an angular correlation would be evidence
for neutral currents in muonic atoms. The presently measured value
of the Weinberg angle for the vector hadronic coupling implies an
angular correlation asymmetry of almost 10^{-5}.

3.1.7 Feasibility Studies of Doing Parity Violation Experiments in Muonic Atoms

L.M. Simons
Kernforschungszentrum Karlsruhe, IK II und Universität Karlsruhe

J. Missimer
Institut für Physik, Johannes Gutenberg Universität, Mainz,
Federal Republic of Germany

A direct way of resolving the controversies existing between atomic physics experiments studying parity violation effects would be the measurement of parity violating effects in atomic hydrogen or in muonic atoms. Moreover an experiment in muonic atoms would also provide a test of lepton universality in the weak neutral current regime and it would measure a different combination of coupling constants than is done in deep inelastic scattering of electrons[1].

The effects of weak neutral currents should be observable as an angular correlation between emitted X-rays and the spins of the muon or of the nucleus. The correlation results from the interference between E1 and E2 multipole amplitudes in transitions from the muonic 3d state to the ground state[2]. Carefully examining nuclei at Z≈70 an optimal case was found in the mixing of F = 3 levels in muonic Thulium where in contrast to earlier work[3] also dynamical excitation of the nucleus was taken into account.

The two levels

$$|1^- M\rangle = .59|(3p_{1/2}\ 1/2)1M\rangle - .55|(3p_{3/2}\ 1/2)1M\rangle$$
$$+ .58|(3p_{1/2}\ 3/2)1M\rangle$$

and

$$|1^+M> = .88|(3d_{3/2\ 1/2})1M> - .46|(3d_{3/2\ 3/2})1M>$$

$$+ .13|(3d_{5/2\ 3/2})1M>$$

are found to have nearly optimum energy distance which results
in a forward-backward asymmetry of the 3→1 transition of

$$\alpha \approx -1 \times 10^{-5}.$$

With a dedicated coincidence arrangement measuring the 3d→1s
transition with a novel CsF detector in coincidence with its
feeding transitions detected by an array of Ge detectors such an
effect should be measurable on a three standard deviation level in
a reasonable measuring time of about a month.

References

[1] C.Y. Presuett et al., Phys. Lett. 77B(1978)347;
   C.Y. Presuett et al., Phys. Lett. 84B(1979)524

[2] L.M. Simons, Helv. Phys. Acta 48(1975)141

[3] J. Missimer and L.M. Simons, Nucl. Phys. A 316(1979)413.

3.1.8 The Energy Levels of Muonic Atoms[*]

E. Borie
Kernforschungszentrum Karlsruhe, IK II und Universität Karlsruhe

G. A. Rinker
Theoretical Division, Los Alamos National Laboratory,
Los Alamos, NM 87545

The theory of muonic stoms is a complex and highly developed combination of nuclear physics, atomic physics, and quantum electrodynamics. Perhaps nowhere else in microscopic physics are such diverse branches so intimately intertwined and yet readily available for precise experimental verification or rejection. In the present review, we summarize and discuss all of the relevant components of muonic atom theory, and show in selected cases how this theory meets experimental measurements.

3.1.9 More Nuclear Size Corrections to the Lamb Shift[*]

E. Borie
Kernforschungszentrum Karlsruhe, IK II und Universität Karlsruhe

An evaluation of previously uncalculated finite size effects on the Lamb shift of normal atoms, using methods which are well-known from muonic atoms, gives corrections which are larger than the experimental uncertainties (40 ppm for the Lamb shift in hydrogen). The additional corrections tend to restore agreement between theory and experiment.

3.1.10 Use of Furry-Sommerfeld-Maue Wave Functions in Pair Production at Medium and High Energies[*]

E. Borie

Kernforschungszentrum Karlsruhe, IK II und Universität Karlsruhe

The analytic expression for the differential pair production cross section, obtained using full Furry-Sommerfeld-Maue wave functions for the electron and positron, is integrated numerically over angles without further approximation. The resulting Coulomb corrections to the total pair production cross section are compared with existing interpolations in the energy range 10 MeV to 50 MeV, and their experimental relevance is discussed.

3.2   PIONIC, KAONIC and ANTIPROTONIC ATOMS

3.2.1   Isotope Effects in Light Pionic Atoms[*]

I. Schwanner, R. Abela, G. Backenstoss, W. Kowald,
P. Pavlopoulos, L. Tauscher, H.J. Weyer

Institut für Physik, Universität Basel, Basel, Switzerland

P. Blüm, M. Dörr, W. Fetscher, D. Gotta, R. Guigas,
H. Koch, H. Poth, G. Schmidt, H. Ullrich

Kernforschungszentrum Karlsruhe, IK II und Universität Karlsruhe

Direct comparison of the pionic K-series X-ray transitions for $^{16}O/^{18}O$ and $^{6}Li/^{7}Li$ has been made and a new measurement of the same transitions in ^{3}He has been performed.

3.2.2 Results of the Search for K-Series X-Rays from Kaonic Hydrogen[*]

M. Izycki, G. Backenstoss, L. Tauscher
Institut für Physik der Universität, Basel, Switzerland

P. Blüm, R. Guigas, N. Hassler, H. Koch, H. Poth
Kernforschungszentrum Karlsruhe, IK II und Universität Karlsruhe

K. Fransson, A. Nilsson
Research Institute of Physics, Stockholm, Sweden

P. Pavlopoulos, K. Zioutas
CERN, Geneva, Switzerland

The X-ray spectrum associated with K^- stopping in liquid hydrogen was measured with high resolution Si(Li) detectors. The total K X-ray yield is not larger than 8×10^{-4} per stopped K^- assuming no line broadening. A weak line pattern was found, which was tentatively ascribed to the K^-H K-series X-rays. The shift and width of the 1s level, deduced from this pattern, are $\varepsilon_{1s} = +270\pm80$ eV and $\Gamma = 560\pm260$ eV, respectively.

3.2.3 Results on the Measurement of K-Series X-Rays from Antipro- tonic Hydrogen[*]

M. Izycki, G. Backenstoss, L. Tauscher
Institut für Physik der Universität Basel, Basel, Switzerland

P. Blüm, R. Guigas, N. Hassler, H. Koch, H. Poth
Kernforschungszentrum Karlsruhe, IK II und Universität Karlsruhe

B. Emmoth, K. Fransson, A. Nilsson
Research Institute of Physics, Stockholm, Sweden

P. Pavlopoulos, K. Zioutas
CERN, Geneva, Switzerland

The X-ray spectrum emerging from a liquid-hydrogen target when stopping antiprotons was measured with high resolution in order to determine the strong interaction shift and width of the atomic 1s level. Owing to strong Stark quenching only weak structures could be observed. The upper limit of the yield of any one of the K-series transitions is 3.5×10^{-4} (95% C.L.) per stopped antiproton, assuming no broadening of the 1s level. Possible identifications of the weak lines with the K-series transitions are discussed.

3.2.4 Study of Rare Annihilation Channels and Search for Deeply Bound Baryonium States

B. Richter, P. Blüm, R. Guigas, H. Koch, Th. Köhler, M. Meyer, H. Poth, U. Raich

Kernforschungszentrum Karlsruhe, IK II und Universität Karlsruhe

G. Backenstoß, M. Hasinoff, P. Pavlopoulos, J. Repond, L. Tauscher, D. Tröster

Institut für Physik, Universität Basel, Switzerland

L. Adids, I. Bergström, K. Fransson, A. Kerek
Research Institute for Physics, Stockholm, Sweden

M. Suffert
CNR, Strasbourg, France

K. Zioutas
Nuclear Physics Department, University of Thessaloniki, Greece

The data of an experiment to search for narrow baryonium states below threshold via detection of high energy gammas has been analysed. The experimental set up, which collected these data, consisted of a modular NaI spectrometer (54 modules) and a 10" x 12" NaI monocrystal. The anti-protons were stopped in a LH_2-target, which was surrounded by an annihilation detector of nearly 4π solid angle allowing the definition of charged and γ-multiplicities.

The performance of the γ-detectors was studied with pions stopping in hydrogen. The absolute and relative calibration and the long term stability of the γ-detection system were controlled with a light pulser system. An energy resolution of 5% at 130 MeV was achieved for the modular NaI. The 10" x 12" NaI had a resolution of about 8%. As a demonstration of the performance we show Fig.1, where reasonable agreement is found between the shapes of the spectra collected with the modular NaI at two different times, and the spectrum obtained in a Monte-Carlo-simulation of the experiment (1).

At the high energy part of the spectrum the background is particularly low. The contributions of rare annihilation channels with a monoenergetic π^0 or γ to the gamma spectrum could be studied and are displayed in Table 1.
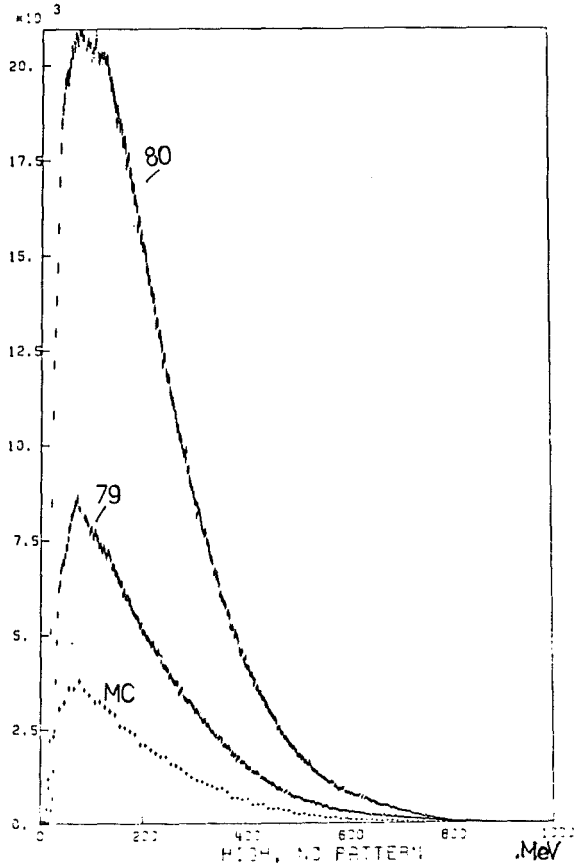
Fig. 1: Total gamma spectrum in $\bar{p}p$

Table 1: Preliminary results on rare annihilation channels (Relative errors are about 30%)

	data of 1979	data of 1980
$\bar{p}p \rightarrow x\pi^+,\ y\pi^-,\ z\pi^0$		
$\quad \hookrightarrow \pi^- p \rightarrow n\gamma$	$8 \cdot 10^{-3}$	$4 \cdot 10^{-3}$
$\rightarrow \rho^0\pi^0,\ \omega\pi^0$	$6.2 \cdot 10^{-2}$	$6.4 \cdot 10^{-2}$
$\rightarrow \eta'\gamma,\ \phi\gamma$	$1.4 \cdot 10^{-3}$	$9 \cdot 10^{-4}$
$\rightarrow \eta\gamma$	$4 \cdot 10^{-4}$	$2.5 \cdot 10^{-4}$
$\rightarrow \pi^0\pi^0,\ \pi^0\gamma$	-	$3 \cdot 10^{-5}$

The low energy part of the spectrum dominated by the π^0 decay photons of the different annihilation channels is the energy domain where possibly baryonium states would show up. In contrast to our previous experiment (2) the sensitivity for the detection of narrow structures was increased by a factor of 5 due to higher statistics and better energy resolution.

Again, one finds hints for weak structures at 180 and 220 MeV as in our previous experiment, however, with a 3 times lower yield. The 420 MeV-line is not found in this experiment, but a line at 320 MeV can be reported. In Table 2, the preliminary results are summarized and compared with the results of the previous experiment.

Table 2: Preliminary results on narrow bound states in $\bar{p}p$-systems

E_γ [MeV]	significance		yield		
	1979	1980	1979	1980	previous exp.
180	3σ	3σ	$2.4 \cdot 10^{-3}$	$2.9 \cdot 10^{-3}$	$7 \cdot 10^{-3}$
220	2σ	3σ	$2 \cdot 10^{-3}$	$2.2 \cdot 10^{-3}$	$6 \cdot 10^{-3}$
320	3σ	8σ	$5.7 \cdot 10^{-3}$	$6.7 \cdot 10^{-3}$	-
420	-	-	-	-	$8 \cdot 10^{-3}$

Relative errors about 30%.

References

(1)   Th. Köhler, Diplomarbeit, Universität Karlsruhe (unpublished)
(2)   P. Pavlopoulos et al., Phys. Let. 72B(1978)415.

3.2.5 Study of Strong Interaction Effects in Antiprotonic Isotopes ^{6}Li/^{7}Li

R. Guigas, P. Blüm, H. Koch, M. Meyer, H. Poth, B. Richter
Kernforschungszentrum Karlsruhe, IK II und Universität Karlsruhe

G. Backenstoß, M. Izycki, P. Pavlopoulos, L. Tauscher
Institut für Physik, Universität Basel, Switzerland

K. Fransson, A. Nilsson
Research Institute for Physics, Stockholm, Sweden

K. Zioutas
Nuclear Physics Department, University of Thessaloniki, Greece

Low energetic antiprotons have been stopped in thin targets of iso-topically pure lithium. The x-rays emitted during the atomic deexci-tation were measured with four high resolution Si(Li) detectors. The two identically shaped targets were alternately exposed to the beam. Their positions were automatically exchanged at regular intervalls, thus providing a relative measurement of isotope effects, which is expected to be free of systematic errors.

Due to the surprisingly low yield of the last observable transition, i.e. the 3d-2p transition, the analysis of the data turned out to be difficult. Nevertheless, the high statistics and the improved signal to background ratio (as compared to a previous experiment at Brook-haven (1)) allowed to detect lines with yields as small as several 10^{-4} per stopped antiproton. All background lines could be identified. Fig. 1 displays that part of the spectrum, where the 3d-2p-transition is detected.

The strong interaction effects in the lower level $(\varepsilon_{2p}, \Gamma_{2p})$ could be obtained immediately from the 3d-2p transition. The upper width Γ_{3d} is extracted from the intensity of the L_α-line related to the M-series. Table 1 displays the result.
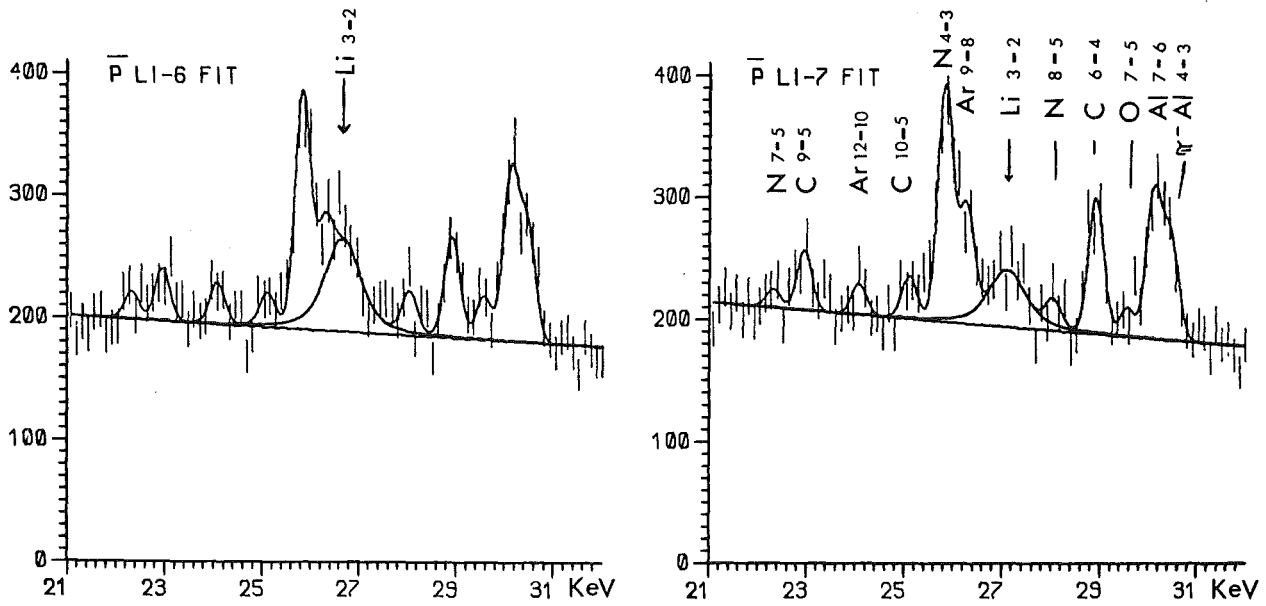
Fig.1: 3d-2p transition in $\bar{p}^6$Li and $\bar{p}^7$Li

Table 1: Strong interaction effects in $\bar{p}^6$Li and $\bar{p}^7$Li

		^{6}Li	^{7}Li
E_{exp}:	keV	26.65 ± .72	27.11 ± .06
ε_{2p}:	eV	-230 ± 72	-336 ± 60
Γ_{2p}:	eV	443 ± 210	456 ± 190
Γ_{3d}:	eV	.13 ± .045	.21 ± .062
Y_{rel}:		0.48 ± .017	.030 ± .009
Y_{abs} per $\bar{p}_{stop}$		∼ .011	∼ .007

In comparison to the previous experiment (1) we achieved a much higher significance (8σ) for both isotopes. Moreover the transitions were not properly assigned in the previous experiment.

Comparison of the data with the prediction of a simple optical model with two free parameters (real and imaginary part of an effective scattering length) showed agreement in the strong interaction effects of the lower level(2p), however, disagreement in the width of the 3d-ni-veau. As a best fit of the data together with the results of an experi-

ment on the elements ^{14}N, ^{16}O, ^{32}S (Ref.2) we found an effective
scattering length of a = 1.1 ± 1.9 fm. The large isotope effects
in the 2p-shift and the 3d-width couldn't be explained and will
need an elaborated microscopic model.

References

(1) R. Robertson et al., Phys. Rev. C16(1977)1945
(2) H. Poth et al.,   Nucl. Phys. A294(1978)435

3.2.6 Low Energy Kaon and Antiproton Nucleon Interactions

K. Kilian, H. Poth[+], J.-M. Richard[++]
CERN, Geneva, Switzerland

[+] Kernforschungszentrum Karlsruhe, IK II
[++] Division de Physique Théorique, IPN Orsay

The installation of an internal target in LEAR allows, apart from other application, the creation of antineutrons through the $\bar{p}$ charge exchange reaction $\bar{p}p \rightarrow \bar{n}n$ with highest production rates, when compared to other methods. The internal target technique, in conjunction with beam cooling provides a windowless source, the recuperation of non-interacting antiprotons, highest energy and angular resolution, and gives access to lowest energies (see Fig. 1).

The number of antineutrons produced on an internal target installed in LEAR are estimated for an optimized operation (cf. Fig.2). It turned out that the antineutron rates are comfortable to study the charge exchange and antineutron induced reactions in detail. CM-energy resolution of some KeV can be achieved with this technique.

The main aspects of the physics interest in reactions involving antineutrons are the disentanglement of isospin singlet and triplet scattering amplitudes, tests of particular terms of boson exchanges, access to extremely low energy $\bar{n}p$ and $\bar{n}n$ interactions and a specific approach to annihilation. Experimental results in this field would considerably help to understand the low energy $\bar{N}N$ interaction on the basis of a working model.

$\bar{p}p \rightarrow \bar{n}n$
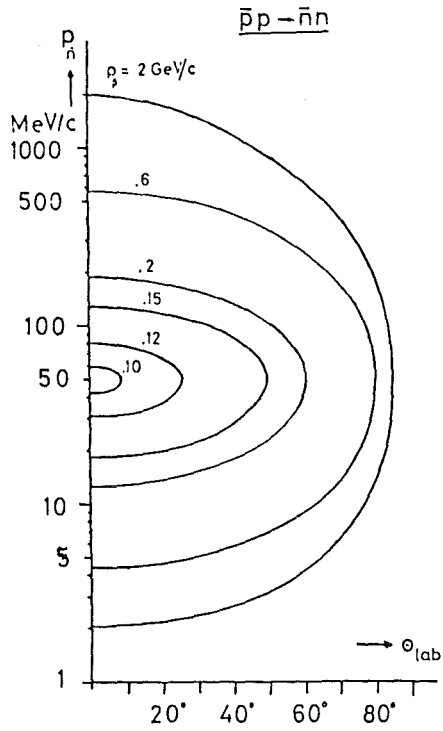
Fig. 1: Antineutron momentum versus n production angle for incident antiproton momenta of 2, 0.6, 0.2, 0.15, 0.12 and 0.10 GeV/c.
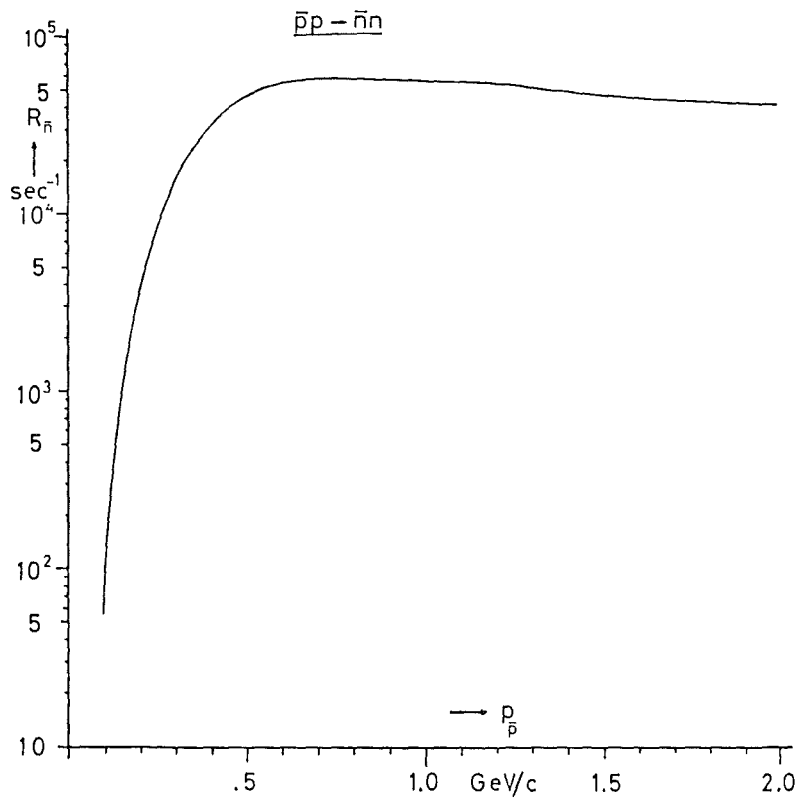
Fig. 2: Integral antineutron rates for an optimized internal target in LEAR.

3.3 PION NUCLEUS INTERACTION

3.3.1 Pion Absorption in ^{3}He

D. Gotta, M. Dörr, W. Fetscher, S. Ljungfelt, G. Schmidt, H. Ullrich
Kernforschungszentrum Karlsruhe, IK II und Universität Karlsruhe

G. Backenstoß, W. Kowald, I. Schwanner, H.J. Weyer
Universität Basel, Institut für Physik, Klingelbergstr. 82,
CH-4056 Basel, Switzerland.

Two- and three-body decays following the absorption of stopped negative pions in ^{3}He have been investigated for the first time in a kinematically complete measurement. nn, pn and dn coincidences have been measured using 2 m long position sensitive TOF-counters and a total absorption counter, respectively. Additionally, coincidences with pionic K-X-rays have been recorded which allows to distinguish between absorption from atomic S- and P-orbits. The experiment was done at the πE1-channel at SIN. A cooled (5 K) gas target has been used.

Results from the 3-body decay are available in the form of a Dalitz-Plot. As a one-dimensional representation, the density distribution along the (circular) circumsphere of the kinematically allowed region is given in Fig. 2. Four peaks in this distribution can be seen corresponding to the nn final state interaction FSI(nn) region, the quaifree absorption on a pp-pair QFA(pp), the np final state interaction FSI(pn), and to the quasifree absorption on a np-pair QFA(pn), respectively. The ratios of the corresponding peak areas are

$$FSI(nn):QFA(pp):FSI(pn):QFA(pn)$$

$$=(1.6\pm0.3):(5.9\pm0.2):(11.8\pm0.5):(80.7\pm8.7)$$

for S- and P-absorption. They do not seem to change drastically
for pure S-absorption. The nnp/nd ratio is $9.54 \, ^{+2.96}_{-1.50}$. The rather
strong concentration of the events at 180° can be seen in the an-
gular distributions for the QFA(pp) and FSI(pn) peak, respective-
ly (Fig. 3).
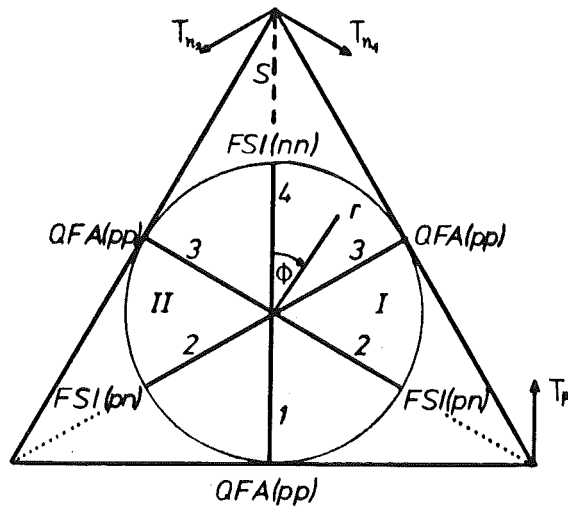
Fig. 1: Dalitz plot in triangular coordinates.
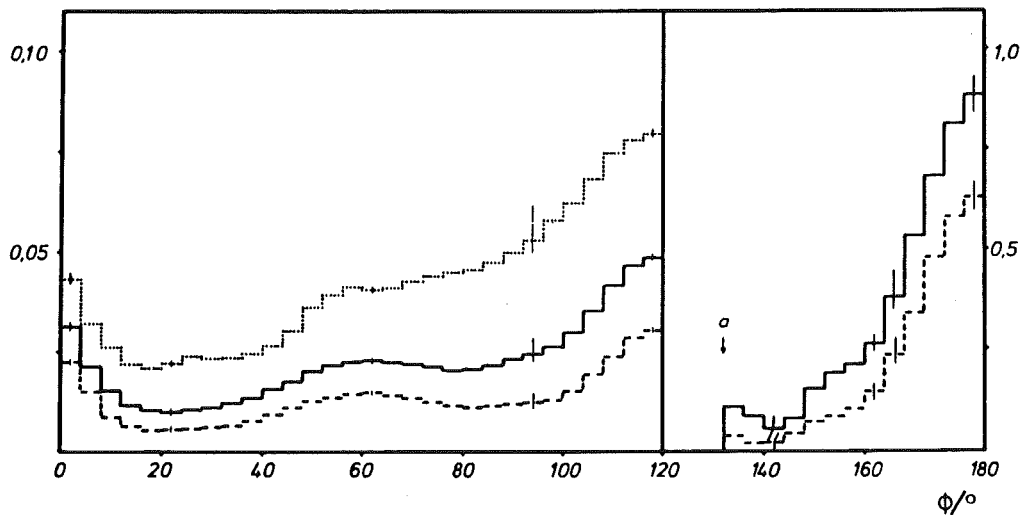
Fig. 2: Density distributions in polar coordinates (see Fig.1).
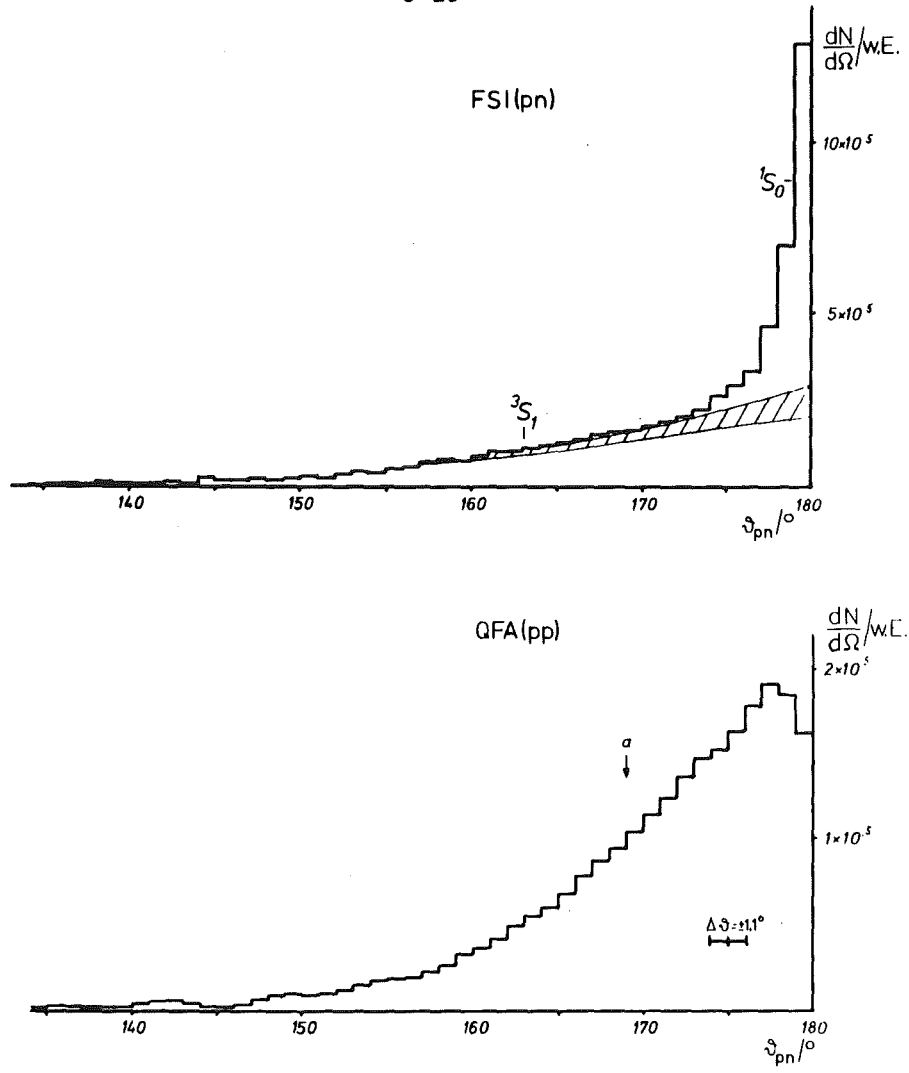
Fig. 3: Angular distributions of the QFA(pp) and FSI(nn) peak.

3.3.2 Absorption of Stopped Negative Pions in ^{6}Li

M. Dörr, D. Gotta, W. Fetscher, G. Schmidt, H. Ullrich
Kernforschungszentrum Karlsruhe, IK II und Universität Karlsruhe

G. Backenstoß, W. Kowald, I. Schwanner, H.J. Weyer
Institut für Physik der Universität Basel, Klingelbergstr. 82,
CH-4056 Basel, Switzerland.

The aim of the experiment is to explore the mechanism of pion absorption, with special emphasis on the composite particles (deuterons, tritons) emitted with high energies. In order to minimize sequential processes we have chosen the target ^{6}Li, being a rather light nucleus with well-known properties.

The measurements have been performed at SIN. All pairs of particles, being combinations of neutrons, protons, deuterons and tritons have been detected simultaneously, using two large (2 m long) position sensitive TOF counters (for n, p, d, t)and a 3 x 4 matrix of total absorption counters, 17 cm x 17 cm x 8 cm each, in connection with MWP-chambers (for p, d, t). All counters are capable of particle identifications. Table 1 shows the measured branching ratios for the respective reaction channels. In addition, for all particle combinations the following distributions are available: E_1 versus E_2, recoil momentum versus missing energy, opening angle and angle between sum and difference of the particle momenta.

Table 1: Observed branching ratios for 150° - 180°.
The numbers give percentages. The thresholds are
17, 21, 28 and 32 MeV for n, p, d and t, respectively.

	n	p	d	t
n	$\sim$ 80			
p	6	<0.01		
d	9.2	0.12	0.17	
t	4.4	0.24	0.47	0.105
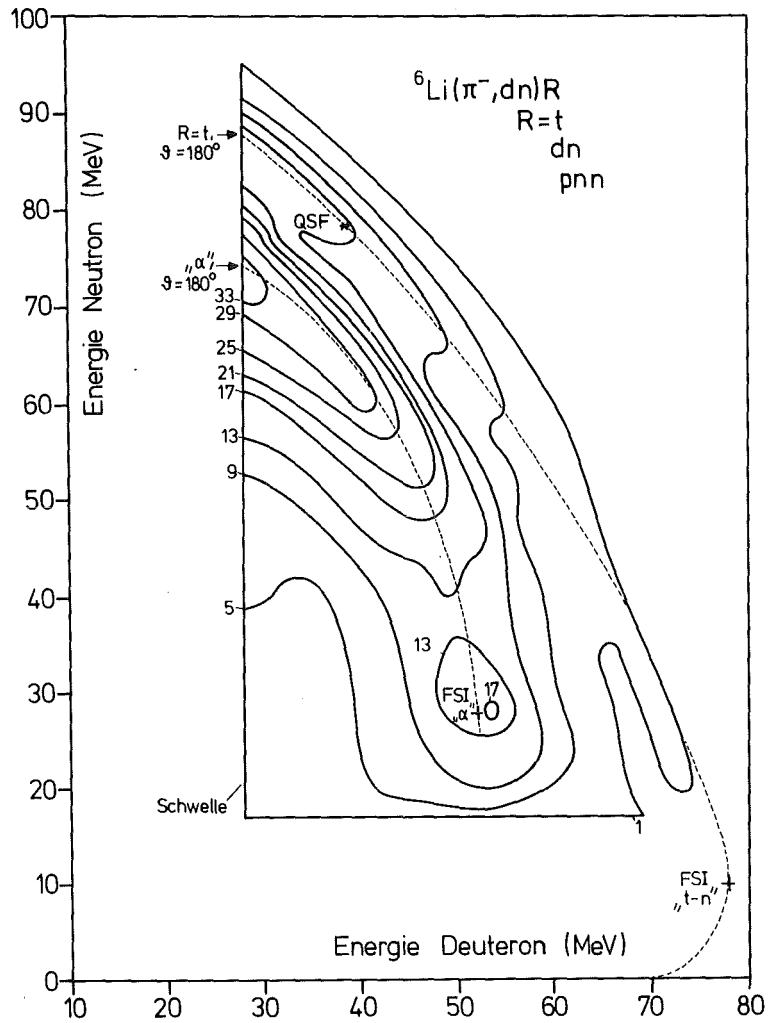
Fig. 1: Dalitz plot of the nd-channel. The solid lines are equal density lines. The quasifree absorption on a (npp)-subsystem (upper dashed line) and on an α-cluster (lower dashed line) is clearly visible.
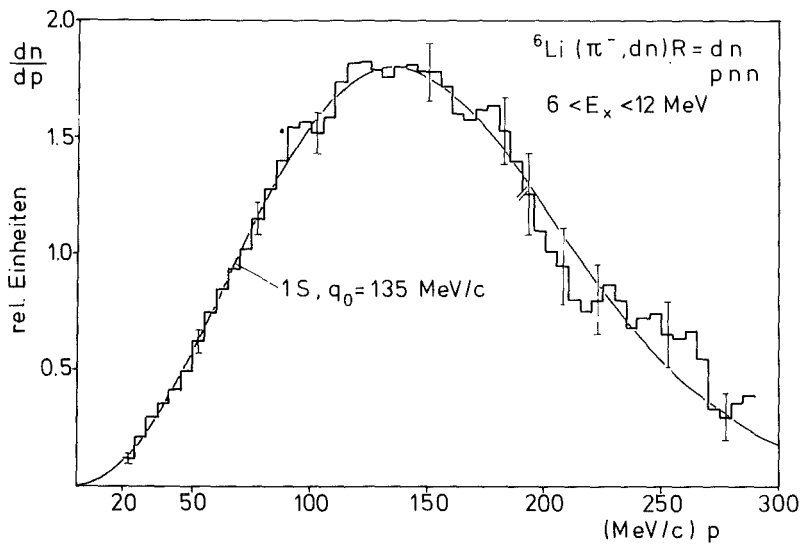
Fig. 2: Recoil momentum distribution for the nd-channel. The curve shows a simple calculation for a 1 S (t-^{3}He)-intercluster motion.
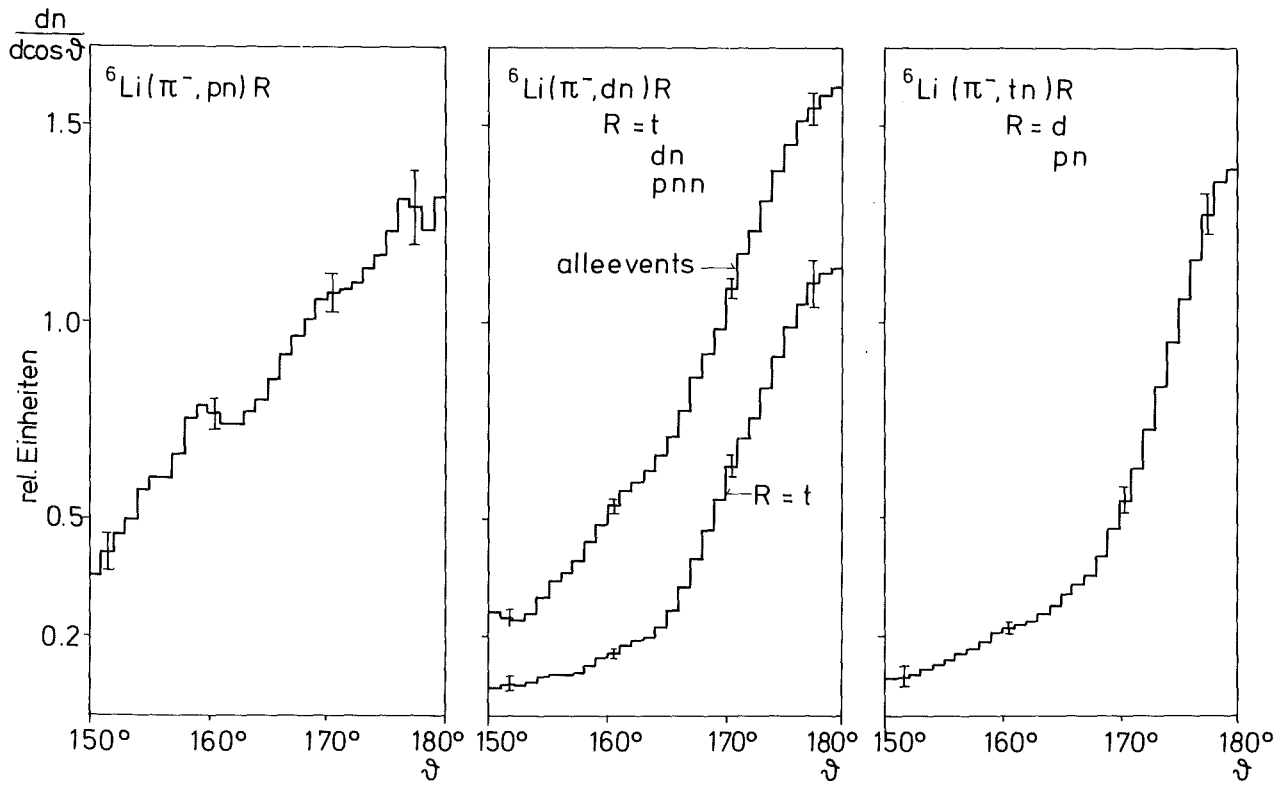
Fig. 3: Angular distributions for (np), (nd) and (nt) pairs.

3.3.3 Measurements of the Elastic $\pi^{\pm}$ ^{12}C Scattering at Forward Angles and of the Total Cross-Sections for the $\pi^{\pm}$ ^{12}C Interaction at Energies Below the (3.3)-Resonance

H. Degitz, U. Klein, K. Hofmann, W. Kluge, R. Markus, H. Matthäy, U. Wiedner
Kernforschungszentrum Karlsruhe, IK II und Universität Karlsruhe

In the last year first measurements of the elastic scattering of $\pi^{\pm}$ ^{12}C for 60 and 80 MeV covering an angular interval between 7.5° and 27.5° and of the total cross-sections of $\pi^{\pm}$ ^{12}C for energies between 50 and 90 MeV were carried out. These measurements aim at a detailed investigation of the Coulomb-nuclear interference in order to determine the real and imaginary parts of the nuclear forward scattering amplitude, which represent an important input for forward dispersion relations. The experimental set-up for the elastic scattering of pions on carbon is particularly suited for the rejection of decay muons, which represent the main background for pion nucleus scattering at forward angles. Six multiwire proportional chambers register the incident and scattered particles. In addition the scattered particles are detected by a matrix of six 3 mm thick Si(Li) detectors of an area 50 x 30 mm^2 in order to determine their energy losses, by a plastic scintillator to determine their time-of-flight and by a NaI(Tl) detector of 15 x 15 x 15 cm^3 to determine their full energies. The set-up for the measurement of total cross-sections is modified such that large area multiwire proportional chambers (384 x 384 wires, 2 mm apart) are used for the detection of the scattered particles and that the six Si(Li) detectors, the time-of-flight counter and the NaI are omitted. The data taken are evaluated presently.

This activity is also regarded as a preparation of future measurements of the elastic scattering of $\pi^{\pm}$ on protons at low energies and small angles and as a preparation of measurements with a new magnetic spectrometer at SIN. For that purpose soft ware developments, studies of the muon background and developments of new wire chambers are necessary.

3.3.4 Neutron and Proton Components of Nuclear Transitions in Pion Inelastic Scattering on ^{26}Mg*

C.-A. Wiedner, K.R. Cordell, W. Saathoff
Max-Planck-Institut für Kernphysik, D-6900 Heidelberg

S. T. Thornton
Max-Planck-Institut für Kernphysik, D-6900 Heidelberg
and Department of Physics, University of Virginia, Charlottesville,
VA 22901, USA

J. Bolger, E. Boschitz, G. Pröbstle
Kernforschungszentrum Karlsruhe, IK II und Universität Karlsruhe

J. Zichy
Schweizerisches Institut für Nuklearforschung (SIN), CH-5234 Villigen,
Switzerland

The elastic and inelastic scattering of 180 MeV positive and negative pions from ^{26}Mg has been measured. From these data the ratios of neutron and proton nuclear transition matrix elements have been determined for the first and second excited states. These ratios are compared with those obtained from electromagnetic transitions in mirror nuclei and with shell model predictions.

3.3.5 Wide Angular Range Study of the Reaction $^{16}O(\pi^-, 2n)^{14}N$ With Stopped Pions[*]

B. Bassalleck, H.D. Engelhardt, W.D. Klotz, C.W. Lewis, F. Takeutchi, H. Ullrich
Kernforschungszentrum Karlsruhe, IK II und Universität Karlsruhe, and CERN, Geneva, Switzerland

M. Furić
'R. Bošković' Institute, Zagreb, Croatia, Yugoslavia, and CERN, Geneva, Switzerland

A first kinematically complete investigation of the reaction $^{16}O(\pi^-,2n)^{14}N$ with stopped pions has been performed at the CERN SC over a wide angular range.

Measured distributions in excitation energy of the residual nucleus, recoil momentum, and angle between the two neutrons are presented. They are compared with theoretical predictions on two-hole states and with detailed calculations on the quasi-free two-nucleon absorption process.

3.4 PROTON-PROTON INTERACTION EXPERIMENTS

3.4.1 Measurement of the Spin Correlation Parameter A_{oonn} and the Polarization A_{oono} in Elastic p-p Scattering Between 400 and 600 MeV[*]

D. Besset, Q.H. Do, B. Favier, R. Hausammann, E. Heer, R. Hess,
C. Lechanoine-Leluc, W.R. Leo, D. Rapin, D.W. Werren
DPNC, University of Geneva, Switzerland

Ch. Weddigen
Kernforschungszentrum Karlsruhe, IK II und Universität Karlsruhe

J.M. Cameron, S. Jaccard, S. Mango
SIN - 5234 Villigen, Switzerland

We have measured the spin correlation parameter A_{oonn} and the polarization A_{oono} for p-p elastic scattering in the c.m. angular range between 30° and 90° at seven energies between 400 and 600 MeV. The experiment was performed at SIN using a polarized beam and target and a fast on-line event reconstruction method. The results are compared with phase-shift predictions.

3.4.2 A Phenomenological Interpretation of the Production Cross Section for the Reaction $p + p \rightarrow \pi^+ + d$ [*]

Ch. Weddigen
Kernforschungszentrum Karlsruhe, IK II

Using new data on the unpolarized differential cross section for the reaction pp→πd, obtained by the NESIKA collaboration at SIN, the energy dependence of the anisotropy parameters γ_0, γ_2, and γ_4 is interpreted phenomenologically. Especially the energy dependence of γ_4, which is stronger than predicted theoretically, could be understood as being due to the behaviour of a production amplitude with $\ell_\pi = 3$ near threshold.

3.4.3 Energy Dependence of the pp→π$^+$d Differential Cross Section Between 500 and 600 MeV[*]

J. Hoftiezer, Ch. Weddigen
Kernforschungszentrum Karlsruhe, IK II und Universität Karlsruhe

B. Favier, S. Jaccard, P. Walden
SIN, CH-5234 Villigen, Switzerland

P. Chatelain, F. Foroughi, C. Nussbaum, J. Piffaretti
Institut de Physique, Université de Neuchâtel, CH-2000 Neuchâtel,
Switzerland

The unpolarized differential cross section for the reaction pp→π$^+$d
has been measured at SIN at seven energies between 514 and 583 MeV.
Data are presented in terms of a Legendre polynominal expansion.
An observed strong energy dependence of the 4th order coefficient
can be understood as a threshold phenomenon in a phenomenological
NΔ resonant description. No evidence was found for a $^1D_2$ dibaryon
resonance near 600 MeV.

3.4.4 Measurements on the Pion Production from the Reaction $pp \rightarrow \pi^+d$

P. Chatelain[+], B. Favier[++], F. Foroughi[+], J. Hoftiezer[+++], S. Jaccard[++],
C. Nussbaum[+], J. Piffaretti[+], P. Walden[++++], Ch. Weddigen[+++]

+   Université de Neuchâtel, CH-2000 Neuchâtel
++   Schweizerisches Institut für Nuklearforschung, CH-5234 Villigen
+++   Kernforschungszentrum, IK II und Universität Karlsruhe
++++ SIN, Guest from TRIUMF, Vancouver, B.C. V6T 1W5, Canada.

The reaction $pp \rightarrow \pi^+d$ is a fundamental process for the description of pion production and absorption in nuclear matter. At SIN energies it is restricted to small angular momenta so that only few production amplitudes contribute. The purpose of our activity is to gain increased, detailed information about these production amplitudes, step by step. The measurements are of current interest due to conjectured dibaryon resonances ($^1D_2$ and $^3F_3$) which could effect the $pp \rightarrow \pi^+d$ reaction.

The differential cross section $(d\sigma/d\Omega)_0$ for unpolarized particles is governed between 500 and 600 MeV by singlet amplitudes, so that it should be sensitive to an anomaly in the $^1D_2$ initial state. The analysing power A exists as an interference between singlet and triplet amplitudes, therefore it should give information with regard to the state $^3F_3$.

1. The Differential Cross Section $(d\sigma/d\Omega)_0$

The angular distribution of the production cross section was measured with the priviously described method[1] using the arrangement sketched in Fig.1a, for seven proton energies E_p from 514 to 583 MeV. The telescopes p1 and p2 served as beam monitor. They detect pp elastic scattering at $90°$ in the CM system, and were calibrated absolutely according to the diagram shown in Fig.1b. A third telescope p3 recorded the incident protons (about 1.5×10^7/sec) while a target detector p4 ($1 \times 1 \times .5\ cm^3$) determined the portion (70 to 85%) of the beam which struck the CH_2 target in the measurement of $(d\sigma/d\Omega)_0$.

The anisotropy parameters a_{2i}^{00} are obtained from the normalized angular distribution according to the parametrization[2]

$$(d\sigma/d\Omega)_0 = \frac{1}{4\pi} \sum_{i=0}^{2} a_{2i}^{00} P_{2i}(\cos\Theta_{cm}) \qquad (1)$$

(P_{2i} = Legendre Polynomials). Our Results (Fig.2) show a strong energy dependence, especially in a_4^{00} which is not predicted by microscopic theories. For reference a phenomenological interpretation[3] considering the known data from $E_p=0$ to 1 GeV can reproduce the energy dependence of a_{2i}^{00} as being due to threshold behaviour of an $\ell_\pi=3$ amplitude. No indication for a $^1D_2$ dibaryon resonance was found[4].
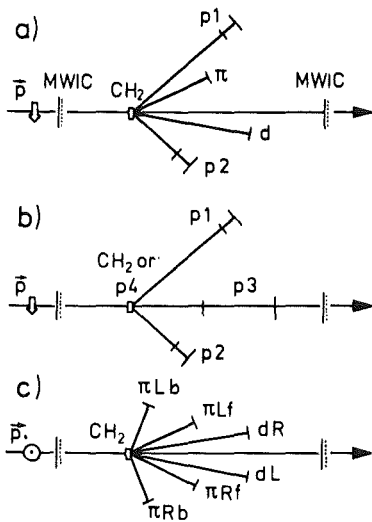
Fig. 1:
Schematic drawing of the arrangement
for measuring the differential cross
section $(d\sigma/d\Omega)_0$ (a), the absolute
normalization (b), and the analysing
power A (c). The detectors are labelled
according to the particles they detect
(p,π or d), MWIC = multiwire ionisation
chambers.
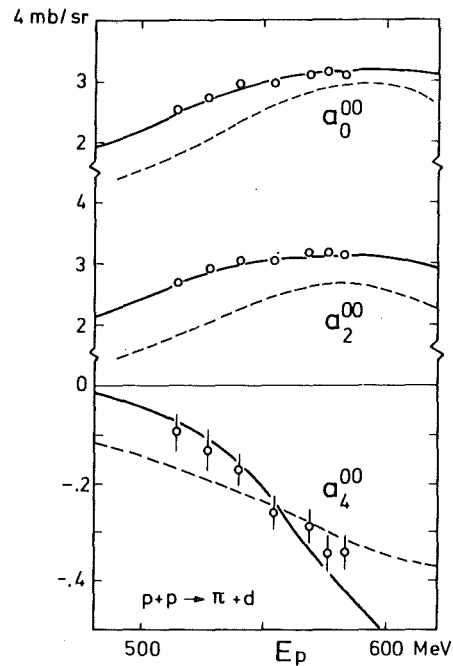
Fig. 2:
Comparison of our results for the para-
meters a_{2l}^{00} (Eq.1) with the result of a
phenomenological interpretation (Ref.3)
(solid lines) and a theoretical pre-
diction (Ref. 5) (dashed lines).
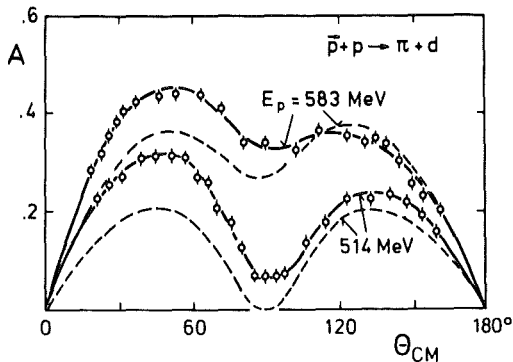
Fig. 3:
Experimental results for the analysing
power A with fitted curves (Ref. 7)
and theoretical predictions (Ref. 5)
(dashed lines).

2. The Analysing Power A

The analysing power describes the spin dependent part of the differential
cross section $d\sigma/d\Omega = (d\sigma/d\Omega)_0 (1+AP\cos\Theta_{cm})$. For the measurement of A a
symmetric arrangement (Fig.1c) was employed. As a result of the double
valued nature of the deuteron angle in the lab. system two detectors, πf

and πb can be operated in coincidence with each of the detectors dL and dR. To eliminate spurious asymmetries, the direction of the proton polarisation P (.4165 ± .0040[6]) was rotated 180° by a superconducting solenoid between two measurements. The coincidence count rates N, after background subtraction give the analysing power

$$A = \frac{1}{p} \times \frac{r-1}{r+1}, \text{ with } r = \left[\frac{N_{L\uparrow} \times N_{R\downarrow}}{N_{L\downarrow} \times N_{R\uparrow}}\right]^{1/2}.$$

Angular dependencies obtained are given in Fig. 3. Additional data at intermediate energies are not yet evaluated. The solid lines in Fig. 3 are fitted curves for obtaining parameters similar to those defined in Eq.(1)[7]. Our results differ significantly from theoretical predictions[5].

References:

1) B. Favier et al., SIN Newsletter 12(1979)56
2) J.A. Niskanen, private communication
3) Ch. Weddigen, KfK-Report 2926B(1980)
4) J. Hoftiezer et al., Phys. Lett. 100B(1981)462
5) J.A. Niskanen, Phys. Lett. 79B(1978)190
6) B. Favier, Thèse n° 1984, Université de Genève (1979)
7) J. Hoftiezer et al., SIN Newsletter 13(1980)30.

3.4.5 Evidence for a Dibaryon Signal in the Measurement of Elastic π^+-d_{pol} Scattering[*]

J. Bolger, E. Boschitz, G. Pröbstle, G.R. Smith
Kernforschungszentrum Karlsruhe, IK II und Universität Karlsruhe

S. Mango
Schweizerisches Institut für Nuklearforschung, CH-5234 Villigen, Switzerland

F. Vogler
Physikalisches Institut, Universität Erlangen-Nürnberg, 8520 Erlangen,
Federal Republic of Germany

R.R. Johnson
Physics Department, University of British Columbia, Vancouver, British
Columbia V6T 1W5, Canada

J. Arvieux
Laboratoire National Saturne, F-91190 Gif-sur-Yvette, France, and
Institut des Sciences Nucléaires, F-38026 Grenoble, France

The vector analyzing power (iT_{11}) in elastic π-d_{pol} scattering has been measured for several angles at T_π=142 and 256 MeV. The results are compared with calculations reported in the literature. At the lower energies, Faddeev calculations agree fairly well with the data. At the higher energies, the experimental results differ markedly from any conventional calculation, but agree surprisingly well with predictions in which effects of dibaryon resonances are explicitly included.

3.4.6 Effects of Transverse Polarization Components in Parity
       Tests with Longitudinally Polarized Nucleons[*]

M. Simonius, R. Henneck, Ch. Jacquemart, J. Lang
Laboratorium für Kernphysik, Eidg. Techn. Hochschule, 8093 Zürich,
Switzerland

W. Haeberli
University of Wisconsin, Madison, Wisconsin 53706, USA

Ch. Weddigen
Kernforschungszentrum Karlsruhe, IK II und Universität Karlsruhe

In the study of parity violation by the scattering of longitudinally
polarized spin $\frac{1}{2}$ particles, systematic errors arise from the presence
of small polarization components perpendicular to the beam. A quantita-
tive treatment of these errors is presented. It is shown that non-uni-
form polarization distributions over the beam profile give sizeable
effects even if the average transverse polarization vanishes. Methods
are presented which permit accurate correction of the parity measure-
ments of the presence of transverse polarization components. It is
shown that the necessary information can be obtained by measuring four
suitably chosen one-dimensional intensity and polarization distribu-
tions within the beam. Finally, possible origins of the non-uniform
polarization distributions are outlined.

3.4.7 Test of Parity Violation in pp-Scattering with Longitudinally Polarized Protons at 45 MeV

R. Balzer[+], W. Haeberli[++], R. Henneck[+], S. Jaccard[+++], Ch. Jacquemart[+],
J. Lang[+], T. Roser[+], M. Simonius[+], Ch. Weddigen[++++]

+   Laboratorium für Kernphysik, ETHZ, CH-8093 Zürich
++   University of Wisconsin, Madison, WI 53706, USA
+++   Schweizerisches Institut für Nuklearforschung, CH-5234 Villigen
++++   Kernforschungszentrum Karlsruhe, IK II und Universität Karlsruhe

According to modern weak interaction theories a small weak, strangeness-conserving contribution is expected in the nucleon-nucleon-interaction. This contribution should manifest itself through the parity violating signature of the weak interaction. Since parity is (assumed to be) conserved in the strong nuclear interaction the observation of parity violation in nuclear processes is a clear indication of a weak interaction contribution, whose structure can then be studied.

Although parity violation has been clearly observed in several nuclear processes involving medium and heavy nuclei[1] the quantitative interpretation of the results is difficult, because one has to know the nuclear wave functions accurately. In view of these difficulties processes involving only few nucleon systems are better suited for a detailed investigation of these effects. We studied parity violation in pp-scattering following a suggestion by Simonius[2].

The principle of measurement consists essentially of measuring the relative change in cross section (suitably angle integrated) as the polarization vector is changed from positive to negative helicity. Since the scattering cross section is proportional to the ratio of the number of scattered protons, N_s, to the number of incident protons, N_p, the longitudinal analyzing power A_z can be written as

$$A_z = (\sigma^+ - \sigma^-)/(\sigma^+ + \sigma^-) = \frac{1}{|P_z|} (N_s^+/N_p^+ - N_s^-/N_p^-) / (N_s^+/N_p^+ + N_s^-/N_p^-)$$

where P_z is the magnitude of the beam polarization.

We briefly describe our experimental setup (cf. Fig.1): Polarized protons (1.2 µA on target) are produced in the SIN polarized ion-source. After accelerating the beam in the SIN injector cyclotron to 50 MeV a solenoid (S) precesses the vertical polarization (P_y) into the horizontal plane, and a 47.6° defelction magnet (M) produces a longitudinally polarized beam. Protons scattered in a 100-atm H_2 target (T) by 23°-52° enter a cylindrical ionization chamber (diameter 4 cm) filled with 1 atm H_2.
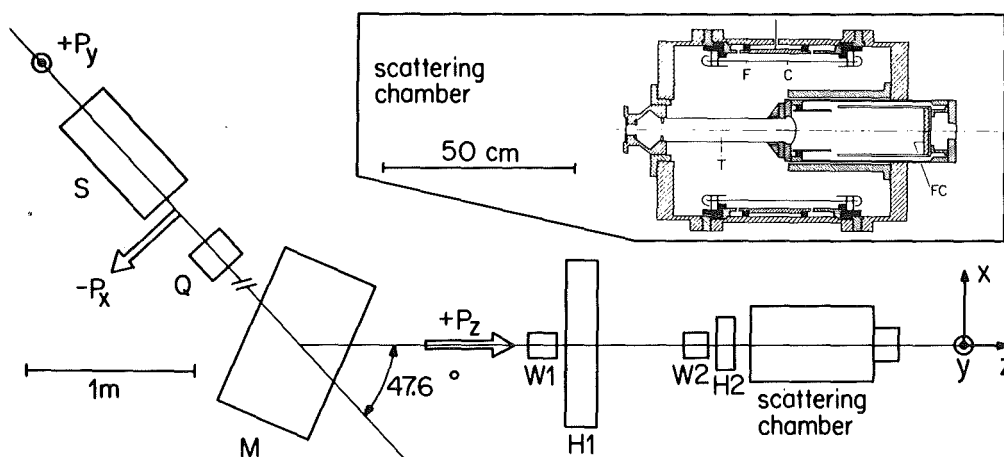
Fig. 1: Schematic diagram of the experimental arrangement. The figure shows the spin precession elements (solenoid S, deflection magnet M), the beam scanners H1 and H2, the beam modulation elements Q, W1, W2 and the scattering chamber. The inset shows the scattering chamber in more detail: the target vessel (T), the Faraday cup (FC), and the ionization chamber which consists of an aluminium foil (F) at 10 kV and the ion collector (C).

To obtain $N_s^\pm$ and $N_p^\pm$, the currents from the ionization chamber and the Faraday cup are integrated for 20 msec. Individual 20 msec measurements are separated by 10 msec dead time, during which the polarization is reversed, the digitized integrated charges are stored in a computer and beam scanners move through the beam.

The principal problem of the experiment is the elimination of systematic errors. We consider the following instrumental effects:(1) transverse polarization components, (2) beam intensity modulations correlated with spin reversal, (3) beam position and emittance modulations correlated with spin reversal, (4) spurious electronic effects, (5) asymmetry of β-decays of activated nuclei, (6) influence of the regular analyzing power in double scattering.

For pp-scattering, calculations[1] show that A_z has a broad maximum near 50 MeV (determined solely by kinematics and the pp strong phase shifts), whereas the absolute value of A_z depends of course on the weak force. Recent calculations[1] predict A_z around -3×10^{-7} at 45 MeV. The experimental results obtained so far at 15 MeV and 45 MeV by several groups give $(-2.4 \pm 0.7) \times 10^{-7}$, when all measurements are referred to 45 MeV, a result which is heavily dominated by our result $(-2.3 \pm 0.8) \times 10^{-7}$, which includes previous data[3].

References
1) W. Haeberli, Proceedings of the 5th Int. Symp. on Polarization Phenomena in Nuclear Physics, Santa Fe 1980, p.1340
2) M. Simonius, Phys. Lett. 41B(1972)415
3) R. Balzer et al., Phys. Rev. Lett. 44(1980)699

3.5 INSTRUMENTATION AND APPLICATIONS

3.5.1 A New Magnetic Spectrometer for the Scattering of Low Energy Pions on Nuclei to be Installed at SIN

H.A. Enge[+], W. Kluge, H. Matthäy, H.A. Thiessen[++], and C.A. Wiedner[+++]

Kernforschungszentrum Karlsruhe, IK II und Universität Karlsruhe

[+] MIT Boston, Laboratory for Nuclear Science
[++] LAMPF, Los Alamos; MPI für Kernphysik,Heidelberg; CERN, Geneva
[+++] MPI für Kernphysik,Heidelberg

A new magnetic spectrometer for the scattering of low energy pions on nuclei will be built during 1981/1982. The concept was developed in the last year. The spectrometer will consist of a quadrupole triplet and a split-pole magnet (QQQDD type). The split-pole part of the instrument will be a stand-alone spectrometer capable of analyzing a range of 70 to 240 MeV/c pions with a solid angle of 20 msr at a field strength of 1.33 T. The quadrupole triplet refocuses the target spot onto an object detector about 50 cm from the entrance of the split-pole and to a waist in the middle of the split-pole. The momentum range will be ±20%, the dispersion D = 1.45 cm/% in the focal plane, the magnification M = 0.67, the D/M ratio consequently 2.16 cm/%. The mean radius of the dipoles will be 50 cm, the deflection angle 60°. Raytrace calculations showed that the aberrations for the split-pole are remarkable small. In particular, the smallness of the x/θ^3 and $x/\theta^2\delta$ terms are unusual for this kind of instrument. Remaining aberrations are of passing interest since the momentum will be determined between the object and the focal plane by multiwire chambers. Further optimizations in order to maximize the transmitted phase space through the quadrupole triplet are presently underway. Fig.1 shows a preliminary sketch of the spectrometer.
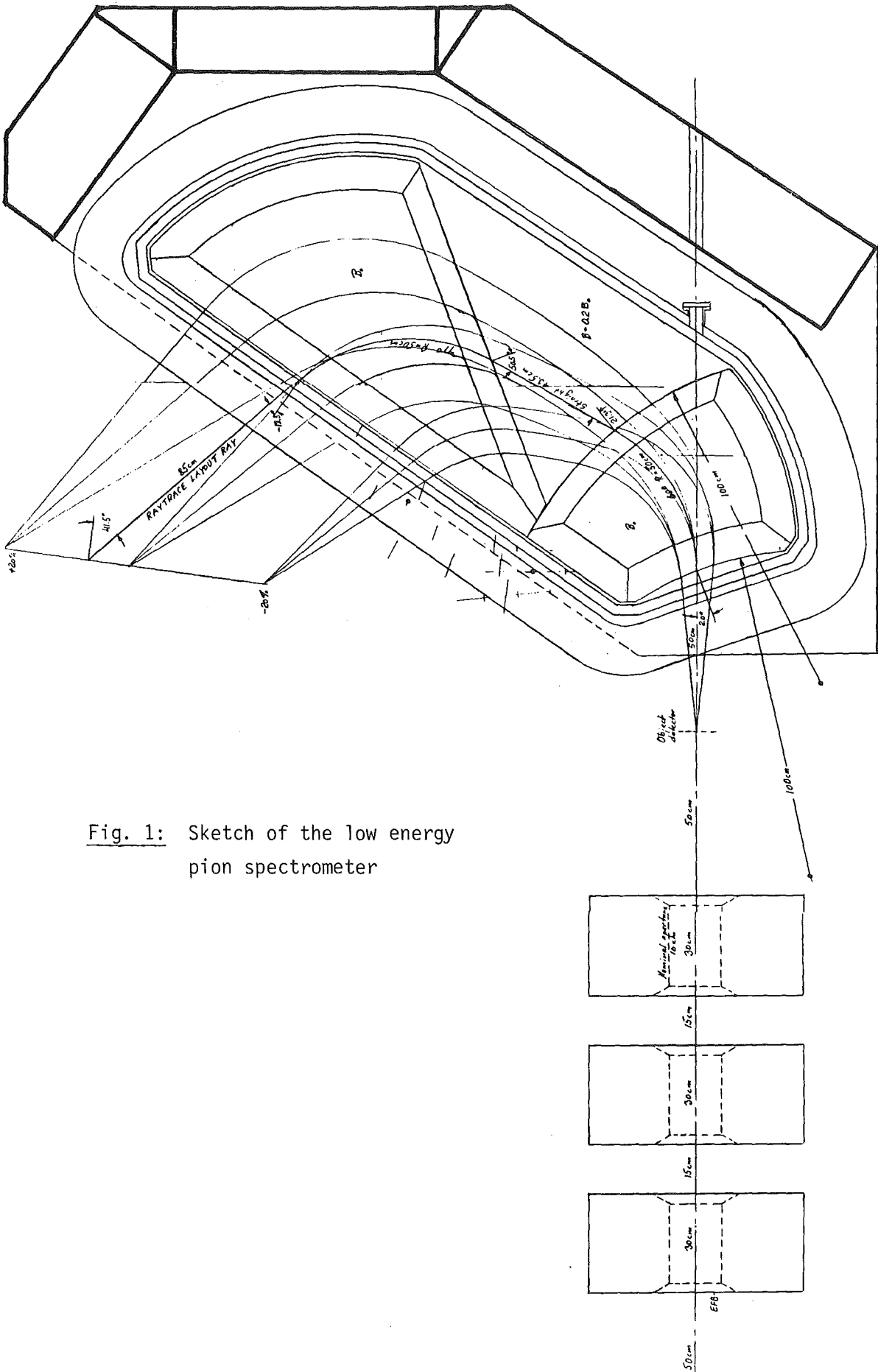
Fig. 1: Sketch of the low energy pion spectrometer

3.5.2 <u>A Computer Simulation of the Orbits of Charged Particles in a</u>
       <u>Cyclotron Trap</u>

P. Blüm, L.M. Simons

Kernforschungszentrum Karlsruhe, IK II und Universität Karlsruhe

The measurement of antiprotonic K_α X-rays in hydrogen (deuterium)
is a long standing problem still not solved in medium energy physics.

Recent calculations[1] show that it should be possible to observe
this transition in gaseous targets with pressures less than 10 Torr.
Here, the difficulty arises that only a small number of antiprotons
can be stopped in such a target if not special means are developed.

In a proposal to CERN we developed the idea to use a cyclotron
like field where the antiprotons are injected with a certain momen-
tum corresponding to its radial position at a given magnetic field.
Guided by the focussing properties at the cyclotron field the anti-
proton will then spiral into the center of the system.

Several calculations were performed in order to determine the in-
fluence of multiple scattering at different target pressure on the
beam dynamics at the antiproton. It was studied which momentum width
and angular divergence of the initial beam can be accepted by our system.

As criteria for the determination of the acceptance a cylindrical vo-
lume for the stopping region was defined with a radius of 4 cm and
a length of 10 cm with the axis of this cylinder coincident with the axis
of the system.

It could be shown that even a beam with a $\Delta p/p$ at about 20% can be
accepted the better the lower the pressure. The angular divergence of

40 mrad which is typical for the beam we want to inject will be easily accepted.

Also the focussing properties compensate for multiple scattering of particles in the course of the slowing down process resulting in a well defined stopping distribution in the center of the system.

The calculations performed served as a basis for the design of a superconducting split coil magnet system, which is now under discussion.

References

1) Edith Borie, unpublished report (1979)

3.5.3 An Experimental Ensemble Used for the Study of Proton-Proton Scattering at SIN[*]

D. Besset, Q.H. Do, B. Favier, L.G. Greeniaus, E. Heer, R. Hess,
C. Lechanoine-LeLuc, D. Rapin, D.W. Werren
DPNC, University of Geneva, Switzerland

M. Daum, S. Mango, E. Steiner, G. Vecsey
SIN, Villigen, Switzerland

Ch. Weddigen
Kernforschungszentrum Karlsruhe, IK II

An experimental program on the proton-proton scattering is presently running at SIN. This article gives the technical details of the employed instruments and equipments. It reviews in particular the SIN polarized proton beam, the large scale equipments, the LH_2 and the polarized targets, the detectors, the electronics, the on-line computer and the different basic layouts. Eventually these materials may be splitted into separated articles. However, we found more valuable to present here a complete picture which reflects the "state of the art".

3.5.4 An Azimuthal Segmented Cylindrical Drift Chamber System with Two-Dimensional Readout[*]

U. Raich, P. Blüm, M. Meyer
Kernforschungszentrum Karlsruhe, IK II

The construction of a low mass, self-supporting cylindrical drift chamber, which is segmented in the azimuthal direction, is described. The second coordinate is determined by the charge division method. The left-right ambiguity is solved by staggering the five anode-wires of each module by ±0.25 mm. In addition to the constructional problems the electronic processing of the chamber signals and first measurements on a test module are presented.

3.5.5 Set-Up and Test Measurements on a Segmented Drift Chamber with Two-Dimensional Readout

U. Raich, P. Blüm, R. Guigas, H. Koch, Th. Köhler, M. Meyer, B. Richter
Kernforschungszentrum Karlsruhe, IK II und Universität Karlsruhe

During the last years we studied the possibility to measure drift time and charge amplitude from one wire simultaneously without loosing accuracy. Optimal performance was found by applying a grated negative high voltage to the cathode in order to get a constant drift velocity and a positive high voltage to the readout wire in order to optimize the gas amplification.

We developed a concept of a modular system of drift chambers consisting of 15 modules forming a cylinder of 1 m length. The mechanical details, calculations of the grated drift field and first results of a test module are described elsewhere (1). A further test of a first module was performed at CERN with p and π^- of 600 MeV/c, with the aim to optimize the electronical set-up, to determine space resolution and to develop an evaluation program. As result we found a constant drift velocity over the whole drift space and a resolution of ± 0.3 mm. The resolution along the wire was measured to 100 mm FWHM in the middle of the wire, which corresponds to 1% of the length of the wire. The resolution gets worse to about 2% at the ends of the wire. Fig.1 shows a beam spot (triggered by a scintillation counter of 0.5x0.5 cm^2) along the wire. Using the total charge amplitude of each of the 5 wires we selected the three smallest values as dE/dx information of the chamber. Thus we achieved an enormous reduction of the Landau tail of the energy loss distribution and we were able to distinguish between antiprotons and pions due to their energy loss.

Meanwhile the total system is assembled and is under test at the PS in CERN.

Reference

(1) U. Raich et al., NIM 176(1980)163
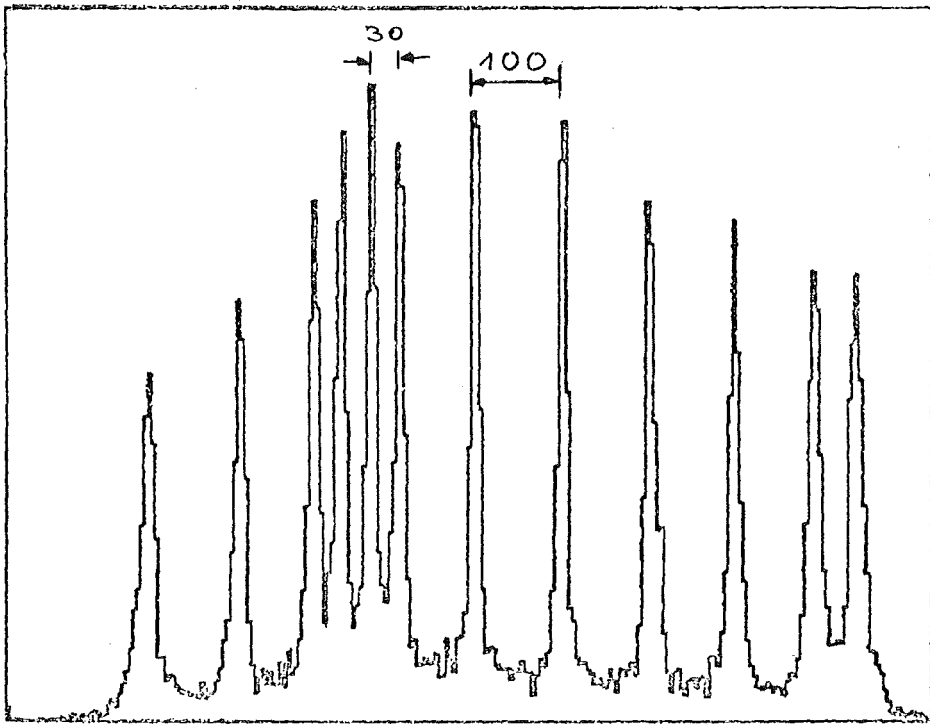
Fig. 1: Resolution along a wire

3.5.6 Development and Tests of Multiwire Proportional Chambers

H. Degitz, A. Höhne, K. Kärcher, U. Klein, R. Markus, H. Matthäy,
A. Moline[+], U. Wiedner, W. Kluge
Kernforschungszentrum Karlsruhe, IK II und Universität Karlsruhe

[+]Schweizerisches Institut für Nuklearforschung, CH 5234 Villigen

Multiwire proportional chambers of various sizes and shapes were developed and tested during the last years. They were used for various experiments:

1. for the external visualization of the pion range[1]
2. for measurements of small angle pion scattering[2]
3. for low energy elastic scattering of pions on ^{12}C and total cross-section measurements,
4. for measurements of the beam properties of the PIOTRON[3].

During the last year plane large area chambers of a size of 80x80 cm^2 and a prototype low mass cylindrical chamber of 17 cm diameter and 33 cm active length were built. The large plane chambers consist of two readout planes (x- and y-coordinates) and three high voltage planes. Each readout plane contains 384 wires of 20 μm diameter, 2 mm apart. The high voltage planes contain wires of 100 μm diameter, 1 mm apart. The measured efficiency equals 98% per plane.

The cylindrical chamber consists of 255 readout wires of 20 μm diameter, 2 mm apart fixed parallel to the cylinder envelope on two circular supports of glass fibre strengthened plastics (GFK material). High voltage is supplied by a special 140 μm thick high voltage foil with 80 strips (of 3 mm width, 1 mm apart), which is attached to an inner cylinder of Rohacell 31. The strips are inclined relatively to the readout wires by an angle of 49°. The gap widths are 5 mm, the readout wire tension is 60 p. The high voltage is supplied by a copper plated capton foil attached to the inner side of an outer Rohacell cylinder. The inner and outer Rohacell cylinders contain the detector gas. Readout electronics is applied as well to the readout wires as to the 80 high voltage strips. This way the coordinates of an incident charged particle can be registered in two dimensions.
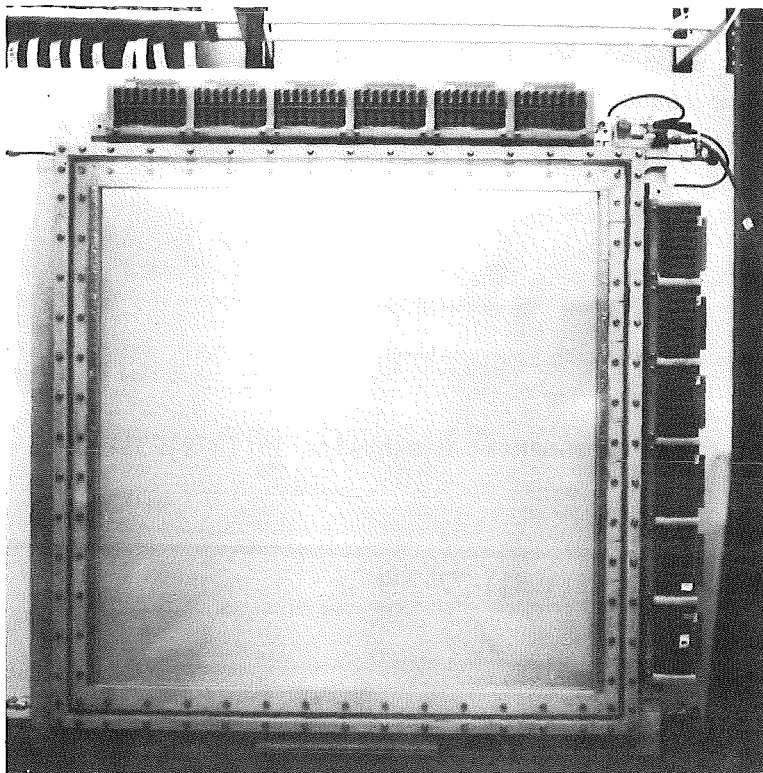
Fig.1: Plane multi-
wire proportional
chamber of a size
of 80 x 80 cm^2
(384 x 384 wires).
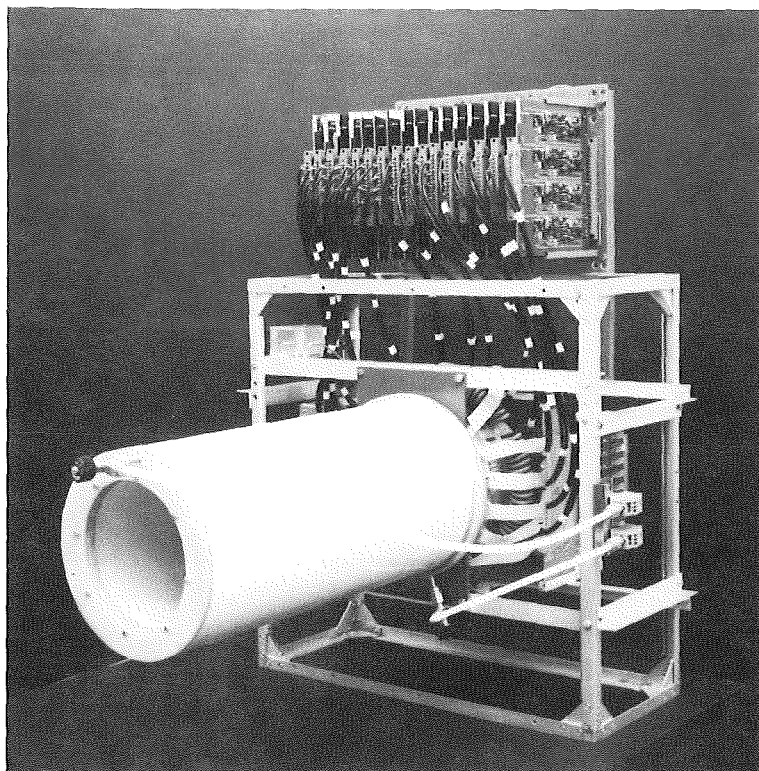
Fig. 2: Cylindrical multi-
wire proportional
chamber.

3-56

Fig. 1 shows a plane large area chamber, while Fig. 2 shows the cylindrical chamber, revealing the readout wires parallel to the cylinder envelope and the high-voltage strips, inclined by 49° to the readout wires.

References

[1] H. Matthäy et al., Radiation and Environmental Biophysics 16(1979)231-237; SIN Newsletter 11(1979)58

[2] H. I. Amols et al., Phys. Med. Biol. 26(1981)277-289

[3] H. Degitz et al., SIN Newsletter 13(1980)46.

3.5.7 Experimental Investigations of the External Visualization of Stopping Density Distributions of Pions in Biological Matter

K. Hofmann, H. Matthäy, H. Degitz, W. Kluge, U. Klein
Kernforschungszentrum Karlsruhe, IK II und Universität Karlsruhe

The aims of this work were twofold:
to clarify the basic physical aspects of an external pion range monitor and to propose a practicable device for pion irradiations at SIN. The following processes occurring within the stopping region were exploited for the external visualization:

1. The radiative capture of pions on protons $\pi^- p \rightarrow n\gamma$
   (by means of the registration of $n\gamma$-coincidences)

2. The decay sequence $\pi^+ \rightarrow \mu^+ \rightarrow e^+$ (for positive pions only)
   (by means of the detection of positrons)

3. The radiative capture of pions on nuclei like carbon or oxygen
   (by means of the detection of high energetic photons).

In the last year detailed investigations for the optimization of the external visualization detecting the high energetic photons from the radiative capture of negative pions on carbon and oxygen, carried out in 1979, were evaluated. These photons were converted into electrons and positrons either within the target material itself or in an external Pb-converter. They were collimated by a Pb-collimator in order to define their direction. Three cases were distinguished electronically:
a) the emission of charged particles, i.e. protons, or electrons due to the conversion of photons within the target volume;
b) the emission of neutral particles, i.e. neutrons and photons from the target converted in the Pb-collimator and Pb-converter;
c) the emission of neutral particles from the target, converted in the Pb-converter exclusively.

Fig. 1 shows the measured full width at half maximum (FWHM) of the pion range peak as a function of the minimum energy of the detected particles for a water

target. Full circles indicate case a), open circles indicate case b), triangles and squares denote case c) with a 3 mm and 6 mm thick Pb-converter, respectively. It turnes out that the best possible spatial resolution for monitoring the pion range is obtained for cases a) and c). The spatial resolution of the range monitor not including the stopping density distribution of pions equals 16 mm (FWHM). In addition the detection efficiencies as function of the minimum energy of the detected particles were measured, the multiple scattering within the target volume by varying the target extensions perpendicular to the beam axis was investigated and the possible use of high energetic protons and neutrons from the stopping region for visualization purposes was studied. The proposed range monitor appears to be of particular value for tests of therapy plans at the new medical pion facility PIOTRON at SIN. The restricted available space at the PIOTRON complicates the operation of such a range monitor in vivo, i.e. during patient irradiations.
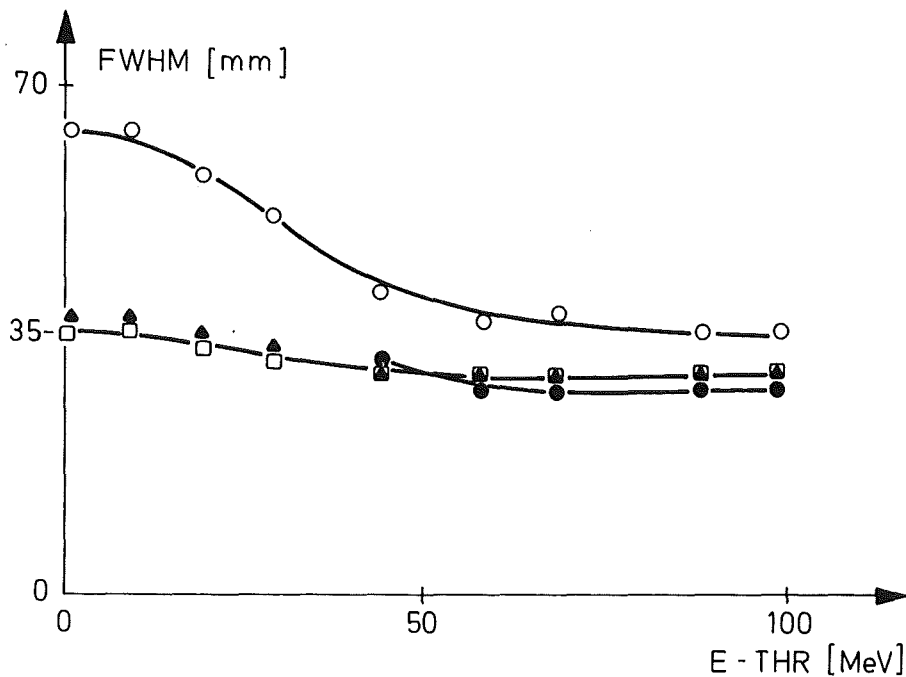
Fig. 1: Full width at half maximum (FWHM) of the pion range peak as a function of the minimum energy of the detected particles for a water target. For the various symbols used see text.

3.5.8 Test of a Pion Range Monitor Using the Radiative Capture of Pions on Protons $\pi^- p \to n\gamma$ [*]

G. Büche, W. Kluge, H. Matthäy, A. Moline[+], D. Münchmeyer, D. Schmidt
Kernforschungszentrum Karlsruhe, IK II und Universität Karlsruhe

[+]Schweizerisches Institut für Nuklearforschung (SIN), CH-5234 Villigen, Switzerland

The present paper demonstrates that neutron-photon pairs from radiative capture of stopped pions on chemically bound protons can be used to measure the range of negative pions within phantoms or a patient. Experimental results are given for a polyethylene and a water target of realistic size as well as for a Rando phantom. Monte-Carlo calculations were carried out in order to study the influence of various sizes of treatment volumes, detector geometries and neutron scattering within the targets upon the accuracy of the pion range determination. The results reveal clearly that a pion range monitor for the control of therapy plans and for actual patient irradiations can be designed according to the proposed principle. The absorbed dose required for a measurement is of the order of 0.1 Gy for a single pion beam, if one aims at an accuracy of range determination of a few millimeters.

3.5.9 Distributions of Absorbed Dose from π^--Meson Beams Calculated from a New Monte Carlo Program[*]

G. Büche, G. Przybilla
Kernforschungszentrum Karlsruhe, IK II and Universität Karlsruhe

We describe the structure and the physical input data of a new
Monte Carlo program for calculations of the absorbed dose which
is transferred by negatively charged pions to tissue equivalent phantoms.
The program is based mainly on experimentally determined input data.
Contributions to absorbed dose from nuclear reactions of pions in flight
and from nuclear fragmentation following the absorption of stopped pions
were studied in detail. The resulting dose distributions are presented
for cases of narrow as well as extended parallel beams of π^--mesons
with an initial average momentum of 170 MeV/c.

3.5.10 Energy Deposition Spectra of π^--Particles Calculated from Pion Nucleus Interaction Data

G. Büche

Kernforschungszentrum Karlsruhe, IK II

The biological effectiveness of an irradiation with negatively charged pions is not fully parametrized by the physical dose at a given site. Therefore, at least the ionization density connected with the energy transfers to the matter should be known. More exactly, the relative biological effectiveness (RBE) of a given absorbed dose can be deduced from the distributions of linear energy transfer (LET) or lineal energy (y). Continuing our work[1] on distributions of absorbed dose from pions, we have calculated LET- as well as y-spectra for the two characteristic regions of a depth dose curve on the basis of a comprehensive set of data from experimental intermediate energy physics with pions.

The main results are reproduced in Fig.1. The two upper parts show the relative doses for the plateau and Bragg-peak regions, respectively, as a function of LET_∞. The plateau spectrum (left) reveals a large contribution from fast pions within a narrow interval of LET_∞ and only a small amount of energy is lost from particles generated within strong interaction processes on nuclei of the phantom. The Bragg-peak spectrum shows a very broad shape, where all of the various secondary particles generated from nuclear capture processes contribute with their corresponding energy losses. This spectrum is characterized by a peak of contributions from hydrogen isotopes, a flat part at intermediate values of LET, the so-called ^{4}He edge, and a small contribution from heavy fractions.

For the matter of a comparison between the calculated LET-spectra and the measured spectra of lineal energy y at least two effects have to be taken into account: the distribution of cord lengths of particles crossing the detector volume and the production of δ-rays including their escape from the detection volume. The former was regarded assuming a spherical shape of 1 μm radius for the sensitive volume. The latter effect has been treated in a semi-empirical way. The average energy of δ-rays, which is

transported out of a cylinder of 1 μm radius around the particle track was calculated using the formalism of Butts and Katz[2], whereas the shape of the y-spectrum for these electrons was taken from the work of Kliauga and Dvorak[3], who used photoelectrons of appropriate energies. The results from this approximate transformation of the LET-spectra into energy deposition spectra are given by the histograms in the lower half of Fig. 1. The points reproduce experimentally obtained spectra of lineal energy from the work of Schuhmacher et al.[4]. The overall agreement between the calculated and the experimental energy deposition spectra is very good and illustrates the equivalence of data which were obtained from microdosimetry and from nuclear physics experiments with negatively charged pions. Further agreement may be obtained in the case of the plateau-spectrum by the microscopical treatment of small energy transfers and in the case of the Bragg-peak spectrum by inclusion of dose contributions from pion energy straggling which are expected around 1 keV μm^{-1}. The main advantages of our method are to give a simple way for the calculation of energy deposition spectra, to include automatically the individual beam conditions, and to get a further parameterization of the dose, at a fixed value of y, by the particle nature from which the dose is transferred. The last point is expecially useful with respect to estimates of radiation quality for biomedical purposes in view of the existence of track structure effects.

References

[1] G. Büche and G. Przybilla, Nucl. Instr. and Meth. 179(1981)321

[2] J.J. Butts and R. Katz, Radiat. Res. 30(1967)855

[3] P. Kliauga and R. Dvorak, Radiat.Res. 73(1978)1

[4] H. Schuhmacher, H.G. Menzel, H. Blattmann, and M. Salzmann
Proc. 7th Symposium on Microdosimetry, Oxford, U.K., 1980
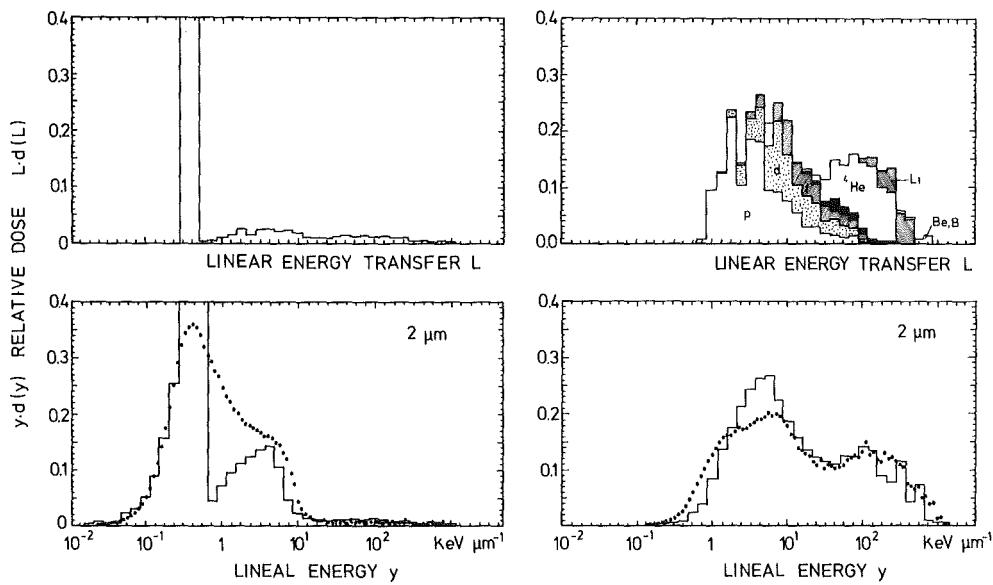
Fig.1: The relative absorbed doses in the plateau region (left half) and in the Bragg-peak region (right half) of the dose distribution originating from an irradiation of the water phantom by a beam of negatively charged pions (initial momentum 176 MeV/c ± .85% FWHM), water depths 14.2 and 20.1 g cm^{-2}). The dotted curves are reproduced from the experimental work of Schuhmacher et al.[4]

3.5.11 Multiple Scattering Distributions for Therapeutic Pion Beams[*]

H.I. Amols[+], G. Büche, W. Kluge, H. Matthäy, A. Moline[++],D.Münchmeyer
Kernforschungszentrum Karlsruhe, IK II and Universität Karlsruhe

[+] Cancer Research and Treatment Center, University of New Mexico, Albuquerque, NM

[++]Swiss Institute for Nuclear Research, 5234 Villigen, Switzerland

Accurate treatment planning for therapeutic beams of negative pions requires knowledge of the multiple scattering of pions in biologically relevant materials. Complete spatial and angular scattering distributions have been measured for pions in scatterers of carbon, water and calcium. Measurements were made for targets varying in thickness from 0.5 to 21 g cm^{-2} and for pions with ranges of approximately 12 and 20 g cm^{-2}. An array of scintillators, multiwire drift and multiwire proportional chambers was used to record the scattering of individual particles. These data are compared with the results of Molière scattering theory. The implications for pion treatment planning are discussed.

3.5.12 Measurements of the Properties of 60 Single Beams of the New Medical Pion Channel 'PIOTRON' at SIN

U. Wiedner, H. Matthäy, H. Degitz, K. Hofmann, U. Klein, W. Kluge, R. Markus, A. Moline[+]
Kernforschungszentrum Karlsruhe, IK II and Universität Karlsruhe

[+]Schweizerisches Institut für Nuklearforschung, CH 5234 Villigen (AG), Switzerland

The precise knowledge of the beam properties is one of the basic requirements of therapy planning for radiation therapy with negative pions. For the new SIN superconducting pion therapy channel an appropriate device was constructed which can be rotated with high precision around the axis of the patient treatment chamber in order to determine the parameters of the 60 single beams. The detection system consisted of three scintillation counters and three multiwire proportional chambers to identify electrons, muons, and pions and to reconstruct the particle trajectories. Beam profiles and divergencies in both x- and y-direction (which are parallel to the extensions of a beam slit) were measured[1]. Figs.1 and 2 show map displays of the phase space distributions in the $x-\Theta_x$ and $y-\Theta_y$ planes of a single beam, respectively. The shape of the emittance polygons, which is similar to parallelogrammes, is in accordance with magnetooptical calculations. Fig.3 shows as an example a polar diagramme indicating the position in beam direction (z-coordinate) of the x-waist, i.e. the focus in the x-direction for all 60 beams. The mean z-position is 80 mm off the centre of the PIOTRON. The deviations from exact cylinder symmetry of the x-waist position are of the order of ± 5 mm.

Reference

[1]H. Degitz et al., SIN Newsletter 13(1980)46
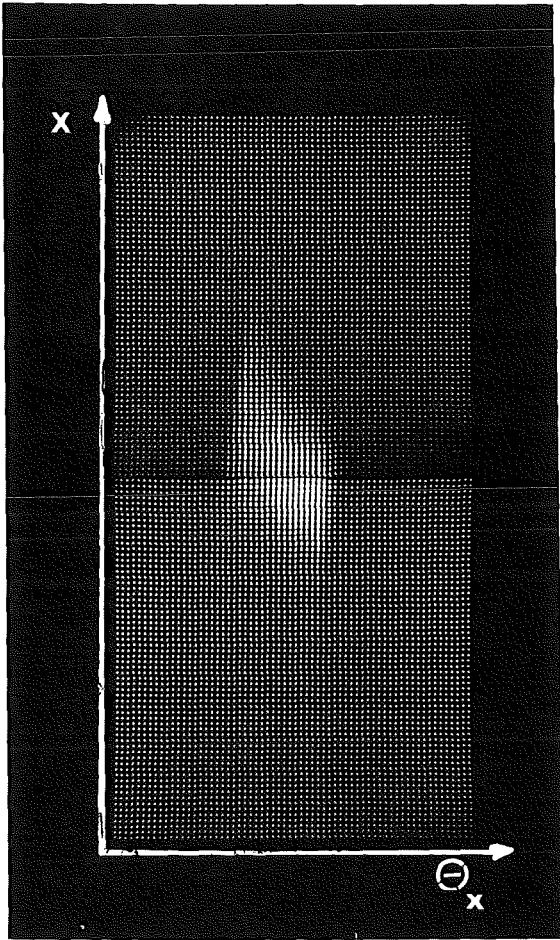
Fig.1: Map display of the phase space distribution in the x-Θ_x plane for a single beam
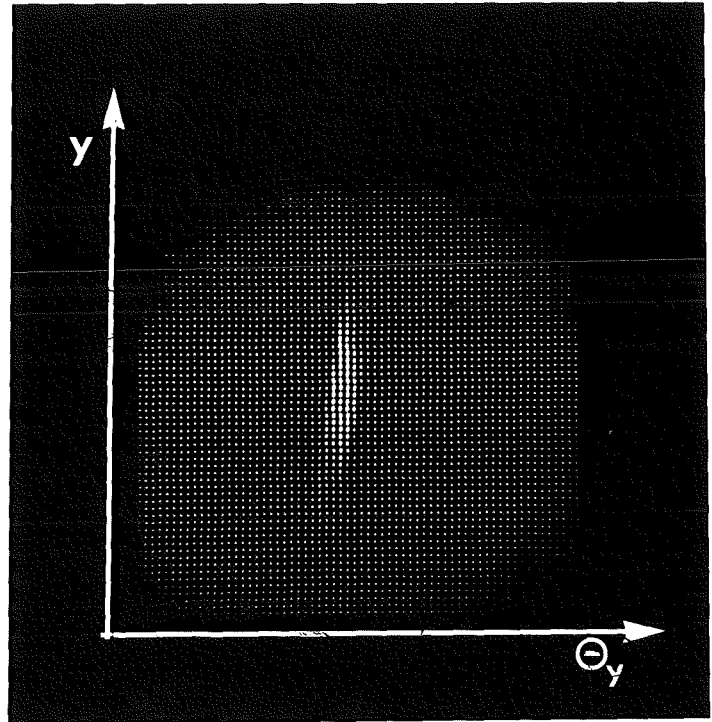
Fig.2: Map display of the phase space distribution in the y-Θ_y plane for a single beam
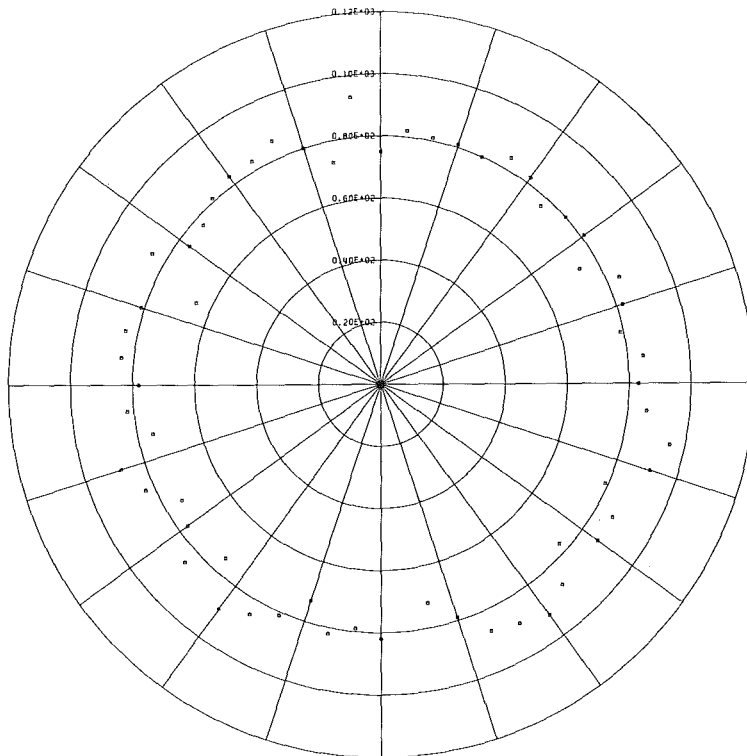
Fig.3: Polar diagramme of the position in beam direction of the x-waist for all 60 beams.

3.5.13 Calculations on Electron Cooling in Storage Rings

H. Poth, A. Wolf
Kernforschungszentrum Karlsruhe, IK II

The aim of the calculations is to predict the performance of electron cooling in LEAR on stored proton and antiproton beams in various operation conditions. In a computer simulation program, the force exerted by the electrons on individual particles of a sample during single passages of the electron beam region is calculated. This procedure is based on the work of M. Bell[1] in which cooling rates are found to be in agreement with the results of the experiments at the ICE storage ring.

The simulation, so far limited to the description of the decrease of the phase space volume of an initial distribution, is now being extended to arrive at a stationary sample distribution representing a real, continously stored particle beam. To this end, the scattering of the particles by gas molecules inside the ring and the intrabeam scattering is taken into account by applying mean growth rates for beam size and momentum spread derived from the widths of emittance and momentum distributions of the actual stored beam.

The simulation program will be used to predict the equilibrium state of the circulating beam; the working of electron cooling can be studied in the presence of additional actions of the stored beam by, e.g., stochastic longitudinal beam blow-up in connection with a slow extraction, and for different properties of the electron beam, considering variations of the electron energy and the electron motion transverse to the stored particle beam.

Reference

[1]M. Bell, Cooling in ICE, CERN-EP/79-10

3.5.14 Implications of an Internal Target for Antineutron Production in LEAR[*]

M. Giesch, J. Gspann[+], W. Hardt, K. Kilian, P. Lefèvre, D. Möhl,
H. Poth[++], P. Riboni

CERN, Geneva, Switzerland
[+] Kernforschungszentrum Karlsruhe, IKVT
[++]Kernforschungszentrum Karlsruhe, IK II

Starting from the required characteristics on an internal cluster beam target for antineutron production we discuss the implications for the machine. The admissible target thickness in the presence of the beam cooling system is worked out and the resulting vacuum requirements are evaluated. The compatibility of the basic machine design with the later installation of the target is examined.

3.5.15 On the Production of Antideuterons[*]

H. Pilkuhn[+], H. Poth

Kernforschungszentrum Karlsruhe, IK II

[+]Institut für Theoretische Kernphysik, Universität Karlsruhe

We examine the possibility of producing antideuterons in antiproton-antiproton collisions through the process $\bar{p}\bar{p} \rightarrow \bar{d}\pi^-$ at the maximum of the reaction cross-section (530 MeV/c antiproton lab.-momentum) for low energy experiments. Luminosities are estimated for a collider consisting of two rings having the characteristics of LEAR. For this case the luminosity and production rates turn out to be rather low. However, with a dedicated collider for the antideuteron production, rates can be improved for experiments with low energy and stopped antideuterons. Antideuteron stop experiments could be performed directly at the intersection region. No further handling of the $\bar{d}$ would be required owing to their low energy. The advantages of this production scheme are pointed out.

3.5.16 Results from the Electron Cooling Experiments at CERN[*]

P. Møller-Petersen, M. Bell, J. Chaney, S. Cittolin, H. Herr, H. Koziol, F. Krienen, G. Lebée, G. Petrucci, H. Poth[+], T. Sherwood, G. Stefanini, C. Taylor, L. Tecchio, G. Rubbia, S. van der Meer and T. Wikberg

CERN, Geneva, Switzerland

[+]Kernforschungszentrum Karlsruhe, IK II

Through the interaction of stored protons with an electron beam of small transverse velocities and a well-defined longitudinal velocity the beam properties of the circulating protons can be highly improved within short times. This process (called electron cooling of protons) was studied experimentally on 10^8 protons circulating in the ICE (Initial Cooling Experiment) storage ring at 46 MeV.

A short introduction to the electron cooling theory is given followed by a description of the experimental technique. The results of the measurements are presented. Transverse (reduction of proton beam divergence and diameter) and longitudinal (reduction of the proton beam momentum spread) cooling were investigated in detail. Cooling times (1/e) of 1.2 s (transverse) and 0.3 s (longitudinal) could be achieved. Equilibrium proton beam sizes of about 0.8 mm (FWHM) and beam divergence of about 0.2 mrad were obtained. The minimal proton beam momentum spread which could be reached was 4×10^{-5}. The production rate of neutral hydrogen originating from electron capture of protons in the cooling region was measured for various configurations.

3.5.17   On the Use of the ICE-GUN for Electron Cooling in LEAR[*]

H. Haseroth, Ch. Hill, P. Møller-Petersen, H. Poth[+]

CERN, Geneva, Switzerland

[+]Kernforschungszentrum Karlsruhe, Institut für Kernphysik II

The possibility of using the ICE-cooling system (see 3.5.16) for electron cooling of antiprotons stored in LEAR (Low Energy Antiproton Ring) is studied. A short description of the ICE-system and the relevant cooling results are given. The cooling performance in LEAR is worked out for various operation conditions. It turned out that the ICE-cooler, after some improvements would be a very efficient cooling system in the momentum range between 100 MeV/c - 300 MeV/c, considerably improving the stored beam quality and allowing the operation of an internal target. An upgrading to 600 MeV/c seems to be possible. The various modifications of the ICE-system to be performed prior to installation in LEAR are described and cost, manpower and time schedule are estimated.
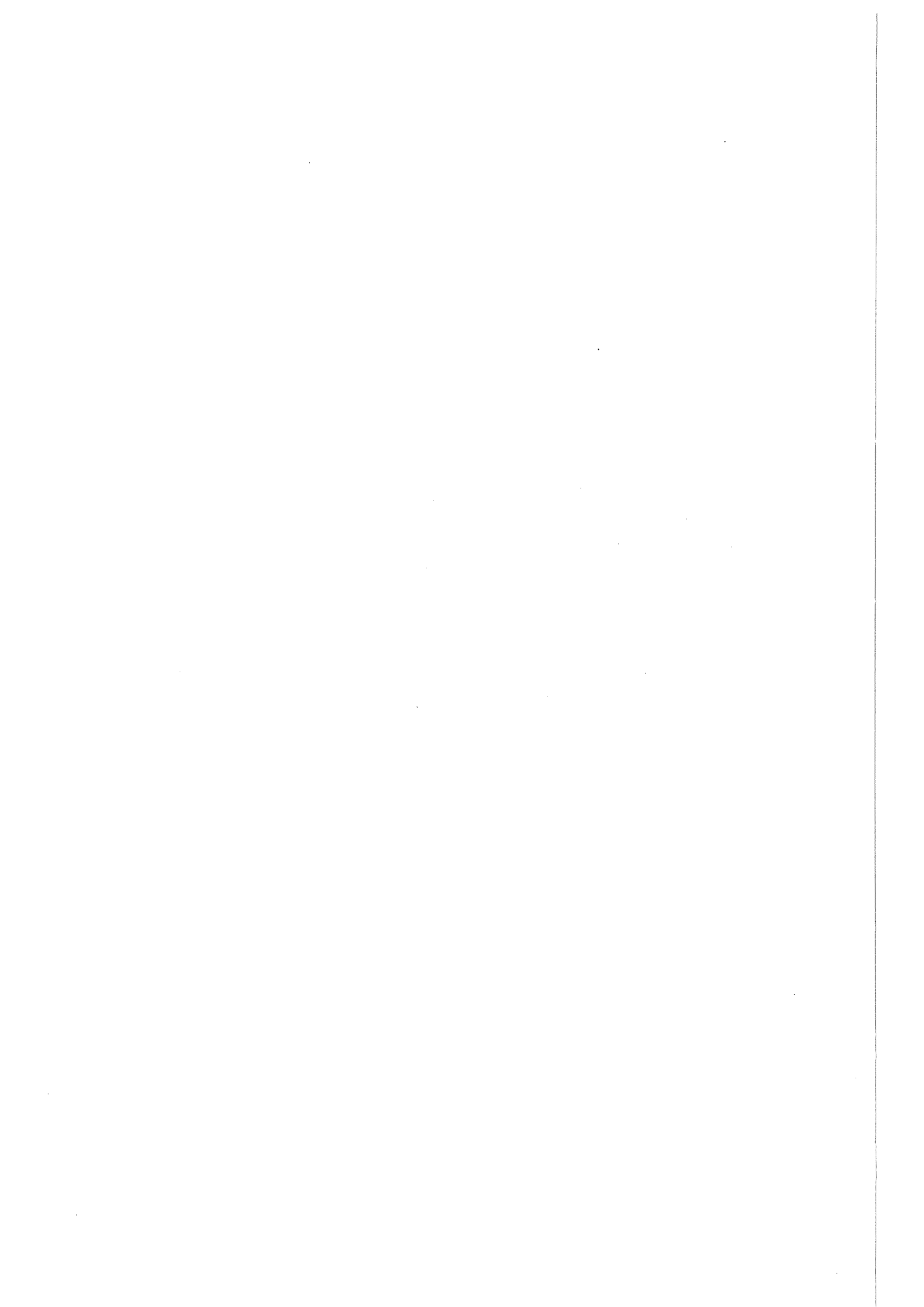
4. HIGH ENERGY PHYSICS

4.1 PION- AND PHOTOPRODUCTION EXPERIMENTS

For two major experimental activities of the past years - the study of neutral final states at Serpukhov and the investigation of photoproduction of proton antiproton pairs at DESY - the data analysis and dissertation work has been finished[1,2,3]. Two final publications are in preparation, two others have been submitted already.

4.1.1 Analysis of the Reaction $\pi^-p \to \pi^0\eta n$ at 40 GeV Beam Momentum *

W.D. Apel, K.H. Augenstein, F. Abdel-Khalek, M. Krüger,

H. Müller, H. Schneider

Kernforschungszentrum Karlsruhe, IK 1 and Universität Karlsruhe

The reaction $\pi^-p \to \pi^0 \eta$ has been analyzed using data of an
$\big|_{\to 2\gamma}\big|_{\to 2\gamma}$
experiment performed at Serpukhov 70 GeV accelerator, with the NICE 648 channel hodoscope spectrometer for γ ray detection. Events with 4γ seen are used for the analysis. A method is applied, which allows the determination of the number of $\pi^0\eta$ events for each mass, $\cos \theta_{GJ}$ and t bin. Mass-spectra, t-distributions and decay angular distributions for the $\pi^0\eta$ system are presented. The cross section for the production of A_2^0 is found to be 2.7 ± 1.1 µb at 40 GeV/c beam momentum.

No indication of a resonant 1^- state in the $\pi^0\eta$ system is observed, in spite of the fact that this state is allowed for the $\pi^0\eta$ system on the same footing as the observed 0^+ and 2^+ resonances. A $q\bar{q}$ state however with $J^P = 1^-$ cannot decay into $\pi^0\eta$. The absence of this resonant state provides one of the simplest supporting evidences for the quark model of the hadrons.

* in Collaboration with Pisa, Serpukhov, Wien and CERN; submitted to Nucl.Phys.

4.1.2 Cross Section and $p\bar{p}$ Invariant Mass Distribution of the Reaction $\gamma p \rightarrow p\bar{p}p$ at $4.7 < E < 6.6$ GeV *

J. Bodenkamp, D.C. Fries, A. Markou, E. Seitz
Kernforschungszentrum Karlsruhe, IK 1 and Universität Karlsruhe

The photoproduction of proton antiproton pairs in a 7 GeV tagged photon beam at DESY has yielded the following results[1,2]:

- a measurement of the total cross section of the reaction $\gamma p \rightarrow p\bar{p}p$ at 5 energy bins in the energy range $4.74 \leq E_\gamma \leq 6.55$

- an uncovering of the cross dynamical features of the reaction $\gamma p \rightarrow p\bar{p}p$ in the above energy range

- the observation of a small signal in the invariant $p\bar{p}$ mass spectrum at 2.023 ± 0.005 GeV with a width of 27 ± 12 MeV, which confirms in position and width a $p\bar{p}$ mass signal reported previously by two groups[4]. which is however controversial due to two other experiments[5].

---

* in Collaboration with DESY, Hamburg;
submitted to Phys.Lett. B

References

1) A. Markou, Photoerzeugung von $p\bar{p}$ Paaren an Wasserstoff im Energiebereich 4.74 - 6.55 GeV (Dissertation, Karlsruhe), KfK 2886 (1980)

2) J. Bodenkamp, Wirkungsquerschnitt und $p\bar{p}$ Massenspektrum der Reaktion $\gamma p \rightarrow p\bar{p}p$ im Energiebereich 4.74 - 6.55 GeV (Dissertation, Karlsruhe), KfK 3179 (1981)

3) F. Abdel-Khalek, Untersuchung der Reaktion $\pi^- p \rightarrow \pi^0 \eta^0 n$ bei Pionenimpulsen von 25 und 40 GeV (Dissertation, Karlsruhe), KfK 3115 (1981)

4) P. Benkheiri et al., Phys.Lett. 68B (1977) 483
   B.G. Gibbard et al., Phys.Rev.Lett. 24 (1979) 1593

5) S.V. Cheng et al., Phys.Rev.Lett. 45 (1980) 1611
   R.M. Bionta et al., Phys.Rev.Lett. 44 (1980) 909

4.2 PHYSICS AT e^+e^- STORAGE RINGS

W.D. Apel, S. Banerjee, J. Bodenkamp, D. Chrobaczek, J. Engler,
G. Flügge, D.C. Fries, W. Fues, G. Hopp, H. Keim, H. Küster,
H. Müller, H. Randoll, G. Schmidt, H. Schneider
Kernforschungszentrum Karlsruhe, IK 1 and Universität Karlsruhe

Most efforts of the High Energy Physics group in Karlsruhe have been concentrated on an exploitation of the large CELLO spectrometer[1] which came into operation at the e^+e^- storage ring PETRA early in 1980. The CELLO detector was built and is run by a collaboration of three German (KfK and Universität Karlsruhe, MPI München and DESY) and three French institutes (Orsay, Paris, Saclay). In the following chapters performance and physics results from the first year of running are reported.

References

1) CELLO Collaboration, H.-J. Behrend et al., Phys. Scripta 23 (1981) 610
   G. Flügge et al., Phys. Scripta 23 (1981) 498

4.2.1 Layout and Performance of the CELLO LAr-Calorimeter

The calorimeter serves to detect mainly electrons and photons, which manifest themselves by their typical electromagnetic shower developing in material of high atomic number. In the CELLO calorimeter the shower propagates in plates of lead, which are grouped to stacks giving a total thickness of 20 radiation lengths. The gaps between the plates are filled with liquid argon of high purity, from which the deposited ionisation charge is collected by an electric field.

The calorimeter assembly consists of three cryostats and 20 stacks, namely 16 stacks in a large cylindrical cryostat and 2 stacks each in two end caps, which close the two forward regions in the beam direction (see fig. 1). All three cryostats are connected to one refrigerator, which reliquifies the evaporated argon gas into a common buffer tank.

CELLO

1   Beam Pipe
2   Cyl. Proportional Chambers
3   Cyl. Drift Chambers
4   Superconducting solenoids
5   Liquid Argon Calorimeters
6   Hadron Filter
7   Muon Chambers
8   End Cap Proportional Chambers
9   Drift Chambers
10 Scintillation Trigger Counters
11 Lead glass Counters
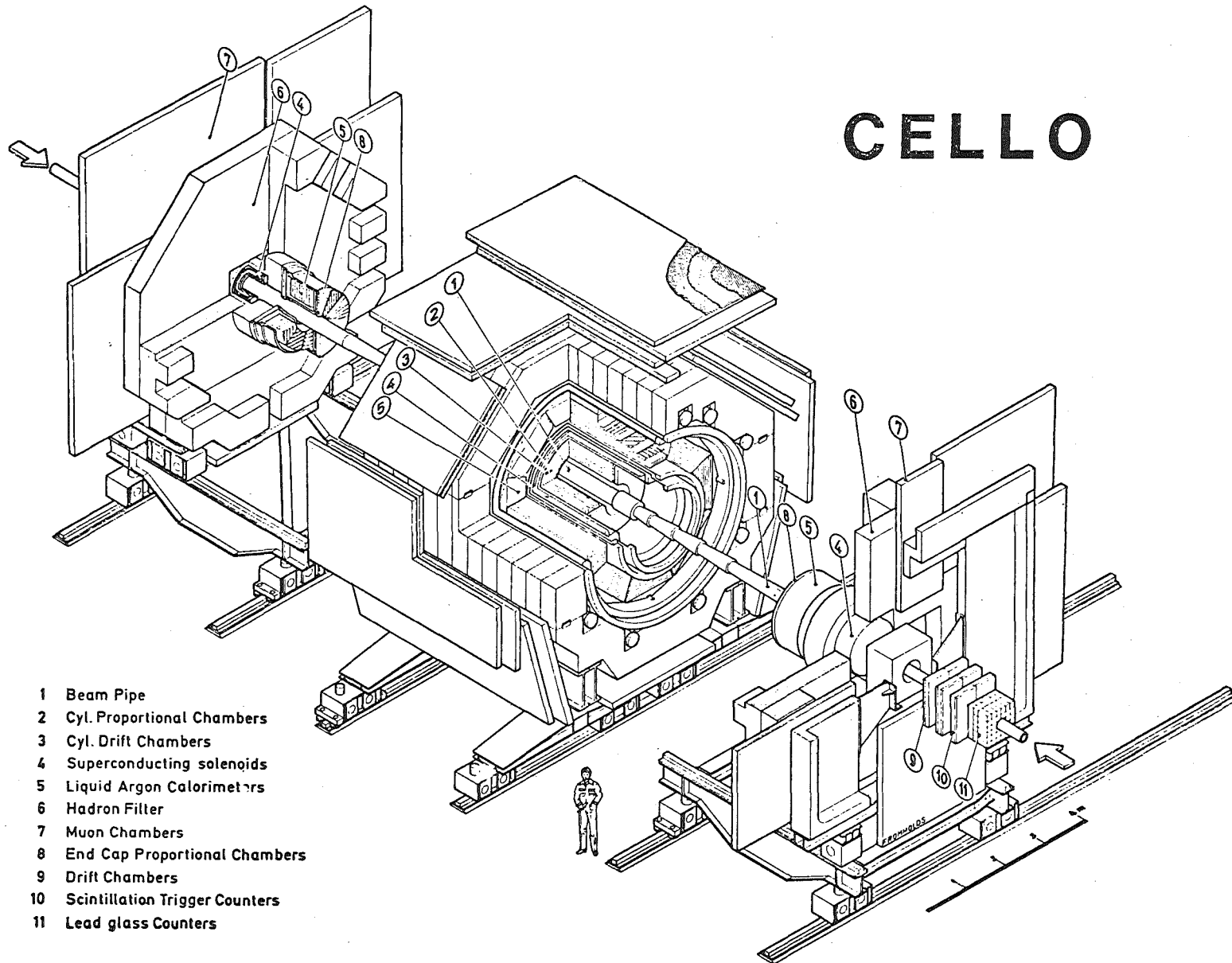
Fig. 1: Layout of the CELLO detector

The liquid flows back through regulation valves keeping the level in the cryostats constant.

The croygenic system has worked satisfactorily throughout the years 1980/81. Especially, no indication of unpurification at a 1 ppm level could be observed, the content of oxygen and other gases being continuously monitored by a Herschmeter and a gas chromatograph.

The purity of the argon with respect to electronegativ molecules is corroborated also by the high current of charge output: The collected charge is a function of the applied high voltage and the degree of purification, which is usually parametrized in equivalent O_2 impurity. By applying different voltages we obtained for the parameter 1.3 ppm O_2 equivalent. This means, that at the nominal voltage of 15 kV/cm we collect 81% of the deposited ionisation charge.

The longterm stability is monitored by the amount of charge for electromagnetic shower Q in elastically scattered Bhabha events. Over a period of months we obtained Q = (0.515 ± 0.005) pC/GeV, the stability being better than 1%.

The energy resolution is shown in fig. 2, where the charge Q for Bhabhas in one stack is plotted. A fit to the upper half of the distribution gives a resolution of σ = 3.2%. This figure deteriorates to about σ = 4%, when all stacks of the calorimeter are used. This means that the intercalibration has to be improved.

Very stable operation with respect to pick-up noise has been achieved. This enables good trigger possibilities. With a tolerable rate of $\sim$ 0.3 trigger/sec for the data acquisition system we could lower the threshold to 1.3 GeV shower energy. The coincidence conditions are: either two showers in two separate stacks or one shower in one stack and one track in the central detector. With these conditions the calorimeter trigger recuperates an appreciable amount of physical events which escape the charge particle trigger.
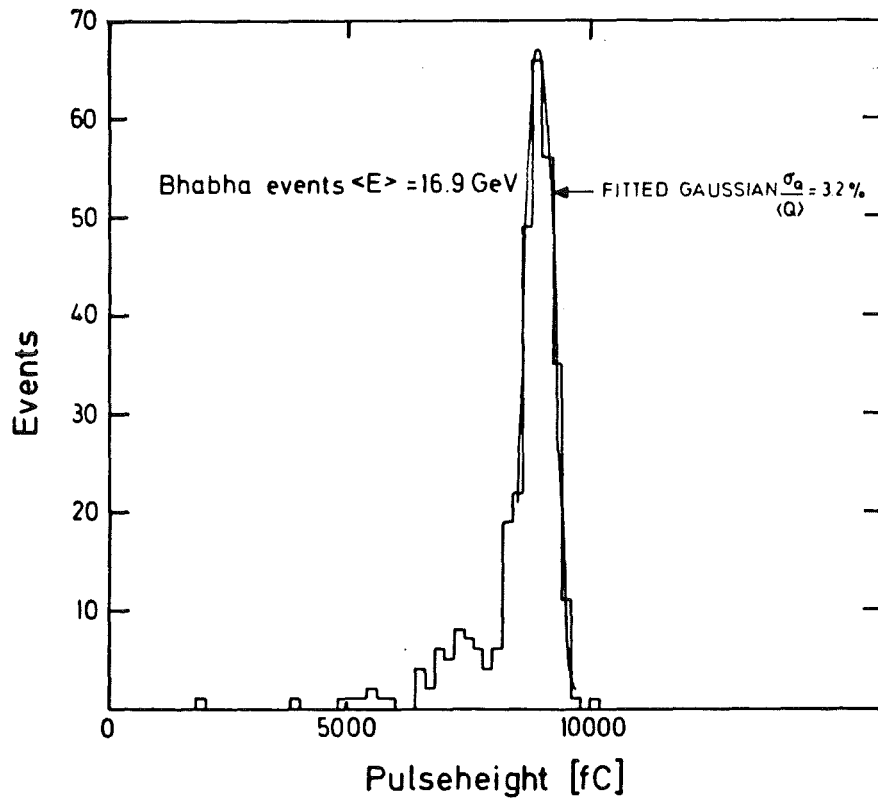
Fig. 2: Pulseheight distribution from Bhabha-scattering at 16.9 GeV beam energy.

4.2.2 The Analog-to-Digital Electronic of the Liquid Argon Calorimeter of the CELLO Detector

General layout

The electronics has been designed to be used in a system of 8000 channels of the CELLO calorimeter. Therefore, emphasis has been placed on compactness, stability against oscillations in the system and low costs. In particular the last point has influenced the choise of transistors, diodes, cables and connectors and in some cases the use of discrete components has turned out to be cheaper than hybrid circuits.

The preamplifier is directly attached to the croystat to minimise the length of the input cable. Four channels are on a board. The signals are transmitted to the counting room by an unshielded twisted pair

cable and fed into the main amplifier with 16 channels on a board.

Digitizing takes place in a sample-and-hold circuit and a comparator, which compares the pulse with a staircase voltage function generated for 24 mainamplifier cards in a common CAMAC crate simultaneously. The final data handling is organized on a read-out card, where only channels with signals above a certain noise level are transmitted via CAMAC to the computer. 64 channels are handled in one multiplexer. In the following chapter, the electronic chain will be described in more detail:

Preamplifier

The matching transformer with a core of 303 material serves to adapt the amplifier input capacitance to the capacitance of the plates of the individual detector channels. The corresponding winding ratios for minimal noise <-> signal ratio were determined experimentally. Because the transformer introduces additional parallel noise it is useful only at higher capacitance (> 500 pF).

The σ of the noise peak for all channels of a stack in the final set-up with all 8000 channels working at a time is shown in fig. 1. The plotted curve indicates the noise performance of the prototype amplifier chain under optimal conditions in the laboratory. In the final set-up the mean noise is about 30% higher.

In contrast to other LAr electronics systems, the first filter circuit is already put on the preamplifier card. This ensures better stability and facilitates the transmission to the main amplifier, for which an unshielded 64 channel twisted pair cable is used.

Main amplifier

The differential input of the main amplifier rejects noise induced on the cable very efficiently. It is followed by a second filter circuit. The signal is then fed to a sample-and-hold circuit and is stored on a charging capacitor when the trigger pulse has passed. Digitalization is performed by comparing the charging capacitor voltage with a staircaise voltage common to all channels. Duration of a step is 1 μsec.

The dynamic range of the amplifier chain output extends from noise level up to 10 Volts which corresponds to 1024 steps in the staircase
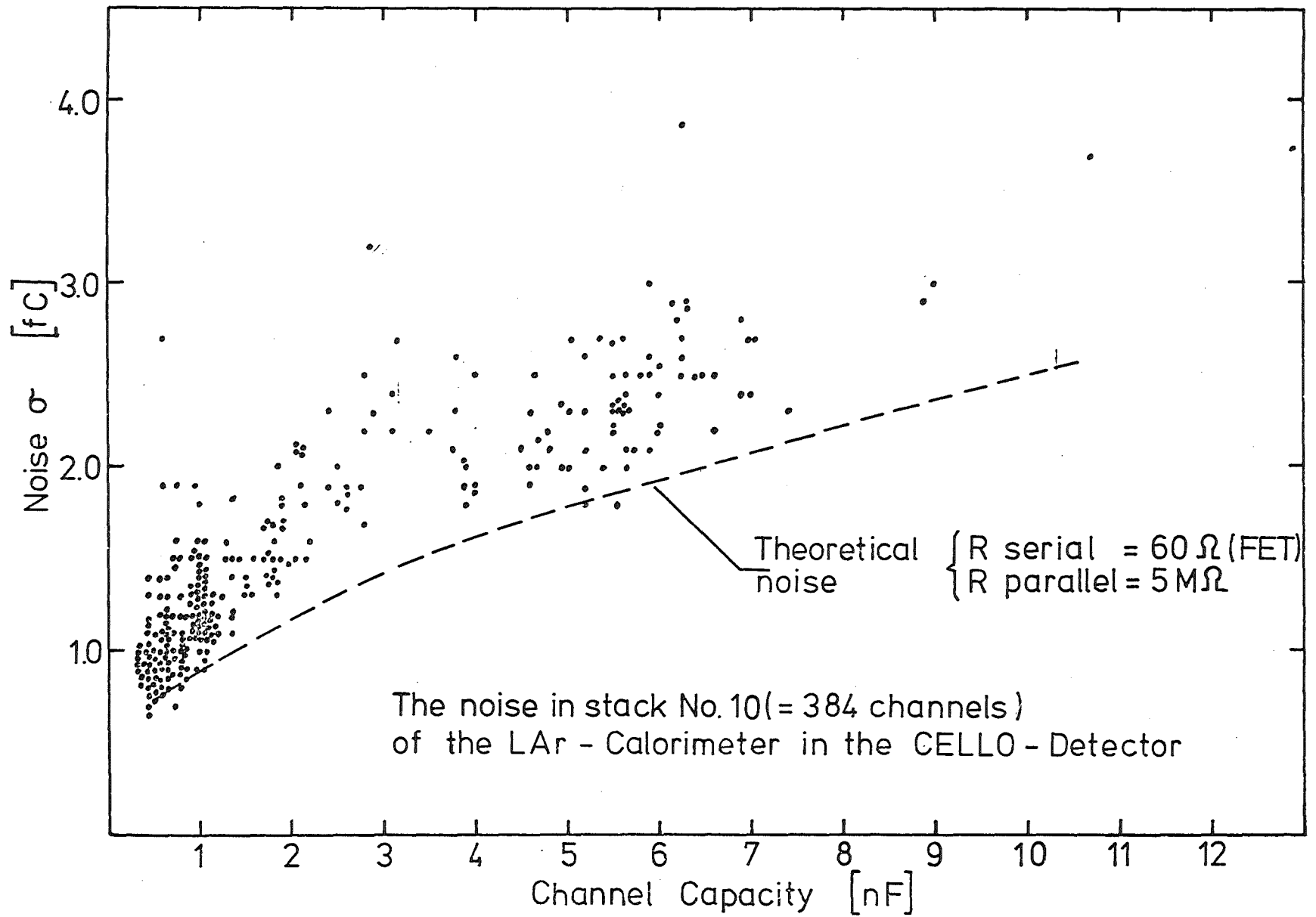
Fig. 1: Noise as a function of input capacitance

voltage (1024 counts). Deviation from linearity is about 1 in 1000. The amplification does not vary very much from channel to channel. Deviation from the mean of more than 10% is rather rare. The pedestal is normally set to about 30 channels. For trigger purposes, four discriminators are included in the circuit. An upper and lower discrimination level for the sum of 8 neighbouring channels can be set. Also the analog sum of 8 channels for a total trigger is provided at the output connector.

The Read-out Multiplexer

The 16 channels of a main amplifier are transmitted during 1 μsec by a synchronized serial signal on a coax line to the read-out multiplexer. A complete conversion time lasts 1024 μsec. To one multiplexer 4 main-amps are connected, which are transmitted in parallel. During read-out the content of each channel is compared with a level stored in a separate "threshold memory". The channels below the threshold are suppressed during read-out ("zero-suppression"). This internal scanning takes 100 nsec per channel. The thresholds can be set individually for all channels by computer.

Performance

The lead LAr calorimeter with the elctronics described above is working satisfactorily under running conditions since May 1980.

The amount of charge collected for elastic scattered electrons and positrons (Bhabha scattering) at 17 GeV is shown in fig. 2. In the upper plot the mean for the individual lead stacks is given (stack 7 is not connected). The resolution as determined for the shown sample is typically 3-4%.

As different high voltage is applied to the individual stacks, we can obtain the voltage dependence of the collected charge. The mean of channels 1-6 and channels 9-16 is plotted in fig. 3 together with a theoretical fit. The fit has as a free parameter the amount of oxygen (or other electro-negative solvents) dissolved in the LAr. From the two points one obtains the result that the loss of charge corresponds to (1.3±0.1) ppm O_2. Extrapolating to the asymptotic value we see that at
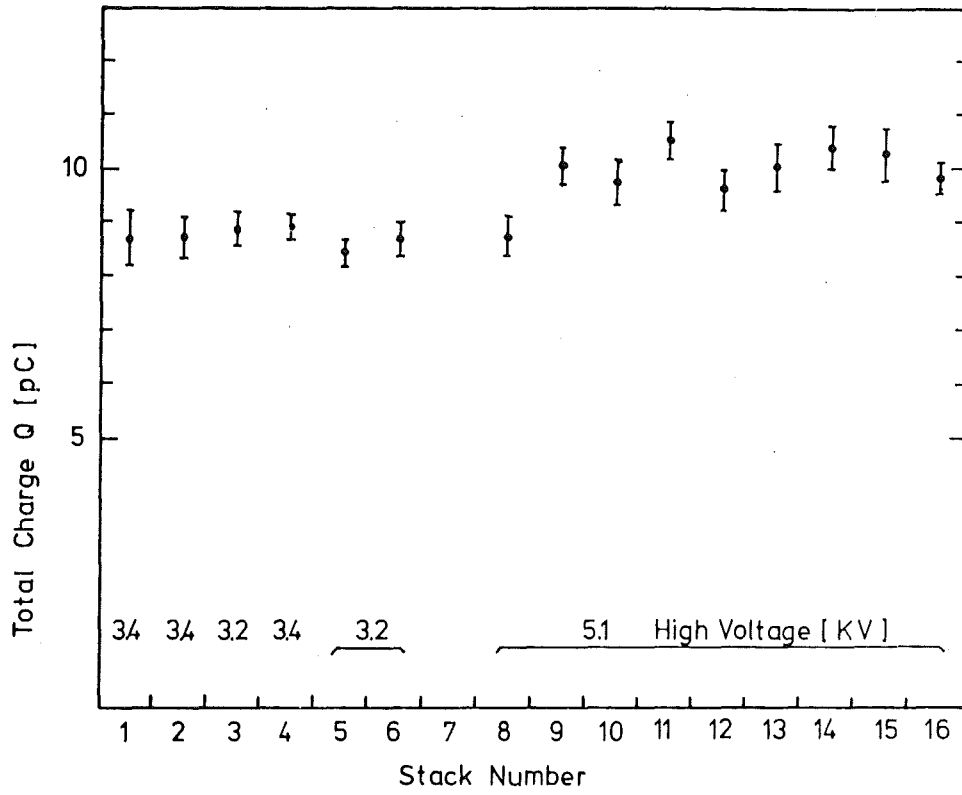
Fig. 2: Total charge collected in different stacks from 17 GeV Bhabha events.
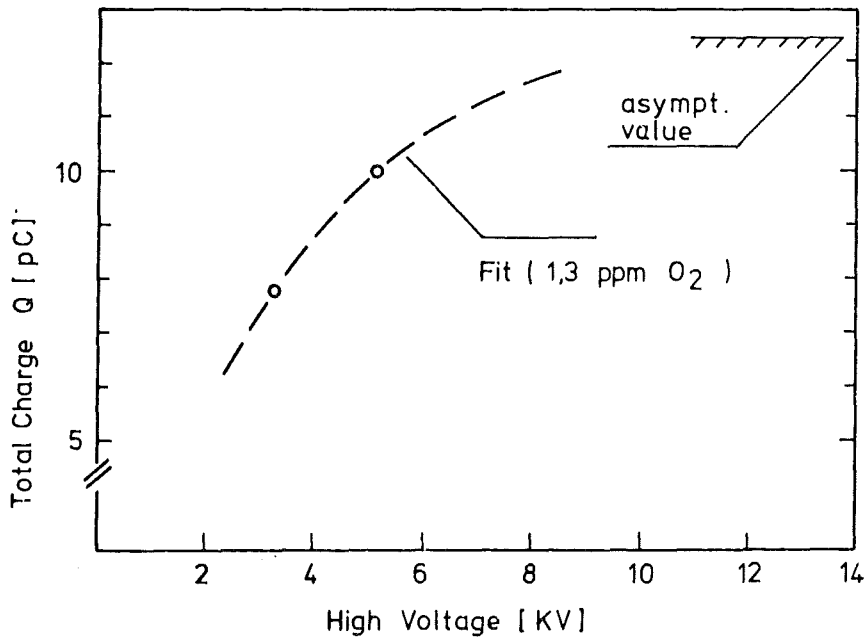
Fig. 3: Total charge collected as a function of high voltage

5.1 kVolt we collect 75% of the liberated charge.

Out of the 8000 channels implemented in the CELLO detector typically only 1% is not working properly due to defects in the analog or digital part of the electronics. The pedestal stability has been checked over a period of about one month. All channels are stable within 1 ADC count.

The zero-suppression has been implemented and is presently working at a level of 1 σ (noise) above pedestal. A 50% increase of the number of electronics channels is planned for the next year to increase space resolution and facilitate pattern recognition.

4.2.3 Calibration of the Liquid Argon Calorimeter of the CELLO Detector

The CELLO liquid argon calorimeter consists of 6000 electronical channels in the central part and 2000 channels in the endcap part.

The energy of a particle shower in the calorimeter is distributed over about 50-100 channels. Therefore it is very important to have an exact relative calibration between the single channels if one wants to obtain a good energy resolution.

Calibration is done by injecting a known amount of charge through a capacitor into the detector capacitance. The experience shows, that due to cross-talk effects between the channels the amplifier signal varies very much with the number of channels pulsed simultaneously. Therefore currently only 1/16 of the 384 channels of one stack are calibrated at one time, but all 16 stacks of the central part in parallel.

Each electronic channel matches the capacitance of the detector channel and therefore the amplification slope varies with the detector capacitance. Fig. 1 shows the dependence of calibration slopes from detector-capacitance for all channels of the central calorimeter.
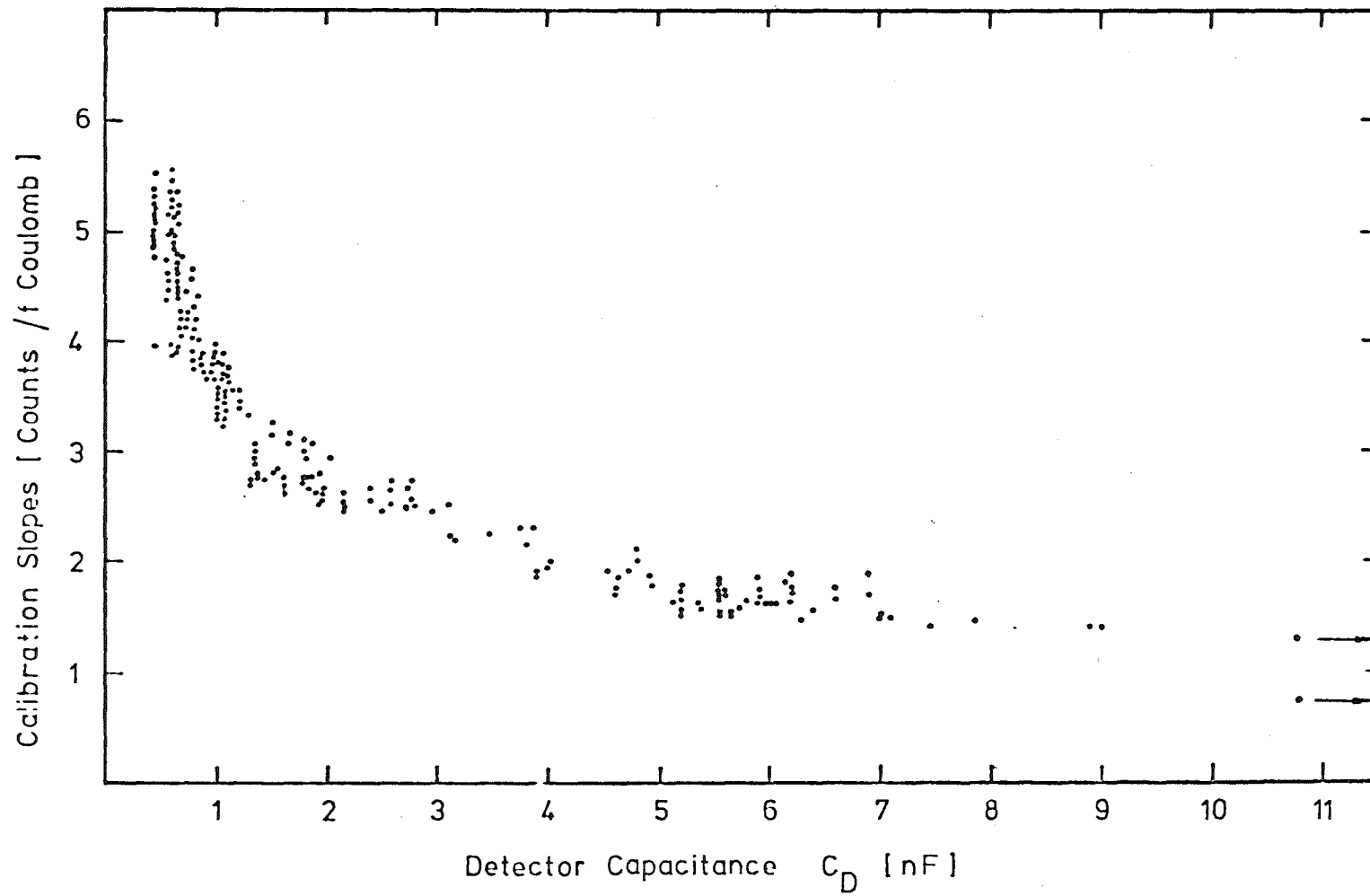
Fig. 1: Calibration slopes in one stack for different input capacitance

The calibration procedure is controlled by a micro computer and is repeated in several time intervals. The difference of slopes measured before and after a running period of 2 months is shown in fig. 2. The uncertainty of the calibration can be explained by the tolerances of the calibration capacitor ($\pm$ 0.5%) and of the resistors of the pulse distribution network ($\pm$ 1%). This is of the same magnitude as the statistical error (see fig. 2).

In addition during normal data taking every 10-20 sec a calibration pulse is given (controlled by microcomputer) and read out like a normal event. This specially marked monitor events allow a quick cross check of the calorimeter.

The relative calibration supplies a factor for calculating the charge collected on the lead electrodes. To get the energy absorbed in the calorimeter the absolute efficiency of the detector must be known. This value can be obtained by looking at physical events, which deposit a well-known amount of energy in the calorimeter. This has been done with low energy electrons (about 1 GeV), from which the momentum has been measured in the tracking device of the CELLO detector. After subtracting muonic and hadronic background a value of $Q/E = 0.5 \pm 0.01$ fC/MeV is obtained. In fig. 3 the low energy data is compared with the calibration obtained from elastically scattered electron (Bhabha scattering), which have the full beam-energy (17 GeV). The energy resolution measured with the low energy electrons is shown in fig. 4. The result of $13.3\%/\sqrt{E}$ is in good agreement with the resolution of $13\%/\sqrt{E}$ obtained from Bhabha scattering electrons.
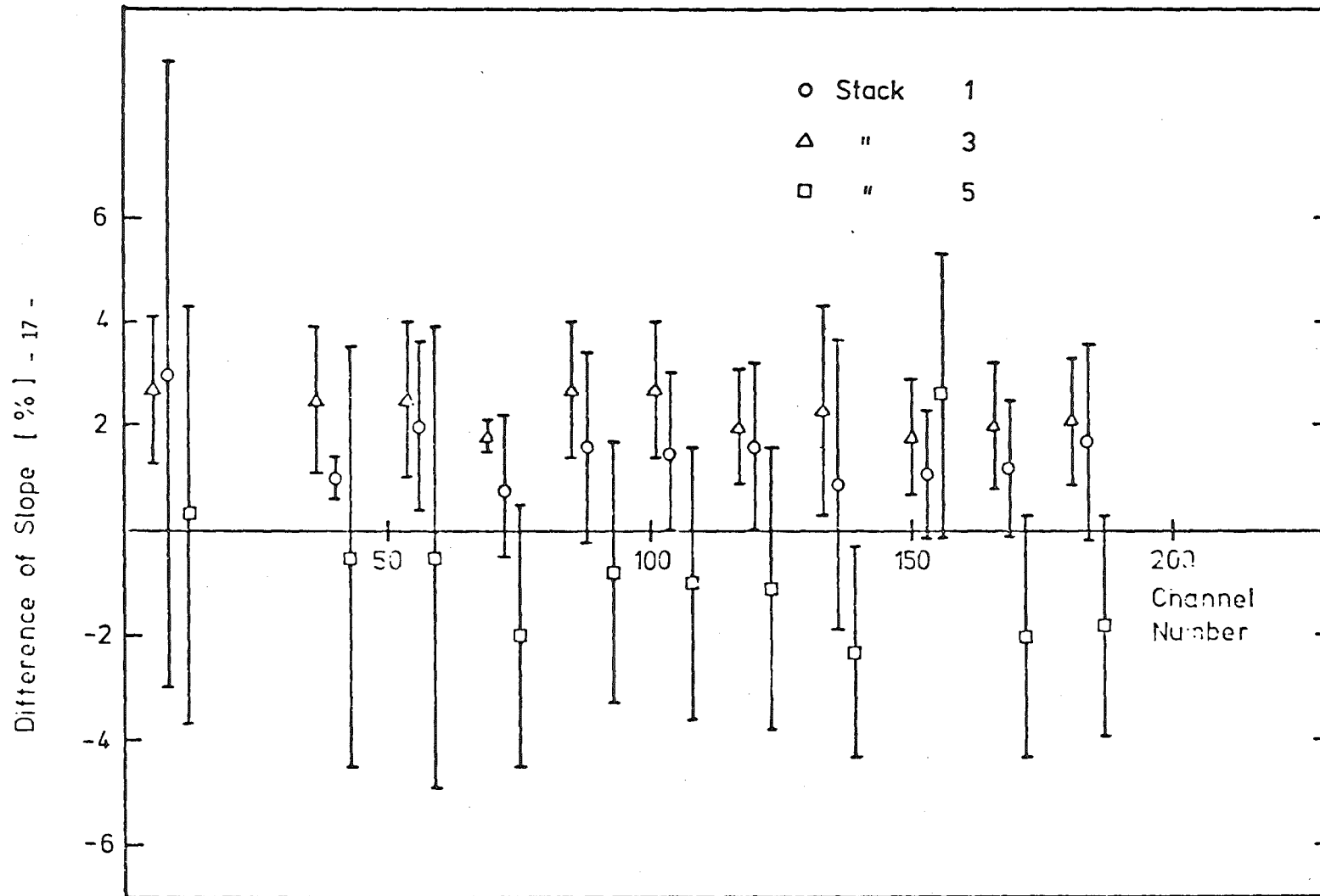
Fig. 2: Variation of the calibration slopes over two months
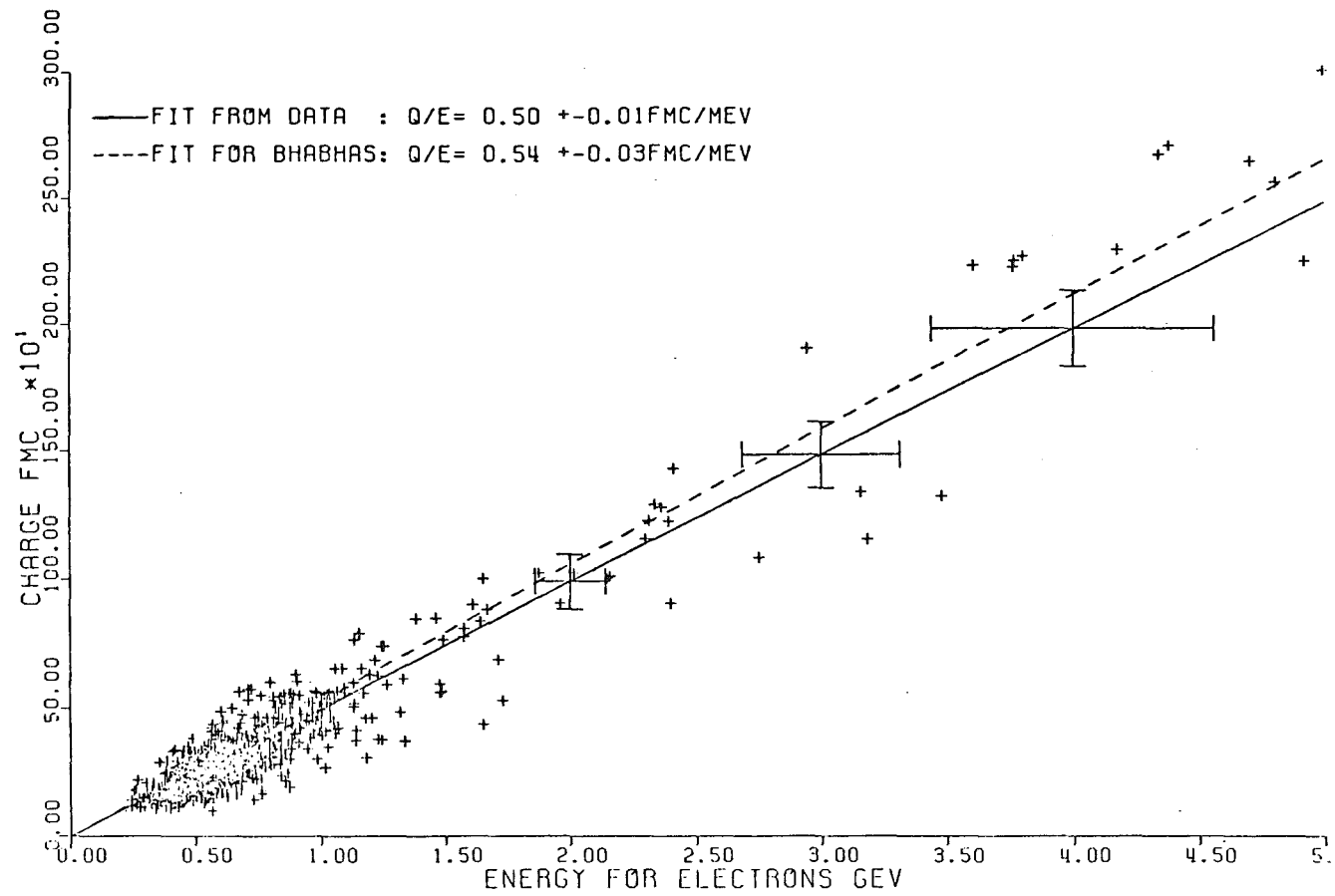
Fig. 3: Charge/energy calibration for electrons up to 4.5 GeV. The Bhabha calibration is given for comparison
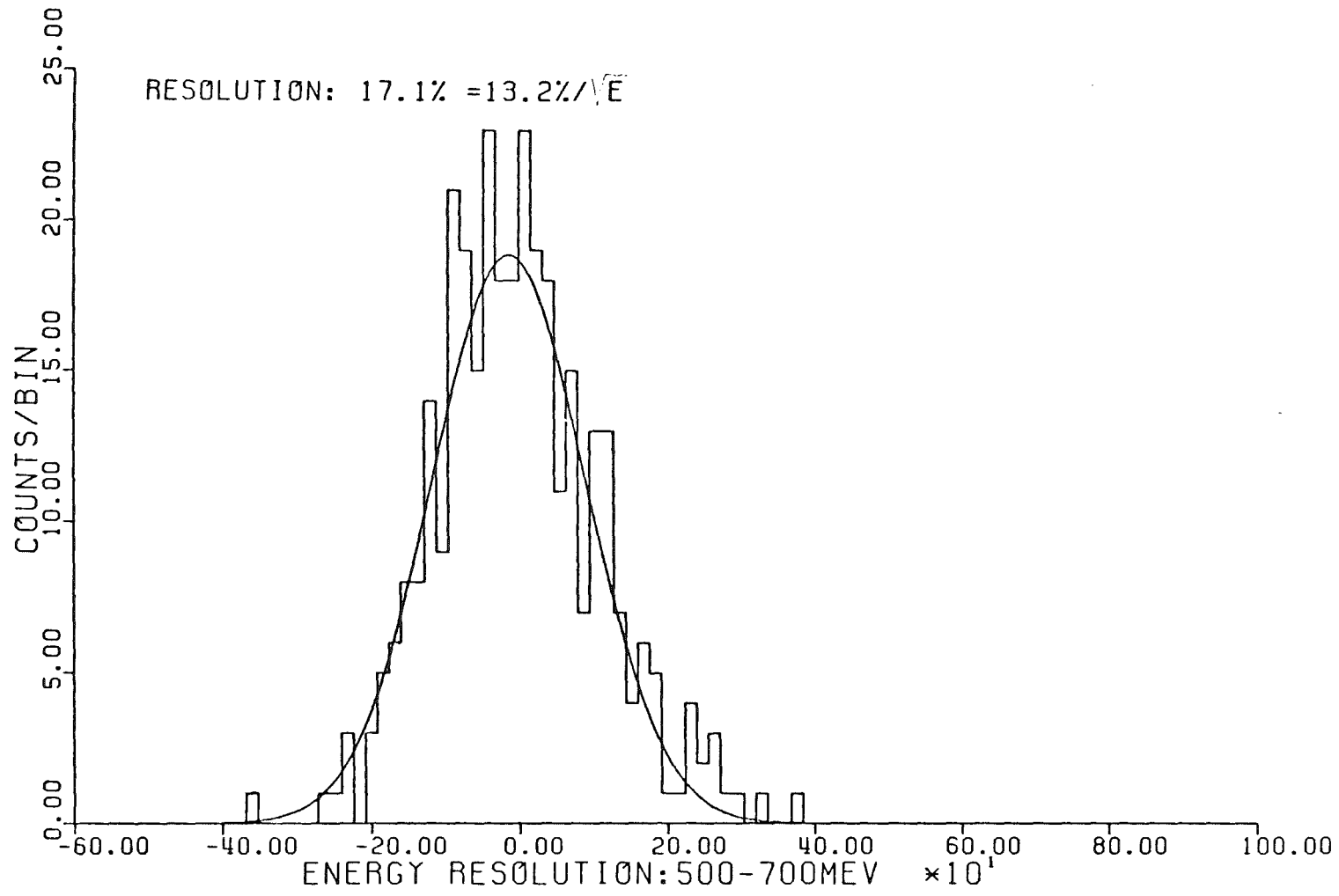
Fig. 4: Energy resolution for low energy electrons

4.2.4 Measurement of $e^+e^- \rightarrow e^+e^-$ and $e^+e^- \rightarrow \gamma\gamma$ at Energies up to 36.7 GeV

The measurement of the production of lepton and photon pairs in high energy e^+e^- reactions provides a stringent test of the validity of quantum electrodynamics (QED) at large momentum transfer. In addition, at highest accessible PETRA energies weak neutral current effects get increasingly important for Bhabha scattering. This allows to test weak interaction phenomena in purely leptonic processes.

The CELLO detector at the e^+e^- storage ring PETRA was used to measure the reactions

$$e^+e^- \rightarrow e^+e^- \quad \text{(Bhabha scattering)}$$

and

$$e^+e^- \rightarrow \gamma\gamma$$

at CM energies between 33.0 and 36.7 GeV.[1]

Fig. 1 shows the resulting differential cross section for Bhabha events. The data was corrected for radiative effects in order α^3 and hadronic vacuum polarisation. The expectation from QED is indicated in the figure.

To determine quantitative limits on the validity of QED the reaction amplitude is modified by introducing form factors, which are usually parametrized in terms of the cutoff parameters $\Lambda_\pm$. The magnitude of $\Lambda_\pm$ sets the energy scale, to which any deviation of the observed process from QED can be excluded. CELLO measured

$$\Lambda_+ > 83 \text{ GeV} \qquad \Lambda_- > 155 \text{ GeV} \qquad (95\% \text{ C.L.})$$

indicating that the electron is structureless down to distances of about 10^{-16} cm.

Similar form factor fits for the 2 photon annihilation $e^+e^- \to \gamma\gamma$ (Fig. 2) yield

$$\Lambda_+ > 43 \text{ GeV} \qquad \Lambda_- > 48 \text{ GeV} \qquad (95\% \text{ C.L.}) \quad .$$

Here $\Lambda_+ = M_e+/\lambda$ can be regarded as the ratio of the mass of a hypothetical heavy electron mediating the reaction and its coupling constant λ.

Deviations from the QED prediction are expected from weak neutral current effects. Including γ-Z^0 interference the Bhabha cross section depends on the vector and axial weak coupling constants g_V and g_A and the Z^0 mass M_{Z0}. In the standard $SU(2) \times U(1)$ model they are determined by one single parameter, $\sin^2\Theta_W$:

$$M_Z = \frac{37.4}{\sin \Theta_W \cos \Theta_W}$$

$$g_A^2 = \frac{1}{4}$$

$$g_V^2 = \frac{1}{4} (1 - 4 \sin^2\Theta_W)^2 \quad .$$

The predictions for the cross section of Bhabha scattering for various values of $\sin^2\Theta_W$ are indicated in fig. 3.

A fit to the CELLO data yields the following values

$$\sin^2\Theta_W = 0.25 \pm 0.13$$

$$0.01 < \sin^2\Theta < 0.48 \qquad (95\% \text{ C.L.}) \quad ,$$

which shows that data start to be sensitive to weak neutral current effects.
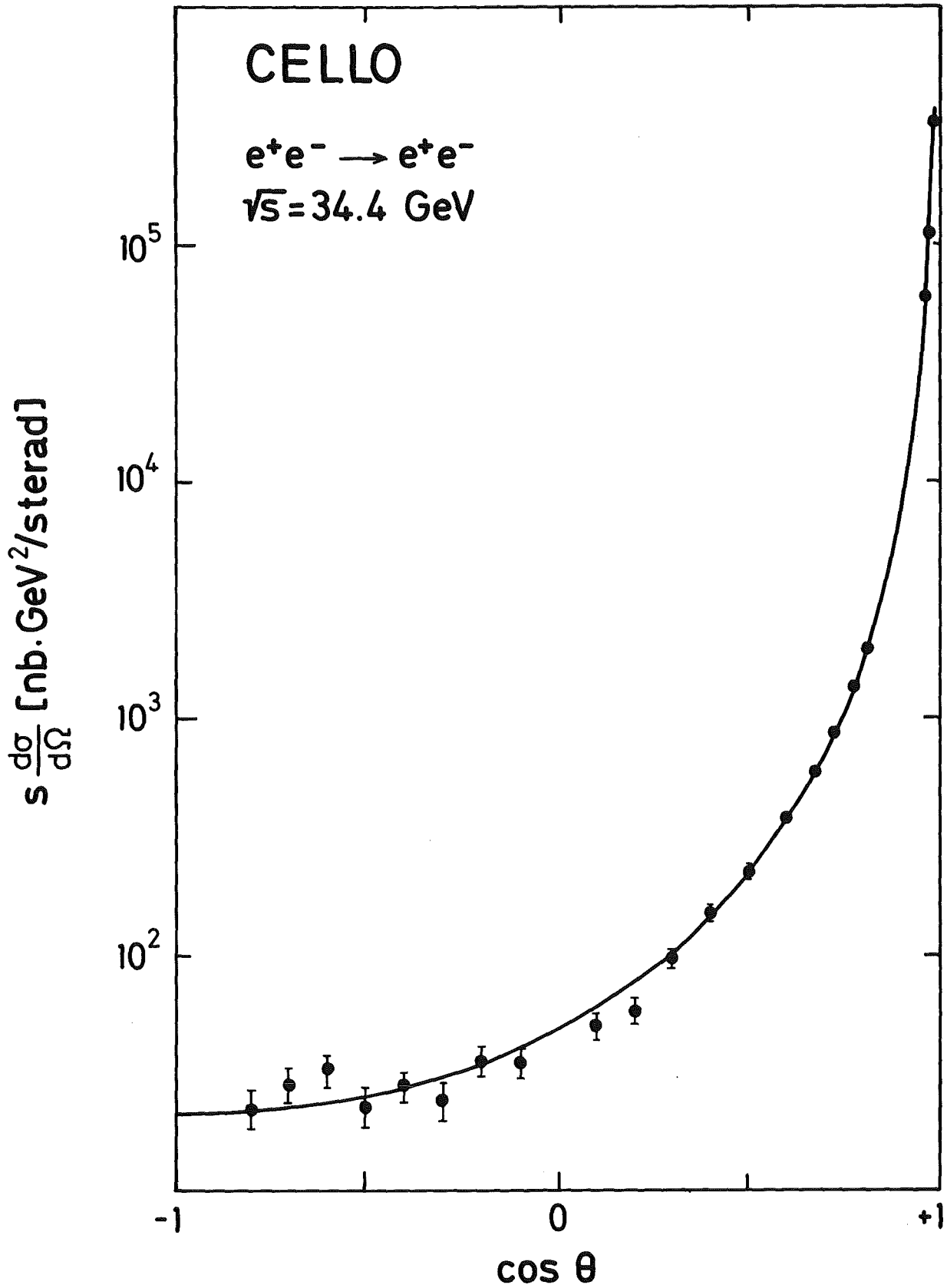
Fig. 1: Differential cross section of the reaction $e^+e^- \rightarrow e^+e^-$ in the central detector and endcap calorimeter range. Only statistical errors are plotted. The QED prediction (full curve) is normalized to the endcap points.
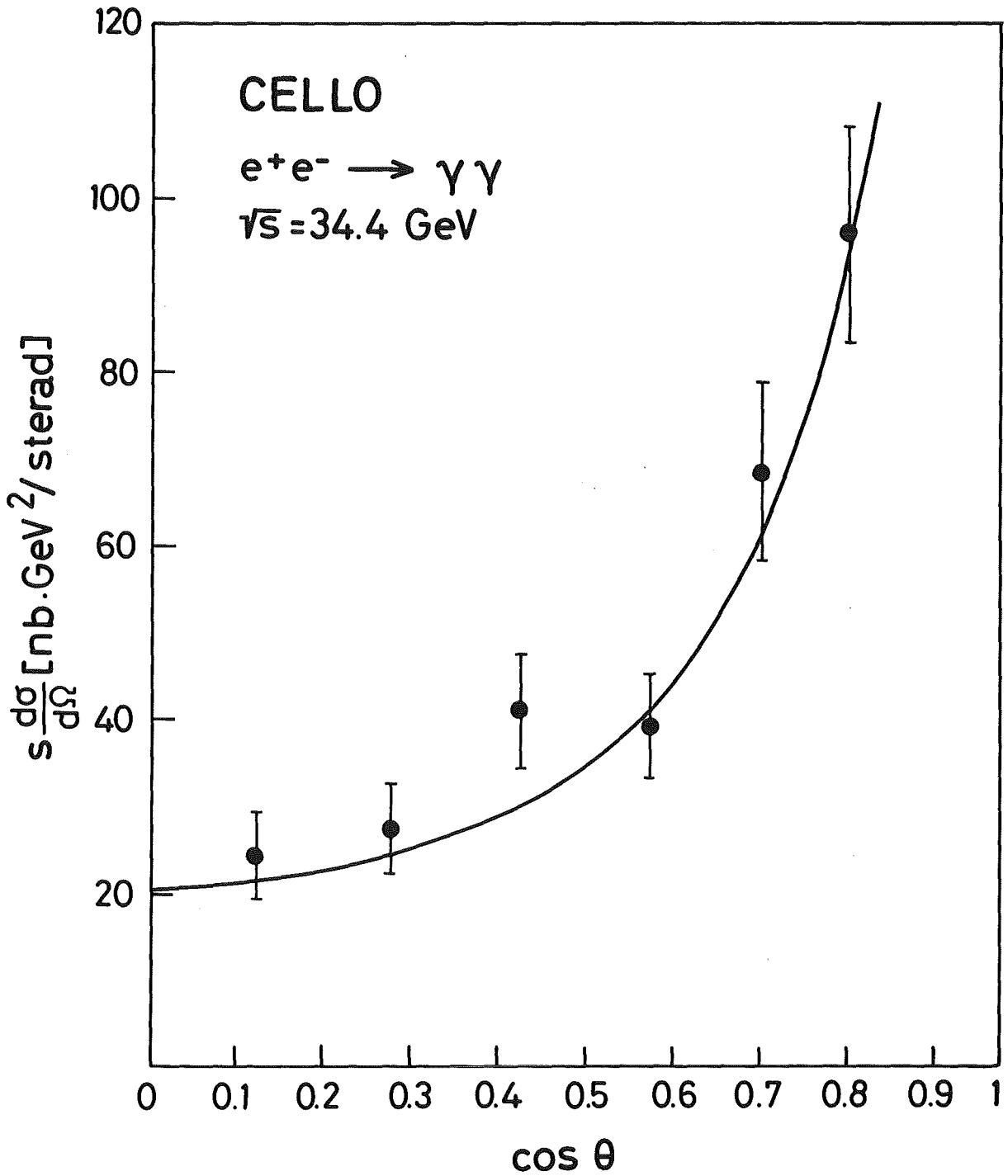
Fig. 2: Differential cross section of the reaction $e^+e^- \to \gamma\gamma$ compared to the QED prediction. Only statistical errors are plotted.
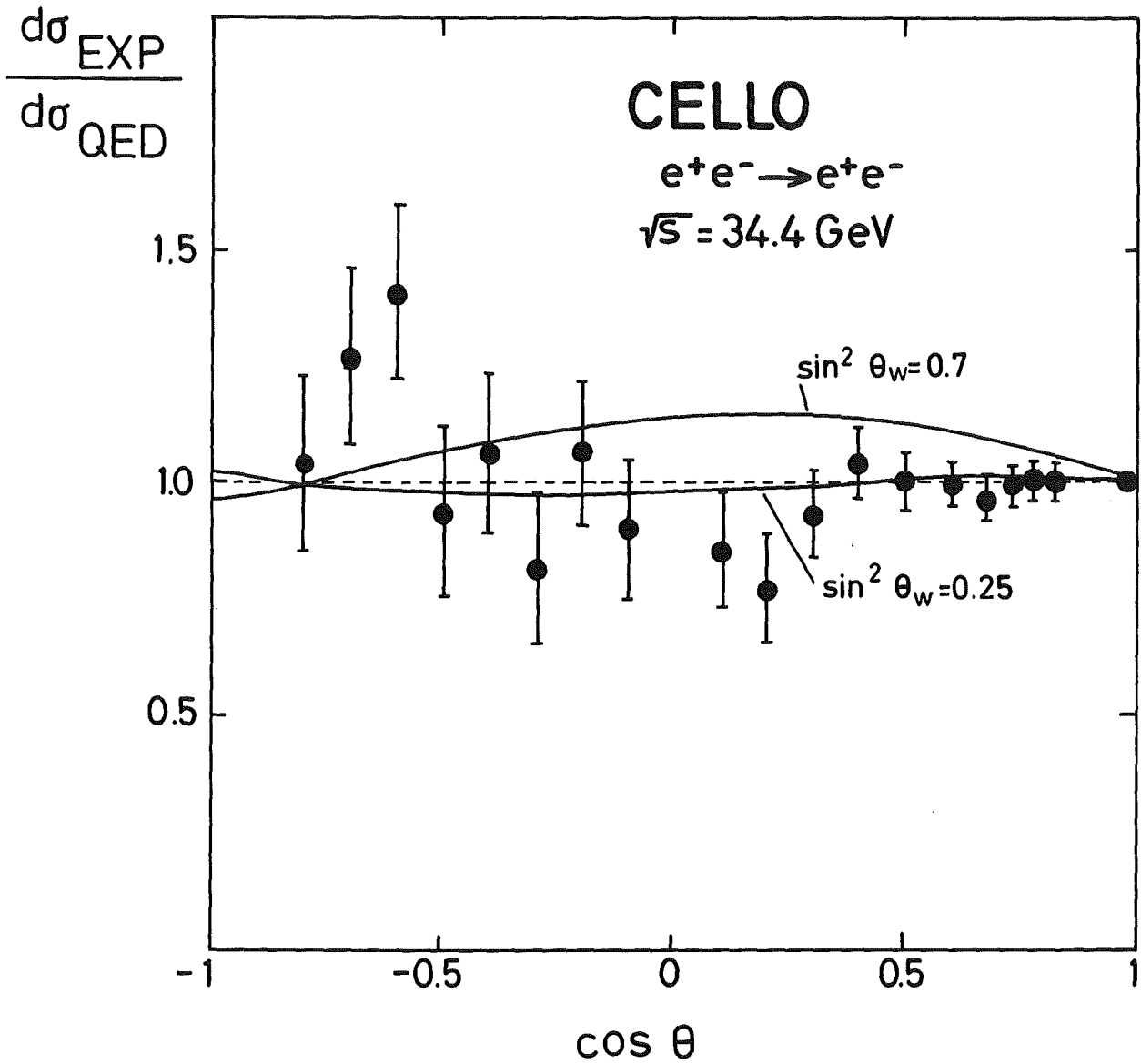
Fig. 3: Relative deviation of the measured cross section from QED pre-
diction. Errors are statistical only. The expectation for dif-
ferent values of $\sin^2\theta_W$ is indicated.

The analysis was performed on data taken from May to November 1980 with an integrated luminosity of about 3.8 pb^{-1}. Till summer 1981 CELLO added twice this statistics, the analysis of this new data is under way.

Reference

1) CELLO collaboration, H.-J. Behrend et al., Phys.Lett. 103B (1981) 148

4.2.5 Study of Hadronic Events in the CELLO Detector

Total cross section

One of the most important reactions in e^+e^- physics is the annihilation into hadrons:

$$e^+e^- \rightarrow \text{hadrons} . \tag{1}$$

The total cross section for reaction (1) is usually measured in terms of

$$R = \sigma_{had}/\sigma_{\mu\mu} ,$$

where σ_{had} is the total hadronic annihilation cross section and $\sigma_{\mu\mu}$ is the cross section for μ pair production.

In the quark parton model R is related to the charges Q_q of quarks involved in reaction (1) through the simple formula

$$R = 3 \sum_q Q_q^2 ,$$

where the sum runs over all types ("flavours") of quarks contributing to (1). A new flavour of quarks should show up by an increase of R. Moreover, close to threshold, $q\bar{q}$ bound states should be produced and exhibit narrow resonances.

Fig. 1 shows the results from an energy scan in the highest available energy regime of PETRA[1]. The distribution of R shows no significant resonance structure. The mean value of

$$<R> = 3.85 \pm 0.12 \text{ (stat.) } \pm 0.31 \text{ (syst.)}$$

is well compatible with the expectation of
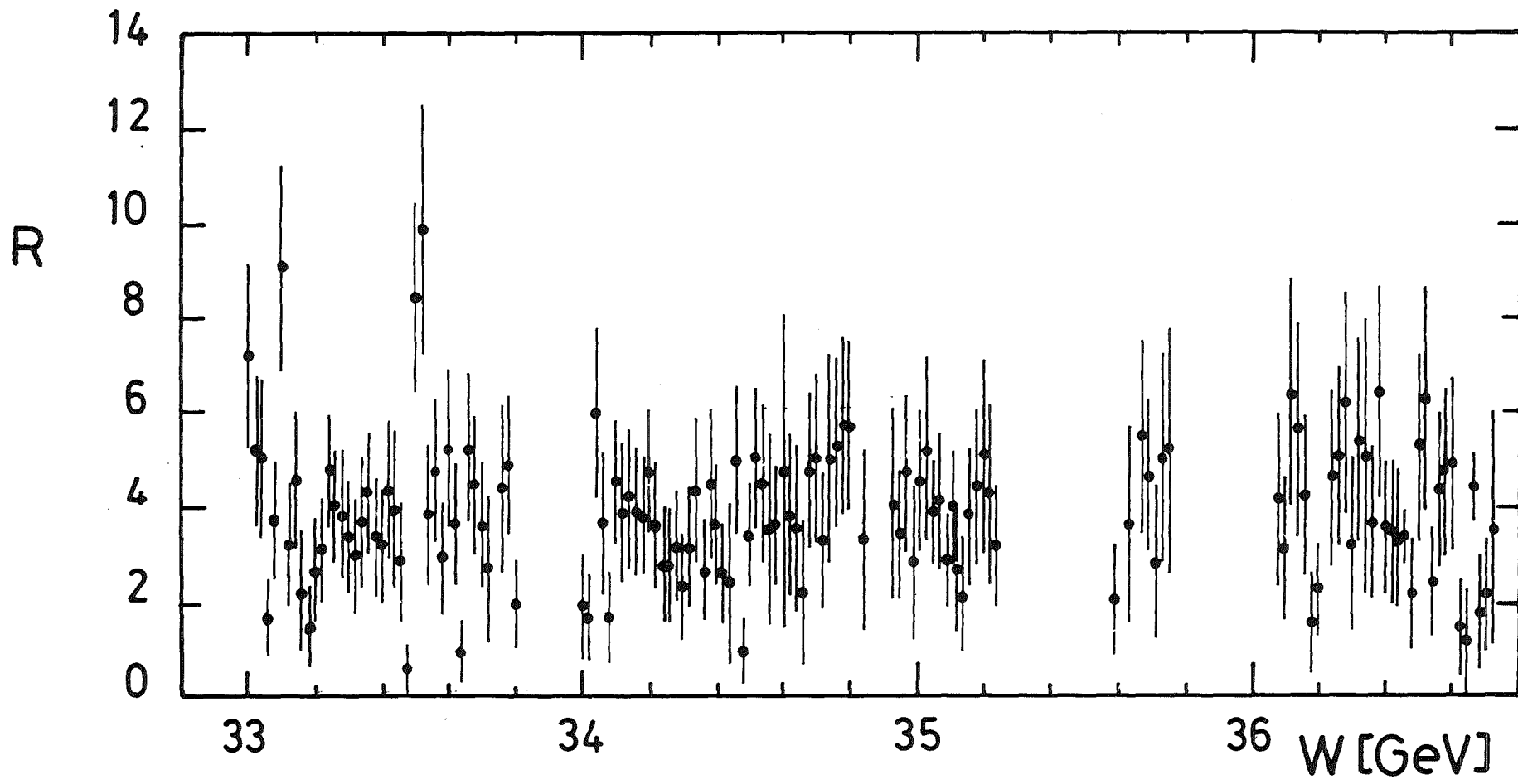
Fig. 1: $R = \sigma(e^+e^- \rightarrow \text{hadrons}) / \sigma_{\mu\mu}$ vs c.m. energy. Only statistical errors are shown.

$$R = 3 \Sigma Q_q^2 (1 + \frac{\alpha_s}{\pi}) \simeq 3.88$$

for udscb-quarks including QCD corrections.

Event shape analysis

This result is corroborated by a detailed event shape analysis. The topology of events originating from a new heavy quark pair should differ strongly from the pronounced two jet structure from "light" quarks. This is simply due to the small Lorentz boost and the larger transverse momenta of the heavy quark jets.

To search for such anomalous event shapes the data are analysed in terms of quantities called sphericity S and aplanarity A. S and A are evaluated for each event by submitting it to a Q-analysis. The three major axes and the corresponding normalized total momentum components Q_i along these axes are determined diagonalizing the momentum tensor. This procedure is similar to the determination of the moments of inertia of a rigid body. The sphericity S is then defined from the two smaller components

$$S = \frac{3}{2} (Q_1 + Q_2) \quad .$$

S may take values between 0 for an ideal two jet structure and 1 for a spherical event. The aplanarity is defined from the smallest component

$$A = \frac{3}{2} Q_1 \quad .$$

It measures to what extent the event differs from a flat shape (A = 0).

Fig. 2 shows the result of an analysis of the hadronic events taken by CELLO in 1980. Data are compared with Monte Carlo calculations assuming udscb quark production (Fig. 2b). Fig. 2c shows the MC simula-
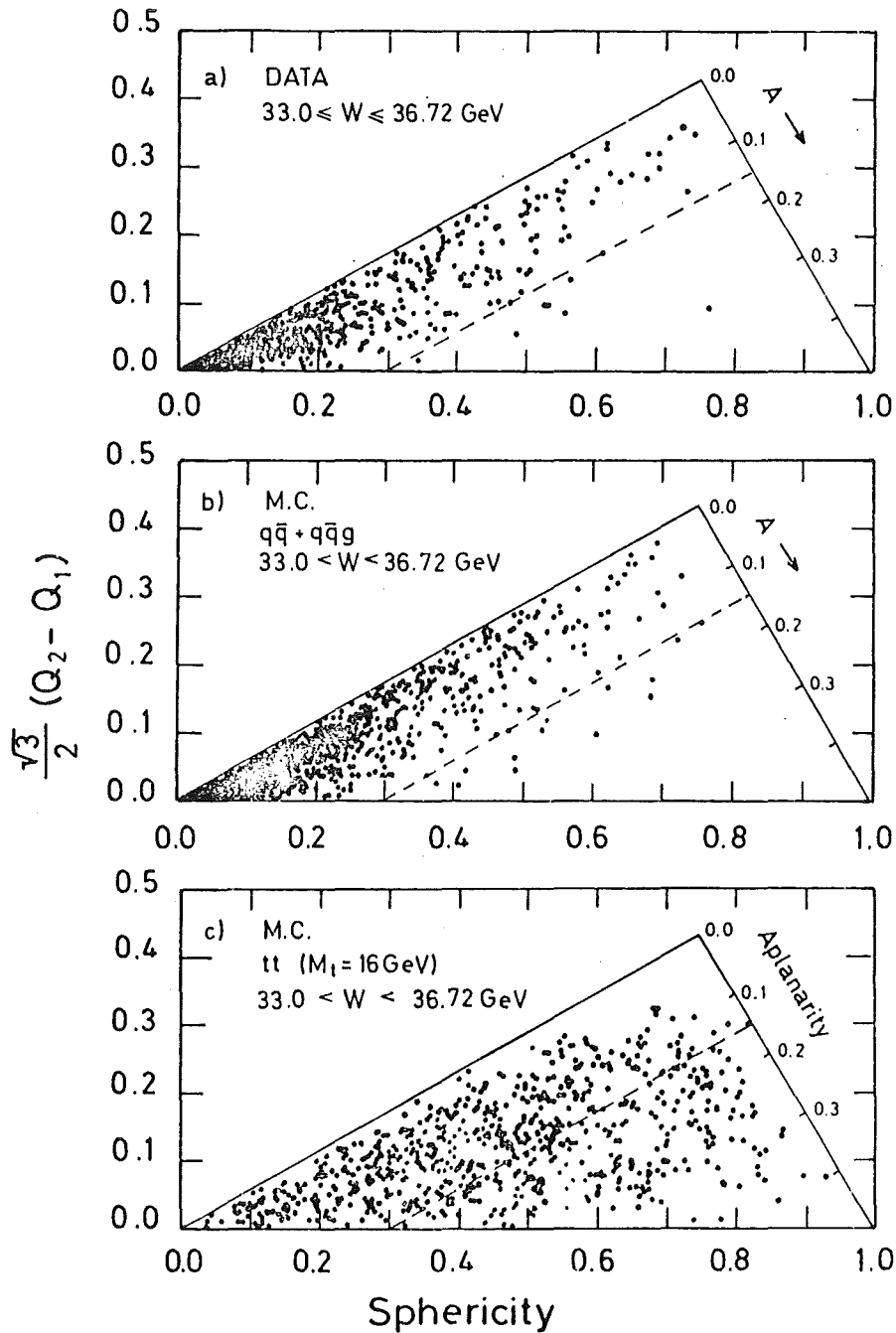
Fig. 2: Distribution of events in aplanarity and sphericity

a) all data, 33.00 ≤ W ≤ 36.72 GeV

b) MC simulation of qq̄ and qq̄g production and fragmentation in the energy range covered by this experiment (q = u,d, s,c and b).

c) MC simulation of non-resonant tt̄ production in the energy range covered by this experiment using M_t = 16 GeV

The cut at A = 0.15 is used to isolate events of large A as expected from tt̄ production

tion of additional t quark production. The absence of events with large
S and A in the data clearly rules out the existence of a new heavy quark
at these energies. Quantitatively we get the following result:
A new heavy quark with charge 2/3 e (1/3 e) is excluded by 14 (7.7)
standard deviations.

Jet studies and determination of α_s

Inspection of Fig. 2 shows that the population of events in the
Q-diagram extends to large values of sphericity S but stays clustered
at small values of aplanarity A. The current interpretation of this
phenomenon is given by quantum chromodynamics (QCD): in addition to
the prominent two jet structure (q$\bar{\text{q}}$) at small S there are planar events
with three jets from gluon bremsstrahlung (q$\bar{\text{q}}$g). Three methods were
used for further investigation. In the first two charged and neutral
particles were used, whereas the third is based on charged particles
only.

- Standard Analysis:

We performed a standard topology analysis using the sphericity
tensor. From the number of planar events, i.e. events with a spheri-
city larger 0.25 and an aplanarity smaller 0.08 in our data and in
the Monte Carlo simulation we deduce a value of α_s = 0.17±0.03±0.03
at 34 GeV and α_s = 0.20±0.04±0.04 at 22 GeV. Fig. 3 shows the aplanarity
distribution at the two energies. The two jet process (q$\bar{\text{q}}$, dashed
curve) cannot reproduce the data, whereas QCD (full curve) is in good
agreement with the data.

We made sure that this result is stable against variation of the
cuts within the quoted statistical errors. We also checked the sensi-
tivity of this α_s-evaluation on the shape of the Monte Carlo $p_\perp$ dis-
tribution used. Contrary to the cluster method (see below) all measured
particles enter this analysis. Hence the method is more sensitive to
tails in the $p_\perp$ distribution. Still the variation of α_s for different
$p_\perp$ distributions (i) and (ii) (see below) stays within the quoted sys-
tematic erros ($\simeq$ 20%).
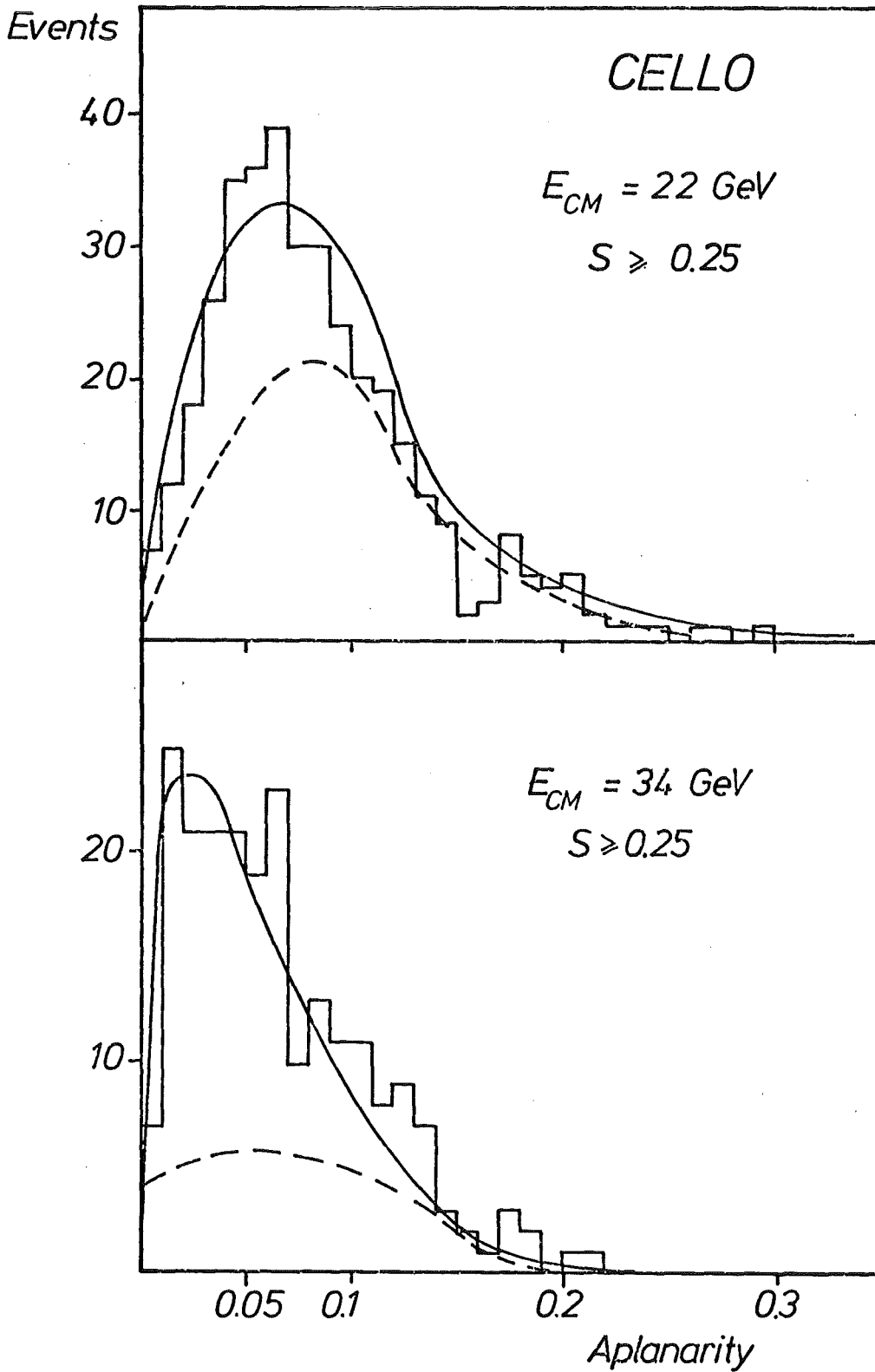
Fig. 3: Aplanarity distribution for hadronic events with S ≥ 0.25 compared to 2 jet (dashed curve) and QCD predictions (full curve).

- Cluster Analysis:

    Particles (neutral and charged) are submitted to the following cluster algorithm[2]:

1) Particles emitted close to each other are merged into preclusters. The procedure is started with the most energetic particle. The next energetic particle occuring within 30° is added. The procedure is iterated taking as the new starting direction the sum of the momenta of all particles already merged in the precluster.

2) Preclusters are grouped into clusters if their axes are less than 45° apart.

3) Clusters with more than 2 GeV total energy containing at least two particles (charged or neutral) are retained and treated as separate jets.

Data are compared to model calculations which include gluon bremsstrahlung. To describe the quark and gluon fragmentation we adapt the phenomenological model of Feynman and Field assuming two types of functions for the transverse momentum in the fragmentation chain:

(i)   gaussian: $p_T \cdot \exp(-p_T^2/\sigma_q)$

(ii)   exponential: $\exp(-p_T/\sigma_e)$

Monte Carlo (MC) generated events are passed through a realistic detector simulation and through the reconstruction chain. Initial state radiative corrections are taken into account.

    Different values for σ_q and σ_e have been tried within the range which gives a reasonable agreement between Monte Carlo simulation and data in the $p_\perp$ distribution of particles in the jets. The mean value of the experimental distribution is reproduced by $\sigma_q \approx 300$ MeV and $\sigma_e \approx 420$ MeV.

Recently it was claimed that the data might be explained without gluon bremsstrahlung. To study this we compare our data with pure $q\bar{q}$ Monte Carlo simulations. Fig. 1a shows the experimental $p_\perp$ distribution (i) and the results of two model predictions. The model with the gaussian distribution in the fragmentation (ii) underestimates the high $p_\perp$ tails whereas the exponential model (iii) is systematically higher at large $p_\perp$. The neutral tracks show analogue behaviour.

Both $q\bar{q}$ model calculations yield 3 jet events due to statistical fluctuations, however, their number cannot explain the data. To quantify this further we study the event thrust of the three jet events which is defined by the jet momenta p_i

$$T_j = \max\left\{ \sum_{i=1}^{3} |p_i^\perp| / \sum_{i=1}^{3} |p_i| \right\}$$

The data shown in fig. 4b are compared to model calculations (i) and (ii) normalized to the observed number of events. Neither of them can reproduce the data. Using the number of events below $T_j < .93$ the hypothesis $q\bar{q}$ is ruled out by 7 s.d..

The three jet sample at 34 GeV is finally analysed to study the dynamics of the proposed underlying QCD process and to determine the value of the strong coupling constant α_s.

For vector gluons the differential cross section with respect to the energy fraction of the most energetic parton is given by

$$\frac{1}{\sigma_0} \frac{d\sigma}{dx_1} = \frac{2}{3} \frac{\alpha_s}{\pi} \cdot \frac{1}{1+\alpha_s/\pi} \cdot \frac{1}{1-x_1} \cdot \left| \frac{2(3x_1^2-3x_1+2)}{x_1} \cdot \ln \frac{2x_1-1}{1-x_1} - 3(3x_1-2)(2-x_1) \right| \quad (1)$$

The event thrust T_j calculated from the 3 jet momenta turns out to measure x_1 to a very good approximation. MC studies show that in our

(a)   (b)
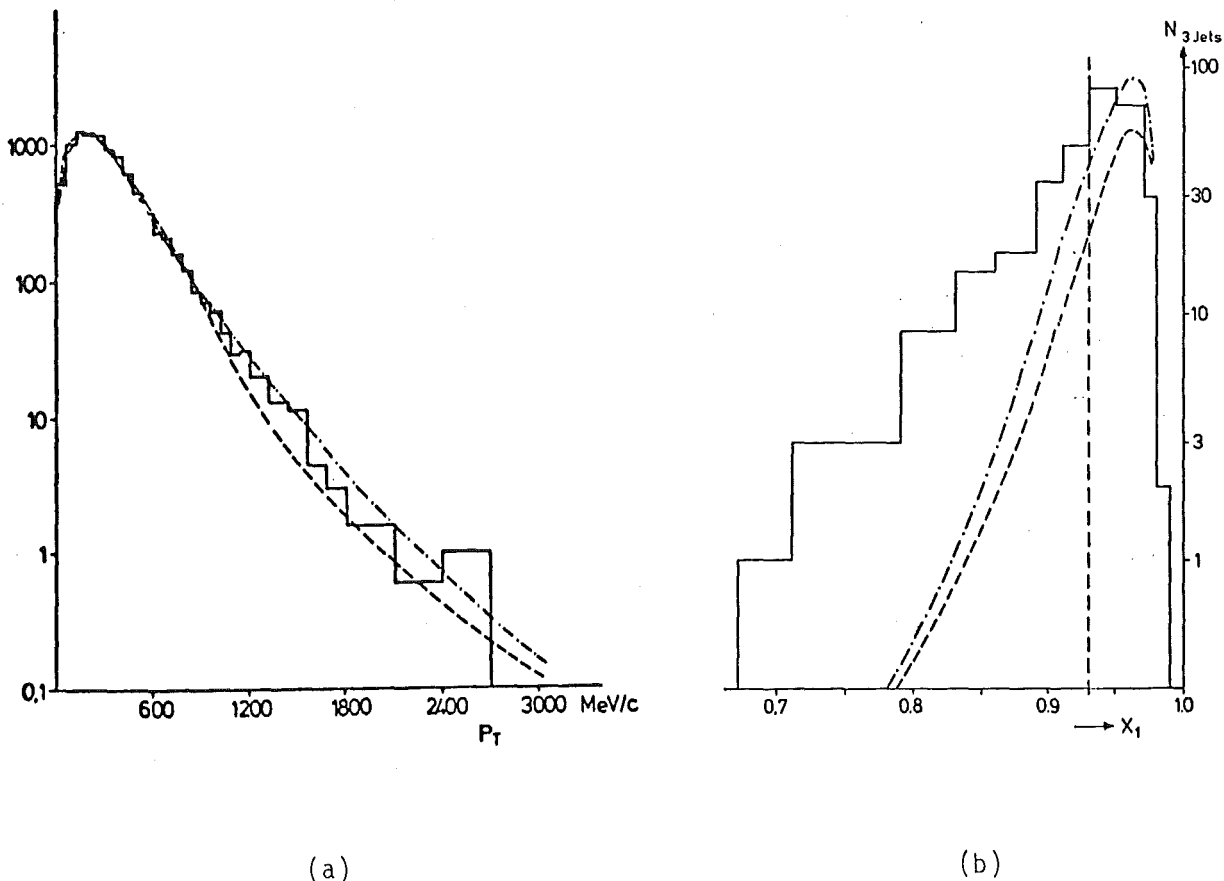
Fig. 4: Comparison of data with different $q\bar{q}$ fragmentation models

    a) distribution of p_T in a jet for charged particles in the
       2 jet sample
       (i) (histogram) experimental distribution
      (ii) (dashed curve) gaussian dependence in the fragmenta-
          tion process with σ_q = 300 MeV/c
      (ii) (dashed-dotted) exponential dependence with σ_e = 420
          MeV/c. High $p_\perp$ values are overestimated.

    b) Distribution of thrust T calculated from the jet momenta in
       3 jet events

       experimental distribution (histogram) and $q\bar{q}$ model calcula-
       tions (dashed and dashed-dotted curves) using the $p_\perp$ distri-
       bution (ii) and (iii) described in a).

       Both models fail to describe the data.

detector T_j determine x_1 with an error of $\simeq 0.02$ and a constant efficiency of (45±3)% in the region $x_1 \leq 0.91$, dropping smoothly to about 38% at 0.95. If we restrict ourselves to this region ($x_1 \leq 0.95$) we retain 314 events. The migration of genuine two jet events into the three jet class is determined by MC simulation. It is 19%, contributing mainly to the region $x_1 > 0.9$.

The resulting x_1 distribution corrected for 2 jet contribution, efficiency and radiation is shown in fig. 5. A comparison with (1) yields good agreement with vector gluon bremsstrahlung as shown in fig. 5 (solid curve). The distribution for a hypothetical scalar gluon does not reproduce the data (fig. 5, dashed curve).

The only free parameter in comparing data and theory in fig. 3 is the strong coupling constant α_s, which in 1st order QCD is directly related to the normalisation of the data. To get a safer value for this absolute number only events are considered in which all jets have $|\cos \Theta \text{ jet}| < 0.8$ which guaranties that the jets are well inside the cylindrical part of our detector. A best fit to the data in the region $x_1 \leq 0.93$ yields

$$\alpha_s = 0.15 \pm 0.02 \pm 0.03 \qquad (34 \text{ GeV})$$

The last point at 0.94 was neglected in the fit because of its large 2 jet correction. The systematic (second) error reflects the uncertainties due to background and absolute normalisation between data and Monte Carlo.

A similar analysis is carried out with the 22 GeV data. The number of genuine 3 jet events is smaller and the corrections from migrating 2 jet events are more important. Within the resulting large errors we find good agreement with QCD, in particular in the x_1 distribution. The value of α_s is

$$\alpha_s = 0.19 \pm 0.04 \pm 0.04 \qquad (22 \text{ GeV})$$
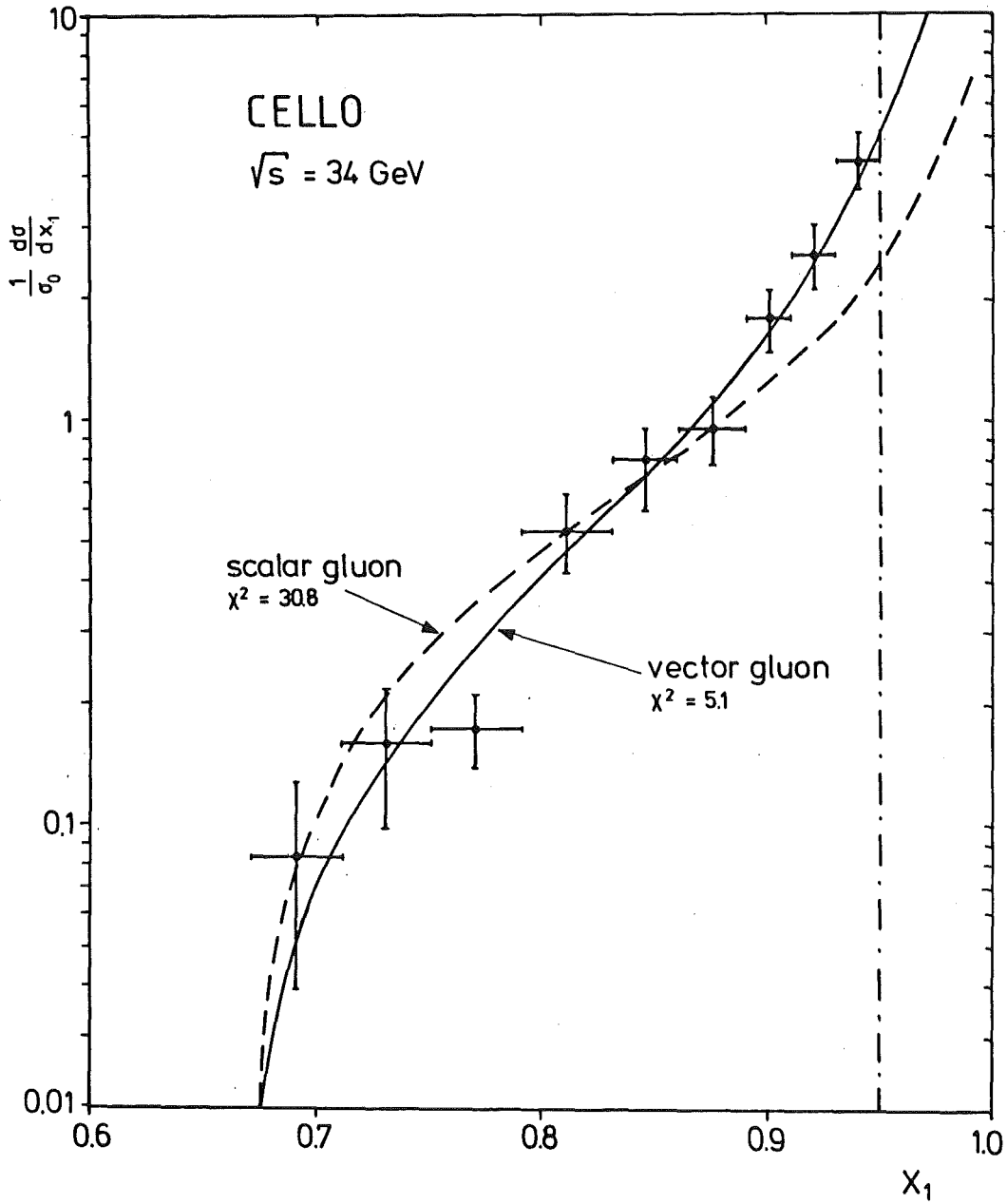
Fig. 5: Differential cross section of three jet events with respect to the energetic fraction x_1 carried by the most energetic parton. Data are compared to the QCD prediction of vector gluons (full curve) and a scalar gluon model (dashed curve).

- Energy Energy Correlations:

We study the semi-inclusive differential cross section of two hadrons in an annihilation process[3,4]:

$$f(\Theta_{ab}) = \frac{2}{\sigma} \cdot \sum_{ab} \int \frac{d^3\sigma(e^+e^- \to a+b+z)}{dz_a \ dz_b \ d\Theta_{ab}} \ z_a \ z_b \ dz_a \ dz_b$$

where Θ_{ab} is the angle between the two hadrons a and b of the final
state,

z_a, z_b are the relative energies of a and b

σ is the total hadronic annihilation cross section.

The sum has to be taken over all hadrons occuring.

f(Θ) normalized to the total annihilation cross sections is usually referred to as 'energy-energy correlation distribution'. One distinguishes:

- the central area (CA) around $\Theta_{ab} \approx \pi/2$. which is predominantely affected by the emission of hard gluons, and
- the regions where Θ_{ab} is small (same distribution (SS)) or where Θ_{ab} is close to π (away-side distribution (AS)), where predominantely virtual color radiative processes during the fragmentation are assumed to influence the distribution.

In the angular range $\Theta_{ab} \approx \pi/2$ (central area) the forward-backward asymmetry $\chi(\Theta_{ab})$

$$\chi(\Theta_{ab}) = f(\pi-\Theta_{ab}) - f(\Theta_{ab})$$

is of special interest. According to a QCD calculation of order α_s by Basham et al. (BBEL)[4], it is essentially single hard gluon emission, which contributes in this angular region to the two jet annihilation channel. The asymmetry distribution $\chi(\Theta_{ab})$ in particular is supposed

to be free of the non-perturbative contributions. Figs. 6a,b show corrected experimental data together with the prediction of BBEL for the asymmetry distribution. We find a reasonable agreement in a restricted angular range around $\Theta_{ab} = \pi/2$. We have fitted the data in this angular region and deduced values for $\alpha_s(Q^2)$ at two energies:

$$E_{CM} = 22 \text{ GeV} \qquad \alpha_s = 0.15 \pm 0.02 \ \{\pm 0.03\}$$

$$E_{CM} = 34 \text{ GeV} \qquad \alpha_s = 0.15 \pm 0.02 \ \{\pm 0.03\}$$

The systematic error { } was estimated by variing the angular limits used for the fit.

Taking the above evaluated α_s one can compute the BBEL prediction for $f(\Theta_{ab})$. The data differs substantially from the QCD computation, presumably due to the presence of non-perturbative effects. If we add a fragmentation term of the form $C \cdot <p_\perp> = E_{CM}^{-1} \cdot \sin^{-2}(\Theta)$ we obtain fair agreement with the data for values

$$E_{CM} = 22 \text{ GeV} \qquad C \cdot <p_\perp> = 1.65 \pm 0.04$$

$$E_{CM} = 34 \text{ GeV} \qquad C \cdot <p_\perp> = 1.89 \pm 0.04$$

fitting BBEL and the fragmentation term to the data.

For the angular region of Θ_{ab} close to π we investigated $f(\Theta_{ab})$ considering only hadrons emitted into opposite hemispheres (AS-distribution). The data show again good agreement with Monte Carlo simulated events, figs. 7a,b.

For a comparison of the AS-distribution with the theoretical prediction we considered the work of Y.I. Dokshitzer et al.[3]. This approach is based on summing in all orders of QCD the diagrams with maximum power n of the terms $(\ln (Q^2/\Lambda^2))^n$, where Q^2 is the total center of mass energy squared. By introducing an effective semi-inclusive
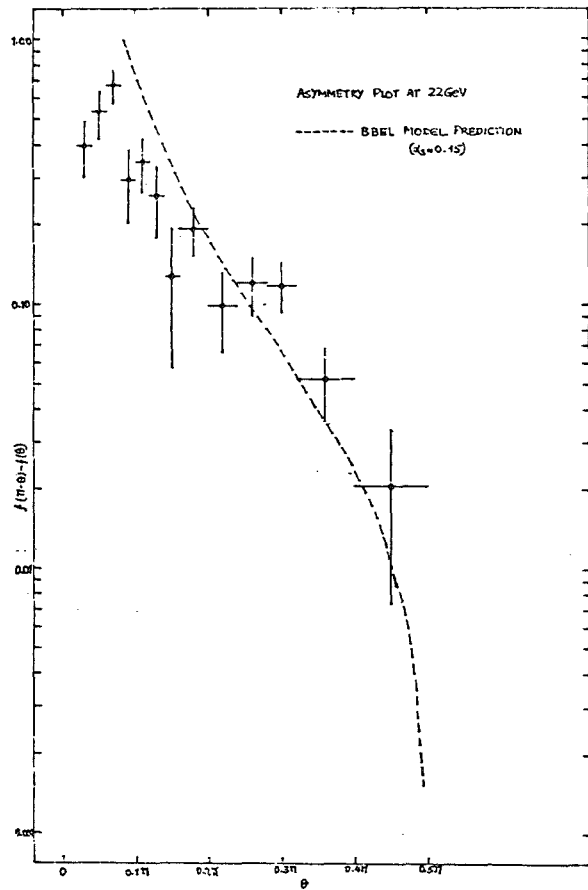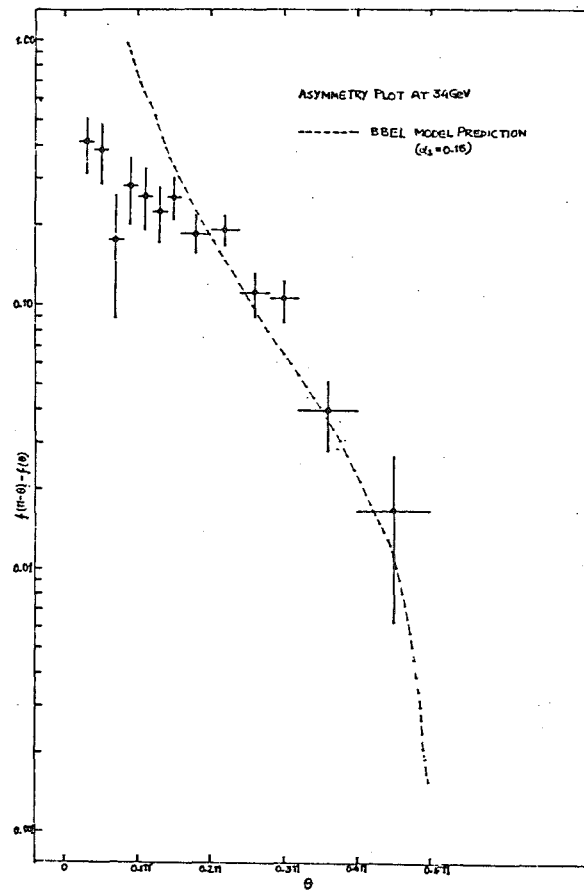
(a)　　　　　　　　　　　　　　　　　　　(b)

Fig. 6:　Asymmetry $f(\pi-\Theta)-f(\Theta)$ compared to BBEL
　　　　　a)　22 GeV data
　　　　　b)　34 GeV data
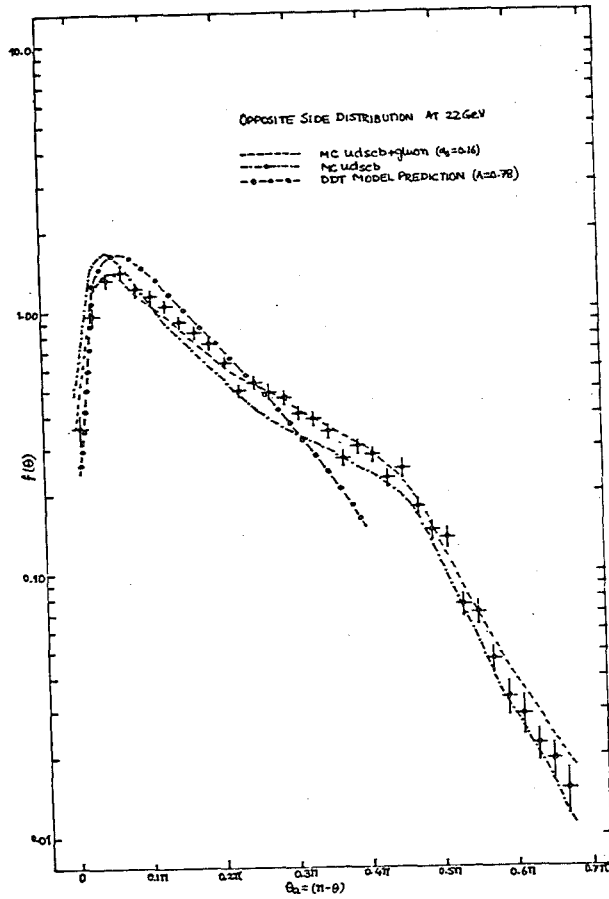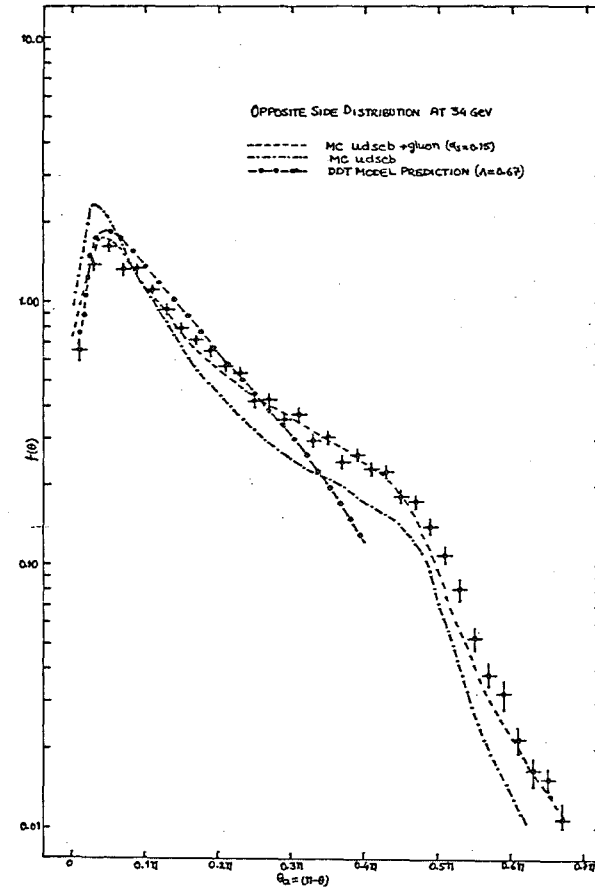
Fig. 7: Opposite side correlations compared to different model calcula-
tions

a) 22 GeV data

b) 34 GeV data

formfactor $T_F(Q^2,\Theta)$ the model is expected to account for the major virtual and real parton processes, which occur in the parton-gluon cascade after annihilation. (This method is called 'leading log approximation', LLG).

More explicitely for the theoretical AS-distribution we evaluated the function

$$f(\Theta) = \frac{2}{\sigma} \Sigma \int_0^1 \frac{d^3 z_a z_b}{dz_a dz_b d\Theta_{ab})} dz_a dz_b = \frac{1}{2} \frac{\partial}{\partial\Theta} T_F(Q^2,\Theta_{ab})$$

where for $T_F(Q^2,\Theta)$ we used an approximated expression.

The data have been corrected for acceptance losses and neutrals. The corrections appeared to be a rather flat function of Θ_{ab} contributing a 10% effect in average.

The LLG-QCD calculation seems to provide a fair description of the AS-distribution both in shape and order of magnitude.

For a study of $f(\Theta_{ab})$ close to 0 ((SS)-distribution) we compared our data with the work of Konishi et al.[5], who considered in their approach higher order QCD effects on $f(\Theta_{ab})$ in the approximation Θ_{ab} = small, arguing that here the fragmentation process involves only one parent quark or gluon.

They computed a differential cross section for the semi-inclusive distribution which we compared with our data, figs. 8a,b. Also for the same-side distribution the QCD calculation yields a fair representation of the data without being able to describe finer details.
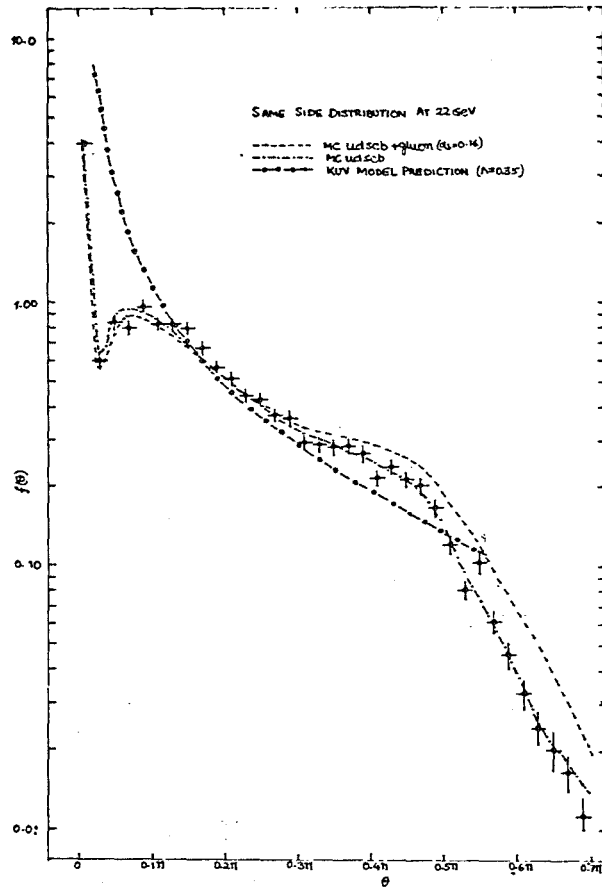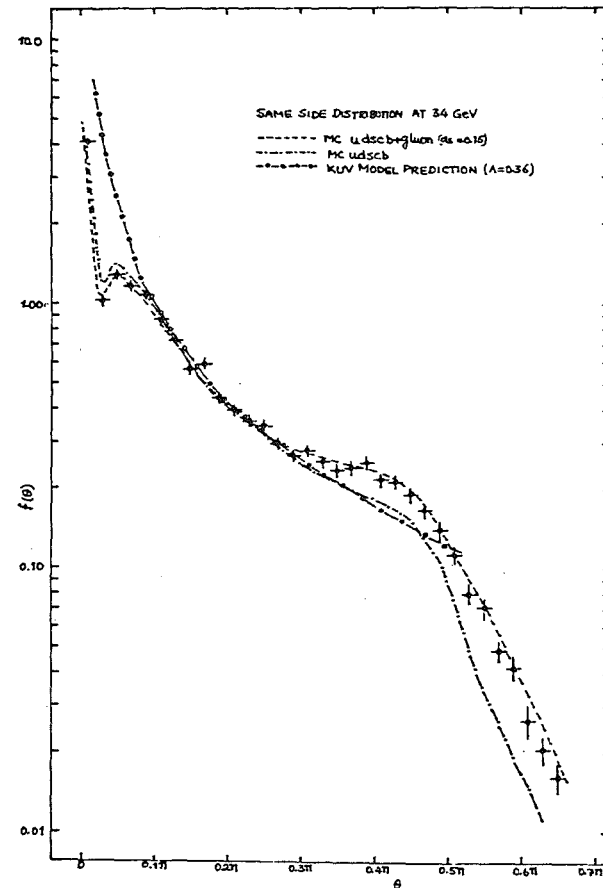
Fig. 8: Same side correlation compared to different model calculations
   a)   22 GeV data
   b)   34 GeV data

References

1) CELLO Collaboration, H.-J. Behrend et al., Search for narrow quar-
   konium states and pair production of new heavy quarks at c.m.
   energies from 33.0 to 36.7 GeV, to be published

2) H.J. Daum, H. Meyer and J. Bürger, Zeitschr. f. Physik C
   J. Dorfan, Zeitschr. f. Physik C

3) Y.L. Dokshitser, D.I. D'yakonov, and S.I. Troyan,
   Phys.Lett. 78B (1978) 290
   Y.L. Dokshitser, D.I. D'yakonov, Fizika Elementarnykh Chastits
   (Leningrad 1979) and DESY L-Trans-234 (1979) and
   Physics reports 58, No. 5 (1980) 269

4) C.L. Basham, L.S. Brown, T.S. Ellis, S.T. Love, Phys.Rev.Lett. 41
   (1978) 1585 and Phys.Rev. D19 (1979) 2018

5) K. Konishi, A. Ukawa and G. Veneziano, Phys.Lett. 80B (1979) 259

4.2.6 Study of Two Photon Interactions

The storage ring PETRA provides a nice tool to investigate the two-photon exchange reaction in a detailed way. The reaction under study and its corresponding graph are shown in fig. 1, where X can be lepton pairs or hadrons.
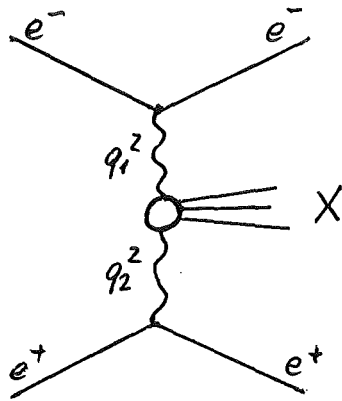
$$e^+ e^- \to e^+ e^- + X \quad (1)$$

For example

$$X = e^+ e^-, \; \mu^+ \mu^-, \; \tau^+ \tau^-$$

or

$$X = \pi's$$

Fig. 1:   Graph of two photon exchange reaction

If the system X consists of lepton antilepton pairs QED-predictions can be tested using the experimental data of the said type. We studied the reaction

$$e^+ e^- \quad \to \quad e^+ e^- e^+ e^- \qquad (2)$$

This is an exactly computable process for which a Monte Carlo simulation program was written. This model calculation has to take into account higher order corrections in the single photon channel which give rise to the same final state as reaction (2). The comparison between the QED predictions and our data are shown in fig. 2.

Both curves given by the Monte Carlo calculations and the data are in very good agreement except the mass region below 900 MeV. These losses are due to the fact that our electron recognition at such low energies is not well established yet.
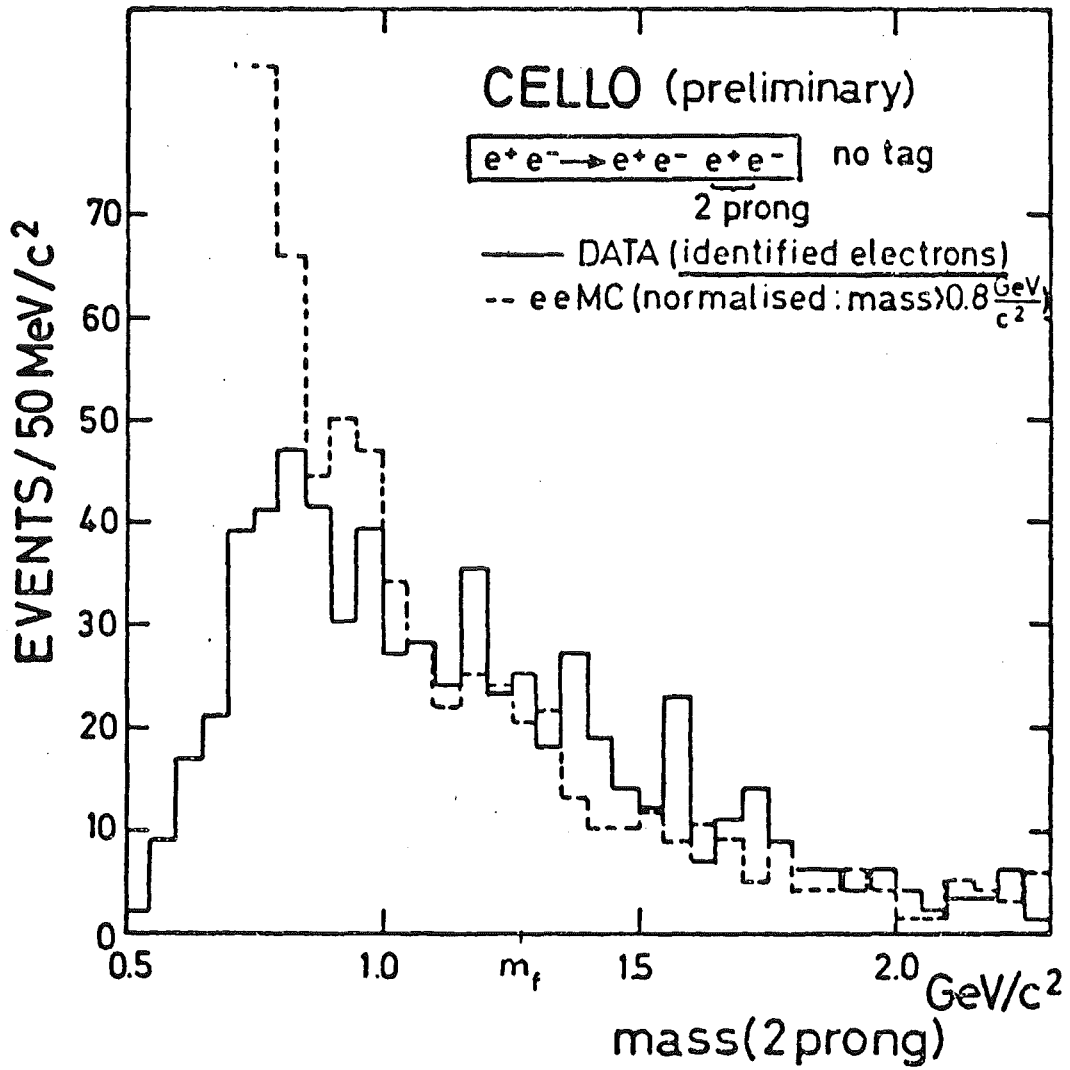
Fig. 2: Invariant mass of the two electrons in the inner detector for no tag two photon events compared to a MC simulation.

If the system X is consisting of hadrons several interesting re-
sults on resonance production can be obtained. We have investigated the
processes $e^+e^- \rightarrow e^+e^-\pi^+\pi^-$, $e^+e^- \rightarrow e^+e^-\mu^+\mu^-$, $e^+e^- \rightarrow e^+e^-e^+e^-$. Only two
tracks with opposite charge were requested to be in the inner detector
(so called no tag events). Fig. 3 gives an invariant mass distribution
of those two prong events. One can clearly see an enhancement of data
in the f = 1270 MeV mass region. Subtracting the QED background
by the help of the Monte Carlo program one is left with the f signal
as shown in the insert of fig. 3. A calculation of the $\gamma\gamma$-width assu-
ming helicity state λ = 2 gives

$$\Gamma_{\gamma\gamma}^{\lambda=2} = 3.4 \pm 0.2 \pm 0.7 \text{ keV}$$

The exclusive channel $\gamma\gamma \rightarrow \rho^0\rho^0 \rightarrow 4\pi^{\pm}$ and its strong threshold enhance-
ment have been first observed at PETRA by the Tasso-Group. The nature of
this $\rho^0\rho^0$ signal is still an open question. A new resonance at 1600 MeV
or glueball decay have been suggested. The results of the study of this
particular channel done by the CELLO-collaboration is shown in fig. 4.

The plot gives the invariant mass distribution of one $\pi^+\pi^-$ combi-
nation versus the other for 1.5 <= E_{cms} <= 1.9 GeV, assuming the events
found in our analysis to be $e^+e^- \rightarrow e^+e^-\pi^+\pi^-\pi^+\pi^-$. The clear enhancement
of the data near the ρ^0 mass region in both projections is evidence for
the $\rho^0\rho^0$ final state.
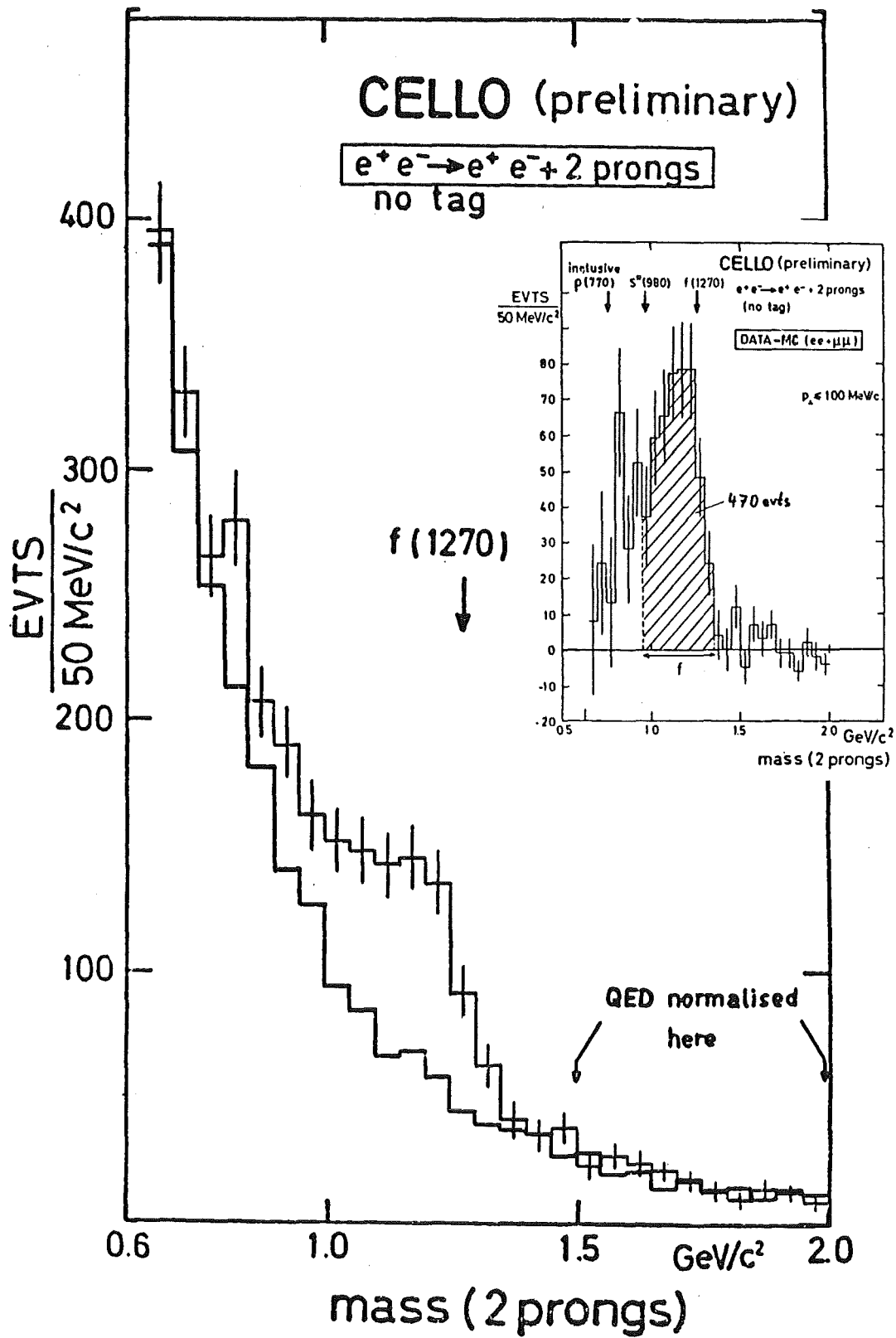
Fig. 3: Invariant mass of all two prong two photon events.

MASS OF TWO PION SYSTEM FOR 1.5<ECM<1.9
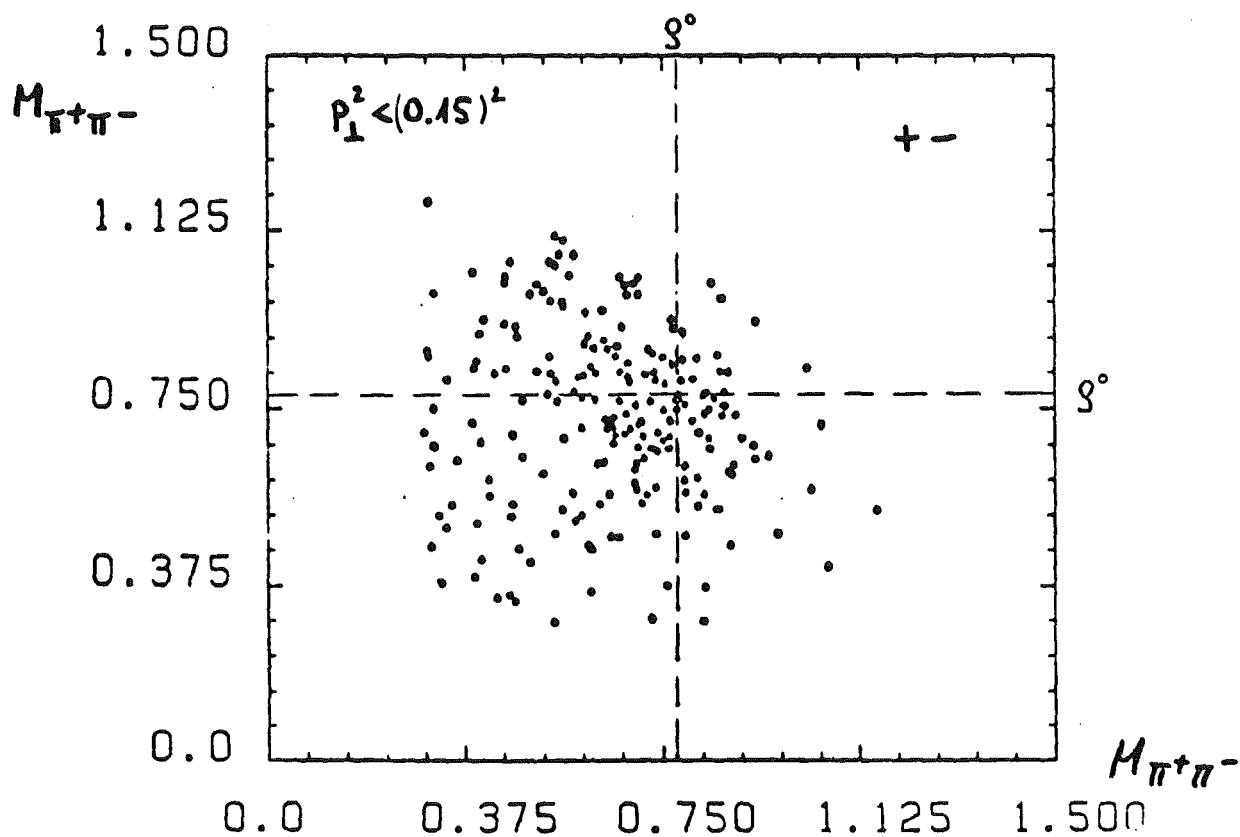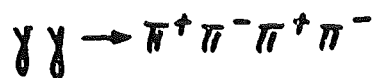
Fig. 4: Scatter plot of the invariant masses of two pion pairs in the reaction $e^+e^- \rightarrow e^+e^-\pi^+\pi^-\pi^+\pi^-$.
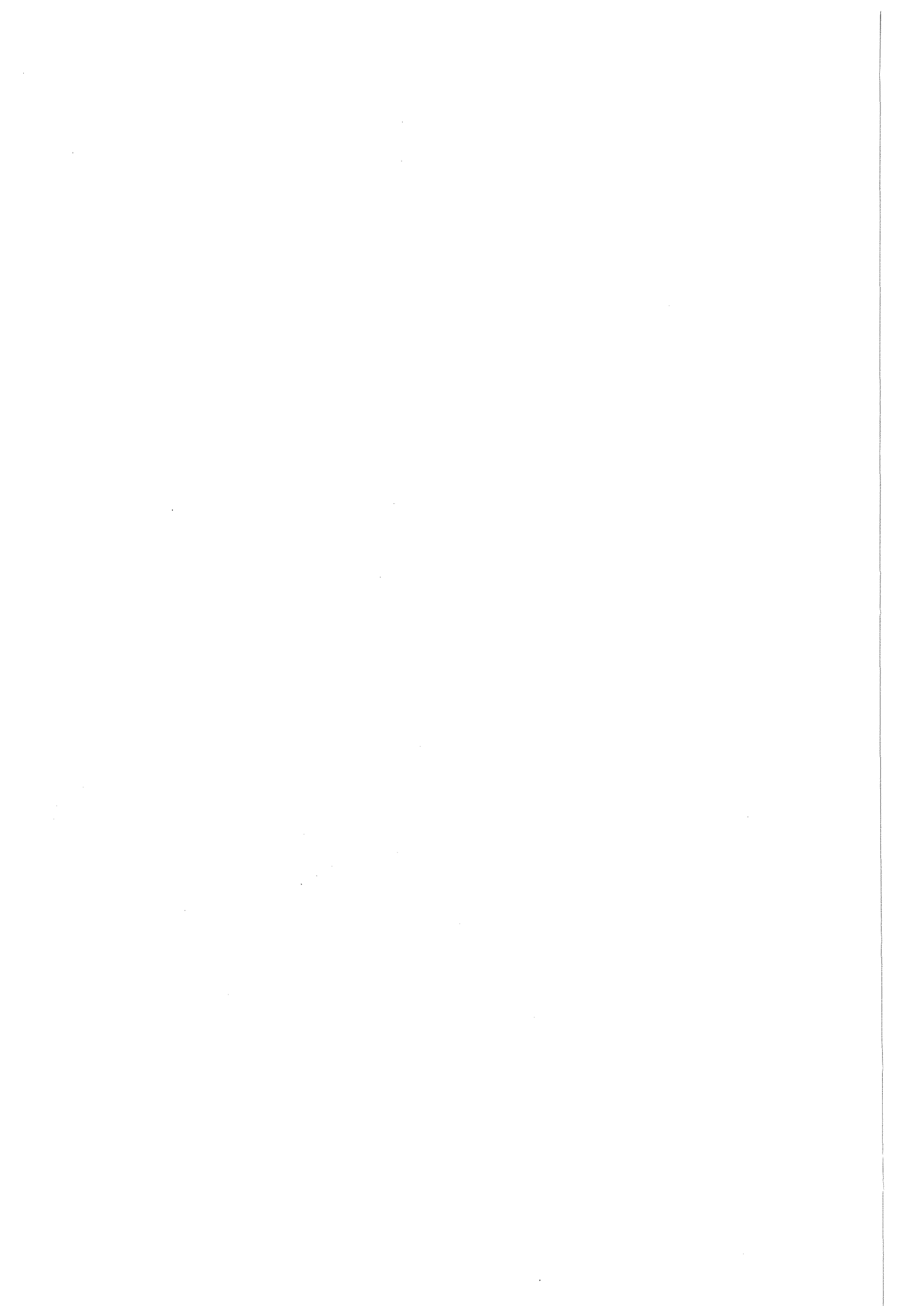
5.   LIST OF PUBLICATIONS

Institut für Kernphysik

Publications

14384   80   ZS;
IK;
ABELA, R.; KUNOLD, W.; SCHNEIDER, M.; SIMONS,
L.
Observation of the 2s-2p muonic x-ray
transition in ^{68}Zn.
SIN Newsletter, No 12(1979) S.36-37

15075   80   ZS;
IK;
ABELA, R.; KUNOLD, W.; SIMONS, L.; SCHNEIDER,
M.
Search for a dynamical E0 excitation in the
muonic ^{68}Zn atom.
Physics Letters B, 94(1980) S.331-34

14391   80   ZS;
IK;
ALBANESE, J.P.; ARVIEUX, J.; BOSCHITZ, E.;
CORFU, R.; EGGER, J.P.; GRETILLAT, P.;
INGRAM, Q.; LUNKE, C.; PEDRONI, E.; PERRIN,
C.; PIFFARETTI, J.; PFLUG, L.; SCHWARZ, E.;
WIEDNER, C.; ZICHY, J.
The SIN high resolution pion channel and
spectrometer.
Nuclear Instruments and Methods, 158(1979)
S.363-70

15153   80   ZS;
IK;
AMOLS, H.; BUECHE, G.; DEGITZ, H.; HOFMANN,
K.; JETTER, K.H.; KLEIN, U.; KLUGE, W.;
MATTHAEY, H.; MOLINE, A.; MUENCHMEYER, D.;
PRZYBILLA, G.; RANDOLL, H.; SCHMIDT, D.;
STABL, F.
Beitraege zum Projekt Strahlentherapie mit
negativen Pionen.
SIN-Jahresbericht 1979, S.C66-C68

14382   80   ZS;
IK;
ARVIEUX, J.; ALBANESE, J.P.; BOLGER, J.;
BOSCHITZ, E.; BUENERD, M.; GABATHULER, K.;
GRAM, P.A.M.; JANSEN, J.; MISCHKE, R.;
PROEBSTLE, G.; VOGLER, F.
Pionic excitation of giant resonances in ^{89}Y.
SIN Newsletter, No 12(1979) S.16-18

14383   80   ZS;
IK;
ARVIEUX, J.; BOLGER, J.; BOSCHITZ, E.; CORFU,
R.; PIFFARETTI, J.; ZIOCK, H.J.; ELLIS, R.J.;
ZIOCK, K.O.H.
A measurement of the ratio sigma(^{12}C[π^+, π^+p]
^{11}B/sigma(^{12}C[π^-, π^-p] ^{11}B).
SIN Newsletter, No 12(1979) S.19-20

15010   80   ZS;
IK;
ARVIEUX, J.; ALBANESE, J.P.; BUENERD, M.;
BOLGER, J.; BOSCHITZ, E.; PROEBSTLE, G.;
VOGLER, F.; GABATHULER, K.; GRAM, P.A.M.;
JANSEN, J.; MISCHKE, R.
Pionic excitation of giant resonances in ^{89}Y.
Physics Letters B, 90(1980) S.371-74

15444   80   ZS;
IK;
ARVIEUX, J.; BOLGER, J.; BOSCHITZ, E.;
PROEBSTLE, G.; JOHNSON, R.R.; MANGO, S.;
SMITH, G.R.; VOGLER, F.
Evidence for a dibaryon signal in the
measurement of elastic π^+d(pol.) scattering.
SIN-Newsletter, (1980) No 13, S.15-16

14387   80   ZS;
IK;
BACKENSTOSS, G.; DOERR, M.; KOWALD, W.;
KRAUSE, H.; SCHMIDT, G.; ULLRICH, H.; WEYER,
H.J.
Variable pion energies from a moderated fixed
energy pion beam.
SIN Newsletter, No 12(1979) S.50-54

15159   80   ZS;
IK;
BACKENSTOSS, G.; KOWALD, W.; SCHWANNER, I.;
TAUSCHER, L.; WEYER, H.J.; GOTTA, D.; GUIGAS,
R.
Precision determination of the difference of
the charge radii of ^{16}O and ^{18}O.
Physics Letters B, 95(1980) S.212-14

14390   80   ZS;
IK;
BALZER, R.; HAEBERLI, W.; HENNECK, R.; LANG,
J.; SIMONIUS, M.; JACQUEMART, CH.; JACCARD,
S.; REICHART, W.; WEDDIGEN, CH.;
Measurement of parity violation in p-p
scattering at 45 MeV.
SIN Newsletter, No 12(1979) S.76-81

14541   80   ZS;
IK;
BALZER, R.; HENNECK, R.; JACQUEMART, CH.;
LANG, J.; SIMONIUS, M.; HAEBERLI, W.;
WEDDIGEN, CH.; REICHART, W.; JACCARD, S.
Measurement of parity nonconservation in pp
scattering at 45 MeV.
Physical Review Letters, 44(1980) S.699-702

15152   80   ZS;
IK;
BALZER, R.; HAEBERLI, W.; HENNECK, R.;
JACCARD, S.; JACQUEMART, CH.; LANG, J.;
REICHART, W.; ROSER, T.; SIMONIUS, M.;
WEDDIGEN, CH.
Measurement of parity violation in p-p
scattering at 45 MeV.
SIN-Newsletter, (1980) No 13, S.50-52

14954   80   ZS;
IK;
BASSALLECK, B.; ENGELHARDT, H.D.; KLOTZ,
W.D.; LEWIS, C.W.; TAKEUTCHI, F.; ULLRICH,
H.; FURIC, M.
Wide angular range study of the reaction
$^{16}O(\pi^-, 2n)^{14}N$ with stopped pions.
Nuclear Physics A, 343(1980) S.365-81

15307   80   KfK; VOR;
IK;
BAUER, W.
Fabrication of niobium cavities.
In: Proceedings of the Workshop on RF
Superconductivity, Karlsruhe, July 2-4, 1980.
KfK-3019 (November 80) S.271-88

14880   80   SO;
IAK; IK;
BEER, H.; CIERJACKS, S.; DICKMANN, F.; ERBE,
D.; HAGE, W.; HINTERBERGER, F.; KAEPPELER,
F.; LEUGERS, B.; MUELLER, R.; NAQVI, A.A.;
ROSSEN, P.VON; SCHMALZ, G.; WICKENHAUSER, J.;
WISSHAK, K.
Nuclear data research in the Institut fuer
Angewandte Kernphysik, Kernforschungszentrum
Karlsruhe.
In: NEANDC(E)-212 U Vol.5 (June 80)
Progress Report on Nuclear Data Research in
the Federal Republic of Germany for the
Period April 1, 1979 to March 31, 1980 S.1-19

14392   80   ZS;
IK;
BESSET, D.; DO, H.Q.; FAVIER, B.; GREENIAUS,
L.G.; HESS, R.; LECHANOINE, C.; RAPIN, D.;
WERREN, D.W.; WEDDIGEN, CH.
Proton-carbon analyzing power between 300 and
560 MeV.
Nuclear Instruments and Methods, 166(1979)
S.379-89

14736   80   ZS;
IK;
BESSET, D.; DO, H.Q.; FAVIER, B.; GREENIAUS,
L.G.; HESS, R.; LECHANOINE, C.; RAPIN, D.;
WERREN, D.W.; WEDDIGEN, CH.
Measurement of the spin-dependent parameters
D, R, A, and P for small-angle p-p elastic
scattering between 300 and 600 MeV.
Physical Review D, 21(1980) S.580-98

15163   80   ZS;
IK;
BESSET, D.; DO, H.Q.; FAVIER, B.; HAUSAMMANN,
R.; HEER, E.; HESS, R.; LECHANOINE-LELUC, C.;
LEO, W.R.; RAPIN, D.; WERREN, D.W.; WEDDIGEN,
CH.; CAMERON, J.M.; JACCARD, S.; MANGO, S.
Measurement of the spin correlation parameter
Asub(00nn) and the polarization Asub(00n0) in
elastic p-p scattering between 400 and 600
MeV.
Nuclear Physics A, 345(1980) S.435-56

14542   80   ZS;
IK;
BIANCHI, M.; DIEHL, I.; BAARLI, J.; SULLIVAN,
A.H.
Dose fractionation effects with negative
pions.
British Journal of Radiology, 53(1980)
S.509-10

14386   80   ZS;
IK;
BLOMBERG, A.; GRAM, P.A.M.; INGRAM, Q.;
JANSEN, J.; MISCHKE, R.; PROEBSTLE, G.;
VOGLER, F.; ZICHY, J.
Study of the reaction $^{16}O(\pi, \pi p)$ in a
coincidence experiment.
SIN Newsletter, No 12(1979) S.48-49

14385   80   ZS;
IK;
BOLGER, J.; BOSCHITZ, E.; CORDELL, K.R.;
JOHNSON, R.; PROEBSTLE, G.; SAATHOFF, W.;
THORNTON, S.T.; WIEDNER, C.; ZICHY, J.
π^{+-}-scattering from ^{26}Mg at $Tsub(\pi) = 180$
MeV.
SIN Newsletter, No 12(1979) S.44-45

15484   80   ZS;
IK;
BOSCHITZ, E.
Neutron and proton components of nuclear
transitions in pion inelastic scattering on
^{26}Mg.
Physics Letters B, 97(1980) S.37-41

14393   80   ZS;
IK;
BUECHE, G.; KLUGE, W.; MATTAEY, H.; MOLINE,
A.; MUENCHMEYER, D.; SCHMIDT, D.
Test of a pion range monitor using the
radiative capture of pions on protons
$\pi^- p -->n\gamma$.
Radiation and Environmental Biophysics,
17(1980) S.169-85

14881   80   SO;
INR; IK;
BUTH, L.; CIERJACKS, S.; RAINBOW, M.T.;
SWINHOE, M.T.
Nuclear data research in the Institut fuer
Kernphysik, Kernforschungszentrum Karlsruhe.
In: NEANDC(E)-212 U Vol.5 (June 80)
Progress Report on Nuclear Data Research in
the Federal Republic of Germany for the
Period April 1, 1979 to March 31, 1980
S.20-24

15150   80   ZS;
IK;
CHATELAIN, P.; FAVIER, B.; FOROUGHI, F.;
HOFTIEZER, J.; JACCARD, S.; PIFFARETTI, J.;
WALDEN, P.; WEDDIGEN, CH.
Recent analyzing power measurements for the
reaction p(pol.)p-->πd.
SIN-Newsletter, (1980) No 13, S.30-31

14367   80   ZS;
IAK; IK;
CIERJACKS, S.; HINTERBERGER, F.; SCHMALZ, G.;
ERBE, D.; ROSSEN, P.VON; LEUGERS, B.
High precision time-of-flight measurements of
neutron resonance energies in carbon and
oxygen between 3 and 30 MeV.
Nuclear Instruments and Methods, 169(1980)
S.185-98

14902   80   SO; VOR;
INR; IK;
CIERJACKS, S.; RAINBOW, M.T.; SWINHOE, M.T.;
BUTH, L.
Neutron yields and spectra from 590 MeV(p, n)
reactions on lead targets.
Symp.on Neutron Cross-Sections from 10 to 50
MeV. Upton, N.Y., May 12-14, 1980
BNL-NCS-51245-Vol.1 of 2 (July 80) S.201-12
Zugl.: DOE/NDC-21/L; NEANDC(US)-208/L;
INDC(USA)-84/L

15331   80   KfK; VOR;
IK;
CIERJACKS, S.; RAINBOW, M.T.; SWINHOE, M.T.;
BUTH, L.
Neutron and charged particle production
yields and spectra from thick metal targets
by 590 MeV protons.
Meeting of the Internat.Collaboration on
Advanced Neutron Sources ICANS-IV, Tsukuba,
J, October 20-24, 1980
KfK-3097B (Oktober 80)

14543   80   PROC; VOR;
IK;
CITRON, A.
Superconducting accelerators. Invited paper.
Rizzuto, C. [Hrsg.]
Proc.of the 8th Internat.Cryogenic
Engineering Conf.ICEC 8, Genova, I, June 3-6,
1980.
Guildford, Surrey: IPC Science and Technology
Pr.1980. S.49-58

14903   80   KfK; VOR;
IK;
CITRON, A.
Compilation of experimental results and
operating experience.
In: Proceedings of the Workshop on RF
Superconductivity, Karlsruhe, July 2-4, 1980
KfK-3019 (November 80) S.3-26

14904   80   PROC; KfK; VOR;
IK;
CITRON, A.
Summary of the workshop on
RF-superconductivity at Karlsruhe, July 2-4,
1980.
Newman, W.S. [Hrsg.]
11th Internat.Conf.on High-Energy
Accelerators, Geneva, CH, July 7-11, 1980
Basel: Birkhaeuser 1980. S.864-77
In: Proceedings of the Workshop on RF
Superconductivity, Karlsruhe, July 2-4, 1980
KfK-3019 (November 80) S.323-37

15151   80   ZS;
IK;
DEGITZ, H.; HOFMANN, K.; KLEIN, U.; KLUGE,
W.; MARKUS, R.; MATTHAEY, H.; MOLINE, A.;
WIEDNER, U.
First measurements of the Piotron beam
properties.
SIN-Newsletter, (1980) No 13, S.46-49

15154   80   ZS;
IK;
ELLIS, R.J.; ZIOCK, H.J.; ZIOCK, K.O.H.;
BOLGER, J.; BOSCHITZ, E.; ARVIEUX, J.; CORFU,
R.; PIFFARETTI, J.
Coincidence measurements of the reactions
$^{12}C(\pi^{+-},\pi^{+-}d)^{10}B$ and $^{12}C(\pi^{+-},\pi^{+-}t)^{9}B$.
Physics Letters B, 88(1979) S.253-56

14388   80   ZS;
IK;
FAVIER, B.; FOROUGHI, F.; JACCARD, S.;
NUSSBAUM, C.; VUILLEUMIER, B.; WEDDIGEN, CH.
Pion production in the reaction p+p-->d+π.
SIN Newsletter, No 12(1979) S.56-60

15309   80   SR;
IK;
FAVIER, B.; FOROUGHI, F.; JACCARD, S.;
NUSSBAUM, C.; VUILLEUMIER, B.; WEDDIGEN, CH.
Pion-Produktion ueber die Reaktion
p+p-->π+d.
SIN Jahresbericht 1979, S.C22-C24

14772   80   KfK; VOR;
IK;
FLUEGGE, G.
Recent e+e- physics.
8th Internat.Winter Meeting on Fundamental
Physics, Ronda, E, March 24-29, 1980
KfK-2995 (Juli 80)

14905   80   KfK; VOR;
IK;
FLUEGGE, G.; KOPPITZ, B.; KOTTHAUS, R.;
LIERL, H.
Review of contributed papers on
experimentation at LEP.
Internat.Conf.on Experimentation at LEP,
Uppsala, S, June 16-20, 1980
KfK-3040B (Juni 80)

14394   80   KfK; DPL;
IK;
GLOECKNER, H.
Bestimmung der Trajektorien einlaufender
Antiprotonen in einem Experiment zur
Untersuchung gebundener Zustaende im
Antiproton-Proton-System.
KfK-2916B (Februar 80)
Diplomarbeit, Univ.Karlsruhe 1980

14461   80   ZS; VOR;
IK;
GRUNDNER, M.; HALBRITTER, J.
XPS and AES studies on oxide growth and oxide
coatings on niobium.
Journal of Applied Physics, 51(1980)
S.397-405

14545   80   ZS;
IK;
HALBRITTER, J.
On surface states at superconductor oxide
interfaces.
Solid state communications, 34(1980) S.675-78

15299   80   ZS;
IK;
HALBRITTER, J.; GRUNDNER, M.
On surface coatings and secondary yield of
Nb_3Sn and Nb.
Journal of Applied Physics, 51(1980)
S.5396-405

15310   80   KfK; VOR;
IK;
HALBRITTER, J.
Theoretical aspects in rf-superconductivity.
In: Proceedings of the Workshop on RF
Superconductivity, Karlsruhe, July 2-4, 1980.
KfK-3019 (November 80) S.190-214

15011   80   KfK; VOR;
IK;
HEERINGA, W.
Polarized targets in nuclear and high energy
physics.
5th Internat.Symp.on Polarization Phenomena
in Nuclear Physics, Santa Fe, N.M., August
11-15, 1980
KfK-3062 (November 80)

14395   80   KfK; DIS;
IK;
HENSLEY, F.
Eine Methode zur Bestimmung der
Neutroneneinfangquerschnitte von
Kryptonisotopen.
KfK-2918 (Februar 80)
Dissertation, Univ.Heidelberg 1980

15448   80   KfK;
IK;
HOEHLER, G.; KAISER, F.
Review and tables of pion-nucleon forward
amplitudes.
KfK-3027 (August 80)

15328   80   PROC; SO;
IK;
INGRAM, Q.
Pion-nucleus scattering around the 3-3
resonance.
Hungerford, E.V. [Hrsg.]
Meson-Nuclear Physics - 1979. Proc.of the 2nd
Internat.Topical Conf., Houston, Tex., March
5-9, 1979
New York, N.Y.: American Institute of Physics
1979 S.455-500. (AIP Conference Proceedings.
Nr 54)
DOE-CONF-790347

15160   80   ZS;
IK;
IZYCKI, M.; BACKENSTOSS, G.; TAUSCHER, L.;
BLUEM, P.; GUIGAS, R.; HASSLER, N.; KOCH, H.;
POTH, H.; FRANSSON, K.; NILSSON, A.;
PAVLOPOULOS, P.; ZIOUTAS, K.
Results of the search for K-series X-rays
from kaonic hydrogen.
Zeitschrift fuer Physik A - Atoms and Nuclei,
297(1980) S.11-15

15161   80   ZS;
IK;
IZYCKI, M.; BACKENSTOSS, G.; TAUSCHER, L.;
BLUEM, P.; GUIGAS, R.; HASSLER, N.; KOCH, H.;
POTH, H.; EMMOTH, B.; FRANSSON, K.; NILSSON,
A.; PAVLOPOULOS, P.; ZIOUTAS, K.
Results on the measurement of K-series X-rays
from antiprotonic hydrogen.
Zeitschrift fuer Physik A - Atoms and Nuclei,
297(1980) S.51-59

15313   80   PROC; VOR;
IK;
KIRCHGESSNER, J.; KNEISEL, P.; PADAMSEE, H.;
PETERS, J.; PROCH, D.; SUNDELIN, R.; TIGNER,
M.
Design studies for a 1500 MHz superconducting
accelerator cavity for use in an e^+e^- storage
ring.
11th Internat.Conf.on High Energy
Accelerators, Geneva, CH, July 7-11, 1980
Basel: Birkhaeuser 1980. S.886-891

15314   80   KfK; VOR;
IK;
KNEISEL, P.
Surface preparation of niobium.
In: Proceedings of the Workshop on RF
Superconductivity, Karlsruhe, July 2-4, 1980.
KfK-3019 (November 80) S.27-40

12325   80   PAT; DAS;
IK;
KUEHN, W.
Verfahren und Schaltungsanordnung zum Regeln
der Eigenfrequenz und der Phasenlage mehrerer
supraleitender Resonatoren.
DE-AS 27 00 122 (19.6.1980)
US-PS 4 196 398 (1.4.1980)   (PLA 76/74)

15315   80   KfK;
IK;
KUNTZE, M.; [HRSG.]
Proceedings of the workshop on rf
superconductivity.
Karlsruhe, Federal Republic of Germany, July
2-4, 1980
KfK-3019 (November 80)

15316   80   KfK; VOR;
IK;
KUNTZE, M.
Additional design criteria for low
β structures.
In: Proceedings of the Workshop on RF
Superconductivity, Karlsruhe, July 2-4, 1980.
KfK-3019 (November 80) S.237-42

15155   80   ZS;
IK;
MISCHKE, R.; BLOMBERG, A.; GRAM, P.A.M.;
JANSEN, J.; ZICHY, J.; BOLGER, J.; BOSCHITZ,
E.; INGRAM, Q.; PROEBSTLE, G.
Inelastic pion double charge exchange on ^{16}O
at 240 MeV.
Physical Review Letters, 44(1980) S.1197-1200

14892   80   ZS;
IAK; IK;
PATIN, Y.; CIERJACKS, S.; LACHKAR, J.;
SIGAUD, J.; HAOUAT, G.; COCU, F.
Fission fragment energy-velocity correlation
measurements for the ^{233}U(d, pf)-reaction.
Nuclear Instruments and Methods, 160(1979)
S.471-85

14649   80   ZS;
IK;
POTH, H.; ABELA, R.; BACKENSTOSS, G.; BLUEM,
P.; FETSCHER, W.; HAGELBERG, R.; IZYCKI, M.;
KOCH, H.; NILSSON, A.; PAVLOPOULOS, P.;
SIMONS, L.; TAUSCHER, L.
The antiprotonic X-ray spectrum of liquid
helium.
Physics Letters B, 76(1978) S.523-26

14389   80   ZS;
IK;
PRZYBILLA, G.; JETTER, K.H.; BUECHE, G.;
KLUGE, W.; MATTHAEY, H.
A new Monte-Carlo-programme for the
calculations of dose distributions from
π^--beams stopped in tissue equivalent
phantoms.
SIN Newsletter, No 12(1979) S.70-73

15333   80   KfK; DPL;
IK;
PRZYBILLA, G.
Ein neues Monte-Carlo-Programm zur Berechnung
der Energieuebertragung von einem
π^--Mesonenstrahl auf ein gewebeaehnliches
Phantom.
KfK-3022 (November 80)
Diplomarbeit, Universitaet Karlsruhe 1980

14396   80   KfK; DIS;
IK;
SCHWARZ, W.
Charakterisierung von Tunnelbarrieren durch
Leitfaehigkeitsmessungen an
Niob-Nioboxid-Blei Kontakten.
KfK-2913 (Maerz 80)
Dissertation, Univ.Karlsruhe 1980

14546   80   PROC; VOR;
IK;
SCHWARZ, W.; HALBRITTER, J.
Tunnel barriers in Nb-Nbsub(x)Osub(y)-Pb
junctions.
Abeles, F.; Croset, M. [Hrsg.]
Proc.of the 8th Internat.Vacuum Congress,
Cannes, F, September 22-26, 1980.
Paris: Societe Francaise du Vide 1980. Vol. 1
S.443-46

14807   80   KfK;
IK;
WEDDIGEN, CH.
A phenomenological interpretation of the
production cross section for the reaction
p+p-->w+d.
KfK-2996B (Juli 80)

15566   81   ZS;
IK;
BREUER, H.; WAGNER, G.J.; KNOEPFLE, K.T.;
MAIRLE, G.; DOLL, P.
Charged particle decay of hole states in ^{16}O.
Physics Letters B, 96(1980) S.35-38

15567   81   ZS;
IK;
DAKOWSKI, M.; DOLL, P.; GOBBI, A.; RUDOLF,
G.; SANN, H.; BOCK, R.; LYNEN, U.; OLMI, A.
Structure effects in dissipative collisions.
Physics Letters B, 90(1980) S.379-83

15568   81   ZS;
IK;
SYMONS, T.J.M.; DOLL, P.; BINI, M.; HENDRIE,
D.L.; MAHONEY, J.; MANTZOURANIS, G.; SCOTT,
D.K.; BIBBER, K.VAN; VIYOGI, Y.P.; WIEMAN,
H.H.; GELBKE, C.K.
High energy proton emission in reactions
induced by 315 MeV ^{16}O ions.
Physics Letters B, 94(1980) S.131-34

15569   81   ZS;
IK;
BINI, M.; GELBKE, C.K.; SCOTT, D.K.; SYMONS,
T.J.M.; DOLL, P.; HENDRIE, D.L.; LAVILLE,
J.L.; MAHONEY, J.; MERMAZ, M.C.; OLMER, C.;
BIBBER, K.VAN; WIEMAN, H.H.
Alpha particle emission in peripheral heavy
ion reactions at 20 MeV/u.
Physical Review C, 22(1980) S.1945-50

15573   81   ZS;
IK;
ALBANESE, J.P.; ARVIEUX, J.; BOLGER, J.;
BOSCHITZ, E.; INGRAM, Q.; JANSEN, J.; ZICHY,
J.
Elastic scattering of positive pions by ^{16}O
between 80 and 340 MeV.
Nuclear Physics A, 350(1980) S.301-31

15578   81   ZS;
IK;
SIMONIUS, M.; HENNECK, R.; JACQUEMART, CH.;
LANG, J.; HAEBERLI, W.; WEDDIGEN, CH.
Effects of transverse polarization components
in parity tests with longitudinally polarized
nucleons.
Nuclear Instruments and Methods, 177(1980)
S.471-80

15599   81   ZS;
IK;
BUECHE, G.; PRZYBILLA, G.
Distributions of absorbed dose from π^--meson
beams calculated from a new Monte Carlo
program.
Nuclear Instruments and Methods, 179(1981)
S.321-41

15600   81   ZS;
IK;
NOGUCHI, S.; KOJIMA, Y.; HALBRITTER, J.
Measurement of a superconducting 500 MHz Nb
cavity in the TM_{010}-mode.
Nuclear Instruments and Methods, 179(1981)
S.205-15

15673   81   KfK; DIS;
IK;
ABDEL-KHALEK, F.
Untersuchung der Reaktion $\pi^-p \rightarrow \pi^0 eta^0 n$ bei
Pionimpulsen von 25 und 40 GeV/c.
KfK-3115 (Maerz 81)
Dissertation, Universitaet Karlsruhe 1981

15674   81   ZS;
IK;
AMOLS, H.I.; BUECHE, G.; KLUGE, W.; MATTHAEY,
H.; MOLINE, A.; MUENCHMEYER, D.
Multiple scattering distributions for
therapeutic pion beams.
Physics in Medicine and Biology, 26(1981)
S.277-89

15675   81   ZS;
IK;
BOLGER, J.; BOSCHITZ, E.; PROEBSTLE, G.;
SMITH, G.R.; MANGO, S.; VOGLER, F.; JOHNSON,
R.R.; ARVIEUX, J.
Evidence for a dibaryon signal in the
measurement of elastic π^+-dsub(pol)
scattering.
Physical Review Letters, 46(1981) S.167-70

15676   81   KfK;
IK;
ZEITNITZ, B.
Neutrino physics at the spallation neutron
source.
KfK-3155 (Maerz 81)

15840   81   KfK; SO;
IK;
CELLO-COLLABORATION
Measurement of $e^+e^- \longrightarrow e^+e^-$ and
$e^+e^- \longrightarrow$ gammagamma at energies up to 36.7 GeV.
KfK-3181 (Mai 81)
DESY-81-021 (Mai 81)

15841   81   KfK;
IK;
GABRIEL, T.A.; LILLIE, R.A.; BISHOP, B.L.;
WILCZYNSKI, J.; ZEITNITZ, B.
Neutrino physics at the spallation neutron
source.
II. Neutrino fluxes, shielding considerations
and detector analysis.
KfK-3174 (Juni 81)

15842   81   ZS;
IK;
HOFTIEZER, J.; WEDDIGEN, CH.; FAVIER, B.;
JACCARD, S.; WALDEN, P.; CHATELAIN, P.;
FOROUGHI, F.; NUSSBAUM, C.; PIFFARETTI, J.
Energy dependence of the pp-->π^+d
differential cross section between 500 and
600 MeV.
Physics Letters B, 100(1981) S.462-65

15843   81   KfK;
IK;
VETTER, J.E.; [HRSG.]
The basic concept of the SNQ linear
accelerator.
KfK-3180B (Juni 81)

15971   81   ZS;
IK;
PASSOW, C.
Physik der Teilchenstrahlen hoher Dichte.
KfK-Nachrichten, 13(1981) No 1-2, S.130-36

15972   81   ZS;
IK;
FLUEGGE, G.
Untersuchung von Quarks und Leptonen im
CELLO-Detektor.
KfK-Nachrichten, 13(1981) No 1-2, S.137-43

15973   81   ZS;
IK;
KLAGES, H.O.
Experimente mit Schnellen Neutronen am
Karlsruher Zyklotron.
KfK-Nachrichten, 13(1981) No 1-2, S.144-49

15981   81   ZS;
IK;
BAARLI, J.; BIANCHI, M.; DIEHL-MARSHALL, I.;
RAFFNSOE, R.C.; RIEDEL, M.; SOTIRIOUS, D.;
SULLIVAN, A.H.; TUYN, J.W.N.
The biological effect of very high energy
hadrons.
International Journal of Radiation Biology,
39(1981) S.559-63

15982   81   ZS;
IK;
CELLO-COLLABORATION
CELLO - a new detector at PETRA.
Proc.of the Internat.Conf.on Experimentation
at LEP, Uppsala, S, June 15-20, 1980
Physica Scripta, 23(1981) S.610-22

15984   81   ZS;
IK;
DIEHL-MARSHALL, I.; BIANCHI, M.
Induction of micronuclei in bean roots by 250
GeV hadrons.
Radiation and Environmental Biophysics,
19(1981) S.117-24

Conference Contributions

V14257   80   VOR;
IK;
ABDEL-WAHAB, M.S.; BENTE, H.; DOBIASCH, H.;
HAESNER, B.; HUSSON, L.; KLAGES, H.O.;
SCHMALZ, G.; SCHWARZ, P.; WILCZYNSKI, J.;
HINTERBERGER, F.; EVERSHEIM, P.D.
Der totale Neutronenwirkungsquerschnitt des
10B und 11B.
Fruehjahrstagung DPG, Kernphysik, Muenchen,
17.-21. Maerz 1980. Verhandlungen der
Deutschen Physikalischen Gesellschaft, R.6,
Bd15(1980) S.1240

V14238   80   VOR;
IK;
ABELA, R.; KUNOLD, W.; SCHNEIDER, M.; SIMONS,
L.
Messung der EO-Anregung des ^{68}Zn-Kerns mit
myonischen Atomen.
Fruehjahrstagung DPG, Kernphysik, Muenchen,
17.-21. Maerz 1980. Verhandlungen der
Deutschen Physikalischen Gesellschaft, R.6,
Bd15(1980) S.1072

V15165   80   VOR;
IK;
ABELA, R.; KUNOLD, W.; SCHNEIDER, M.;
OESTERLE, W.; SIMONS, L.; WUEST, J.
Time differential and integral measurements
of the ground state polarisation of muonic
atoms.
Fruehjahrstagung der Schweizerischen
Physikalischen Gesellschaft, Zuerich, CH,
10.-12.April 1980

V14504   80   VOR;
IK;
ALBANESE, J.P.; ARVIEUX, J.; BOLGER, J.;
BOSCHITZ, E.; BUENERD, M.; GRAM, P.A.M.;
INGRAM, Q.; JANSEN, J.; LEBRUN, D.; MISCHKE,
R.; PROEBSTLE, G.; SAATHOFF, W.; VOGLER, F.;
WIEDNER, C.; ZICHY, J.;
KARLSRUHE-GRENOBLE-HEIDELBERG-ERLANGEN-
SIN-KOLLABORATION
Inelastische π-Streuung im Gebiet der
(3,3)-Resonanz.
Fruehjahrstagung DPG, Kernphysik, Muenchen,
17.-21.Maerz 1980. Verhandlungen der
Deutschen Physikalischen Gesellschaft, R.6,
Bd 15(1980) S.1054-55

V14259   80   VOR;
IK;
APEL, W.D.; AUGENSTEIN, K.H.; BERTOLUCCI, E.;
DONSKOV, S.V.; INYAKIN, A.V.; KACHANOV, V.A.;
KRASNOKUTSKY, R.N.; KRUEGER, M.; LEDER, G.;
LEDNEV, A.A.; MANNELLI, I.; MIKHAILOV, YU.V.;
MUELLER, H.; PIERAZZINI, G.M.; PROKOSHKIN,
YU.D.; QUAGLIA, M.; SCHNEIDER, H.; SKRIBANO,
A.; SERGIAMPIETRI, F.; SHUVALOV, R.S.;
SIGURDSSON, G.; VINCELLI, M.L.
Measurement of $\pi^-p-->\pi^0\pi^0n$ at 25 GeV/c.
Fruehjahrstagung DPG, Teilchenphysik,
Dortmund, 27.-29.Februar 1980. Verhandlungen
der Deutschen Physikalischen Gesellschaft,
R.6, Bd 15(1980) S.894

V14262   80   VOR;
IK;
APEL, W.D.; ENGLER, J.; MOENNIG, F.; SCHMIDT,
G.; SCHNEIDER, H.; GROSSE-WIESMANN, P.;
GUNDERSON, B.; LUERS, D.; MEYER, T.;
OBERLACK, H.; SCHACHT, P.; SCHACHTER, M.J.;
STEINER, H.
Das Argon-Kalorimeter des CELLO-Detektors.
Fruehjahrstagung DPG, Teilchenphysik,
Dortmund, 27.-29.Februar 1980. Verhandlungen
der Deutschen Physikalischen Gesellschaft,
R.6, Bd 15(1980) S.900-01

V14232   80   VOR;
IK;
ARVIEUX, J.; BOLGER, J.; BOSCHITZ, E.;
JOHNSON, R.; MANGO, S.; PROEBSTLE, G.; SMITH,
G.; VOGLER, F.;
KARLSRUHE-GRENOBLE-ERLANGEN-SIN-KOLLABORATION
Messung der Vektoranalysierstaerke in der
elastischen πD-Streuung.
Fruehjahrstagung DPG, Kernphysik, Muenchen
17.-21. Maerz 1980. Verhandlungen der
Deutschen Physikalischen Gesellschaft, R.6,
Bd15(1980) S.1055

V14264   80   VOR;
IK;
BAUER, W.; BRANDELIK, A.; CITRON, A.;
HALBRITTER, J.; KOJIMA, Y.; KUNTZE, M.;
NOGUCHI, S.
Messung von Beschleunigungsfeldstaerken und
Gueten an supraleitenden Resonatoren fuer
e^+-e^--Speicherringe.
Fruehjahrstagung DPG, Teilchenphysik,
Dortmund, 27.-29.Februar 1980. Verhandlungen
der Deutschen Physikalischen Gesellschaft,
R.6, Bd 15(1980) S.902-03

V14601   80   VOR;
IK;
BAUER, W.
Messungen an 500-MHz Resonatoren fuer DORIS.
Vortr.: Institut fuer Experimentalphysik,
Gesamthochschule Wuppertal, 3.Juni 1980

V14260   80   VOR;
IK;
BLUEM, P.; GUIGAS, R.; KOCH, H.; MEYER, M.;
POTH, H.; RAICH, U.; RICHTER, B.;
BACKENSTOSS, G.; PAVLOPOULOS, P.; TAUSCHER,
L.; ADIELS, L.; BERGSTROEM, I.; FRANSSON, K.;
KEREK, A.; SUFFERT, M.; ZIOUTAS, K.
Suche nach Baryonium-Zustaenden unterhalb der
Schwelle.
Fruehjahrstagung DPG, Teilchenphysik,
Dortmund, 27.-29.Februar 1980. Verhandlungen
der Deutschen Physikalischen Gesellschaft,
R.6, Bd 15(1980) S.894-95

V15046   80   VOR;
IK;
BLUEM, P.
Experimente mit gestoppten Antiprotonen am
Lear.
Vortr.: Arbeitstreffen Mittelenergiephysik,
Todtnauberg, 2.-8.Oktober 1980

V14261   80   VOR;
IK;
BODENKAMP, J.; FRIES, D.C.; MARKOU, A.;
SEITZ, E.; BEHREND, H.J.; HESSE, W.P.;
MCNEELY, W.A.; MIYACHI, T.; SCHROEDER, V.
Abschliessende Ergebnisse einer
experimentellen Untersuchung der Reaktion
γp-->Proton Antiproton Proton.
Fruehjahrstagung DPG, Teilchenphysik,
Dortmund, 27.-29.Februar 1980. Verhandlungen
der Deutschen Physikalischen Gesellschaft,
R.6, Bd 15(1980) S.898-99

V15308   80   VOR;
IK;
BOLGER, J.; BOSCHITZ, E.; PROEBSTLE, G.;
SMITH, G.; MANGO, S.; VOGLER, F.; JOHNSON,
R.R.; ARVIEUX, J.
Evidence for a dibaryon signal in the
measurement of elastic π-d scattering.
Internat.Symp.on High Energy Physics with
Polarized Beams and Polarized Targets,
Lausanne, CH, September 25 - October 1, 1980

V15485   80   VOR;
IK;
BOSCHITZ, E.
Experimental search for dibaryon resonances.
From Collective States to Quarks in Nuclei.
Workshop, Bologna, I, November 24-28, 1980

V14263   80   VOR;
IK;
CELLO-KOLLABORATION; SCHMIDT, G.
Arbeitsweise und erste Resultate der
LAr-Kalorimeter-Elektronik am CELLO-Detektor.
Fruehjahrstagung DPG, Teilchenphysik,
Dortmund, 27.-29.Februar 1980. Verhandlungen
der Deutschen Physikalischen Gesellschaft,
R.6, Bd 15(1980) S.901

V15329   80   VOR;
IK;
CIERJACKS, S.; RAINBOW, M.T.; SWINHOE, M.T.;
BUTH, L.
Angular and depth dependent neutron yields
and spectra from 590 MeV (p,n) reactions in
thick lead targets.
5th Nat.Soviet Conf.on Neutron Physics, Kiev,
SU, September 15-19, 1980

V15330   80   VOR;
IK;
CIERJACKS, S.; SCHMALZ, G.; HINTERBERGER, F.;
ROSSEN, P.VON
Experimental study of isospin mixing in ^{12}C +
n-->^{13}C(T=3/2) and ^{16}O +
n-->^{17}O(T=3/2)resonances.
5th Nat.Soviet Conf.on Neutron Physics, Kiev,
SU, September 15-19, 1980

V15463   80   VOR;
IK;
CIERJACKS, S.
Accelerator-based white neutron sources.
Invited paper.
IAEA Consultants' Meeting on Neutron Source
Properties, Debrecen, H, March 17-21, 1980

V15464   80   VOR;
IK;
CIERJACKS, S.
Methods of absolute fast fission cross
section determinations employing the (n,p)
standard. Invited paper.
Internat.Symp.on Selected Topics of the
Interaction of Fast Neutrons and Heavy Ions
with Atomic Nuclei, Dresden, 17.-21.November
1980

V14233   80   VOR;
IK;
DOERR, M.; FETSCHER, W.; GOTTA, D.; RAICH,
U.; SCHMIDT, G.; ULLRICH, H.; BACKENSTOSS,
G.; KOWALD, W.; SCHWANNER, I.; WEYER, H.J.
Emission von Teilchenpaaren nach
π^--Absorption in ^6Li und ^7Li.
Fruehjahrstagung DPG, Kernphysik, Muenchen,
17.-21. Maerz 1980. Verhandlungen der
Deutschen Physikalischen Gesellschaft, R.6,
Bd15(1980) S.1056

V14254   80   VOR;
IK;
DOERR, M.; FETSCHER, W.; GOTTA, D.; RAICH,
U.; SCHMIDT, G.; ULLRICH, H.; BACKENSTOSS,
G.; KOWALD, W.; SCHWANNER, I.; WEYER, H.J.
Dalitzplot der Reaktion $\pi^{-3}He \longrightarrow pnn$.
Fruehjahrstagung DPG, Kernphysik, Muenchen,
17.-21. Maerz 1980. Verhandlungen der
Deutschen Physikalischen Gesellschaft, R.6,
Bd15(1980) S.1211

V14544   80   VOR;
IK;
DOERR, M.; FETSCHER, W.; GOTTA, D.; RAICH,
U.; SCHMIDT, G.; ULLRICH, H.; BACKENSTOSS,
G.; KOWALD, W.; SCHWANNER, I.; TAUSCHER, L.;
WEYER, H.J.
Absorption of stopped negative pions in ^3He.
9th Internat.Conf.on the Few-Body Problem.
Eugene, Or., August 17-23, 1980

V15047   80   VOR;
IK;
GOTTA, D.
π^--Absorption in ^3He.
Vortr.: University of British Columbia,
Vancouver, CDN, September 9, 1980

V14602   80   VOR;
IK;
GRUNDNER, M.; HALBRITTER, J.
XPS and AES studies on oxide growth and oxide
coatings on niobium.
Vortr.: Universitaet und Istituto Nazionale
di Fisica Nucleare, Genova, I, 31.Maerz 1980

V14237   80   VOR;
IK;
GUIGAS, R.; BLUEM, P.; KOCH, H.; MEYER, M.;
POTH, H.; RICHTER, B.; ZIOUTAS, K.;
BACKENSTOSS, G.; PAVLOPOULOS, P.; TAUSCHER,
L.; BERGSTROEM, I.; FRANSSON, K.; NIELSON, A.
Messung starker Wechselwirkungsparameter am
antiprotonischen $^{6,7}Li$.
Fruehjahrstagung DPG, Kernphysik, Muenchen,
17.-21. Maerz 1980. Verhandlungen der
Deutschen Physikalischen Gesellschaft, R.6,
Bd15(1980) S.1071

V14214   80   VOR;
IK;
HALBRITTER, J.
On oxide growth on Nb and Nb_3 Sn.
Vortrag: Univ.de Paris, L'Ecole Normale
Superieure, January 24, 1980

V14215   80   VOR;
IK;
HALBRITTER, J.
On surface coatings and secondary yield of
Nb₃Sn and Nb.
Vortr.: Univ.de Paris, Orsay, January 25,
1980
Vortr.: Univ.und Istituto Nazionale di Fisica
Nucleare, Genova, I, 1.April 1980

V14278   80   VOR;
IK;
HALBRITTER, J.
Ueber Oberflaechenzustaende an
Metall-Oxyd-Grenzflaechen und den Tunnelstrom
(leakage current) durch diese Zustaende.
Fruehjahrstagung DPG, Festkoerperphysik,
Freudenstadt, 24.-28.Maerz 1980.
Verhandlungen der Deutschen Physikalischen
Gesellschaft, R.6, Bd 15(1980) S.387-88

V15166   80   VOR;
IK;
HALBRITTER, J.; PHILIPP, A.
On the temperature and frequency dependence
of the surface resistance of superconducting
Nb.
Applied Superconductivity Conf.'80, Santa Fe,
N.M., September 29 - October 2, 1980

V15167   80   VOR;
IK;
HALBRITTER, J.
Electron loading in superconducting 500 MHz
Nb cavities.
Vortr.: Physikalisches Institut, Universitaet
Wuppertal, 26.Juni 1980

V15168   80   VOR;
IK;
HALBRITTER, J.
On residual rf losses and tunnel currents
caused by interface states.
Applied Superconductivity Conf.'80, Santa Fe,
N.M., September 29 - October 2, 1980

V15311   80   VOR;
IK;
HALBRITTER, J.
Supraleitende Nb-Hohlraumresonatoren und
deren Oberflaechenprobleme.
Vortr.: Elektrotechnik Kolloquium,
Ruhruniversitaet Bochum, 25.Juni 1980

V15312   80   VOR;
IK;
HALBRITTER, J.
On Nb-Nb$_2$O$_5$-interfaces tunnel anomalies and
electron emission.
Vortr.: Departement de Physique de la Matiere
Condensee, l'Universite de Geneve, Geneve,
CH, 18.November 1980

V15170   80   VOR;
IK;
HENNECK, R.; JACQUEMART, CH.; LANG, J.;
SIMONIUS, M.; BALZER, R.; HAEBERLI, W.;
JACCARD, S.; REICHART, W.; WEDDIGEN, CH.
Parity violation in pp scattering at 45 MeV:
discussion of systematic error sources.
5th Internat.Symp.on Polarization Phenomena
in Nuclear Physics, Santa Fe, N.M., August
11-15, 1980

V14258   80   VOR;
IK;
HINTERBERGER, F.; EVERSHEIM, P.D.;
ABDEL-WAHAB, M.S.; BENTE, H.; DOBIASCH, H.;
HAESNER, B.; HUSSON, L.; KLAGES, H.O.;
SCHMALZ, G.; SCHWARZ, P.; WILCZYNSKI, J.
21Ne(T=3/2) Resonanzen im totalen
Neutronenwirkungsquerschnitt des 20Ne.
Fruehjahrstagung DPG, Kernphysik, Muenchen,
17.-21. Maerz 1980. Verhandlungen der
Deutschen Physikalischen Gesellschaft, R.6,
Bd15(1980) S.1241

V14906   80   VOR;
IK;
HINTERBERGER, F.; EVERSHEIM, P.D.; ROSSEN,
P.VON; CIERJACKS, S.; KECSKEMETI, J.; KLAGES,
H.O.
High-resolution study of
isospin-nonconserving neutron and proton
resonances.
Internat.Symp.on High Precision Nuclear
Physics, Bad Honnef, June 9-11, 1980

V15169   80   VOR;
IK;
HOFTIEZER, J.; WEDDIGEN, CH.; FAVIER, B.;
JACCARD, S.; CHATELAIN, P.; FOROUGHI, F.;
NUSSBAUM, C.
Differential cross section for pion
production in the reaction pp-->πd between
500 and 600 MeV.
5th Internat.Symp.on Polarization Phenomena
in Nuclear Physics, Santa Fe, N.M., August
11-15, 1980

V14234   80   VOR;
IK;
KLAGES, H.O.; SCHWARZ, P.
Ueber einen neuartigen Detektor fuer schnelle
Neutronen mit hoher
Ansprechwahrscheinlichkeit (Black-Detektor).
Fruehjahrstagung DPG, Kernphysik, Muenchen,
17.-21. Maerz 1980. Verhandlungen der
Deutschen Physikalischen Gesellschaft, R.6,
Bd15(1980) S.1057-58

V14907   80   VOR;
IK;
KLAGES, H.O.; DOBIASCH, H.; FISCHER, R.;
HAESNER, B.; HEERINGA, W.; SCHWARZ, P.;
WILCZYNSKI, J.; ZEITNITZ, B.
Analysing power of the elastic $N-^3He$
scattering.
5th Internat.Symp.on Polarization Phenomena
in Nuclear Physics, Santa Fe, N.M., August
11-15, 1980

V15332   80   VOR;
IK;
KLOSE, W.; STILLER, H.
The status of the German spallation source
project (SNQ).
Meeting of the Internat.Collaboration on
Advanced Neutron Sources ICANS-IV, Tsukuba,
J, October 20-24, 1980

V14216   80   VOR;
IK;
MITTAG, K.
Bericht ueber das Vorhaben
'Spallationsneutronenquelle'.
Vortrag: Institut fuer Angewandte Physik,
Univ.Frankfurt, 1.Maerz 1980

V15136   80   VOR;
IK;
MOELLER-PETERSEN, P.; BELL, M.; CHANEY, I.;
CITTOLIN, S.; HERR, H.; KOZIOL, H.; KRIENEN,
F.; LEBEE, G.; PETRUCCI, G.; POTH, H.;
SHERWOOD, T.; STEFANINI, G.; TAYLOR, G.;
TECCHIO, L.; RUBBIA, C.; VAN DER MEER, S.;
WIKBERG, T.
Electron cooling experiments in the ICE
storage ring at CERN.
5th European Symp.on Nucleon-Antinucleon
Interactions, Brixen, I, June 23-28, 1980

V15171   80   VOR;
IK;
PADAMSEE, H.; PROCH, D.; KNEISEL, P.;
MIODUSZEWSKI, J.
Field strength limitations in superconducting
cavities - multipacting and thermal
breakdown.
Applied Superconductivity Conf.'80, Santa Fe,
N.M., September 29 - October 2, 1980

V14955   80   VOR;
IK;
PASSOW, C.
Nichtlineare Elektrodynamik.
Vortr.: Institut fuer Theoretische Physik,
Universitaet Karlsruhe, 4.Februar 1980

V15183   80   VOR;
IK;
PASSOW, C.
Physik der Teilchenstrahlen hoher Dichte.
VDI Tagung 'Beschleunigertechnik', Karlsruhe,
28.-31.Oktober 1980

V14279   80   VOR;
IK;
PHILIPP, A.; HALBRITTER, J.
Untersuchungen der Hochfrequenzeigenschaften
von Nb bei Frequenzen von 12 bis 18 GHz.
Fruehjahrstagung DPG, Festkoerperphysik,
Freudenstadt, 24.-28.Maerz 1980.
Verhandlungen der Deutschen Physikalischen
Gesellschaft, R.6, Bd 15(1980) S.390

V14908   80   VOR;
IK;
PILKUHN, H.; POTH, H.
On the production of antideuterons.
5th European Symp.on Nucleon-Antinucleon
Interactions, Brixen, I, June 23-28, 1980

V14547   80   VOR;
IK;
POTH, H.
Bericht ueber den geplanten Niederenergie
Antiprotonen Ring am CERN.
Vortr.: 43.Physikertagung 1979 Ulm, Deutsche
Physikalische Gesellschaft, Oesterreichische
Physikalische Gesellschaft und Schweizerische
Physikalische Gesellschaft, Ulm,
25.-29.September 1979

V15172   80   VOR;
IK;
POTH, H.
Der Niederenergie - Antiprotonring LEAR.
Vortr.: IV.Arbeitstreffen
Mittelenergiephysik, Todtnauberg,
2.-8.Oktober 1980

V14603   80   VOR;
IK;
RAICH, U.; BLUEM, P.; MEYER, M.
An azimuthal segmented cylindrical
drift-chamber system with two-dimensional
readout.
Wire Chamber Conf., Wien, A, February 27-29,
1980

V14287   80   VOR;
IK;
SCHWARZ, W.; KROENER, F.; HALBRITTER, J.
Tunnelbarrieren von Nb-Nbsub(x)Osub(y)-Pb
Kontakten.
Fruehjahrstagung DPG, Festkoerperphysik,
Freudenstadt, 24.-28.Maerz 1980.
Verhandlungen der Deutschen Physikalischen
Gesellschaft, R.6, Bd 15(1980) S.420

V15246   80   VOR;
IK;
VETTER, J.E.
A linear accelerator for the German
spallation neutron source.
Tagung der Internat.Collaboration on Advanced
Neutron Sources ICANS-IV, Tsukuba, J.,
October 20-24, 1980

V15524   81   VOR;
IK;
HALBRITTER, J.; HUEBNER, H.
Untersuchung der Elektronen-Feldemission bei
hohen Frequenzen.
Fruehjahrstagung DPG, Festkoerperphysik,
Muenster, 9.-14.Maerz 1981. Verhandlungen der
Deutschen Physikalischen Gesellschaft, R.6,
Bd.15(1981) S.385

V15535   81   VOR;
IK;
PHILIPP, A.; HALBRITTER, J.
Temperatur- und Frequenzabhaengigkeit des
Oberflaechenwiderstandes von supraleitendem
Nb.
Fruehjahrstagung DPG, Festkoerperphysik,
Muenster, 9.-14.Maerz 1981. Verhandlungen der
Deutschen Physikalischen Gesellschaft, R.6,
Bd.15(1981) S.500

V15538   81   VOR;
IK;
HALBRITTER, J.
Grenzflaechenzustaende an
Nb-Nb$_2$O$_5$-Grenzflaechen und ihre
Tunnelanomalien.
Fruehjahrstagung DPG, Festkoerperphysik,
Muenster, 9.-14.Maerz 1981. Verhandlungen der
Deutschen Physikalischen Gesellschaft, R.6,
Bd.16(1981) S.504-05

V15544   81   VOR;
IK;
BOLGER, J.; BOSCHITZ, E.; PROEBSTLE, G.;
SMITH, G.R.; MANGO, S.; MEYER, M.; VOGLER,
F.; JOHNSON, R.R.; ARVIEUX, J.
Search for dybarion resonances in pion
scattering on vector polarized deuterons.
45.Physikertagung der DPG, gemeinsam mit der
Fruehjahrstagung Kern- und Teilchenphysik,
Kurzzeit- und Plasmaphysik, Hamburg,
23.-27.Maerz 1981. Verhandlungen der
Deutschen Physikalischen Gesellschaft, R.6,
Bd.16(1981) S.655

V15545   81   VOR;
IK;
ABELA, R.; WUEST, J.; EFFENBERGER, B.;
KUNOLD, W.; OESTERLE, W.; SIMONS, L.;
SCHNEIDER, M.
Bestimmung des Quadrupolmomentes von
myonischem Arsen.
45.Physikertagung der DPG, gemeinsam mit der
Fruehjahrstagung Kern- und Teilchenphysik,
Kurzzeit- und Plasmaphysik, Hamburg,
23.-27.Maerz 1981. Verhandlungen der
Deutschen Physikalischen Gesellschaft, R.6,
Bd.16(1981) S.656-57

V15546   81   VOR;
IK;
DOLL, P.; HAESNER, B.; KECSKEMETI, J.;
KLAGES, H.O.; SCHWARZ, P.; CHALUPKA, A.;
VONACH, H.
Kalibrierung von Neutronendetektoren mit
Hilfe bekannter Neutronenfelder.
45.Physikertagung der DPG, gemeinsam mit der
Fruehjahrstagung Kern- und Teilchenphysik,
Kurzzeit- und Plasmaphysik, Hamburg,
23.-27.Maerz 1981. Verhandlungen der
Deutschen Physikalischen Gesellschaft, R.6,
Bd.16(1981) S.677

V15547   81   VOR;
IK;
BALZER, R.; HENNECK, R.; JACQUEMART, CH.;
LANG, J.; ROSER, T.; SIMONIUS, M.; HAEBERLI,
W.; JACCARD, S.; REICHART, W.; WEDDIGEN, CH.
Parity violation in p-p scattering at 45 MeV.
45.Physikertagung der DPG, gemeinsam mit der
Fruehjahrstagung Kern- und Teilchenphysik,
Kurzzeit- und Plasmaphysik, Hamburg,
23.-27.Maerz 1981. Verhandlungen der
Deutschen Physikalischen Gesellschaft, R.6,
Bd.16(1981) S.679-80

V15560   81   VOR;
IK;
GUNDERSON, B.;
CELLO-KOLLABORATION
Totaler hadronischer Wirkungsquerschnitt in
e+e--Vernichtung.
45.Physikertagung der DPG, gemeinsam mit der
Fruehjahrstagung Kern- und Teilchenphysik,
Kurzzeit- und Plasmaphysik, Hamburg,
23.-27.Maerz 1981. Verhandlungen der
Deutschen Physikalischen Gesellschaft, R.6,
Bd.16(1981) S.821

V15561   81   VOR;
IK;
CELLO-KOLLABORATION;
RANDOLL, H.
Aufbau und Betrieb des CELLO-LAR-Kalorimeters
bei PETRA.
45.Physikertagung der DPG, gemeinsam mit der
Fruehjahrstagung Kern- und Teilchenphysik,
Kurzzeit- und Plasmaphysik, Hamburg,
23.-27.Maerz 1981. Verhandlungen der
Deutschen Physikalischen Gesellschaft, R.6,
Bd.16(1981) S.838

V15562   81   VOR;
IK;
CELLO-KOLLABORATION;
HOPP, G.
Energieeichung des CELLO-LAR-Detektors bei
PETRA.
45.Physikertagung der DPG, gemeinsam mit der
Fruehjahrstagung Kern- und Teilchenphysik,
Kurzzeit- und Plasmaphysik, Hamburg,
23.-27.Maerz 1981. Verhandlungen der
Deutschen Physikalischen Gesellschaft, R.6,
Bd.16(1981) S.838

V15563   81   VOR;
IK; ITP;
BAUER, W.; BRANDELIK, A.; CITRON, A.; GRAF,
F.; HALBRITTER, J.; HERZ, W.; KNEISEL, P.;
LEHM, R.; LEHMANN, W.; SZECSI, L.
Erste Ergebnisse eines Experiments mit einem
supraleitenden Beschleunigungsresonator in
DORIS.
45.Physikertagung der DPG, gemeinsam mit der
Fruehjahrstagung Kern- und Teilchenphysik,
Kurzzeit- und Plasmaphysik, Hamburg,
23.-27.Maerz 1981. Verhandlungen der
Deutschen Physikalischen Gesellschaft, R.6,
Bd.16(1981) S.841

V15564   81   VOR;
IK;
RICHTER, B.; BLUEM, P.; GUIGAS, R.; KOCH, H.;
MEYER, M.; POTH, H.; RAICH, U.; BACKENSTOSS,
G.; PAVLOPOULOS, P.; REPOND, J.; TAUSCHER,
L.; TROESTER, D.; ADIELS, L.; BERGSTROEM, I.;
FRANSSON, K.; KEREK, A.; SUFFERT, M.;
ZIOUTAS, K.
Suche nach Baryonium unterhalb der
Proton-Antiproton-Schwelle.
45.Physikertagung der DPG, gemeinsam mit der
Fruehjahrstagung Kern- und Teilchenphysik,
Kurzzeit- und Plasmaphysik, Hamburg,
23.-27.Maerz 1981. Verhandlungen der
Deutschen Physikalischen Gesellschaft, R.6,
Bd.16(1981) S.846

V15601   81   VOR;
IK;
ZIEHER, K.W.; HORNUNG, A.
Investigation of a modified helix loaded
superconducting resonator for acceleration of
heavy ions.
Particle Accelerator Conf., Washington, D.C.,
March 11-13, 1981

V15642   81   VOR;
IK;
BUECHE, G.
Dosis Verteilungen von negativ geladenen
Pionen aus Monte-Carlo Rechnungen.
Vortr.: Institut fuer Biophysik, Universitaet
des Saarlandes, Homburg/Saar, 26.Januar 1981

V15749   81   VOR;
IK;
CHU, Y.; DOLL, P.; GOBBI, A.; HILDENBRAND,
K.; HO, H.; KUEHN, W.; LOEHNER, H.; LYNEN,
U.; MUELLER, W.; OLMI, A.; PELTE, D.; SANN,
H.; SANTO, R.; WINKLER, U.
Collective effects in ^{12}C induced reactions
at 86 MeV/u.
Proc.of the Internat.Conf.on Nuclear Physics.
Berkeley, Calif., August 24-30, 1980.
(Abstract)
LBL-11118 S.557

V15750   81   VOR;
IK;
DAKOWSKI, M.; DOLL, P.; GOBBI, A.; LYNEN, U.;
OLMI, A.; RUDOLF, G.; SANN, H.; BOCK, R.
Nuclear structure information in dissipative
collisions.
Internat.Symp.on Continuum Spectra of Heavy
Ion Reactions, San Antonio, Tex., December
3-5, 1979

V15751   81   VOR;
IK;
GOTTA, D.
Analyse von Proton Antiproton Annihilationen
in Ruhe.
Vortr.: Universitaet Mainz, 4.Mai 1981

V15752   81   VOR;
IK;
HALBRITTER, J.
On resonant absorption of phonons and photons
at interfaces
16th Internat.Conf.on Low Temperature
Physics(LT-16), Los Angeles, Calif., August
19-26, 1981

V15753   81   VOR;
IK;
HOFTIEZER, J.; WEDDIGEN, CH.; FAVIER, B.;
JACCARD, S.; WALDEN, P.; CHATELAIN, P.;
FOROUGHI, F.; NUSSBAUM, C.; PIFFARETTI, J.
Differential cross section and analysing
power measurements of the pp-->π^+d reaction.
9eme Conference Internationale sur la
Physique a Haute Energie et la Structure
Nucleaire(ICOHEPANS-9), Versailles, F,
Juillet 6-10, 1981

V15754   81   VOR;
IK;
KNOEPFLE, K.T.; SAUTER, A.; WAGNER, G.J.;
DOLL, P.; HENDRIE, D.L.; WIEMAN, H.
K-splitting of isoscalar giant quadrupole
resonances in Ca-isotopes.
Proc.of the Internat.Conf.on Nuclear Physics.
Berkeley, Calif., August 24-30, 1980.
(Abstract)
LBL-11118 S.262

V15983   81   VOR;
IK;
BODENKAMP, J.; FRIES, D.C.; MARKOU, A.;
SEITZ, E.; BEHREND, H.J.; FENNER, H.; HESSE,
W.P.; MIYACHI, T.; MCNEELY, W.A.; SCHROEDER,
V.
Cross section and proton antiproton invariant
mass distribution of the reaction
gammaproton-->proton antiproton proton at
$4.7 <= E_{sub(gamma)} <= 6.6$ GeV.
Conf.on High Energy Physics, Lisboa, P, July
9-15, 1981

V15985   81   VOR;
IK;
MASCHUW, R.
Polarized targets for neutron scattering
experiments.
Polarized Target Meeting, Braunschweig,
14.-15.Mai 1981

V15986   81   VOR;
IK;
MITTAG, K.
SNQ linear accelerator beam dynamics.
ICANS-V Meeting of the Internat.Cooperation
on Advanced Neutron Sources, Karlsruhe, June
25-26, 1981

V15987   81   VOR;
IK;
SCHULZE, D.
New methods of rf control for the spallation
neutron source.
ICANS-V Meeting of the Internat.Cooperation
on Advanced Neutron Sources, Karlsruhe, June
25-26, 1981

V16003   81   VOR;
IK;
BAUER, G.S.; VETTER, J.E.
The German project for a high power
spallation neutron source for fundamental
research.
IIASA Workshop on a Perspective on Adaptive
Nuclear Energy Evolutions - Towards a World
of Neutron Abundance, Laxenburg, A, May
25-27, 1981

V16004   81   VOR;
IK;
HALBRITTER, J.
Eigenschaften von realen Metalloberflaechen.
Vortr.: Physikkolloquium, Karlsruhe, 24. Juli
1981

Institut für Angewandte Kernphysik II

Publications

Almeida, J.; Beer, H.; Käppeler, F.; Wisshak, K.
Neutroneneinfang und die Entstehung der chemischen Elemente
KfK-Nachrichten, 12 (1980) No. 3, S. 3-11

Appel, H.; Raudies, J., Thies, W.-G., Hanser, A.; Sellschop, J.P.F.
Residence Sites for ^{111}In Implanted in Diamond
Hyperfine Interactions 10 (1981), North Holland Publ. Company,
735-740.

Bechtold, V., Chan-Tung, N.; Dousson, S.; Geller, R.; Jacquot, B.,
Jongen, Y.
ECR Ion Source for Multiply-Charged Oxygen Beams
Nuclear Instr. Meth. 178 (1980) S. 305-08

Beck, R.; Mihailovic, M.V.; Poljsak, M.
Calculation of Nuclear Reaction Parameters with the Generator
Coordinate Method and Their Interpretation
Nucl. Phys. A, 351 (1981) 295-311

Beck, R.; Krivec, R.; Mihailovic, M.
The Three-Cluster Structures in ^{7}Li.
Nucl. Phys. A,363 (1981) 365-80.

Beer, H.; Cierjacks, S.; Dickmann, F.; Erbe, D.; Hage, W.;
Hinterberger, F.; Käppeler, F.; Leugers, B.; Müller, R.; Naqvi, A.A.;
Rossen, P. von; Schmalz, G.; Wickenhauser, J.; Wisshak, K.
Nuclear Data Research in the Institut für Angewandte Kernphysik,
Kernforschungszentrum Karlsruhe
NEANDC(E)-212 U Vol. 5 (June 80), Progress Report on
Nuclear Data Research in the Federal Republic of Germany for the
Period April 1, 1979 to March 31, 1980, 1-19.

Beer, H., Käppeler, F., Wisshak, K., Ward, R.A.
^{176}Lu: Cosmic Clock or Stellar Thermometer ?
KfK-3094 (Dezember 1980).

Beer, H.; Ward, R.A.

Neutron-Capture Nucleosynthesis of Nature's Rarest Stable Isotope
Nature, 291 (1981) 308-10

Bekk, K.; Nowicki, G.

Kernstrukturuntersuchungen mit Lasern
KfK-Nachrichten, 12 (1980) No. 3, 12-16

Buschmann, J.; Gils, H.J.; Rebel, H.; Schulz, F.; Neumann, B.;
Klewe-Nebenius, H.

Kernreaktionen mit einem ungewöhnlichen Teilchenstrahl:
156 MeV ^{6}Li-Ionen
KfK-Nachrichten 13 (1981) No. 1-2, 150-53

Dickmann, F.; Hanser, A.;

Annual Report. Teilinstitut Kernphysik des Instituts für
Angewandte Kernphysik.(July 1, 1979 - June 30, 1980)
KfK-3068, Oktober 1980

Friedman, E.; Gils, H.J.; Rebel, H.; Pesl, R.;

The Dependence on Energy and Mass-Number of the Alpha-Particle
Optical Potential: A Justification for the Folding Model Approach.
KfK - 3038 (September 1980) - Nucl. Phys. A 363 (1981) 137

Gils, H.J.; Nowicki, G.; Rebel, H.

Die Unterschiede der räumlichen Verteilung von Protonen und
Neutronen in Calcium-Atomkernen
KfK-Nachrichten, 12 (1980) No. 3, 17-23.

Gils, H.J.; Friedman, E.; Rebel, H.

Radial Sensitivity of Hadronic Probes and How Accurately are
Nuclear Radii Determined.
KfK-3039 (Sept. 1980).

Gils, H.J.

The Karlsruhe Code MODINA for Model Independent Analysis of Elastic
Scattering of Spinless Particles.
KfK-3063 (November 1980).

Gils, H.J.

Design of a Simple Magnetic Spectrograph for the Karlsruhe
Isochronous Cyclotron
KfK-2972 (Dezember 1980).

Hage, W.; Wisshak, K.; Käppeler, F.

Neutron Fission Cross-Section Measurement of ^{241}Am in the Energy
Range from 10 to 1030 keV
Nucl. Sci. Eng. 78 (1981) 248-58

Heck, D.

The Influence of Secondary Fluorescence from Elements Adjacent
to the Microbeam Spot on Local Concentration Determination with PIXE.
Nucl. Instr. Meth. 181 (1981) 135-39.

Mairle, G.; Wagner, G.J.; Knöpfle, K.T.; Pao, Liu Ken,
Riedesel, H., Bechtold, V., Friedrich, L.

Deformation of 1p Shells in (2s,1d) Shell Nuclei from a
Systematic Study of $(\vec{d},\tau)$ Reactions
Nucl. Phys. A 363 (1981), 413-428.

Neumann, B.; Rebel, H.; Buschmann, J.; Gils, H.J.; Klewe-Nebenius, H.;
Zagromski, S.

Projectile Break-up in Continuous Particle Spectra from Nuclear
Reactions Induced by 156 MeV ^{6}Li.
Zeitschrift für Physik A – Atoms and Nuclei, 296 (1980) 113-22.

Rebel, H.; Pesl, R.; Gils, H.J.; Friedman, E.;

Method for Analysis of Inelastic Alpha Particle Scattering
KfK 3104 (May 1981) – Nucl. Phys. 368 (1981) 61

Schweickert, H.

17th European Cyclotron Progress Meeting in Karlsruhe
KfK-Nachrichten, 12 (1980) No. 3, 43-44

Stach, W.; Kretschmer, W.; Wango, M.B., Rebel, H.

Nuclear Shape Effects in Scattering of Alpha Particles and
Polarized Deuterons.
Nukleonika, 25 (1980) 1025-34

Stuirbrink, A.; Knoepfle, K.T.; Mairle, G.; Riedesel, H.;
Schindler, K.; Wagner, G.J.; Bechtold, V.; Friedrich, L.

Spin Determination of Deeply-Bound Hole States from $(\vec{d},^3\text{He})$
Reactions.
5th International Symp. on Polarization Phenomena in Nuclear Physics,
Santa Fe, N.M., August 11-15, 1980
Zeitschrift für Physik – Atoms and Nuclei, A 297 (1980) 307-09

Wisshak, K.; Käppeler, F.

The Neutron Capture and Fission Cross Section of Amerium-241 in the
Energy Range from 10 to 250 keV.
Nucl. Sci. Eng. 76 (1980) 148-62

Wisshak, K.; Käppeler, F.

Determination of the Capture Width of the 27.7 keV s-Wave
Neutron Resonance in Iron-56.
Nucl. Sci. Eng. 77 (1981) 58-70.

Conference Contributions

11th Internat. Quantum Electronics Conf., Boston, Mass., June 23-26, 1980

Andl, A.; Bekk, K.; Göring, S.; Hanser, A.; Nowicki, G.;
Rebel, H.; Schatz, G.

Laser Spectroscopy of Minute Samples of Radioactive Alkaline Earth
Atoms

5th Internat. Conf. on Hyperfine Interactions, Berlin, July 21-25, 1980

Andl, A.; Appel, H.; Büche, G.; Haffner, H.; Wittek, P.

Demonstration of a Hydrogen Bond on Tobacco Mosaic Virus using ^{129}I.

5th Internat. Symp. on Polarization Phenomena in Nuclear Physics,

Santa Fe, N.M., August 11-15, 1980

Mairle, G.; Knoepfle, K.T.; Riedesel, H.; Schindler, K.; Wagner, G.J.;
Bechtold, V.; Friedrich, L.

Configuration Mixing of Particle-Hole States in A = 16 Nuclei
studied by the $^{17}O(\vec{d},t)^{16}O$ and ^{17}O $(\vec{d},\tau)^{16}N$ Reaction.

Mairle, G.; Liu Ken Pao; Knoepfle, K.T.; Riedesel, H.; Schindler, K.;
Wagner, G.J.; Bechtold, V.; Bialy, J.; Friedrich, L.

Spectroscopy of Stretched Configurations with the $(\vec{d},\alpha)$-Reaction
at 52 MeV.

Stuirbrink, A., Knoepfle, K.T.; Mairle, G.; Riedesel, H.; Schindler, K.;
Wagner, G.J.; Bechtold, V.; Friedrich, L.

Spin Determination of Deeply-Bound Hole States from $(\vec{d},^{3}He)$ Reactions

International Conf. on Nuclear Physics, Berkeley, Calif., August 24-30, 1980

Gils, H.J.; Friedman, E.; Pesl, R.; Rebel, H.

Nuclear Sizes of ^{40}Ca, ^{42}Ca, ^{44}Ca, ^{48}Ca, ^{50}Ti, ^{53}Cr from Elastic
Scattering of 104 MeV Alpha Particles.

International Symp. on Radioiodines, Banff, Alberta,
CAN, September 13-16, 1980

Assmus, K.H.; Maier, W.; Schütz, R.; Schulz, F.; Schweickert, H.

Routine Production of Iodine-123 at the Karlsruhe Isochronous Cyclotron.

5th Nat. Soviet Conf. on Neutron Physics, Kiev, SU,
September 15-19, 1980

Wisshak, K.; Wickenhauser, J.; Käppeler, F.

The Isomeric Ratio in Neutron Capture of ^{241}Am at 14.75 meV
and 30 keV.

Europhys. Conf. on Nuclear Physics Methods in Materials Research
Darmstadt, September 23-26, 1980

Essig, G.; Fehsenfeld, P.

Thin Layer Activation Technique and Wear Measurements in Mechanical
Engineering

Study Weekend, "Topics in Heavy Ion Reactions", Daresbury Laboratory,
Warrington, GB, October 4-5, 1980

Neumann, B.; Rebel, H.; Klewe-Nebenius, H.; Gils, H.J.

^{6}Li-Break-Up-Reactions at 26 MeV/Nucleon.

VDI-Konferenz, Karlsruhe, October 26, 1980

Schatz, G.

Technische Anwendungen von Beschleunigern mittlerer Energie.

Workshop on ECR-Ion Sources, GSI Darmstadt, December 8, 1980

Bechtold, V., Friedrich, L.; Schweickert, H.

Status of HISKA and First Results of p-HISKA.

5th Intern. Conf. on Ion Beam Analysis, Sydney, Australia,
February 16-20, 1981

D. Heck

Secondary Fluorescence Induced in Elements in the Micrometer Vicinity
of Ion Microprobe Spots in PIXE Experiments.

Meeting of Krypton-81m Generator Producers, Liege, B, February 27, 198µ

Kernert, N.; Peters, J.

Production of ^{81}Rb/^{81}Kr Generators at Karlsruhe.

Expertentreffen für Kernphysik, Schleching, March 4-13, 1981

Schatz, G.

Der s-Prozeß der Elementsynthese.

Rebel, H.

Ladungs- und Materieverteilung in Atomkernen (4 Vorlesungen)

Frühjahrstagung DPG, Kernphysik, Hamburg, March 23-27, 1981

Almeida, J.; Käppeler, F.; Erbe, D.

Der Einfluß von ^{22}Ne auf die Neutronenbilanz im s-Prozeß

Bechtold, V.; Ehret, H.P.; Friedrich, L.; Möllenbeck, J.;
Schweickert, H.; Ziegler, P.

The ECR-Ion Source HISKA for the Karlsruhe Isochronous Cyclotron

Beck, R.; Krivec, R.; Mihailovic, M.V.

Untersuchung von Zwei- und Drei-Cluster Strukturen in ^{7}Li.

Beer, H.; Käppeler, F.; Ward, R.A.

Messung der Neutroneneinfangquerschnitte ^{152}Sm$(n,\gamma)^{153}$Sm,
^{151}Eu$(n,\gamma)^{152}$Eu und ^{152}Gd$(n,\gamma)^{153}$Gd zur Untersuchung
der s-Prozeßverzweigung beim ^{151}Sm.

Beer, H.; Ward, R.A.

Über die s-Prozeß Herkunft von ^{180}Ta, dem seltensten stabilen
Kern in unserem Sonnensystem.

Bollmann, E.; Fehsenfeld, P.; Kernert, N.; Peters, J.; Schulz, F.;
Schweickert, H.

Applied Nuclear Physics at the Karlsruhe Isochronous Cyclotron

Eyrich, W.; Hofmann, A.; Ortner, H.; Rebel, H.; Scheib, U.;
Stamminger, R.; Steuer, D.; Steuer, H.; Stumm, J.

Direct Spectroscopy of the Neutron-Decay of the Isoscalar Giant
Resonances in ^{208}Pb.

Gerhard, P.; Grabmayr, P.; Knoepfle, K.T.; Liu Ken Pao;
Mairle, G.; Riedesel, H.; Schindler, K.; Schmidt, H.R.;
Stuirbrink, A.; Wagner, G.J.; Bechtold, V.; Friedrich, L.

Spectroscopy of Stretched Configurations with the $(\vec{d},\alpha)$-Reaction
at 52 MeV.

Gils, H.J.; Friedman, E.; Rebel, H.

Radial Sensitivity of Hadronic Probes and How Accurately are
Nuclear Radii Determined.

Grabmayr, P.; Mairle, G.; Riedesel, H.; Seegert, G.; Stuirbrink, A.;
Wagner, G.J.; Bechtold, V.; Friedrich, L.

Deeply-Bound Hole States in Odd-A Nb Isotopes.

Käppeler, F.; Wisshak, K.; Hong, L.D.

Die Wirkungsquerschnitte am Beginn des s-Prozeß-Synthesepfads
und die besondere Rolle des ^{58}Fe.

Neumann, B.; Buschmann, J.; Gils, H.J.; Klewe-Nebenius, H.;
Rebel, H.; Zagromski, S.; Shyam, R.

Continuous Particle Spectra from (^{6}Li+^{40}Ca) Reactions at E_{Li}=156 MeV
and the Complex Structure of the Triton Component.

Planeta, R.; Grotowski, K.; Majka, Z.; Buschmann, J.;
Klewe-Nebenius, H.; Gils, H.J.; Neumann, B.; Rebel, H.

Investigation of Mechanism in the ^{6}Li+^{40}Ca Reaction at E_{Li}=156 MeV.

Rebel, H.; Pesl, R.; Gils, H.J.; Friedman, E.

Method for Analysis of Inelastic Alpha Particle Scattering and
How Good is the Vibrational Model?

Ward, R.A.; Beer, H.

On the Origin of the Solar System Abundances of ^{113}In, ^{114}Sn, and ^{115}Sn.

18th European Cyclotron Progress Meeting, Louvain-la-Neuve, Belgium,
March 26-27, 1981

Bechtold, V.; Friedrich, L.; Schweickert, H.

Status of HISKA and First Results of p-HISKA.

7th Internat. Conf. on Magnet Technology, Karlsruhe, March 30-April 3, 1981

Bechtold, V.; Baran, W.; Ervens, W.; Friedrich, L.; Kessler, S.

Design and Test of a 700 mm Long Hexapole Composed of Rectangular
Rare Earth Cobalt Permanent Magnets.

1st European Conf. on Atomic Physics, Heidelberg, April 6-10, 1981

Andl, A.; Bekk, K.; Göring, S.; Hanser, A.; Nowicki, G.;
Rebel, H.; Schatz, G.; Thompson, R.C.

Laser Spectroscopic Measurements of Isotope Shifts in Calcium Isotopes

3rd Annual Symp. on Safeguards and Nuclear Material Management

Eberle, H.; Matussek, P.; Michel-Piper, I.; Ottmar, H.

Operational Experiences with K-Edge Photon Absorptiometry
for Reprocessing Feed and Product Solution Analysis.

Matussek, P.; Ottmar, H.; Iyer, M.R.; Chakraborty, P.P.;
Choithramani, S.J.; Sharma, D.N.

A Microprocessor-Based Plutonium Waste Monitor with Internal
Matrix Attenuation Correction.

1. Präsentation des BMFT-Förderprogrammes über Tribologie:
Reibung, Verschleiß, Messung '(1

Fehsenfeld, P., Möller, H.

Radionuklidtechnik im Maschinenbau.

Seminar Radionuklidtechnik, Karlsruhe, May 13-15, 1981

Bollmann, E.; Fehsenfeld, P.; Kleinrahm, A.; Roth, H.

Aktivierungstechnik für Verschleißmessungen im Maschinenbau.

Workshop on Nuclear Astrophysics, Schloß Ringberg, Tegernsee,
May 19-22, 1981

Beer, H.

Population of Isomeric States by keV Neutron Capture and its Importance
in Stellar Nucleosynthesis.

Käppeler, F.

s-Process Studies at Karlsruhe.

Europhysics Conf. on Nuclear and Atomic Physics with Heavy Ions,
Bukarest, Rumänien, June 9-12, 1981

Corcalciuc, V.; Gils, H.J.; Rebel, H.; Buschmann, J.; Pesl, R.

104 MeV Alpha Particle Scattering from ^{90,92}Zr: the Radial Shape
of the Extended Optical Potential.

Neumann, B.; Rebel, H.; Gils, H.J.; Klewe-Nebenius, H.;
Planeta, R.; Shyam, R.

^{6}Li Break-up Reactions at 26 MeV/nucleon.

Buschmann, J.; Freindl, L.; Gils, H.J.; Grotowski, H.; Klewe-Nebenius, H.;
Majka, Z.; Micek, S.; Neumann, B.; Planeta, R.; Rebel, H.; Zagromski, S.

Evidence of a Fission Like Mechanism in the ^{6}Li+^{40}Ca Reaction.

Lectures

Bechtold, V.

Status of the Karlsruhe Isochronous Cyclotron
Central Institute for Physics, Bukarest-Magurele, Rumänien,
September 8, 1980

Rebel, H.

Die unterschiedliche Verteilung von elektrischer Ladung
und Kernmaterie in den Ca-Atomkernen
Hahn-Meitner-Institut für Kernforschung, Berlin, July 7, 1980

Rebel, H.

Materie-Verteilung in Atomkernen aus der Alpha-Teilchenstreuung.
'Physik mit dem SUSE-Beschleuniger', Ludwig-Maximilians-Universität
München, November 21, 1980

Rebel, H.

Wie verteilen sich die Neutronen in Atomkernen?
Physikalisches Kolloquium der Universität Mainz, November 11, 1980

Käppeler, F.

Neutron Capture Cross Sections - Clues to s-Process Nucleosynthesis.
Institut Max von Laue - Paul Langevin, Grenoble, February 4, 1981

Käppeler, F.

Neutron Flux and Temperature During s-Process Nucleosynthesis.
Universität Lund, February 18, 1981

Rebel, H.

Optische Spektroskopie und Alphateilchen-Streuung als Informations-
quellen über die Verteilung der nuklearen Materie in Atomkernen.
Physikalisches Koll., Universität Tübingen, May 6, 1981

Schweickert, H.

Applied Nuclear Physics at the Karlsruhe Isochronous Cyclotron
Comision Nacional de Energia Atomica, (CNEA), Institut für
Radioisotope, Buenos Aires, Argentinien, May 5, 1981

Schatz, G.

Bestimmung von Ladungsradien instabiler Kerne, eine Anwendung
der Laserspektroskopie.
Gesellschaft für Schwerionenforschung, Darmstadt, May 26, 1981

Gils, H.J.

^{6}Li-Induced Nuclear Reactions at $E_{Li} = 156$ MeV.
Ben-Gurion University, Beer Sheva, Israel, May 26, 1981

Friedrich, L.

ECR-Ionenquellenentwicklung in Karlsruhe.
Institut für Strahlen- und Kernphysik, Universität Bonn,
June 25, 1981
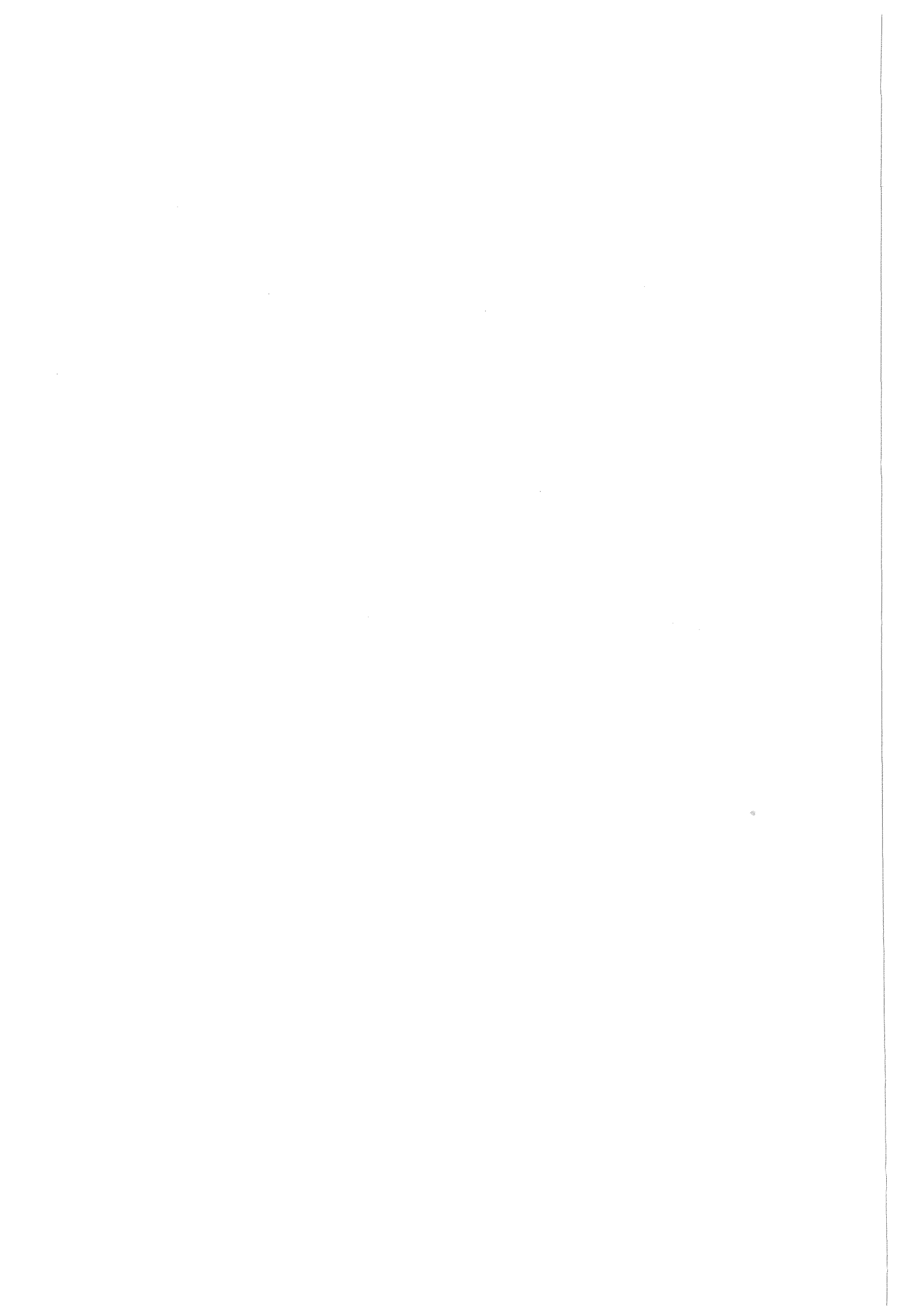
6. PERSONNEL

Institut für Kernphysik

Head of the Teilinstitut 1 (IK 1): Prof.Dr.Bernhard Zeitnitz

Scientific and technical staff:

Apel, W.-D., Dr.	Kecskemeti,J., Dr. (bis 31.7.1981)
Aures,R., DP	Keim, H.
Banerjee,S., Dr.	Kiontke,S., DP
Bodenkamp,J., Dr.	Klages,H.-O., Dr.
Chernohorsky,I.	Krupp,H.
Chrobaczek,D., DP	Küster,H.
Deutsch,G.	Lallemand,V.
Dittmann,R.	Maschuw,R., Dr.
Doll,P., Dr.	Mischok,M.
Engler,J., Dr.	Müller,H., Dr.
Flügge,G., Prof.Dr.	Oexner,M.
Fries,D., Dr.	Plischke,P., Dr.
Fues,W., Dr.	Randoll,H., DP
Gamerdinger,K.	Schmalz,G., DI
Giorginis,G., Dr.	Schmidt,F.K., Dr.
Grundel, G.	Schmidt,G., DP
Gumbsheimer,R., Ing.grad.	Schneider,H., Dr.
Haesner,B., DP	Schwarz,P., DP
Hagert,H.	Skacel,H.
Hansmeyer,J.	Spohrer,G.
Heeringa,W., Dr.	Ullrich,G.
Hiebert,J., Prof.Dr.	Wilczynski,J., DP
Hopp,G.	Zeitnitz,B., Prof.Dr.
Hucker,H.	Ziegler,P.
Husson,L., Ing.	

Head of the Teilinstitut II(IK II): Prof.Dr.Anselm Citron

Scientific and technical staff:

Blüm,P., Dr.	Oesterle,W.
Bolger,J., Dr.	Poth,H., Dr.
Borie,E., Dr.	Pröbstle,G.
Boschitz,E., Prof.Dr.	Przybilla,G.
Büche,G., Dr.	Raich,U., DP
Citron,A., Prof.Dr.	Reich,J.
Degitz,G., DP	Richter,B., DP
Diehl,U.	Schmidt,G., Dr.
Dörr,M., DP	Schneider,M.
Dröge,M.	Simons,L.M., Dr.
Effenberger,B.	Smith,G., Dr.
Engelhardt,D., Prof.Dr.	Ullrich,H., Prof.Dr.
Firl,G.	Weddigen,C., Dr.
Gotta,D., Dr.	Wiedner,U.
Guigas,R., Dr.	Wolf ,A.
Haas,E.	
Höhne,A.	
Hofmann,K.-W.	
Hoftiezer,J., Dr.	
Kärcher,K.	
Klein,U., DP	
Kluge,W., Prof.Dr.	
Koch,H., Prof.Dr.	
Köhler,T.	
Kunold,W., DP	
Ljungfelt,S., DP	
Maier,T.	
Markus,R.	
Mathie,E., Dr.	
Matthäy,H., Dr.	
Meyer,M., DI	

Institut für Angewandte Kernphysik II

Head of the Institut: Prof. Dr. Gerhard Schatz

Scientific and technical staff:

Almeida, J., Dipl.-Phys.	Heck, D., Dr.
Altai, K., Dipl.-Phys.	Käppeler, F., Dr.
Andl, A., Dr.	Kazerouni, M.A., Dipl.-Phys.
Bao, Z.Y., Mars., DP	Kunigkeit, G., Mrs., Ing.
Beck, R., Dr.	Maaß, E., Mrs.
Beer, H., Dr.	Matussek, P., Dipl.-Phys.
Bekk, K., Dr.	Michel-Piper, I., Mrs., Ing.
Buschmann, J., Dr.	Naqvi, S.A.A., Dr.
Chongkum, S.	Ottmar, H., Dr.
Dickmann, F., Dr.	Pesl, R., Dipl.-Phys.
Dohrmann, H., Ing.	Planeta, R., Dr.
Eberle, H., Ing.	Rebel, H.G., Prof. Dr.
Erbe, D.	Rupp, G.
Feißt, K., Mrs.	Schmidt, K.A., Dipl.-Phys.
Feurer, B.	Thompson, R., Dr.
Friederich, H.M., Mrs.	Walter, G., Dipl.-Phys.
Gils, H.J., Dr.	Wisshak, K., Dr.
Göring, S., Dipl.-Phys.	Zagromski, S., Ing.
Hanser, A., Dr.	

Head of the Cyclotron Laboratory: Dr. Hermann Schweickert

Scientific and technical staff:

Acharya, H., Mrs.

Assmus, K.H.

Bauer, G.

Bechthold V., Dr.

Bialy, J., Dipl.-Phys.

Biber, J.

Bibok, G.

Blank, R.

Bollmann, E., Dipl.-Phys.

Depta, A.

Dressen, R.

Ehret, H.P.

Erdel, E.

Fehsenfeld, P., Dr.

Franz, J.

Friedrich, J., Dr.

Gegenheimer, B.

Günther, O.

Haßpacher, G.

Haushahn, G., Dipl.-Phys.

Heasman, K.

Heidenreich, K.

Heinzmann, H., Dipl.-Inf.

Herrmann, P.

Hirth, W.

Holler, H.

Kaltenbaeck, J.

Kappel, W.-R., Ing.

Kauther, P.

Kernert, N., Dipl.-Phys.

Kessel, M.

Kirste, E. Mrs.

Kleinrahm, A.

Kögel, B.

Kuhn, H.

Maier, W.

Mangold, D.

McCann, G.

Möllenbeck, J., Ing.

Peters, J.-W. Dipl.-Phys.

Rämer, Ch., Miss, Ing.

Roth, H.

Schimpf, P.

Schüssler, B.

Schulz, F., Ing.

Seidel, H.

Seitz, J.

Seufert, H.

Sheikh, S.

Stöbener, E., Ing.

Thouw, T., Dr.

Uchatius, R., Mrs.

Wiss, L.

Ziegler, P.